

## **Reactive mixing of silica and rubber for tyres and engine mounts**



The research described in this thesis was financially supported by the Dutch Technology Foundation (STW).



Twente University **Press**

Publisher: Twente University Press,  
P.O. Box 217, 7500 AE Enschede, The Netherlands,  
[www.tup.utwente.nl](http://www.tup.utwente.nl)  
Print: Océ Facility Services, Enschede, The Netherlands

Cover design: by Tom Uitslag

Cover illustration: Front cover shows a tyre with the coupling agent bis-(triethoxysilylpropyl)tetrasulphide and the back cover shows an engine mount.

© L.A.E.M. Reuvekamp, Enschede, 2003.

No part of this work may be reproduced by print, photocopy, or other means without the permission in writing from the publisher.

ISBN 90 365 1856 3

# **REACTIVE MIXING OF SILICA AND RUBBER FOR TYRES AND ENGINE MOUNTS**

INFLUENCE OF DISPERSION MORPHOLOGY ON DYNAMIC  
MECHANICAL PROPERTIES

## **PROEFSCHRIFT**

ter verkrijging van  
de graad van doctor aan de Universiteit Twente,  
op gezag van de rector magnificus,  
prof. dr. F.A. van Vught,  
volgens besluit van het College voor Promoties  
in het openbaar te verdedigen  
op vrijdag 14 februari 2003 om 15.00 uur

door

**Louis-Philippe Antoine Eugène Maria Reuvekamp**

geboren op 16 mei 1973  
te Heino

*Dit proefschrift is goedgekeurd door:*

Promotor: prof. dr. ir. J.W.M. Noordermeer  
Assistent-promotor: dr. R.N. Datta

---

# Voorwoord

---

*“The most beautiful thing we can experience is the mysterious.  
It is the source of all true art and science.”*

*Albert Einstein*

Na 4 jaar is er dan een eind gekomen aan mijn promotietijd binnen de onderzoeksgroep “Rubbertechnologie”. Veel personen hebben door hun aanwezigheid en hulp bijgedragen aan het tot stand komen van dit proefschrift. De eerste bladzijden van dit proefschrift zijn daarom dan ook gereserveerd om deze personen te bedanken. Als eerste wil ik mijn promotor, professor Noordermeer, bedanken voor de gelegenheid die hij mij gegeven heeft om in zijn groep af te kunnen studeren en vervolgens verder te gaan met een promotieonderzoek. De goede begeleiding en kritische beoordeling van mijn werk heb ik altijd gewaardeerd. Daarnaast hebben we ook samen een aantal congressen bezocht, waarbij ook tijd was voor een leuk informeel deel.

Mijn assistent-promotor, Datta, wil ik ook zeer bedanken. Zijn enthousiaste begeleiding en zeer nuttige en leuke discussies zal ik niet gauw vergeten. De STW-begeleidingscommissie wil ik graag bedanken voor de zinvolle en zeer interessante halfjaarlijkse bijeenkomsten. The following persons I would like to thank for their valuable and very interesting discussions during the half-year meetings; Ir. N. Gevers, Dr. A. Guillet, Dr. A. de Hoog, Ir. A. Labruyère, S. de Meij, Dr. K. Menting, Dr. T. Mergenhagen, Ing. J. Mol en Prof. Dr. J. Vancso.

Het samenwerken met Dries of Dr.ies was echt een feest. We hebben vele discussies gehad omtrent het werk en de vergelijking van silica in rubber als een skippybal in een bord spaghetti was toch wel de mooiste. En tussen het fiepenschieten door is mijn organisch chemische kennis toch nog weer wat bijgespijkerd.

All the HPLC work would have been much more difficult without the help of Subhas and Hennie Bevers, thanks! I also would like to thank Marcin Debowski for all the AFM-measurements performed on those “sticky” rubbers. I know it were difficult measurements but I am glad you managed to come up with nice images. Ook Clemens en Steffie heel erg bedankt voor de AFM metingen nadat Marcin was vertrokken. Binnen het Mesa+ onderzoeksinstituut hebben twee personen mij de afgelopen jaren geholpen. Mark Smithers wil ik bedanken voor het vele SEM en TEM werk, ook al zijn de resultaten niet opgenomen in het proefschrift het werk is zeker zinvol geweest, en Albert van de Berg voor de XPS-metingen.

Mijn directe collega en kamergenote Annemieke wil ik bedanken voor alle discussies en het bijdragen aan de leuke sfeer in de groep, het congres in Nürnberg zal ik niet gauw vergeten. Ook alle andere collega's van de vakgroepen RBT, PBM, STEP en MTP wil ik bedanken voor de gezelligheid tijdens de koffie-, thee- en lunchpauzes, de BBQ's en filmavondjes.

En dan waren er natuurlijk nog “mijn” studenten. Stijn, bedankt voor de samenwerking en een deel van je werk kun je terugvinden in Hoofdstuk 4. En dan was er nog het duo Montse en Richard, de periode dat jullie tegelijk aan het afstuderen waren, was echt heel erg plezierig. Montse, despite of all the explosions, ¡muchas gracias por todo el trabajo! Richard ook hartelijk bedankt voor het vele werk.

---

Voor het verhelpen van allerlei administratieve problemen kon ik altijd terecht bij Gerda, Karin en Geneviève en voor de technische ondersteuning altijd bij John en Zlata. Ook de mensen bij Vredestein hartelijk bedankt voor alle hulp, in het bijzonder Luc en Rob en ik moet zeggen: die "leunsessies" zijn een goed initiatief.

Besides all the work there was of course also some time for relaxing, for this I would like to thank the "half-lifers". It was always a heavy competition but remember that Schumy.... Rules! En dan natuurlijk de befaamde bierproefavond (BPA), met Miechel, Leon, Tom, Jurgen en Menno, die inmiddels is uitgegroeid tot een mooie traditie en hopelijk nog jaren stand zal houden! Tom, nogmaals dank voor het ontwerpen van de cover. Special thanks to my friends who made me feel at home here in Enschede, Menno, Geert, Miechel, Kathrin, Leon, Ana, Pedro, Audrey. Of course also thanks to my squash partners, Audrey (was it squash or more the pyramid of info-trading...?), Zhiyuan and Giorgio.

Een woord van dank ook aan mijn huidige kamergenoot en paranimf Geert. Bedankt voor alle hulp en snelle correcties gedurende de laatste paar maanden en het draaiende houden van mijn PC.

Mijn familie wil ik graag bedanken voor alles wat ze voor mij gedaan hebben en de interesse voor mijn werk. Rest mij nog één iemand om te bedanken en dat is Judith. Bedankt voor alle steun en geduld! Het heeft veel voor mij betekend, en ik vind het heel leuk dat jij mijn paranimf wilt zijn.

*Louis*

---

## Contents

---

<b>Chapter 1</b>	General introduction	1
<b>Chapter 2</b>	Mechanisms of filler reinforcement and the effect of mixing conditions on the material properties of silica reinforced tyre tread compounds	5
<b>Chapter 3</b>	Effect of silane coupling agent, TESPT, on the performance of a silica rubber compound as influenced by processing conditions	31
<b>Chapter 4</b>	Effect of zinc oxide on the reaction of TESPT silane coupling agent with silica and rubber	47
<b>Chapter 5</b>	Influence of functional groups of TESPT coupling agent on dynamic and mechanical properties of tyre tread compounds	63
<b>Chapter 6</b>	A study of the influence of the reactivity of the TESPT-sulphur group by model vulcanisation	89
<b>Chapter 7</b>	Distribution of silica filler particles in relation to material properties	111
<b>Chapter 8</b>	Effect of polymer structure on the morphology of rubber compounds as measured with AFM	137
<b>Chapter 9</b>	The effect of silica/coupling agent combinations versus carbon black on the dynamic and mechanical properties of an EPDM-based engine mount compound	149
<b>Main symbols and abbreviations</b>		173
<b>Summary</b>		175
<b>Samenvatting</b>		179
<b>Curriculum Vitae</b>		183



---

# Chapter 1

## *General introduction*

---

### 1.1 Introduction

The first Europeans to see rubber were Columbus and his fellow travellers on their second American expedition (1493-1496). The natives of Haiti played a ball game, the balls being made from the sap, a white milky fluid, of a tree, later named:<sup>1, 2</sup> *Hevea Brasiliensis*.<sup>3</sup> The natural rubber (NR) or caoutchouc is the product condensed from the latex. The name caoutchouc was derived from the indian word “caa-o-chu”, meaning “weeping tree”. It took till 1736, when Charles Marie de la Condamine sent a sheet of natural rubber from Peru to the academy of Sciences in Paris, thereby introducing the material for the first time in Europe. In 1770, the noted scientist Sir Joseph Priestley (discoverer of oxygen) recorded the following: “ I have excellently adapted to the purpose of wiping from paper the mark of black lead pencil.” Europeans were rubbing out pencil marks with small cubes of rubber, which led to the English name “rubber” for this material. However, rubber was not an easy substance to work with, because it deteriorated very easily just like food: rubber would rot.<sup>4</sup>

The invention of useful rubber is commonly attributed to Charles Goodyear.<sup>4, 5</sup> Natural or India rubber, as it was then known, had few uses. Rubber products melted in hot weather, froze and cracked in cold, and adhered to everything they touched. In 1830 Goodyear began experimenting with raw rubber to turn it into a useable product. In 1839, he had managed to harden it by mixing the rubber with sulphur, white lead and oil of turpentine and drying it near a hot stove. The pieces which had come into direct contact with the stove had changed into an elastic, non-sticky product. The process known as vulcanisation had been born. The term vulcanisation was named after Vulcan, the Roman god of fire.

With the invention of the automobile in the late 19<sup>th</sup> century, the rubber boom began. Early automobiles were not very comfortable to ride in. Seats were hard and the rigid wheels made every bump in the road feel like a small mountain to the driver and passengers. Had it not been for the invention of the rubber tyre, the automobile could have remained an interesting novelty.

John Boyd Dunlop invented the pneumatic rubber tyre in 1888.<sup>6</sup> The first tyres consisted of a rubber tube sheet covered with fabric. The first person to consider air filled tyres for cars was a man named André Michelin. Due to many flat tyres with his type of tyre, this tyre was declared a failure. The next 16 years cars travelled on hard metal or wooden tyres. In 1911, the Hardman company was the first to produce a combination of a tyre and tube. An air filled inner tube was surrounded by a hardened rubber tube, which was reinforced with fabric. The automotive rubber tyre had finally been born. In the following years, many improvements and developments have been made on tyres.<sup>6</sup> The latest major development in the tyre industry focused on reduction of fuel consumption of cars. Tyre producers have therefore been concentrating on the development of tyres with low rolling resistance.<sup>7</sup>

Rolling resistance contributes between 18 and 30% of the resistance to the forward motion of a passenger car.<sup>8, 9</sup> The rolling resistance accounts for between the 14-18% of the fuel consumption.<sup>7</sup> This means, that a 30% reduction in rolling resistance results in approximately 4.5% reduction of fuel consumption.<sup>10</sup> This may go as high as around 6%.

Hysteresis within the tyre cords and rubber is the largest contributor to rolling loss and is responsible for 85 to 95% of the total loss.<sup>10, 11</sup> Consequently, modification of the viscoelastic behaviour of tyre materials is an effective way to decrease rolling resistance.<sup>9</sup> Losses due to slipping of the tread on the road surface contributes 5-10% of the total, and friction of the tyre accounts for 0-5% of the total loss.<sup>10, 11</sup>

The major part of the energy losses in a passenger car tyre occurs in the tyre tread:  $\pm$  50%. The sidewall accounts for 10-25% of the rolling resistance of a tyre and the bead region for 10 to 20%. Hence, it is quite evident why the attention of tyre producers has first been drawn to reducing the hysteresis losses, which occur in the tread compound.<sup>12</sup>

A major problem facing tyre designers has traditionally been the compromise between low rolling resistance, high wet grip and high wear resistance. Lowering the rolling resistance commonly results in a reduction in wet grip performance and vice versa. A major step in solving this problem can be achieved by the replacement of carbon black by silica as the filler in the tyre tread compound. This has enabled tyre producers to produce tyres, which provide improved wet grip properties, better winter performance and lower rolling resistance.<sup>13</sup> It has been found that the use of highly dispersible precipitated silica in combination with a coupling agent allows the tyre manufacturers to produce a tyre tread that decreases the tyre rolling resistance by approximately 20%. This corresponds with a decrease of 3-4% in fuel consumption of the car.<sup>14</sup>

Although a lot of research has already been done in the past on this subject,<sup>15-20</sup> it is generally felt that improvements of this technology can still be made by a further study of the mechanism of silica adhesion, or compatibilisation with the rubber matrix by coupling agents.

## 1.2 Aim of this thesis

The aim of the investigations presented in this thesis is to gain a better insight in mixing of silica and rubber in the presence of a coupling agent. A better understanding of the reaction that is taking place between the coupling agent and the silica or the rubber matrix can help to improve the reinforcing performance of silica in rubbers.

During mixing of silica reinforced rubber, processing problems arise such as pre-vulcanisation, which need to be prevented. This can be achieved when more understanding is available about the reaction mechanisms, that are taking place between the coupling agent and the silica or the rubber matrix. Also the effects of the coupling agent on the compound morphology and, consequently, the material properties are of importance.

In the next paragraph the concept of the thesis is described. Different approaches are used to study the effect of the coupling agent on the material properties, ultimately leading to a better understanding of the mechanisms that are involved in the silica reinforced tyre technology.

### 1.3 Concept of this thesis

The research described in this thesis comprises the effect of processing parameters during mixing, several coupling agents and the morphology on the dynamic mechanical properties of silica filled tyre rubbers. The thesis is divided into 9 chapters as outlined:

*Chapter 2* serves as an introduction to topics, that are relevant for the work described in this thesis. The effect of fillers on the dynamic mechanical properties of elastomers is discussed in relation to their role in tyre performance. The processes of dispersion of fillers during mixing are briefly reviewed. Special attention is given to the mixing of silica, regarding the reactions that are taking place in the presence of a silane coupling agent.

*Chapter 3* deals with the influence of the dump temperature and mixing time, applied during mixing, on the material properties of a typical silica reinforced tyre tread. Compounds are mixed at different mixer rotor speeds and fill factors to achieve different dump temperatures. These parameters influence the reaction of the coupling agent bis-(triethoxysilylpropyl)tetrasulphide (TESPT) with the silica surface and the reaction with the rubber matrix.

In *Chapter 4*, the effects of zinc oxide on the reaction of TESPT with the silica surface and also with the rubber matrix are described. The study was performed in-rubber and also by model studies with the aid of High Performance Liquid Chromatography (HPLC) and X-ray Photoelectron Spectroscopy (XPS).

*Chapter 5* focuses on the effect of the different reactive groups of the coupling agent. Several coupling agents are synthesised with different functional groups. The coupling agents are all equivalents of TESPT. Their synthesis routes as well as their effects on the material properties are described.

*Chapter 6* deals with model vulcanisation, which is a vital tool to study the reactivity of the sulphur group of TESPT. In the first part, the reaction of elemental sulphur with different model compounds is described. The different model compounds represent the different butadiene monomer configurations, that can be present in the polymers. The second part describes the reaction between TESPT and a model compound, which is subsequently compared with the elemental sulphur reaction.

*Chapter 7* focuses on the morphology of typical tyre tread compounds mixed with silica and TESPT. The influence of the dump temperature, as shown in Chapter 3, is visualised in this chapter. Different types of common till highly dispersible silica are tested. Macrodispersion and microdispersion are measured with the aid of, respectively, reflective light microscopy and Atomic Force Microscopy (AFM) and are related to the dynamic mechanical properties of the different compounds.

*Chapter 8* discusses soft interstices, which are visible in AFM images. This chapter focuses more on the type of polymer, linear or branched, used during mixing and the occurrence of soft interstices in the AFM phase images.

In *Chapter 9*, all information gained about the silica reinforced tyre tread compounds is used to develop an engine mount recipe based on Ethylene-Propylene-Diene rubber (EPDM). A comparison is made between NR- and EPDM-reinforced recipes with silica vs. carbon black.

## 1.4 References

1. J.A. Brydson, "Rubbery Materials and their Compounds", Elsevier Science Publishers Ltd., Essex (1988).
2. *Natuurrubber*, **20**, (2000), 4.
3. W. Hofmann, "Rubber Technology Handbook", Hanser Publishers, Munich (1996).
4. H.F. Mark, *Rubber Chem. Technol.*, **61**, (1988), G73.
5. C.M. Blow, C. Hepburn, "Rubber Technology and Manufacture", Butterworths, London, second ed., (1982).
6. Internet page, [www.vintagecars.about.com/library/weekly/aa082298.htm](http://www.vintagecars.about.com/library/weekly/aa082298.htm).
7. K.A. Grosch, *Rubber Chem. Technol.*, **69**, (1996), 495.
8. D.L. Illman, *Chem. Eng. News*, (1994), 8.
9. B.A. Hueda, *Rub. Plast. news*, (1992), 27.
10. A. Trono, Tyretech 92, Paris, France, October 27-28, 1992.
11. J.D. Walter, F.S. Conant, *Tyre Sci. Technol.*, **2**, (1974), 235.
12. Y. Bomal, S. Touzet, R. Barruel, Ph. Cochet, B. Dejean, *Kautsch. Gummi Kunstst.*, **50**, (1997), 434.
13. B. Freund, F. Forster, R. Lotz, presented at a meeting of ACS, Rubber Division, Cleveland, Ohio, US, 17-20 October, 1995.
14. R. Rauline (to the Compagnie Generale des Etablissements Michelin - Michelin & Cie), *Eur. Pat.* 0 501227A1 (February 12, 1992).
15. S. Wolff, *Tire Sci. Technol.*, **15**, (1987), 276.
16. S. Wolff, U. Görl, M.J. Wang, W. Wolff, *Eur. Rubber J.*, **1**, (1994), 16.
17. A. Hunsche, U. Görl, A. Muller, M. Knaack, Th. Gobel, *Kautsch. Gummi Kunstst.*, **50**, (1997), 881.
18. U. Görl, A. Parkhouse, *Kautsch. Gummi Kunstst.*, **52**, (1999), 493.
19. U. Görl, J. Munzenberg, H.D. Luginsland, A. Muller, *Kautsch. Gummi Kunstst.*, **52**, (1999), 588.
20. H.D. Luginsland, *Kautsch. Gummi Kunstst.*, **53**, (2000), 10.

---

## **Chapter 2**

### ***Mechanisms of filler reinforcement and the effect of mixing conditions on the material properties of silica reinforced tyre tread compounds***

---

This chapter provides an introduction to topics that are relevant for the work described in this thesis. The effect of fillers on the dynamic mechanical properties of elastomers is discussed in relation to their role in tyre performance. Special attention is given to the mixing of silica, regarding the reactions that are taking place in the presence of a silane coupling agent. The processes of dispersion of fillers during mixing are also briefly reviewed.

#### **2.1 Introduction**

Natural and synthetic rubbers, also called elastomers are rarely applied in their pure form. They are “too weak” to fulfil practical requirements because of lack of hardness, strength properties and wear resistance. Fillers are used in order to improve the properties of rubber compounds. Rubber articles derive many of their mechanical properties from the admixture of these reinforcing fillers at quantities of 30% up to as much as 300% relative to the rubber part. Carbon black is used as the most versatile reinforcing filler for rubber, complemented by silicas in the early nineteen forties. In tyre manufacturing, silicas are more and more used nowadays, mainly to decrease the rolling resistance of the tyres.<sup>1</sup> The increased attitude of protecting the environment, gives rise to a demand for tyres combining a long service life with driving safety and low fuel consumption, achieved by this lower rolling resistance. However, the change from carbon black to silica is not at all obvious because of technical problems involved: in particular the mixing between silica and rubber, two components of opposite polarities. Therefore, coupling agents are applied in order to bridge this polarity difference. The elucidation of the action in the reinforcement process, and the development and production of bifunctional organosilanes as coupling agents, finally paved the way for silicas to enter this area of application.<sup>2, 3</sup>

#### **2.2 Tyre performance versus dynamic mechanical properties**

A tyre has to fulfil many qualifications. Out of all these qualifications, three main performance criteria stand out: traction, wear resistance and rolling resistance. A tyre must deliver high traction and cornering forces on wet and dry roads, also called wet and dry grip. The steering characteristics under all handling situations should be predictable. This high

traction force between tread and road is necessary to create a good grip on the road surface, thereby avoiding slippage. Traction depends on three main type features: the tyre construction; the tyre tread compound and tread profile design; the road conditions.

A tyre must also show low wear and good durability and give a satisfactory driving comfort: the resistance to abrasion should be as high as possible to create a high mileage.<sup>4, 5</sup> With regard to environment and driving costs, the rolling resistance should be as low as possible, leading to low fuel consumption.

These three most important properties: rolling resistance, treadwear and wet grip form the so-called: “magic triangle” of properties, which means that a balance must be found between these properties. These requirements are conflicting, as it is impossible to improve all three characteristics at the same time. For a low rolling resistance, the rubber must have a low hysteresis; the material must be very elastic. For wet grip, it is important that the material has a high hysteresis, the material must not be elastic. In this way, there will be a good contact with the road. A compromise between these characteristics should always be achieved.<sup>3, 4, 6-8</sup>

Tyre rolling resistance is defined as the energy consumed per unit distance of travel as a tyre rolls under load. The energy consumed by the tyre is converted into heat. The proper unit of rolling resistance is [J/m], which equals [N], the unit of force. It should be kept in mind though, that there is a distinct qualitative difference between the two units. Rolling resistance is a energy per unit length and, hence, a scalar – not a vector as the unit [N] would imply.<sup>3</sup>

To get insight in the viscoelastic theory which is necessary to make a relation between tyre performance and dynamic mechanical properties, basic definitions need to be explained. Rubber is a viscoelastic material: as it deforms, a fraction of the energy is stored elastically, and the remainder is dissipated as heat in a hysteric manner. These hysteric losses within a tyre, as well as aerodynamic drag and friction in the contact path and within the rim, are irrecoverable losses and contribute to the total drag force on a moving vehicle.<sup>9</sup>

When a linear viscoelastic material is subjected to a sinusoidal shear deformation  $\gamma$  of angular frequency  $\omega$ :

$$\gamma(t) = \gamma_0 \sin(\omega t) \quad (2.1)$$

where  $\gamma_0$  is maximum strain and  $t$  is time; the shear stress response  $\sigma$  is also sinusoidal, but out of phase with the strain:

$$\sigma(t) = \sigma_0 \sin(\omega t + \delta) \quad (2.2)$$

where  $\sigma_0$  is maximum stress. The strain lags behind the stress by a phase angle  $\delta$ . A vector method of representing the dependence of  $\gamma$  and  $\sigma$  on  $\omega t$  is shown in Figure 2.1. Equation 2.5 can be rewritten as follows:

$$\sigma(t) = (\sigma_0 \cos \delta) \sin \omega t + (\sigma_0 \sin \delta) \cos \omega t \quad (2.3)$$

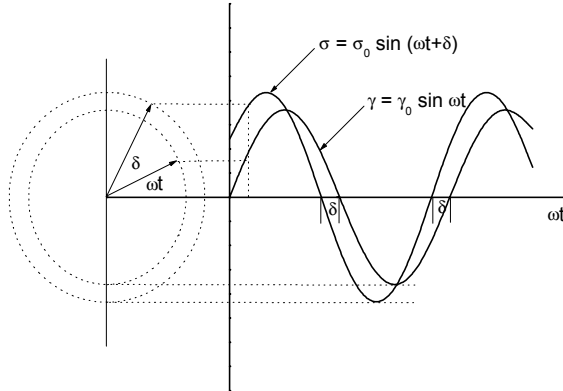


**Figure 2.1** A plot of the phase angle  $\delta$ .

The shear stress consists of two components: one in phase with the strain ( $\sigma_0 \cos \delta$ ); the other  $90^\circ$  out of phase ( $\sigma_0 \sin \delta$ ). Therefore, the relationship between stress and strain can be redefined by writing:

$$\sigma(t) = \gamma_0 [G' \sin \omega t + G'' \cos \omega t] \quad (2.4)$$

in which

$$G' = \frac{\sigma_0}{\gamma_0} \cos \delta \quad (2.5)$$

and

$$G'' = \frac{\sigma_0}{\gamma_0} \sin \delta \quad (2.6)$$

Thus the component of the stress  $G' \gamma_0$  is in phase with the oscillatory strain; the component  $G'' \gamma_0$  is  $90^\circ$  out of phase. A complex representation of the shear modulus ( $G^*$ ) can be written as follows:

$$G^* = G' + iG'' \quad (2.7)$$

$$\text{or } G^{*2} = G'^2 + G''^2$$

$G'$  is called the real part of the shear modulus or storage modulus, and  $G''$  the imaginary part or loss modulus. The tangent of the phase angle, also called loss tangent is:

$$\tan \delta = \frac{G''}{G'} \quad (2.8)$$

$G'$  and  $G''$  are frequency and temperature dependent. A typical frequency-dependence of the dynamic moduli for a viscoelastic material like rubber is shown in Figure 2.2. The course of the plot can be explained by segmental and chain movements in the rubber polymer. At low frequencies of deformation, all changes of the molecular conformation are possible within one cycle of deformation. There is almost no loss of energy. This is generally designed as the terminal zone. The next zone that can be distinguished in Figure 2.2 is the rubber plateau. Within one cycle of deformation entanglements cannot straighten out and act as “artificial” time dependent crosslinks.  $G'$  reaches a plateau, which can be related to the entanglement density. All other movements are still possible and elastic behaviour takes place at these frequencies. Here, there is a minimum in  $G''$ . After the rubber plateau, at even higher frequencies, there is another transition zone, called glass transition, where both  $G'$  and  $G''$  are increasing. Chain segments between the entanglements are not able to follow the applied deformation anymore. This causes another phase shift. Finally, the glassy zone is reached. The frequency is so high that only small local chain movements can occur. The value of  $G'$  equals the glass modulus, while  $G''$  decreases slightly. In every transition zone energy is dissipated which causes a peak in  $G''$ .<sup>10</sup>

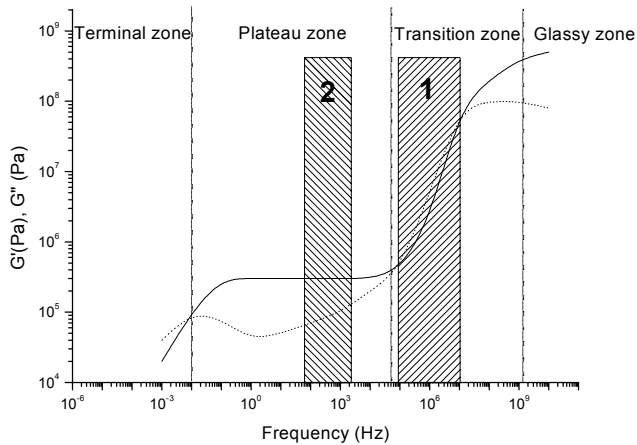


**Figure 2.2** Storage- and loss-modulus versus frequency for a typical non-vulcanised viscoelastic material; (—),  $G'$ ; (·····),  $G''$ ; region 1 is related to wet skid, region 2 is related to rolling resistance.

The rolling resistance, is predominantly related to the loss tangent of the bulk polymer at comparatively low frequencies in the plateau region of the storage modulus: region 2 in Figure 2.2. This low frequency region is in the order of the angular velocity of the rolling tyre. According to the time-temperature equivalence principle, the measurement of the coefficient of wet skid resistance corresponds to a measurement of  $\tan \delta$  in the glass transition region.<sup>11</sup> The wet skid resistance, region 1 in Figure 2.2, is linked with dynamic losses in the glass-rubber transition zone of the bulk polymer, typically in the range of 1 kHz to 1 MHz. The glass transition temperature,  $T_g$  influences the location of the skid process within the transition zone. Therefore, this quantity is often used as a physical criterion in materials development: the higher the  $T_g$ , the higher the wet skid resistance.<sup>12</sup>

A related description of the visco-elastic behaviour of rubber is given by the curve of  $\tan \delta$  against temperature. Nordsiek related the  $\tan \delta$  curve to a number of important functions of a tyre tread rubber without filler: Figure 2.3.

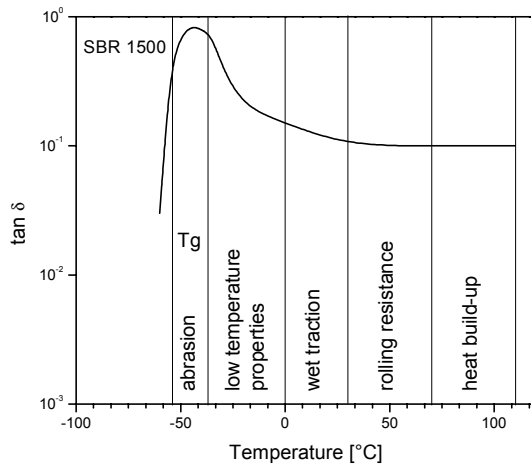


**Figure 2.3**  $\tan \delta$  versus temperature for a typical vulcanised tyre tread rubber compound.

In the low temperature range, the glassy state indicates the limit of elastic behaviour and permits a prediction of rubber suitability for winter use. It was found that the abrasion resistance shows a relationship to the glass transition temperature. Above  $0^{\circ}\text{C}$  in a temperature range till approximately  $+30^{\circ}\text{C}$ , related to prevailing road temperatures, the value of  $\tan \delta$  may be taken as an indication of skid behaviour or traction, particularly on wet roads. The latter is determined by maximum damping. The range between  $+30$  and approx.  $+70^{\circ}\text{C}$  comprises the running temperatures of a tyre. Under these temperatures condition the  $\tan \delta$  essentially determines the degree of rolling resistance. At temperatures exceeding this limit the tyre enters into a region of maximum stress and reaches the limit of safe operation with the risk of destruction. The  $\tan \delta$  values in this range indicate the heat-build-up behaviour and allow an estimate of incipient thermal decomposition and the limit of good tyre performance.<sup>13</sup>

Since the peak in  $\tan \delta$  correlates with the glass transition temperature  $T_g$  of the polymer, this value became a tool for the selection of a suitable tyre rubber. The dependence of  $\tan \delta$  on temperature was studied for several rubber polymers by Nordsiek. The choice of the rubber polymer with the optimum glass transition temperature  $T_g$  plays a key role in achieving a compromise between many tyre requirements.<sup>3, 13, 14</sup>

### 2.3 Types of fillers

Fillers are commonly added to rubber to improve material properties: Figure 2.4. They can be classified as inactive, semi-active and active, although the difference between the various classes cannot be rigidly defined. The designation normally relates to the influence of the filler in the rubber compound on viscosity and mechanical properties such as

tensile strength, abrasion and tear resistance. It is generally assumed that the degree of activity depends on interaction forces between the polymer and the filler.

Generally, active fillers like carbon black and precipitated silica have more influence on the properties of a compound than inactive types like clay, calcium carbonate etc., generally of mineral origin. In many cases, optimum properties as brought about by active fillers, show a minimum or a maximum relative to filler level, whereas in the case of inactive fillers, a change in properties develops in direct proportion to the filler amount.<sup>15</sup> For that reason active fillers are also commonly designated by “reinforcing” fillers.

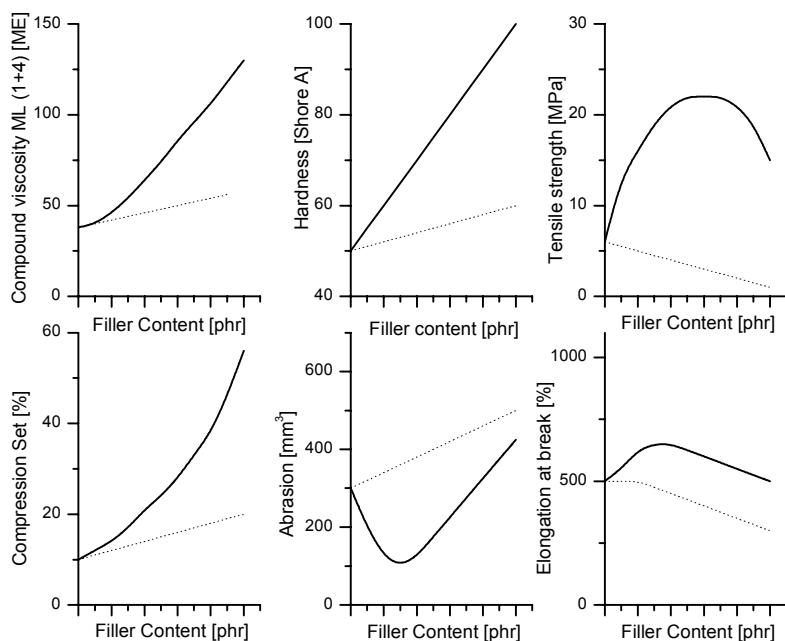


**Figure 2.4** Effect of filler level/type on vulcanisate properties; (.....), inactive; (—), active.

## 2.4 Mechanisms of filler reinforcement

Studies on reinforcement have generally demonstrated, that the surface interaction between fillers and rubber molecules or network segments involves a range of bond energies from relatively weak to very strong. In all cases, physical adsorption undoubtedly occurs to varying degrees depending on the particular surface and molecular segments. In the case of carbon black the level of physical interaction is high.<sup>16</sup> Although chemical reaction between carbon black and rubber is taking place, it occurs only to a minor extent and is not necessary for reinforcement.

When a rubber is filled with reinforcing fillers, above a critical filler concentration filler-filler interaction takes effect. It is determined both by the physical or chemical surface interaction and the distance between filler aggregates in the rubber compound. It can be measured in the range of small deformations. Figure 2.5 gives a schematic representation of

the elastic modulus as a function of the dynamic strain for rubber compounds containing carbon black or silica. According to Payne the enhancement of mechanical properties due to presence of a filler in rubber compounds can be clarified by the “additive effect” as summarised in Figure 2.5. This being the result of the addition to the elastomer’s own mechanical properties in the vulcanised state – the polymer network – of, first an hydrodynamic effect and then the influence of different kinds of interactions: polymer to filler surface i.e. “in-rubber structure” and filler to filler surface interactions.<sup>17, 18</sup>

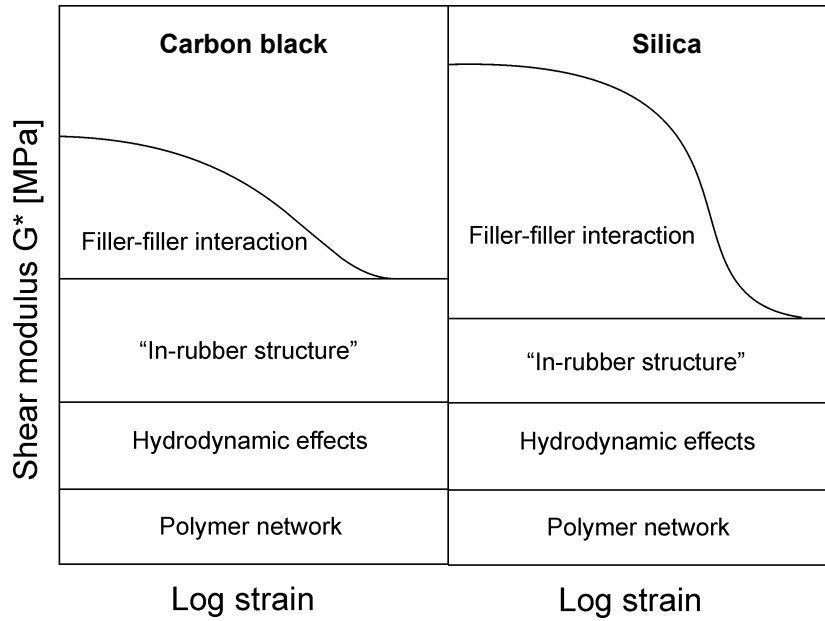


Figure 2.5 Payne effect for carbon black and silica.

The first “additive effect” is the strain independent polymer network, which is the result of the proportionality of the  $G_0$ -modulus to the crosslink density:

$$G_0 = \nu kT \quad (2.9)$$

where  $\nu$  is the number of moles of elastically effective network chains per unit volume, as a result of vulcanisation,  $k$  is the Boltzmann constant and  $T$  is the temperature (K).

When rigid spherical particles are dispersed into a fluid, whether it be a liquid or an elastomer, an increase in viscosity takes place in the case of the liquid or of the modulus in the case of a polymeric matrix. This is commonly designated as the hydrodynamic effect.<sup>19</sup> In 1906 Einstein<sup>20, 21</sup> calculated that, due to the hydrodynamic effect the viscosity of a liquid increases by the addition of uniform spheres according to eq. (2.10):

$$\eta = \eta_0 (1 + 2.5\phi) \quad (2.10)$$

where  $\eta$  and  $\eta_0$  are the viscosities of the filled and unfilled system,  $\phi$  is the volume fraction of the spheres.

There are several conditions for this equation to hold. First, wettability of the particle surface; second, uniform spherical particles and the last condition is, that there should be no interaction between the particles. The last two requirements are never met in real dispersions of fillers in an elastomer. Guth and Gold added a quadratic term to cover higher concentrations to account for the interaction between the spheres.<sup>22</sup>

$$\eta = \eta_0(1 + 2.5\phi + 14.1\phi^2) \quad (2.11)$$

Smallwood showed that for an elastic material filled with rigid spherical particles, the viscosities can be replaced by moduli to give:<sup>23</sup>

$$G = G_0(1 + 2.5\phi + 14.1\phi^2) \quad (2.12)$$

where  $G$  and  $G_0$  are the shear moduli of the filled and unfilled system respectively and  $\phi$  is the volume fraction of the filler. The value for  $G_0$  is obtained from equation 2.9. The shear modulus can also be replaced by the tension elasticity modulus without further change of the equation.

For nonspherical particles, Guth introduced a shape factor,  $f$  (the ratio of the longest dimension of the particle to the shortest), and proposed the following equation:<sup>24</sup>

$$G = G_0(1 + 0.67f\phi + 1.62f^2\phi^2) \quad (2.13)$$

The equations were derived on the assumption that the medium wets the filler particles, but does not chemically react with the filler surface. Brennan suggested that the polymer adsorbed on the filler aggregate surface (bound rubber) should be counted as part of the filler particle.<sup>25</sup> The modulus as given in eq. (2.12) and (2.13) is independent of applied strain.

The effect of the structure of the filler is attributed to the “in-rubber structure”, which can be understood as a combination of the structure of the filler in the in-rubber state and the extent of filler-polymer interaction. The in-rubber structure is amongst others a measure for the occluded rubber, which is shielded from deformation and therefore increases the effective filler content leading also to a strain independent contribution to the modulus. The filler-polymer interaction can be attributed to physical (Van der Waals) as well as to chemical linkages or a mixture of both. In the case of silica-coupling agent systems, this interaction is formed by chemical linkages.<sup>25-28</sup>

The elastic modulus of a filled rubber is experimentally strongly dependent on the deformation and decreases substantially at higher strains. This phenomenon is known as the Payne effect and is attributed to the presence and breakdown of the filler network during dynamic deformation. Payne interpreted the sigmoidal decline from a limiting zero-amplitude value of the storage modulus,  $G_0'$ , to a high-amplitude plateau  $G_\infty'$  as the result of breakage of physical (London and Van der Waals) bonds between filler particles. He also noted that the value  $G_0'$  is largely recoverable upon return to smaller amplitudes and showed that this phenomenon is independent of the polymer, provided enough time is allowed for recovery. It should be noted that when using silica the high level of the elastic modulus and the drop of

the elastic modulus at higher strain amplitudes proves the existence of a stable filler network formed by the silica.<sup>18, 28-31</sup>

A quantitative model of the Payne effect, based on filler agglomeration and deagglomeration, was first presented by Kraus<sup>32</sup> for carbon black agglomerates. He assumed that under a periodic sinusoidal strain  $\gamma$  at fixed frequency  $\omega$ :  $\gamma = \gamma_0 \sin(\omega t)$ , filler contacts are continuously broken and reformed. As the strain amplitude is increased, more and more contacts will be broken and this results in a rate of breakage,  $R_b$ , proportional to some power of the maximum amplitude  $\gamma_0$ . Also, the breakage rate will be proportional to the number of surviving contacts  $N$ :

$$R_b = k_b \gamma_0^m N \quad (2.14)$$

where  $k_b$  is the rate constant. The rate of reagglomeration or making of contacts,  $R_m$ , will be proportional to  $N_0 - N$  and is assumed to vary as  $\gamma_0^{-m}$ :

$$R_m = k_m \gamma_0^{-m} (N_0 - N) \quad (2.15)$$

where  $N_0$  is the number of elastically effective contacts at zero deformation.

From these two basic equations, Kraus derived equations describing the storage- and loss-modulus, resp. the  $\tan \delta$ , and applied those equations to experimental data of Payne and found a good correlation. The equation for the storage modulus is as follows:

$$\frac{G' - G'_\infty}{G'_0 - G'_\infty} = \frac{1}{1 + \left(\frac{\gamma_0}{\gamma_c}\right)^{2m}} \quad (2.16)$$

Where  $\gamma_c$  is a characteristic given by:

$$\gamma_c = \left(\frac{k_m}{k_b}\right)^{1/2m} \quad (2.17)$$

The equation for the loss modulus is:

$$\frac{G'' - G''_\infty}{G''_m - G''_\infty} = \frac{2 \left(\frac{\gamma_0}{\gamma_c}\right)^m}{1 + \left(\frac{\gamma_0}{\gamma_c}\right)^{2m}} \quad (2.18)$$

The loss tangent then becomes:

$$\tan \delta = \frac{G''_{\infty} \left[ \left( \frac{\gamma_0}{\gamma_c} \right)^{m/2} - \left( \frac{\gamma_0}{\gamma_c} \right)^{-m/2} \right]^2 + 2G''_m}{G'_{\infty} \left( \frac{\gamma_0}{\gamma_c} \right)^m + G'_0 \left( \frac{\gamma_0}{\gamma_c} \right)^{-m}} \quad (2.19)$$

Regarding the Payne effect several alternative models have been proposed.<sup>33-36</sup> An extension of the Kraus model was given by Klüppel et al.<sup>34</sup> by using percolation theory. As a result the equation for the storage modulus, eq. 2.16, contains then an elasticity exponent of percolation.

Another interesting model is postulated by Maier and Göritz: they suggested polymer chain adsorption on carbon black, similar to the model of Langmuir, concerning adsorption of gases to planar metal surfaces.<sup>37</sup> The network density in the neighbourhood of a filler particle increases due to adsorption of network chains to the filler particle. A distribution of differently strong links between filler particles and segments of elastomer chains exists. During the mixing process, the first macromolecules which come in contact to the filler see the whole free surface. After formation of the first link the neighbouring segments have a high probability to attach to the net interaction position and so on. This process is ultimately stopped when all neighbouring sites on the surface are occupied. These chains get a strong bond to the filler caused by the stabilisation in the neighbouring positions. Chains, which arrive at the filler surface at a later moment, find the area widely covered and their possibilities of stabilisation are reduced. The last chains attached to these sites have very weak links to the particle. The quantitative description of the storage modulus of a filled rubber sample is caused by entropy elasticity and depending on network density, the Boltzmann constant and the temperature. In the adsorption mechanism the network density is composed of three different parts: (a) the chemical network density; (b) the density of network chains attached by stable bonds to the filler surface; and (c) the density of unstable bonds between chains and filler. An increasing desorption of chains with increasing amplitude leads to a reduced network density. With increasing dynamic deformation these weakly bonded chains are torn off the filler surface and the density of unstable bonds between chains and filler decreases. By means of the theory of entropy elasticity it is then possible to describe the strain dependent modulus.

Freund and Niedermeier studied which mechanism, filler networking or polymer adsorption, prevails for carbon black and for silica.<sup>38</sup> Carbon black and silica were used to vary filler agglomeration and polymer adsorption strength in non-polar NR and polar NBR. Payne-type testing of all compounds, including a relaxation study, led to the conclusion that filler networking is the dominant Payne mechanism in the case of silicas, whereas polymer adsorption dominates in the case of carbon blacks.

Huber and Vilgis investigated how the reinforcement of elastomers by active fillers is influenced by the universal features of the disordered filler structure.<sup>39</sup> They concluded that at small deformations the energy-elastic contribution of the rigid filler network prevails, whereas at large deformations the hydrodynamic effect and the "in-rubber structure" dominates.

The measurement of the Payne effect of silica-reinforced rubber will play a crucial role in the further contents of this thesis. Irrespective of the model background of the effect,

it is clear that it is a very powerful detection method for filler-filler interactions vs. filler-polymer or filler-network interactions in rubber.

## 2.5 Use of silica instead of carbon black as reinforcing fillers in rubber

Carbon black is most commonly used as reinforcing filler. Application of carbon black results in an increase in strength properties, wear resistance and fatigue resistance. In addition, due to its colour it is an excellent absorber of light. It therefore absorbs most of the ultraviolet components of sunlight, which can otherwise initiate oxidative degradation of the rubber.

The effects of the presence of carbon black on the dynamic mechanical properties of various types of filled rubber has been studied by many others, e.g.<sup>40-43</sup> and was reviewed by Medalia.<sup>28</sup> The general conclusion from this early work was that the incorporation of carbon black in different types of rubber gives in most of the cases an increase in the storage and loss moduli,  $G'$  and  $G''$ , and an increase in hysteresis,  $\tan \delta$ . Increases in strain amplitude give decreases in storage modulus  $G'$ : the so-called Payne effect, as mentioned before.

Particularly since the introduction of the Energy<sup>®</sup> tyre by Michelin, silica has become more important as reinforcing filler for the rubber industry. The main reason is the greater reinforcing power of silica when compared to carbon black. The additional effect of temperature dependence of  $\tan \delta$  for reinforced rubber compounds is the result of the characteristics of reinforcing fillers to form a filler network. Comparing the  $\tan \delta$  values at different temperatures for silica and carbon black, a considerably lower  $\tan \delta$  value is found for silica at lower temperatures. In the rubbery state at temperatures beyond 20°C, the  $\tan \delta$  and hysteresis is still higher for carbon black: Figure 2.6.<sup>44-46</sup>

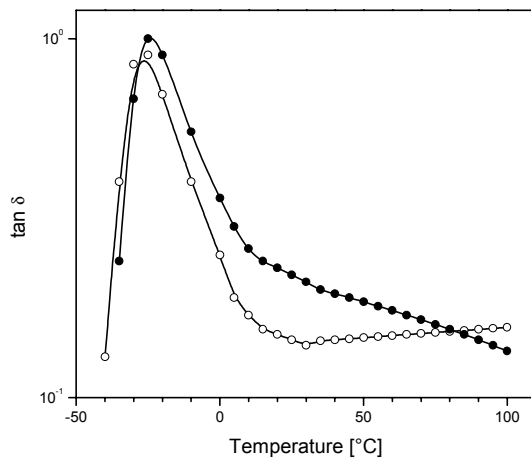


**Figure 2.6** Typical dependence of the temperature dependence of  $\tan \delta$  for a silica (○) and a carbon black (●) reinforced rubber compound.<sup>46</sup>

Replacement of carbon black by silica therefore results in a decrease of  $\tan \delta$  at higher temperatures, and thereby in a reduction of the rolling resistance. The use of silica, in addition leads to a comparable  $\tan \delta$  at lower temperatures, providing a comparable ice and wet grip of a tyre.<sup>1, 3</sup>

The higher hysteresis of carbon black at higher temperatures is mainly due to the energy dissipation during repeated destruction and reconstruction of the filler network due to the Payne effect. This leads to a rapid decrease of  $\tan \delta$  with increasing temperature primarily due to a reduction of filler-filler interaction as well as filler-polymer interaction. Conversely the hysteresis of the silica-filled rubber increases with increasing temperature, finally showing a crossover point with carbon black at about 90°C. Again, this may be anticipated from strongly and highly constructed filler clusters. As the temperature increases, weakening of the filler-filler interaction would result in an increase in the portion of filler network, which can be broken down and reformed during cyclic deformation at low strain amplitudes.<sup>46</sup>

In addition, compounding with silica enables tyre technicians to reduce the filler content, because of the greater reinforcing power of silica. A decrease in filler content corresponds to a higher amount of elastic rubber in proportion to the damping filler phase in the compound and is an effective way to reduce rolling resistance.<sup>3</sup>

In general the use of silica instead of carbon black as a filler in rubber provides, besides the improved rolling resistance, a series of beneficial properties including:<sup>44, 47-49</sup>

- tear, flex, abrasion and heat resistance
- hardness, stiffness and modulus
- adhesion to adjoining compounds during tyre building: tack
- low heat-build-up
- high resilience
- neutral colour

Wagner has reviewed the specific characteristics of silica.<sup>50</sup> He indicated that some important silica properties such as silanol content, adsorbed water, structure and surface area affect the viscosity, cure rate, modulus and abrasion resistance. In general, silica consists of silicon and oxygen tetrahedrally bound into an imperfect three-dimensional crystal structure. The imperfections within the lattice structure leave free silanol groups on the surface.

It is generally agreed that on the smooth non-porous silica surface, that is fully hydroxylated, there are 4 till 5 Si-OH groups  $\text{nm}^{-2}$ , which remain even when the silica is dried at 120-150°C.<sup>51-53</sup> The amount of silanol groups has an influence on the dynamic stiffness  $G'$  at 60°C as shown by Blume.<sup>54</sup> The silanol groups fulfil two important functions. First, the formation of the filler network and second, the reaction with the coupling agent, see later.

Three types of silanol groups can be distinguished on the silica surface. The isolated, vicinal are silanol groups present on adjacent silicon atoms. The third type is the geminal silanol group, in this case two hydroxyl groups are present on the same silicon atom.<sup>55</sup>

The silicas used as rubber fillers possess a degree of hydration which is basically related to their method of manufacture. Fundamentally, the concentration of surface silanols determines the extent of hydration by water vapour. Actual adsorbed water varies with the ambient relative humidity. Adjacent silanol groups are more powerful adsorption sites for water than isolated silanols.<sup>56, 57</sup>

## 2.6 Reaction between coupling agent, silica and rubber phase

The interactions between the polar groups (siloxane, silanol) on the surface of silica aggregates with the non-polar groups (alkyl, olefin, aryl) of hydrocarbon elastomers are weak compared to the hydrogen-bonding interactions between surface silanol groups in silica itself. The dispersive forces between a nonpolar rubber molecule and silica are low. For this reason modification of the silica surface is necessary to improve the compatibility between hydrocarbon elastomers and precipitated silica. Bifunctional organosilanes provide chemical modifications of the silica surface to increase the interaction between the silica and hydrocarbon elastomers.<sup>47</sup> Remarkable improvement in mechanical properties of a silica-filled rubber vulcanisate are obtained with the use of a coupling agent. Improvement of the elastic modulus, tensile strength and elongation at break and a lower  $\tan \delta$  at 60°C, and hence a lower heat-build-up in a tyre.<sup>16, 58, 59</sup> A great many organosilanes were tested in the past.<sup>60-65</sup> The most widely used today is bis-(triethoxysilylpropyl)tetrasulphide (TESPT).<sup>66-68</sup> TESPT was originally developed as a curing agent.<sup>69</sup> When combined with accelerators such as tetramethylthiuramdisulphide (TMTD) and N-cyclohexyl-2-benzothiazolesulphenamide (CBS), TESPT causes silica-containing rubbers to crosslink, without the need for sulphur, and without the mixing problems encountered with silica.<sup>69</sup> The elimination of the mixing problems caused interest to focus on the use of TESPT as a curing agent at first. But as more experience was gained with this agent, its properties as a coupling agent began to attract attention too.<sup>2, 70-75</sup> In recent years, extensive research has been done into both aspects of this agent, e.g. by Luginsland.<sup>76-78</sup>

Since silica does not readily bond to polymers like carbon black does, the tyre tread formulations employ a silane coupling agent (organosilane) to provide the chemical bonding.<sup>79</sup> From a processing point of view, two chemical reactions have to be performed:

- 1) The reaction to bind organosilanes to the silica
- 2) The reaction to bind organosilanes to the polymer

Hunsche et al. studied the reaction of the coupling agent TESPT with silica.<sup>80-84</sup> They suggested that first a single bond with the silica surface was formed: primary reaction. Figure 2.7 presents the assumed course of the silica/TESPT primary reaction. The question whether the triethoxysilyl function reacts directly with the silanol groups on the silica or after hydrolysis (both reactions under formation of ethanol) followed by a condensation reaction, is answered in the literature <sup>85, 86</sup> with the single-step reaction. However, the fact that the silanisation reaction with a pre-dried filler leads to a noticeably lower yield in siloxane bonds suggests, that an initial hydrolysis is also important for the primary reaction.

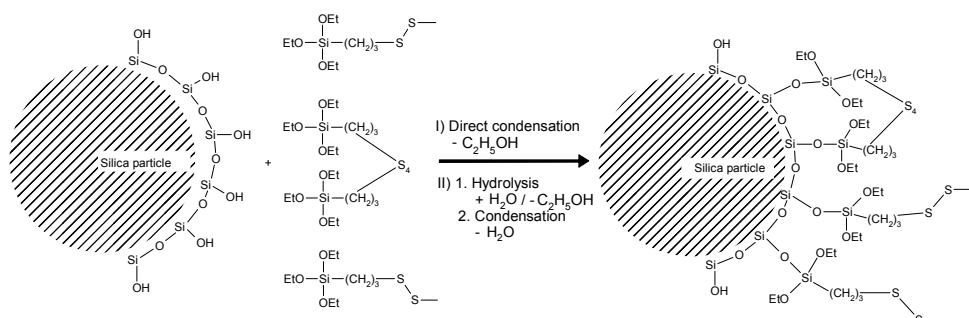


Figure 2.7 Primary reaction.<sup>80</sup>

This primary reaction may be followed, after a hydrolysis reaction, by condensation reactions between pairs of neighbouring silane molecules already bound to the silica surface: secondary reaction. This assumed reaction is presented in Figure 2.8. For mechanical reasons, the secondary reaction is always a two step process. First, the hydrolysis of one or two ethoxy groups and second, the condensation by elimination of water or ethanol. The water required for the intermediate hydrolysis step is adsorbed onto the silica surface as mentioned before.

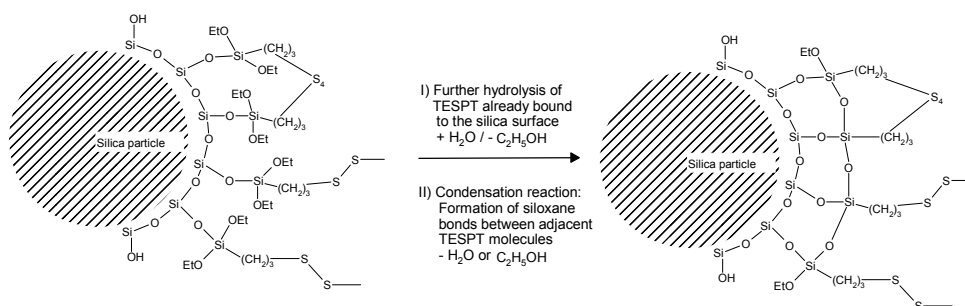


Figure 2.8 Secondary reaction.<sup>80</sup>

It can be seen from Figure 2.7, that during the primary reaction 1 mol of TESPT reacts under the formation of 2 mols of ethanol.<sup>81, 82, 87</sup> The reaction is following first order kinetics. Hunsche et al. determined the kinetic rate constants for the primary and the secondary reaction: Table 2.1. It is seen that the primary reaction is about 10 to 20 times faster than the secondary reaction. A value of 47 kJ/mol was found for the activation energy by Görl for the primary reaction.<sup>82</sup>

**Table 2.1** Kinetic rate constants for the primary reaction ( $k_a$ ) and the secondary reaction ( $k_b$ ) at different temperatures.

Temp. (°C)	120	140	160
$k_a$ (min <sup>-1</sup> )	0.061	0.122	0.229
$k_b$ (min <sup>-1</sup> )	0.0055	0.008	0.012

TESPT is subject to disproportionation. Dependent on the temperature and time that TESPT is exposed to, it disproportionates into a mixture of polysulphides with sulphur chain lengths varying from two to eight sulphur atoms.<sup>88</sup>

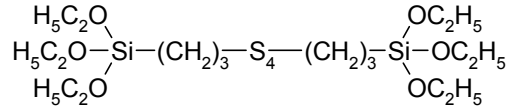


Figure 2.9 bis-(triethoxysilylpropyl)tetrasulphide (TESPT).

Whether this disproportionation reaction occurs during compounding or not has no bearing on the efficiency of TEPST during vulcanisation; the number of polysulphidic (active) sulphur atoms remains unaffected.<sup>88</sup>

Very little is known about the reactivity of the silane compounds toward rubber prior to vulcanisation. It is most likely that the labile tetrasulphidic linkage present in the TESPT undergoes cleavage at a temperature lower than the usual vulcanisation temperature of rubber and that the fragments thus obtained from the coupling agent become chemically linked to the rubber hydrocarbon.<sup>79, 89</sup> First sulphur radicals are formed by mechanical breakdown during mixing.<sup>16</sup> It is a combined process, because at the elevated temperature during mixing the sulphur bonds are more easily broken.<sup>90</sup>

Görl et al. studied the reaction of the coupling agent with the rubber matrix. From the results of a model compound study, the reaction was proposed to take place via an intermediate asymmetric polysulphide, a reaction product of the rubber polymer and the coupling agent. This intermediate product is formed by the reaction of the coupling agent, already linked to the silica surface, and a disulphide accelerator. In the subsequent reaction the polysulphide is substituted into the allylic position of the rubber with release of the accelerator part. A covalent bond between the rubber and the filler was assumed to be formed by this reaction, resulting in a chemical bridge between rubber and filler.<sup>83, 84, 91, 92</sup> A possible reaction of TESPT in a silica filled elastomer can be as follows:

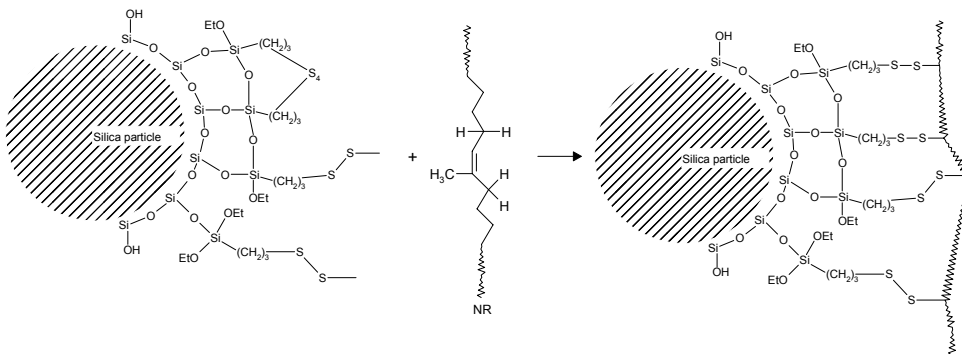
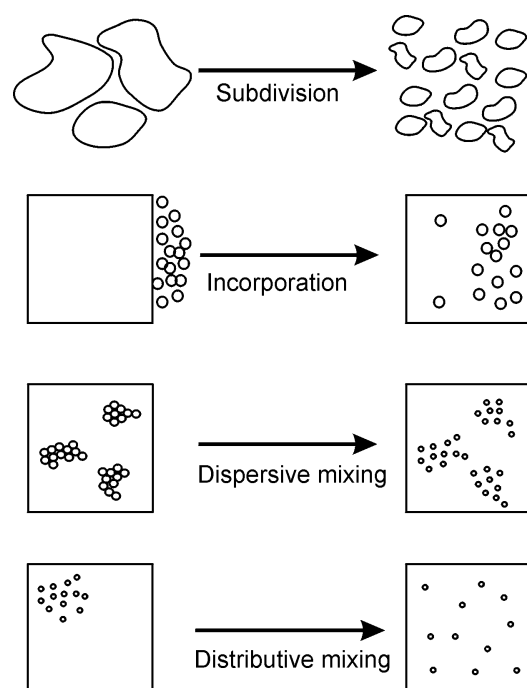


Figure 2.10 Possible reaction of TESPT and rubber.<sup>90</sup>

A disadvantage of the primary reaction of the coupling agent (see Figure 2.7) within internal mixers is, that it is relatively slow at moderate temperatures of for example 120°C commonly employed for rubber mixing. To achieve a shorter reaction time, higher batch temperatures have to be obtained within the first mixing step. At elevated temperatures, however, the reaction of coupling agent with rubber starts, so that scorch problems appear.<sup>93</sup> Another disadvantage is the very difficult mixing of the compound with poor flow properties at the low mixing temperatures required. Modern highly automated tyre production needs compounds which can be extruded, calendered and assembled in an easy manner. Homogeneity, good dispersion, low viscosity and good extrudability are all essential elements.<sup>45</sup> Processability is therefore of paramount importance.

## 2.7 Mixing

As mentioned in paragraph 2.6 mixing problems may occur when silica and silane are mixed in an internal mixer. Before discussing several mixing variables, the basic mixing process will be discussed. The mixing process of fillers into rubbers is in general difficult to describe, and lacks a good theoretical foundation and quantitative approach. In mixing a rubber batch, a number of elementary steps are involved, as shown in Figure 2.11.<sup>94</sup>



**Figure 2.11** Diagrammatic illustrations of the various steps in rubber mixing.

Active fillers are commonly specified by three characteristic sizes, as shown in Figure 2.12. The primary particle typically has cross-sectional dimensions of 5-100 nm. The size of the primary particles is commonly expressed in specific surface area/weight ( $\text{m}^2/\text{g}$ ). Aggregates of multiple primary particles are formed by chemical and physical-chemical

interactions: dimensions: about 100–500 nm. The aggregate can be quantified by the number of primary particles and their geometrical arrangement in the aggregate. The term “structure” is commonly used to describe this arrangement: low structure – linear arrangement; high structure – like grape bundles. The aggregates are further condensed into agglomerates by Van der Waals forces. Typical dimensions of agglomerates are in the order of magnitude of 1–40  $\mu\text{m}$ .<sup>95</sup> Agglomerates are disintegrated during rubber mixing, more or less to the size of aggregates or even primary particles.

Silica aggregates are comparable to those of carbon blacks, but have a higher structure. This structure accounts for a higher reinforcing power relative to carbon black. Because of its high specific component of surface energy, silica has a stronger tendency to agglomerate, is difficult to disperse in rubber and rapidly re-agglomerates after mixing.<sup>3, 53, 96</sup>

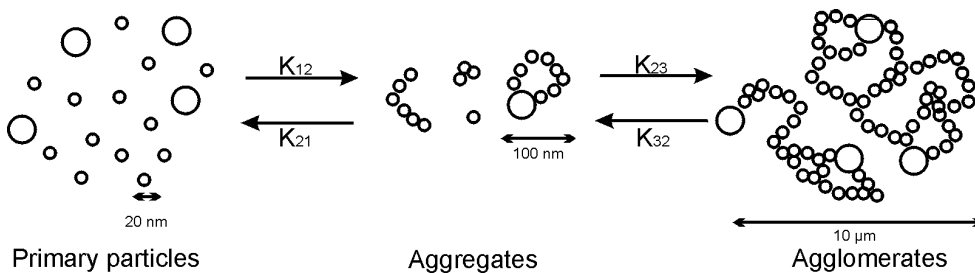


Figure 2.12 Filler aggregation model.<sup>96</sup>

1. The first elementary step of mixing is called the *Subdivision*, which is the breaking down of larger lumps of fillers to smaller ones, suitable for incorporation into the rubber.
2. *Incorporation* of powdered or liquid materials into the rubber to form a coherent mass. Without incorporation, the ingredients are tumbled around in the mixer with little energy being consumed and practically no mixing taking place. During this step the rubber penetrates into the void space of the agglomerates thereby replacing the trapped air.
3. *Dispersion* involves reduction of the size of agglomerates to their ultimate size, the aggregates; i.e. changing their physical state while at the same time distributing the particles formed. This phase is also called dispersive or intensive mixing.
4. “*Distributive*” mixing i.e., moving the particles from one point to another, without changing their physical shape in order to increase randomness or entropy - also called extensive mixing. Mixing in its restricted sense, also defined as “distributive mixing”, is the process whereby the randomness or entropy of a mixture is increased without affecting the physical state of the components.
5. *Viscosity reduction* by mechano-chemical breakdown of the polymer and transforming it to a more easily deformable and less elastic state.

Formation of the dispersion is the most difficult, and therefore the rate-determining step. Distributive mixing is determined mainly by the shear deformation by the mixer, while dispersion largely depends on the shear stress during the process. To obtain a good

dispersion it is often mentioned that a high shear stress is required. A high shear stress can for instance be obtained by a high viscosity of the mass, with the aid of high filler loadings, by using polymers of a high viscosity, low mixing temperatures and finally also by charging the oils at the end of the mixing cycle.<sup>94</sup> In the case of mixing silica with rubber it is more difficult to obtain a good dispersion. Further, low temperatures are not feasible because the primary reaction needs to take place in order to obtain good dispersion of the silica.

### 2.7.1 From agglomerates to aggregates

In general, the incorporation process comprises the wetting of the filler with rubber and displacement of entrapped air. Microscopic examination of the carbon black filled rubber compounds at the early stages of mixing shows that, as the carbon black becomes incorporated, it forms relatively large (10-100  $\mu\text{m}$ ) agglomerates. During the subsequent dispersive mixing stage, these agglomerates are broken down to a size less than 1  $\mu\text{m}$ : the aggregate level.

The effect of mixing time on the development of the physical properties of rubbers containing carbon black was studied by Boonstra and Medalia.<sup>26</sup> They concluded that during the incorporation stage, rubber penetrates into the interstices of the carbon black aggregates. Boonstra and Medalia suggested that the total filled volume should include not only the filler but also the rubber that is occluded within the agglomerates. During the dispersive stage of mixing, these agglomerates are broken down, the amount of occluded rubber decreases, and thus the filled volume decreases, leading to lower viscosity.<sup>27, 97-99</sup>

The plot of mixing torque versus mixing time shows normally an exponential drop, after the addition of the last ingredients, to some limiting value,  $P_\infty$ . Such data can be conveniently fitted by the following equation:<sup>97, 100</sup>

$$\ln \frac{(P_t - P_\infty)}{(P_0 - P_\infty)} = -kt \quad (2.20)$$

where  $P_0$ ,  $P_t$  and  $P_\infty$  represent torque values at the last (second) power peak, at time  $t$ , and the limiting torque after infinitely long mixing. The total change in torque ( $P_0 - P_\infty$ ) is considered proportional to the initial volume of occluded rubber at the second power peak, and ( $P_t - P_\infty$ ) is proportional to the volume of occluded rubber at time  $t$ . Thus, the constant  $k$  represents the rate at which the occluded rubber is dispersed, and thus is proportional to the rate at which carbon black is dispersed. Equation 2.20 is the integral form of an equation describing a process obeying first order kinetics.

Two mechanisms have been proposed for describing the dispersion of carbon black agglomerates:

- 1) The cleavage model, where the agglomerate cleaves into two.
- 2) The Onion peeling model, in which a group of aggregates are peeled off the larger agglomerate.<sup>101</sup>

According to Li et al.<sup>96</sup> there exists a dynamic equilibrium between filler aggregation and breakdown in filled compounds during the mixing process as well as during actual use, see

Figure 2.12. It is found that the mechanism for silica differs from that for carbon black. The rate constants for carbon black aggregation are far greater than for particle separation. However, for silica the differences are much smaller.<sup>96</sup> The sizes of silica aggregates and agglomerates are respectively about 30-40% and 40-50% smaller than those of carbon black. Further, the bound rubber molecules on the silica surface have more freedom of movement. As a result, hysteresis and heat-build-up of silica-filled vulcanisates are lower than the corresponding values for carbon black-filled vulcanisates.<sup>96</sup>

Changes in macrodispersion (>10 microns) and microdispersion (<10 microns) with increased mixing time have different relative effects on physical properties after vulcanisation of the compounds. The macrodispersion changes rapidly in the early stages of mixing. Microdispersion continues to change with longer mixing times, even though macrodispersion remains unchanged. The changes in physical properties, even at constant macrodispersion, highlights the importance of microdispersion, particularly for fatigue and strength properties.<sup>102</sup>

The determination of the quality of the dispersion is difficult. Most common is to use microscopy (optical or electron). However, it is often more preferred to measure physical properties, like tensile strength, tear strength or abrasion resistance.<sup>94</sup>

The final degree of dispersion depends largely upon the processing conditions. All details of the mixing procedure are important in determining the final properties of the compounds, particularly if the rubber is natural rubber reinforced with precipitated silica. To obtain good tyre tread properties, the following parameters are important: the choice of the dump temperature, the sequence of adding ingredients and the necessary processing conditions. These parameters will be discussed in more detail in the following paragraphs.

### **2.7.2 The role of batch temperature during mixing**

The early stages of mixing are crucial to good operation. Poor temperature control of the rotors can lead to excessive slipping of the rubber bale during subdivision and incorporation, drastically reducing the effective mixing time in a mixing cycle. This causes poor mix quality and excessive batch to batch variability.<sup>102</sup>

As described before, silica possesses very strong filler-filler interaction. When no coupling agents are used, compounds show a dramatically high viscosity, see Chapter 3. The Mooney-viscosities at 100°C can reach values of >100 MU (Mooney Units). The handling of those silica-filled compounds is very difficult. When hydrophobing occurs, the surfaces of the silica particles are covered with the coupling agents and filler/filler interactions are dramatically reduced. Fully hydrophobed compounds show Mooney-values of 25-40 MU's at 100°C.<sup>93</sup>

The high viscosities, as described, generate high shear stresses and consequent excessive energy dissipation in the compound, which will lead to a substantial rise in compound temperature in the mixer. As mentioned before in paragraph 2.6, these high temperatures are not acceptable because of scorch problems.

These examples show that silica (tread) compounds need a good temperature controlled mixer, because different levels of hydrophobing will lead to very uneven properties in further processing.<sup>93</sup> In the case of a carbon black compound, the temperature problems can be controlled by adjusting the rotor speed. Although the mechanism for silica

is different than for carbon black, little is known about the actual silica mechanism and therefore the carbon black example will be explained.

Pohl<sup>93</sup> showed that the dispersion quality of a SBR/carbon black compound is a function of rotor speed and fill factor. According to the experiments of Pohl the impact of the speed is huge and stronger than other parameters (i.e. fill factor, time, etc.). Since at high rotor speed the increase in temperature of the compound cannot be stopped, the mixing process has to be interrupted when a critical temperature is reached. To obtain a high quality compound, a second or sometimes even a third mixing stage has to follow. When the rotor speed is reduced the mixer can be used as a cooling unit.

In the case of silica, the batch temperature depends mainly on the coupling agent reaction between the precipitated silica and the rubber. The reaction between the TESPT and the rubber starts only at 170°C. Up to 160°C, the incubation time for the crosslinking reaction of NR with TESPT is thought to assure safe processing.<sup>103</sup>

### 2.7.3 The ram position/pressure

Leblanc has demonstrated that the actual position of the ram, which is the pneumatic plunger of an internal mixer that closes the inlet and exerts force on the contents during mixing, is a key factor of the process. The time for the ram to reach its equilibrium position corresponds to the filler incorporation and dispersion phases of the process. It has been observed that the higher the fill factor, the longer this time, with clear differences due to the nature of the filler.<sup>104</sup>

Funt showed that when the ram pressure is increased, the dump temperature also increases.<sup>102</sup> This is quite logical because a higher ram pressure induces more friction and the latter leads to higher temperatures. Increasing ram pressure also reduces the void volume of the internal mixer. A certain amount of voids are required, however, for good distributive mixing.<sup>105, 106</sup>

### 2.7.4 The order of adding ingredients

The sequence of adding ingredients is also important when mixing rubber and silica. Chemicals that can react with either the alkoxysilyl or the polysulphidic group of a coupling agent like TESPT should not be present during the mixing step where the primary reaction of the coupling agent takes place. The resulting side reactions would consume TESPT to produce unwanted effects. Chemicals containing amino or to a lesser degree aromatic or OH-groups are also suspected of causing side reactions. Processing oils, plasticizers, antioxidants and stearic acid were without significant effect on coupling.<sup>103</sup>

The order of zinc oxide and silica addition to the mix has a profound effect on compound viscosity and modulus. When stearic acid is present and zinc oxide is added early in the mix, the compound viscosity is lower. It was stated, that TESPT is to be added together with the siliceous filler and zinc oxide / stearic acid.<sup>103</sup> That this is not quite correct is the subject of Chapter 4 of this thesis.

The possibility has been reported to calculate the amount of TESPT necessary to obtain products with low heat-build-up together with high tear resistance and good wear resistance.<sup>88</sup>

$$\text{phr}_{\text{coupling agent (TESPT)}} = 0.7 \cdot 10^{-3} \cdot S_{\text{BET}} \cdot \text{phr}_{\text{silica}} \quad (2.21)$$

where  $S_{\text{BET}}$  is the specific surface area measured according to the nitrogen adsorption method or BET (Brunauer, Emmet and Teller) method, phr is the quantity of silica in parts per hundred rubber.

Zinc oxide, an ingredient in most formulations, is a dense material that tends to compact and disperse with difficulty. For optimum dispersion it is most commonly added early in the mix.<sup>107</sup> The curing agents are added in the final mixing step where the temperature is low. The temperature must be low, otherwise premature curing in the mixer will occur.

### **2.7.5 Fill factor**

The fill factor of a mixer, that is the batch size relative to the empty volume of the mixer, can affect the mix quality in two ways. First, overfilling can reduce or eliminate void regions in the mixer, which are required for good distributive mixing, thus leading to greater inhomogeneity of the batch. Perhaps more importantly, the rate of temperature rise increases with increased batch size.<sup>102</sup>

Dizon showed that different types of carbon black need a different fill factor in the internal mixer.<sup>106</sup> This could also be important for silica. The optimum fill factor for silica is about 70%, however this strongly depends on the type of mixer (tangential or intermeshing). Normally a tangential mixer is filled till 70% whereas the intermeshing type is filled till 55%.

Wiedmann showed that the dispersion quality is also dependent on the fill factor, in addition to being dependent on rotor speed and temperature. At constant speed, the quality improves to an optimum and the temperature increases simultaneously with increasing fill factor as a result of a better sticking to the mixer wall. At still higher fill factors the quality decreases again as a result of overfilling, which makes part of the compound end up in the mixer shaft.<sup>105</sup>

### **2.7.6 Relation between the shear modulus and mixing time**

According to Payne<sup>17</sup> there is a relation between mixing time and the ratio of the loss modulus ( $G''$ ) and the storage modulus ( $G'$ ).  $\tan \delta (=G''/G')$  decreases with longer mixing times. A two-stage mixing process shows even lower phase angle values ( $\delta$ ) at high strains as compared to the single stage mixing results.

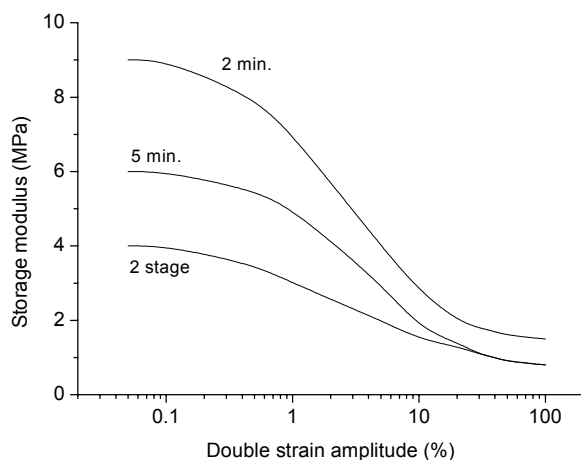


**Figure 2.13** Shear modulus versus strain amplitude and mix time.

Studies by Coran & Donnet<sup>108</sup> showed that  $\tan \delta$  depends on the dispersion of the filler. Generally, when the degree of dispersion improves, both  $G'$  and  $G''$  decrease. However, the storage modulus  $G'$  decreases more rapidly than does the loss modulus  $G''$ . Thus there is an increase in hysteresis as measured by  $\tan \delta$  with improvement in the quality of filler dispersion. The decrease in dynamic moduli with increase of the degree of filler dispersion, can be explained on the basis of a network of agglomerates which exists when the quality of dispersion is poor. As mentioned before in paragraph 2.4 a better dispersion lowers the filler-filler interaction and affects the dynamic properties.<sup>108</sup> The results of Coran & Donnet and Payne (Figure 2.13) are in agreement with the description of the mixing steps as shown in Figure 2.11. More mixing stages generally give a better dispersion.

## 2.8 Summary and experimental mixing approach in accordance with literature survey

Silica reinforcement of rubber is a very complicated technology, which is still very much in development. Literature and patent evidence are growing with a steady pace. As to the silica: the state of the art is, that with the exception of the availability of the easily dispersible silicas like Zeosil® 1165MP, there has not been much development lately. With respect to carbon black technology, the main activity seems to concentrate on the development of silica-coated carbon blacks, which perform like intermediates between carbon black and silica.

A coupling agent is an absolute prerequisite for a proper performance of a silica-reinforced rubber compound, for reasons of:

- ease of dispersion;
- shielding of acidic groups to prevent cure retardation;
- obtaining the right balance between  $\tan \delta$  0°C for optimal wet grip and  $\tan \delta$  60°C for rolling resistance.

Although silicas pre-treated with coupling agents are in principle available, it is standard technology in the rubber industry to add the coupling agent in situ during the mixing operation. A great variety of coupling agents has been and is being explored up till today with varying effectiveness. The most commonly used coupling agent is TESPT. Besides applying TESPT as coupling agent also improved mixing procedures are required when mixing silica and rubber. Literature and patent data suggest that improvements in the mixing process are possible.

Based on these conclusions, the research described in this thesis focuses on improvement of the mixing procedure with emphasis on:

- exploring the effect of mixing parameters such as temperature, time and order of adding ingredients on the dynamic and mechanical properties;
- effect of functional groups of TESPT and type of polymer on the dynamic and mechanical properties;
- morphology study of the dispersion of silica.

Based on literature a mixing procedure was formulated with three mixing stages, to achieve a good dispersion of the silica filler in the rubber matrix. Where a tangential mixer will be applied, the fill factor was set at 70% to achieve a good dispersion of the silica, according to paragraph 2.7.5. In the first mixing step all the ingredients were added, in order to have a good hydrophobation of the silica (paragraph 2.7.4); the second mixing step was done to achieve an even better dispersion of the silica, as mentioned in paragraph 2.7.6. During the final mixing step, the vulcanising agents were added on the two-roll mill at low temperatures to avoid premature vulcanisation.

## **2.9 References**

1. P. Cochet, L. Barriquand, Y. Bomal, S. Touzet, presented at a meeting of ACS, Rubber Division, Cleveland, Ohio, Oct. 17-20, 1995.
2. S. Wolff, Rubber Chem. Technol., **69**, (1996), 325.
3. J.W. ten Brinke, Thesis, University of Twente, (2002).
4. G. Kraus, "Reinforcement of Elastomers", Interscience, New York, (1965).
5. D.J. Schuring, Rubber Chem. Technol., **53**, (1980), 600.
6. I. Indian Rubber Institute, "Rubber Engineering", McGraw-Hill, New York (2000).
7. R. Engehausen, A. Rawlinson, J. Trimbach, Tire Technol. Int. Ann. Review, **2001**, (2001), 36.
8. W.M. Hess, W.K. Klamp, Rubber Chem. Technol., **56**, (1983), 390.
9. J.M. Caruthers, R.E., Cohen, A.I., Medalia, Rubber Chem. Technol., **49**, (1976), 1076.
10. D.E. Hall, J.C. Moreland, presented at a meeting of ACS, Rubber Division, Dallas, Texas, April 4-6, 2000.
11. Y.G. Yanovsky, G.E. Zaikov, "Rheological properties of filled polymers, in Encyclopedia of fluid mechanics volume 9 Polymer flow engineering", Gulf Publishing Company, Houston, (1990).
12. J.D. Ferry, "Viscoelastic Properties of Polymers", John Wiley & Sons, New York (1980).
13. G. Heinrich, Kautsch. Gummi Kunstst., **45**, (1992), 173.
14. K.H. Nordsiek, Kautsch. Gummi Kunstst., **38**, (1985), 178.

15. R. Panenka, *Tire Technol. Int. Ann. Review*, **2001**, (2001), 86.
16. E.M. Dannenberg, *Rubber Chem. Technol.*, **48**, (1975), 410.
17. A.R. Payne, *Rubber Chem. Technol.*, **39**, (1966), 365.
18. A.R. Payne, R.E. Whittaker, *Rubber Chem. Technol.*, **44**, (1971), 440.
19. J.-B. Donnet, *Rubber Chem. Technol.*, **71**, (1998), 323.
20. A. Einstein, *Ann. der Physik*, **19**, (1906), 289.
21. A. Einstein, *Ann. der Physik*, **34**, (1911), 591.
22. E. Guth, O. Gold, *Phys. Rev.*, **53**, (1938), 322.
23. H.M. Smallwood, *J. Appl. Phys.*, **15**, (1944), 758.
24. E. Guth, *J. Appl. Physics*, **16**, (1945), 20.
25. J.J. Brennan, T.E. Jermyn, *J. Appl. Polymer Sci.*, **9**, (1965), 2749.
26. B.B. Boonstra, A.I. Medalia, *Rubber Chem. Technol.*, **36**, (1963), 115.
27. A.I. Medalia, *Rubber Chem. Technol.*, **47**, (1974), 411.
28. A.I. Medalia, *Rubber Chem. Technol.*, **51**, (1978), 437.
29. S. Wolff, U. Görl, M.J. Wang, W. Wolff, *Eur. Rubber J.*, **1**, (1994), 16.
30. A.R. Payne, *J. Appl. Polymer Sci.*, **7**, (1963), 873.
31. A.I. Medalia, *Rubber Chem. Technol.*, **64**, (1991), 481.
32. G. Kraus, *J. Appl. Polymer Sci.*, **39**, (1984), 75.
33. G. Heinrich, M. Klüppel, "Recent advances in the theory of filler networking in elastomers", in *Advances in polymer science*, Springer-Verlag, Berlin, (2002).
34. M. Klüppel, R.H. Schuster, G. Heinrich, *Rubber Chem. Technol.*, **70**, (1997), 243.
35. H.G. Kilian, M. Strauss, W. Hamm, *Rubber Chem. Technol.*, **67**, (1994), 1.
36. G. Heinrich, *Gummi Asbest Kunstst.*, **50**, (1997), 687.
37. P.G. Maier, D. Göritz, *Kautsch. Gummi Kunstst.*, **49**, (1996), 18.
38. B. Freund, W. Niedermeier, *Kautsch. Gummi Kunstst.*, **51**, (1998), 444.
39. G. Huber, T.A., Vilgis, *Kautsch. Gummi Kunstst.*, **52**, (1999), 102.
40. H. Roelig, *Rubber Chem. Technol.*, **12**, (1939), 384.
41. W.S.J. Naunton, J.R.S. Waring, *Trans. Inst. Rubber Ind.*, **14**, (1939), 340.
42. S.D. Gehman, D.E. Woodford, R.B. Stambaugh, *Ind Eng. Chem*, **33**, (1941), 1032.
43. R.B. Stambaugh, *Ind. Eng. Chem.*, **34**, (1942), 1358.
44. C.J. Derham, R. Newell, M.P. Swift, *NR technology*, **19**, (1988), 1.
45. L. White, *Eur. Tyre report*, **9**, (1996), 46.
46. M.J. Wang, *Rubber Chem. Technol.*, **71**, (1998), 520.
47. W.H. Waddell, J.H. O'Haver, L.R. Evans, J.H. Harwell, *J. Appl. Polymer Sci.*, **55**, (1995), 1627.
48. K.P. Jones, P.M. Lewis, P. McL. Swift, I.R. Wallace, *Natural Rubber Sci. Technol.*, (1997), 283.
49. Y. Bomal, Ph. Cochet, B. Dejean, I. Gelling, R. Newell, *Kautsch. Gummi Kunstst.*, **51**, (1998), 259.
50. M.P. Wagner, *Rubber Chem. Technol.*, **49**, (1976), 703.
51. M. Zaborski, A. Vidal, G. Ligner, H. Balard, E. Papirer, A. Burneau, *Langmuir*, **5**, (1989), 447.
52. L.T. Zhuravlev, *Langmuir*, **3**, (1987), 316.
53. R.K. Iler, "The chemistry of silica", John Wiley & sons, New York (1979).
54. A. Blume, *Kautsch. Gummi Kunstst.*, **53**, (2000), 338.
55. J.H. Bachmann, J.W., Sellers, M.P., Wagner, R.F. Wolf, *Rubber Chem. Technol.*, **32**, (1959), 1286.
56. W.D. Bascom, *J. Phys. Chem.*, **76**, (1972), 3188.

57. K. Klier, J.H. Shen, A.C. Zettlemoyer, *J. Phys. Chem.*, **77**, (1973), 1458.
58. S. Wolff, U. Görl, (to Degussa Aktiengesellschaft), *Eur. Pat.* 0 519 188 B1 (26-03-1997).
59. R. Alex, N.M. Mathew, P.P. De, S.K. De, *Kautsch. Gummi Kunstst.*, **42**, (1989), 674.
60. M.P. Cohen, D.K. Parker, L.G. Wideman, (to Goodyear Tire & Rubber Company), *Eur. Pat.* 0 785 207 A1 (23-07-1997).
61. P.H. Sandstrom, R.J. Hopper, J.A. Kuczkowski, (to Goodyear Tire & Rubber Company), *Eur. Pat.* 0 723 991 A1 (31-07-1996).
62. J. Muse, P.H. Sandstrom, L.G. Wideman, (to Goodyear Tire & Rubber Company), *Eur. Pat.* 0 536 701 B1 (21-08-1996).
63. R.J. Zimmer, F. Visel, U.E. Frank, T.F.E. Materne, (to Goodyear Tire & Rubber Company), *Eur. Pat.* 0 794 188 A1 (10-09-1997).
64. G. Agostini, T.F.E. Materne, M. Junio, F. Visel, U.E. Frank, (to Goodyear Tire & Rubber Company), *Eur. Pat.* 0 794 187 A1 (10-09-1997).
65. T. Scholl, H.-J. Weidenhaupt, (to Bayer AG), *Eur. Pat.* 0 680 997 A1 (21-04-1995).
66. B.T. Poh, C.C. NG, *Eur. Polym. J.*, **34**, (1998), 975.
67. R.H. Hess, H.H. Hoekje, J.R. Creasy, F. Strain, (to PPG industries Inc.), *U.S. Pat.* 3,768,537 (30-10-1973).
68. P.E. Cassidy, B.J. Yager, *J. Macromol. Sci. - Revs. Polym. Technol.*, **1**, (1971), 1.
69. S. Wolff, *Kautsch. Gummi Kunstst.*, **30**, (1977), 516.
70. F. Thurn, S. Wolff, *Kautsch. Gummi Kunstst.*, **28**, (1975), 733.
71. S. Wolff, *Kautsch. Gummi Kunstst.*, **34**, (1981), 280.
72. S. Wolff, *Rubber Chem. Technol.*, **55**, (1982), 967.
73. S. Wolff, *Kautsch. Gummi Kunstst.*, **36**, (1983), 969.
74. S. Wolff, E.-H. Tan, J.-B. Donnet, *Kautsch. Gummi Kunstst.*, **47**, (1994), 485.
75. S. Wolff, M.J. Wang, *Kautsch. Gummi Kunstst.*, **47**, (1994), 17.
76. H.D. Luginsland, *Kautsch. Gummi Kunstst.*, **53**, (2000), 10.
77. H.D. Luginsland, R. Kafczyk, W. Lortz, (to Degussa-Huels), *Eur. Pat.* 0997489 A2 (03-05-2000).
78. H.D. Luginsland, A. Hasse, presented at a meeting of ACS, Rubber Division, Dallas, Texas, April 4-6 2000.
79. R.W. Cruse, M.H. Hofstetter, L.M. Panzer, R.J. Pickwell, *Rubber & Plastics News*, (1997), 14.
80. A. Hunsche, U. Görl, A. Muller, M. Knaack, Th. Gobel, *Kautsch. Gummi Kunstst.*, **50**, (1997), 881.
81. A. Hunsche, U. Görl, H.G. Koban, Th. Lehmann, *Kautsch. Gummi Kunstst.*, **51**, (1998), 525.
82. U. Görl, A. Hunsche, presented at a meeting of ACS, Rubber division, Louisville, Kentucky, October 8-11, 1996.
83. U. Görl, A. Parkhouse, *Kautsch. Gummi Kunstst.*, **52**, (1999), 493.
84. U. Görl, J. Munzenberg, H.D. Luginsland, A. Muller, *Kautsch. Gummi Kunstst.*, **52**, (1999), 588.
85. D.W. Sindorf, G.E. Maciel, *J. Phys. Chem.*, **86**, (1982), 5208.
86. D.W. Sindorf, G.E. Maciel, *J. Am. Chem. Soc.*, **105**, (1983), 3767.
87. A. Hunsche, U. Görl, H.G. Koban, Th. Lehmann, presented at a meeting of ACS, Rubber Division, Louisville, Kentucky, October 8-11, 1996.

88. S. Wolff, *Tire Sci. Technol.*, **15**, (1987), 276.
89. R.N. Datta, P.K. Das, S.K. Mandal, D.K. Basu, *Kautsch. Gummi Kunstst.*, **41**, (1988), 157.
90. P.K. Pal, S.K. De, *Rubber Chem. Technol.*, **56**, (1983), 737.
91. A. Hasse, O. Klockmann, A. Wehmeier, H.D. Luginsland, presented at a meeting of ACS, Rubber Division, Cleveland, Ohio, October 16-19, 2001.
92. H.D. Luginsland, J. Fröhlich, A. Wehmeier, Paper No. 3 presented at a meeting of Deutsche Kautschuk Gesellschaft, Fortbildungsseminar "Soft Matter Nano-Structuring and Reinforcement", Hannover, Germany, May 22, 2001.
93. J.W. Pohl, presented at a meeting of ACS, Rubber Division, Cleveland, Ohio, October 21-24, 1997.
94. H. Palmgren, *Rubber Chem. Technol.*, **48**, (1975), 462.
95. G. Wypych, "Handbook of Fillers", ChemTec Publishing, New York, 2nd.ed., (1999).
96. Y. Li, M.J. Wang, T. Zhang, F. Zhang, X. Fu, *Rubber Chem. Technol.*, **67**, (1994), 693.
97. A.Y. Coran J.-B. Donnet, *Kautsch. Gummi Kunstst.*, **47**, (1994), 354.
98. A.I. Medalia, *J. Colloid Interface Sci.*, **32**, (1970), 115.
99. K.E. Polmanteer, C.W. Lentz, *Rubber Chem. Technol.*, **48**, (1975), 795.
100. G.R. Cotten, *Rubber Chem. Technol.* **57**, (1984), 118.
101. S. Shiga, M. Furata, *Rubber Chem. Technol.*, **58**, (1985), 1.
102. M. Funt, *Rubber world*, (1986), 21.
103. Y. Bomal, P. Cochet, B. Dejean, J. Machurat, I. Gelling, *Rubber World*, **208**, (1993), 33.
104. J.L. Leblanc, *Caoutchoucs et Plastiques*, **696**, (1990), 211.
105. W.M. Wiedmann, H.M. Schmid, *Rubber Chem. Technol.*, **55**, (1982), 363.
106. E.S. Dizon, *Rubber Chem. Technol.*, **49**, (1976), 12.
107. R.F. Ohm, "Additives that affect mixing", Chapman&Hall, London, (1997).
108. A.Y. Coran, J.-B. Donnet, *Rubber Chem. Technol.*, **65**, (1992), 1016.

---

## Chapter 3

### *Effect of silane coupling agent, TESPT, on the performance of a silica rubber compound as influenced by processing conditions<sup>#</sup>*

---

The addition of TESPT as a coupling agent to silica-rubber compounds enhances the filler-matrix compatibility. Under certain mixing conditions the surface of the filler may be only partly activated, which may have an adverse effect on the properties in the final product. This coupling agent may also act as sulphur donor and thereby get involved in curing reactions. The dump temperature employed during mixing and the length of time, that the compound is exposed to that temperature, govern the reaction mechanisms of the coupling agent and determine whether the agent leads to the formation of a silica-rubber bond or acts as a curing agent. A temperature of at least 130°C is necessary to ensure that the reaction between the coupling agent and the silica proceeds, whereas the coupling agent starts to react with the rubber or to donate sulphur, resulting in scorch, at temperatures above 160°C. An increase in the 300% modulus and/or G' at 100% strain above 150°C is an indication of scorch caused by the sulphur donor capability of the coupling agent. Another important parameter is the mixing time. It has been observed that the coupling agent must be mixed with the silica for at least 10 minutes at 150°C to obtain a sufficient degree of coupling.

#### 3.1 Introduction

It has long been known that the performance of rubber compounds, e.g. their strength properties, wear resistance and tear strength, can be improved by loading the compounds with particulate fillers. Good dispersion of the fillers is necessary to achieve optimum reinforcement.<sup>1</sup> Silica offers several advantages over carbon black as reinforcing filler. In tyre treads, silica yields a higher wear resistance and better wet grip in combination with a lower rolling resistance than carbon black.<sup>2, 3</sup> When silica is mixed with the commonly used non-polar, olefinic hydrocarbon rubbers, there will be a greater occurrence of hydrogen-bond interactions between surface silanol groups in silica agglomerates, than of interactions between polar siloxane or silanol on the silica and the rubber. So mixing silica with rubber involves major problems.<sup>4</sup>

---

<sup>#</sup>Parts of the work described in this chapter were published in: L.A.E.M. Reuvekamp, J.W. ten Brinke, P.J. van Swaaij, J.W.M. Noordermeer, *Kautsch. Gummi Kunstst.*, **55**, (2002), 41 and: L.A.E.M. Reuvekamp, J.W. ten Brinke, P.J. van Swaaij, J.W.M. Noordermeer, *Rubber Chem. Technol.*, **75**, (2002), 187.

For this reason there is great interest in the possibility of enhancing the compatibility of hydrocarbon rubbers and precipitated silica by modifying the surface of the silica. Bifunctional organosilanes are commonly used to chemically modify silica surfaces in order to promote interactions with hydrocarbon rubbers.

The most widely used bifunctional organosilane for tyre applications is bis-(triethoxysilylpropyl)tetrasulphide (TESPT).<sup>5-7</sup> It has been studied extensively.<sup>8-15</sup> During mixing of silica and rubber in the presence of the coupling agent, several reactions can take place, as already mentioned in Chapter 2. The coupling reaction, also called the primary reaction of the coupling agent with the silica surface during mixing, involves the problem that it takes place at a relatively slow rate at moderate temperatures. The secondary reaction between adjacent coupling agent molecules takes place to an even lesser extent. Higher batch temperatures have to be used then to achieve shorter reaction times. At such elevated temperatures a third coupling reaction may occur, between the coupling agent and the rubber molecules, resulting in scorch of the compound.<sup>16</sup>

The present chapter is divided in two parts. The first part describes the effect of the presence or absence of TESPT coupling agent on the processing and material properties of silica filled tyre tread compounds, in order to demonstrate the elementary need for such compounds. The second part of this chapter covers in more detail the effect of processing conditions on the reaction mechanisms that are taking place, when applying TESPT as a coupling agent.

## 3.2 Experimental

*Compound recipe.* — All experiments were performed using a tyre tread composition as shown in Table 3.1, representing a silica filled recipe corresponding to the fuel-saving green-tyre technology.<sup>17</sup>

**Table 3.1** Tyre tread recipe.

Component	Source	Phr
S-SBR (Buna <sup>®</sup> VSL 5025-1 HM) <sup>a</sup>	Bayer AG	75
BR (Kosyn <sup>®</sup> KBR 01)	Korea Kumho Petrochemical Co. Ltd.	25
Silica (Zeosil <sup>®</sup> 1165 MP)	Rhodia Silices	80
Silane (Silquest <sup>®</sup> A-1289)	Osi Specialties Crompton Corporation	7
Aromatic oil (Enerflex <sup>®</sup> 75)	BP oil Europe	32.5
ZnO	Merck	2.5
Stearic acid	Merck	2.5
Sulphur	J.T. Baker	1.4
CBS (Santocure <sup>®</sup> )	Flexsys B.V.	1.7
DPG (Perkacit <sup>®</sup> )	Flexsys B.V.	2
Total		229.6

<sup>a</sup> vinyl content is 50%, styrene content is 25% and the oil content is 37.5 phr.

*Mixing.* — The compounds were mixed in three steps unless otherwise indicated. The first two steps were effected in a Brabender Plasticorder lab station internal mixer with a

mixing chamber of 390 ml. The mixing procedures employed in the first two steps are indicated in Table 3.2. The starting temperature was 50°C and the cooling water was kept at a constant temperature of 50°C. The dump temperature at the end of the first mixing step was chosen as the main variable in all the experiments. The dump temperature was varied by varying the rotor speed and the mixer's fill factor. The second mixing step was applied to homogenise the compound. After every mixing step the compound was sheeted out on a Schwabenthan 100 ml two-roll mill. The third mixing step was carried out on the same two-roll mill. The accelerators and sulphur were added during this step. The experiments aimed at assessing the effect of extended temperature exposure on a mill were performed using a Schwabenthan Polymix 80T 300 ml two-roll mill with a cooling/heating unit. A Shaw intermeshing 5 liter (5 l) mixer was used to examine the effect of mixer size on the material properties.

**Table 3.2** Mixing procedure.

Step 1:

Time, (min.sec.)	Action
0.00	Open ram; add rubbers
0.20	Close ram
1.20	Open ram; add ½ silica, ½ silane, ½ oil, ZnO and stearic acid
1.50	Close ram
2.50	Open ram; add ½ silica, ½ silane, ½ oil
3.30	Close ram
4.30	Open ram; sweep
4.45	Close ram
6.45	Dump

Step 2:

Time, (min.sec.)	Action
0.00	Load compound
5.00	Dump

*Curing.* — After addition of the curing agents, the compounds' curing properties were determined with the aid of an RPA 2000 dynamic mechanical rheological tester from Alpha Technologies. This is a torsional dynamic rheometer and the only available device, which offers the possibility to test very stiff materials under dynamic conditions.<sup>17</sup> The increase in torque at 160°C, 0.833 Hz and 2.79% strain was measured over a time period of 30 minutes. The optimal vulcanisation time ( $t_{90}$ ) and scorch time ( $t_{02}$ ) of the compounds were determined. The compounds were cured in a Wickert laboratory press WLP 1600/5\*4/3 at 160°C and 100 bar for 12 minutes, according to the  $t_{90}$  of the specific compounds. The cured specimens measured 90 \* 90 mm and were 2 mm thick.

*Characterisation.* — The Mooney viscosity ML(1+4) at 100°C was measured with the aid of a Mooney viscometer 2000E from Alpha Technologies.

Dynamic measurements of the uncured compounds were performed with the aid of the RPA 2000 from Alpha Technologies. The Payne effect is often used as the measure for filler dispersion. To study the filler-filler interactions of the uncured compounds, the storage

modulus was measured as a function of the strain. During the strain sweep measurements, the temperature and frequency were kept constant at 100°C and 0.5 Hz. The  $G'$  was measured in a strain range of 0.56% - 100.04%.

Frequency sweeps were performed with the RPA 2000 to measure the  $\tan \delta$  at 60°C as a measure for the rolling resistance. For this measurement an uncured sample was vulcanised for a time period corresponding to the optimum vulcanisation time. After optimum vulcanisation the sample was cooled down to 60°C and  $\tan \delta$  measured at different frequencies. The  $\tan \delta$  at 15 Hz was taken as a measure for the rolling resistance.

The cured compounds' mechanical properties were determined using a Zwick Z020 tensile tester according to ISO-37.

*Bound rubber.* — Bound rubber was determined by extracting the compound three times for 24 hours with acetone, acetylacetone and tetrahydrofurane, respectively, and weighing the residue. Bound rubber is expressed as the percentage rubber remaining in the residue relative to the total rubber polymer included in the recipe.

### 3.3 Results and discussion

During mixing the batch temperature increases, causing the primary and secondary reaction, and possibly also the silane-rubber reaction, to proceed at different rates. The dump temperature was varied by varying the mixer's rotor speed and fill factor while keeping the other mixing conditions and the mixing time constant. The dump temperature after the first mixing step was significantly higher than after the second mixing step, and therefore it is obvious that the final dump temperature after the first mixing step is the main parameter influencing the degree of reaction. The effect of the dump temperature on the dynamic and mechanical properties of the products obtained after mixing was investigated in the presence and absence of TESPT.

#### 3.3.1 Effect of the presence or absence of TESPT on the properties of uncured and cured compounds

Compounds were mixed according to the recipe and procedure in Table 3.1 and 3.2, in the presence and absence of TESPT silane coupling agent. The Mooney viscosities of the compounds after 2 mixing steps are listed in Table 3.3. Irrespective of dump temperature, the compounds without TESPT show very high Mooney viscosity values. This is a first indication of a poor dispersion of the silica filler, which will lead to subsequent processing problems. When TESPT is present in the compound much lower values for the Mooney viscosity are obtained.

**Table 3.3** Influence of dump temperature after first mixing step on Mooney viscosity after second mixing step.

Without TESPT		With TESPT	
Dump temp., (°C)	Mooney viscosity ML(1+4)100°C	Dump temp., (°C)	Mooney viscosity ML(1+4)100°C
112	158.0	115	-
132	171.7	133	76.8
151	173.0	149	85.6
169	163.1	169	89.7
185	164.7	183	116.3

After the second mixing step the Payne effect was measured with the RPA 2000. The storage modulus at low strain (0.56%) after the second mixing step, a measure for the filler-filler interaction as explained in Chapter 2, is plotted versus the dump temperature after the first mixing step for compounds in absence and presence of TESPT: Figure 3.1. From this graph it is evident that the  $G'$  decreases in linear fashion with increasing dump temperature for the compound without TESPT. Still relatively high values are obtained. This is a second indication, that there is still a large amount of filler-filler interaction due to poor dispersion of the silica. If TESPT is applied as coupling agent, significantly lower  $G'$  values are obtained over the whole dump temperature range. Especially at low dump temperatures, representing more common practical mixing conditions, a much lower  $G'$  is obtained when TESPT is present during mixing of silica and rubber.

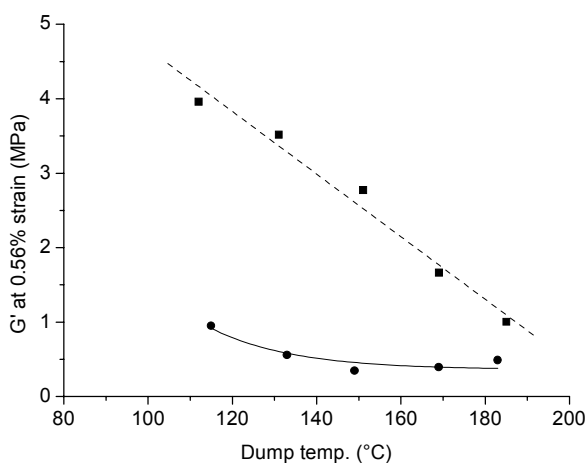


**Figure 3.1** Storage modulus ( $G'$ ) at 0.56% strain as a function of the dump temperature; (■) without TESPT, (●) with TESPT.

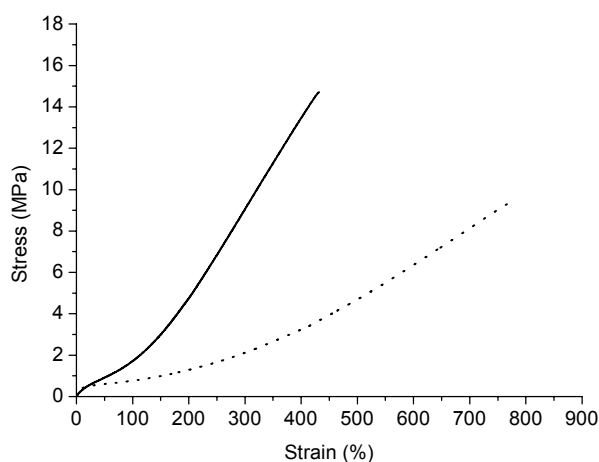


**Figure 3.2** Stress-Strain curve for a compound without TESPT (----) and with TESPT (—).

The effect of the presence or absence of TESPT silane coupling agent is also very clear in stress-strain measurements after curing the compounds: Figure 3.2. When TESPT is absent in the compound, a lower tensile strength and a larger elongation at break are obtained compared to a compound where TESPT is included. It is clear, that the presence of TESPT in silica-filled rubber compounds has a strong effect on mechanical properties.

Other compound properties are depicted in Table 3.4. The Shore A hardness remains more or less constant with increasing dump temperature. In the case that TESPT is present in the compound, slightly lower shore A hardness values are obtained indicating a better dispersion of the silica. The  $\tan \delta$  values at 60°C, a measure for rolling resistance, differ significantly as a function of the dump temperature, irrespective of the presence of TESPT. Another way to look at this rolling resistance is the ratio of the 300% and 100% modulus:  $M_{300}/M_{100}$ .<sup>18</sup> The  $M_{300}/M_{100}$  ratio is basically related to the shape of the tensile curves, Figure 3.2. The greater the tendency of the stress to grow with elongation, the higher the  $M_{300}/M_{100}$  ratio and the lower the  $\tan \delta$  at 60°C.<sup>19</sup> A high value of the  $M_{300}/M_{100}$  ratio corresponds to a low rolling resistance. The  $M_{300}/M_{100}$  is lower for the compound without TESPT than for the compound with TESPT. Dump temperature effects are most clear for compounds with TESPT. An increase in dump temperature results in higher  $M_{300}/M_{100}$  values. For the compound lacking the presence of TESPT, there is no clear effect of the dump temperature visible. Compounds without TESPT are irreproducible and result in large scatter of the data: Table 3.4.

**Table 3.4** Influence of dump temperature and presence of TESPT on material properties.

Without TESPT				With TESPT			
Dump temp., (°C)	Hardness, (shore A)	tan $\delta$ 60°C, (-)	M <sub>300</sub> /M <sub>100</sub> , (-)	Dump temp., (°C)	Hardness, (shore A)	tan $\delta$ 60°C, (-)	M <sub>300</sub> /M <sub>100</sub> , (-)
112	76	0.190	1.84	115	-	-	4.57
132	76	0.144	2.02	133	64	0.183	4.54
151	73	0.147	1.98	149	63	0.176	5.09
169	73	0.181	2.42	169	55	0.143	6.39
185	75	0.161	2.96	183	65	0.131	7.57

The results presented show that, when TESPT is omitted in the tyre tread compound, processing is much more difficult due to high viscosity of the compound. Further, poor dynamic and mechanical properties are obtained when TESPT is left out of the compound during mixing. A coupling agent such as TESPT is necessary to overcome the processing problems and to obtain good dynamic and mechanical properties. In the following paragraphs, the effect of processing conditions on the reaction of the TESPT coupling agent with the silica and the rubber matrix is described.

### 3.3.2 Properties of uncured compounds in relation to the dump temperature in the presence of TESPT silane coupling agent

The most direct indication of a silica-silane-rubber reaction is a change in the compound's Mooney viscosity (see Figure 3.3 A). At dump temperatures above 150°C, a gradual increase in the Mooney viscosity is observed.

The reaction of the coupling agent towards silica and rubber should increase the bound rubber content as given in Figure 3.3 B. Although there is quite some scatter in the data, there is still a slight trend visible. At higher dump temperatures bound rubber tends to increase. The limited accuracy of bound rubber measurements was observed by others as well<sup>20,21</sup> and blamed to the complexity of the system. These measurements only have limited significance.

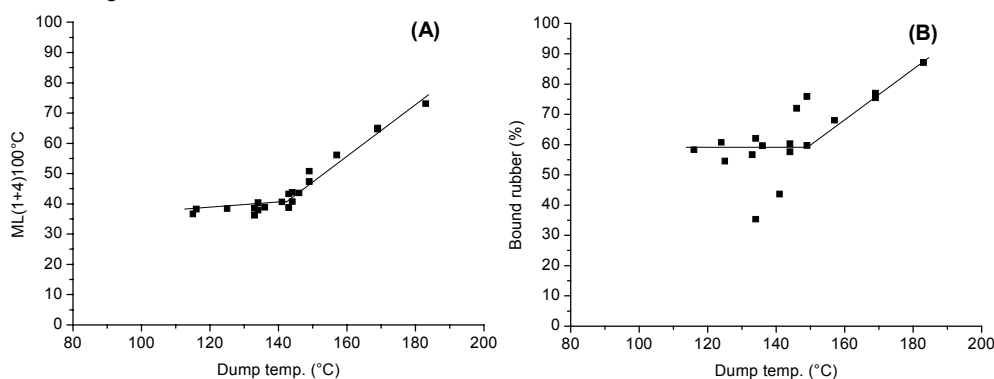


**Figure 3.3** Mooney viscosity (A) and bound rubber (B) as a function of dump temperature (the line in B is drawn as a guide for the eye).

In order to study the reaction between TESPT and silica and that between TESPT and the rubber matrix in greater detail, RPA measurements were performed by subjecting uncured compounds to different strain amplitudes. It should be noted that, as explained in Chapter 2, when using silica the high level of the elastic modulus and the drop of the elastic modulus at higher strain amplitudes are commonly taken to prove the existence of a filler network formed by the silica. Figure 3.4 A shows the effect of the dump temperature on the dynamic storage modulus  $G'$  at the low strain value of 0.56%.  $G'$  can be seen to decrease steadily to a dump temperature of 150°C, after which it slightly increases. At 100% strain the  $G'$  remains constant up to 150°C, after which it increases substantially, Figure 3.4 B.

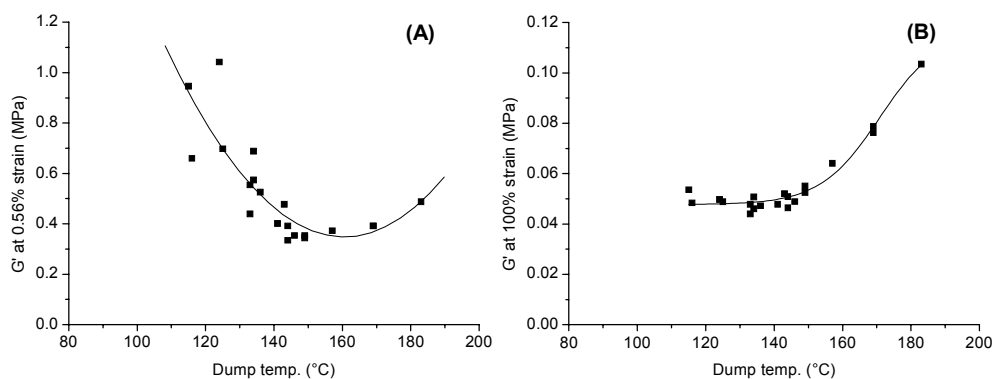


**Figure 3.4** Influence of dump temperature on the storage modulus at 0.56% strain (A) and 100% strain (B).

The decrease in the  $G'$  and the constant compound Mooney viscosity up to dump temperatures of 150°C are obviously due to the primary and secondary reactions of the coupling agent with the silica surface. A higher degree of coupling leads to less filler-filler interaction, and therefore a decrease in  $G'$  at rising temperatures and low strain values. The increase in  $G'$  and Mooney viscosity observable at dump temperatures above 150°C is indicative of scorch attributable to a reaction between the coupling agent and the rubber matrix, resulting in a filler $\leftrightarrow$ coupling agent $\leftrightarrow$ rubber network. The constant value of the compound Mooney up to dump temperatures of 150°C is due to the high strain under which this measurement was performed.  $G'$  also remains constant up to this temperature at high strain values.

The relative increase in  $G'$  measured at 100% strain at dump temperatures of between 150°C and 180°C is 100%, whereas that observed at 0.56% strain is 40%, as can be seen in Table 3.5. This difference is difficult to explain, but is related to performance characteristics of the system concerned. We propose the following interpretation. At low strain values, the silica-filler network is fully developed and has a strong influence on the  $G'$ . At higher strain values, the filler-network is broken and its effect on  $G'$  hence disappears, irrespective of whether measured at 150°C or 180°C. The degree of scorch due to the TESPT measured at 180°C is the same at low and high strain values; the scorch is hence independent of strain and of the filler's reinforcing effect. The greater relative increase in  $G'$  observed at 100% strain, at which the reinforcing effect of the filler is much lower than at 0.56% strain, is clearly indicative of an increase in the modulus of elasticity caused by the scorch occurring in the early curing stages.

**Table 3.5** Relative increase in  $G'$  versus strain at 150°C and 180°C.

Strain (%)	$G'$ (MPa) at 150°C	$G'$ (MPa) at 180°C	Relative increase (%) between 150°C and 180°C
0.56	0.35	0.50	40
100	0.05	0.10	100

### 3.3.3. Interactions between time and temperature as a indication of reaction kinetics of the coupling reaction.

To study the effects of exposure temperature and time in greater detail, experiments were performed using a Schwabenthan Polymix 80T two-roll mill at different milling temperatures. First the compound was mixed in the Brabender mixer using a fill factor of 70% and a rotor speed of 100 rpm as specified for step 1 in Table 3.2. After completing the Brabender mixing cycle with a dump temperature of 150°C, the compounds were milled for 10 minutes on the two-roll mill at different temperatures.

Figure 3.5 A shows the  $G'$  at 0.56% strain as a function of the applied mill temperature. As can be seen in this figure, the same trend was observed as at the different dump temperatures after the Brabender mixing (Figure 3.4 A): the  $G'$  first decreases till temperatures up to 150°C and then increases at higher temperatures. Figure 3.5 B shows the effect of the mill temperature on  $G'$  at 100% strain.  $G'$  remains more or less constant up to 140°C, after which it shows only a slight, virtually insignificant, increase. This is more or less the same behaviour as that observed at different dump temperatures (Figure 3.4 B), except that the effects are now much less discernible.

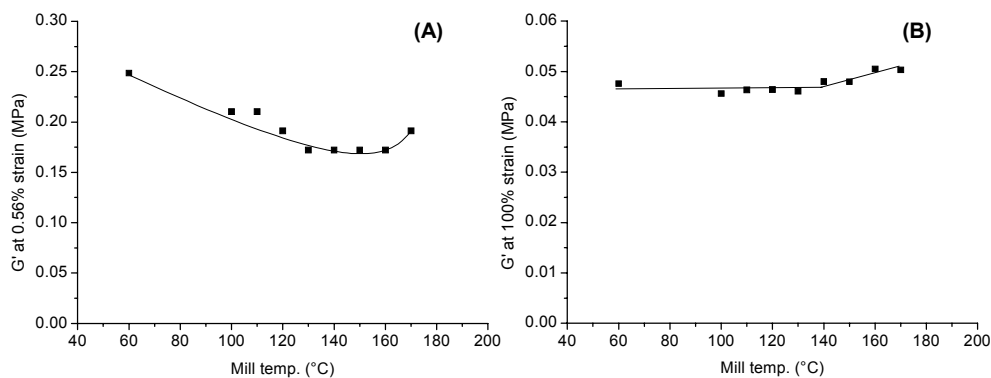


**Figure 3.5** Influence of milling temperature on the storage modulus at 0.56% strain (A) and 100% strain (B).

In spite of the fact that the compounds had reached a dump temperature of 150°C once during the first step in the Brabender mixer, extended milling at 150°C led to a decrease in the  $G'$  at 0.56% strain, even after 10 minutes milling. This implies that the

reaction between the coupling agent and the silica was not completed by the end of the 6.45 minutes mixing in the Brabender mixer at a dump temperature of 150°C.

We used the Brabender mixer to further investigate the effect of different mixing times. In this experiment we varied the further mixing time in the first mixing step after the last addition of the ingredients at 4.45 minutes. The temperature remained constant at 150°C. As can be seen in Figure 3.6 A, the  $G'$  did not reach a constant value after the first mixing step, even after 15 minutes of mixing at a dump temperature of 150°C.

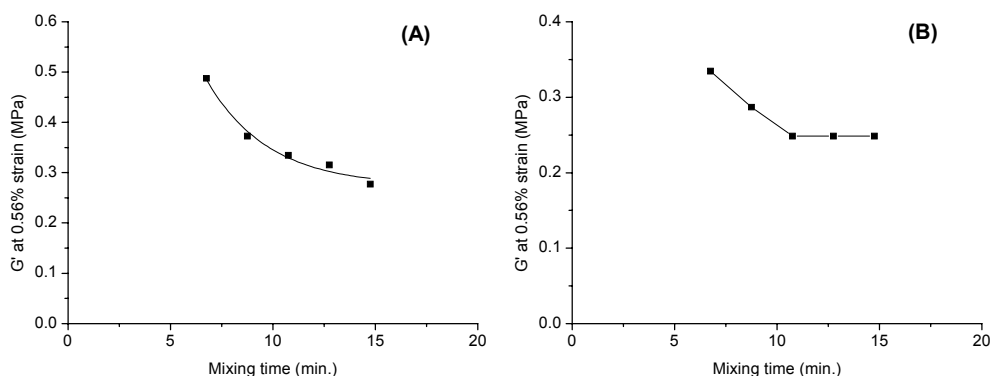


**Figure 3.6** Influence of mixing time on the storage modulus at 0.56% strain after the first mixing step (A) and after the second mixing step (B).

However, in the second mixing cycle of 5 minutes specified in Table 3.2, the  $G'$  reached a constant value after the compound had been mixed for more than 10 minutes in the first step (see Figure 3.6 B). This implies that, to obtain a properly reproducible compound, the compound must be mixed for at least 10 minutes at a temperature of at most 150°C in the first step, preferably followed by a second mixing step of about 5 minutes. Our two experiments confirmed that the primary and secondary reactions between the silane and the silica indeed proceed at a slow rate under the employed conditions, as previously suggested by Hunsche et al.<sup>22</sup> It should however be added that the dump temperature must be kept well below 160°C to prevent the risk of compound scorch.

### 3.3.4 Effect of mixer size

To examine the effect of the dump temperature on the mechanical properties of the compound, also tests were performed on a larger scale. Compounds were mixed with a Shaw intermeshing 5 l mixer. With this mixer, variation of the rotor speed influences the dump temperature more directly than with a tangential mixer like the Brabender.

Several compounds were tested with different rotor speeds and fill factors of the mixers. Results of dynamic measurements after mixing in the 5 l and 390 ml mixers are presented in Figure 3.7. It is clear that the same trend is visible for the two mixers. Slightly lower  $G'$  at 0.56% strain values are obtained for the 5 l mixer, Figure 3.7 A.

Similarly, the same trend in the  $G'$  curve at 100% strain is observed as for the 390 ml mixer, Figure 3.7 B. The temperature where the  $G'$  starts to increase is higher for the larger mixer. The reaction of the coupling agent with the rubber or sulphur donation to the rubber matrix starts in the 5 l mixer at 160°C, whereas the reaction in the 390 ml mixer starts at approximately 150°C. We tend to relate this to problems involved in the measurement of the exact temperature during the mixing operation or to a better heat control in the Shaw intermeshing mixer, resulting in a better heat transfer.

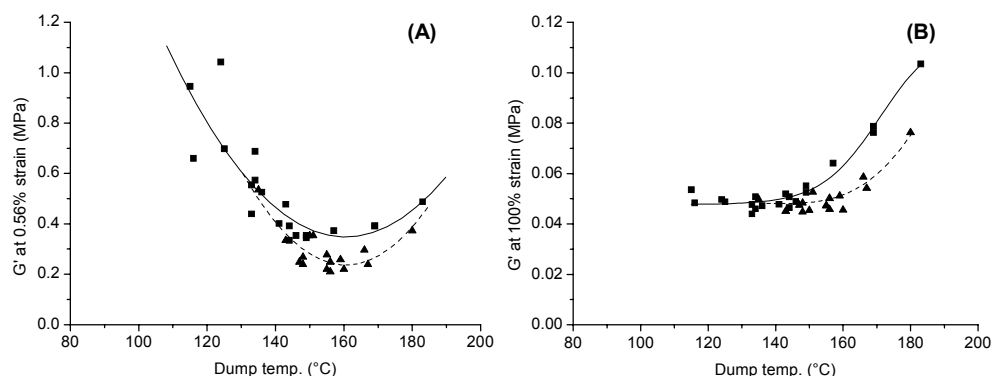


**Figure 3.7** Influence of mixer size on the storage modulus at 0.56% strain (A) and at 100% strain (B); (■) Brabender 390 ml mixer, (▲) Shaw 5 l mixer.

### 3.3.5 Effect of the dump temperature on the tensile properties of cured samples

At dump temperatures above 130°C the elastic modulus of vulcanised samples starts to decrease, as can be seen in Figure 3.8 A. As with the effects observed in the case of the storage modulus  $G'$ , the decrease in the modulus of elasticity must be attributable to a reaction between the silica and the coupling agent, either the primary reaction alone or both the primary and the secondary reaction. As the elastic modulus is per definition a low-strain property, it is as sensitive to filler–filler interaction between silica aggregates as the  $G'$  at low strain amplitudes.

The dump temperature does not have a significant influence on the 100% modulus, as can be seen in Figure 3.8 B. The 300% modulus, however, remains practically constant up to a dump temperature of 150°C and then increases, as can be seen in Figure 3.8 C. The results of the dynamic measurements of unvulcanised compounds at low and high strain amplitudes (Figures 3.4 A and B) bear a strikingly close resemblance to those of the stress–strain measurements of vulcanised compounds at low and high strain amplitudes (Figures 3.8 A and C). The tensile strength shows a slow, steady increase with increasing dump temperatures (Figure 3.8 D). At dump temperatures above 150°C the elongation at break shows a substantial decrease (Figure 3.8 E), as may be expected when crosslinking occurs.

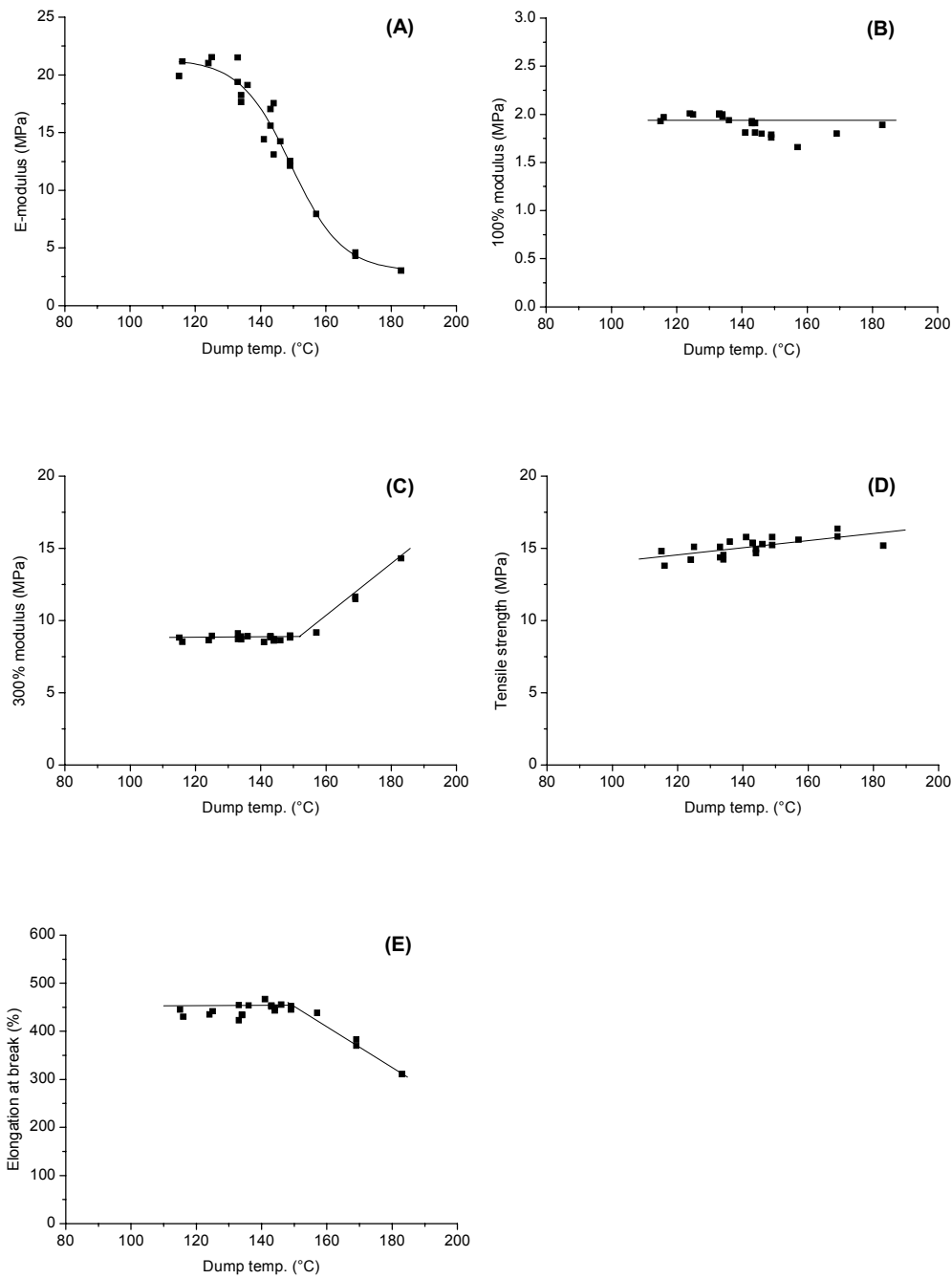


**Figure 3.8** Tensile properties as a function of dump temperature; (A) Elastic modulus, (B) 100% modulus, (C) 300% modulus, (D) Tensile strength, (E) Elongation at break.

Dividing the 300% modulus by the 100% modulus results in a measure for the rolling resistance, see 3.3.1. The values for the two moduli are given in Figure 3.8 B and 3.8 C. If the two properties are divided, the results as given in Figure 3.9 are obtained. In the same figure also the  $\tan \delta$  as a function of the dump temperature is given, as measured with the RPA 2000.

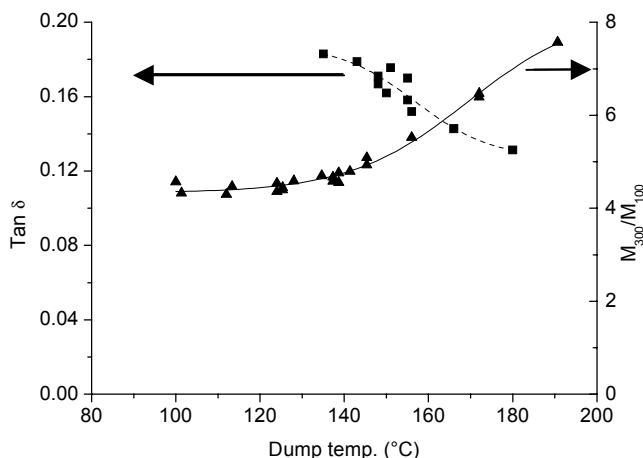


**Figure 3.9**  $\tan \delta$  (■) and  $M_{300}/M_{100}$  (▲) as a function of the dump temperature.

Both material properties show an improvement in the rolling resistance with increasing dump temperature. The  $M_{300}/M_{100}$  is increasing with increasing dump temperature while on the other hand the  $\tan \delta$  is decreasing. The increase of the  $M_{300}/M_{100}$  is mainly due to the increase in the 300% modulus, Figure 3.8 B and C. This increase is caused, as mentioned before, by the coupling of the silica particle to the rubber matrix or sulphur donation to the rubber matrix. High dump temperatures do give lower rolling resistance as shown by the two measurements. On the other hand, at higher dump temperatures a lot of processing problems arise due to scorch of the compound in the mixer.

### 3.4 Considerations on mixer operation

The results of the experiments clearly illustrate the effects of time and temperature on the various reactions which may take place: the primary and secondary reactions between the coupling agent and the silica surface at temperatures up to 150°C and the reaction of the sulphur moiety in the coupling agent with the rubber matrix at temperatures above 160°C. The latter reaction may in principle be the result of two mechanisms. The first is a form of bonding between the coupling agent and the rubber after the coupling agent has reacted with the silica particle. The second is the donation of sulphur to the rubber compound by the coupling agent, which hence accelerates the curing process by making use of its own released sulphur. Which of these mechanisms prevailed under the employed test conditions cannot be inferred from our results.

The results show that a temperature of approximately 160°C should not be exceeded during the mixing when TESPT is used as the coupling agent, to avoid the risk of the silane reacting with the rubber. The graphs illustrating the modulus of elasticity and G' at low strain, which may be regarded as parameters of the coupling reaction between the filler particle and the coupling agent, show that the temperature must however be at least 130°C. Luginsland arrived at similar conclusions via different experiments.<sup>23, 24</sup>

The results of the experiments also show that long mixing times and high temperatures are required to ensure that the TESPT reacts with the silica surface to the desired extent, but that the temperatures must not become too high, because otherwise scorch/curing will occur. Different mixing times and batch temperatures and differences in other parameters such as the specific mixing energy evidently lead to substantial differences in the properties of the cured compound. The mixing time and batch temperature become interdependent during the mixing, and are also influenced by the properties of the employed mixer and the other mixing conditions. So mixing silica compounds with the aid of coupling agents can be regarded as "reactive mixing". Such mixing demands control principles that are a good deal more complex than those commonly used in carbon-black mixing, representing a new dimension in rubber technology.

### 3.5 Conclusions

A coupling agent functionality, like e.g. a silane, is a necessary prerequisite when mixing silica and rubber. The presence of the coupling agent results in considerably lower compound Mooney viscosity and significantly improves the dynamic and mechanical properties of the cured compound.

The dump temperature is a parameter of paramount importance in mixing silica and rubber with the aid of TESPT as a coupling agent. A minimum dump temperature of 130°C is required to ensure that the silica and the coupling agent react to the desired extent, but at temperatures above 160°C either the coupling agent starts to react with the rubber matrix or the TESPT starts to donate sulphur.

It has also been found that a mixing time of at least 10 minutes at 150°C is necessary to ensure complete coupling of the silica and the silane and that the reaction between the silica and the silane takes place primarily during the first mixing step.

### 3.6 References

1. J.-B. Donnet, *Kautsch. Gummi Kunstst.*, **47**, (1994), 628.
2. M.P. Wagner, *Rubber Chem. Technol.*, **49**, (1976), 703.
3. Degussa, Technical information, (1995).
4. R.W. Cruse, M.H. Hofstetter, L.M. Panzer, R.J. Pickwell, *Rubber & Plastics News*, (1997), 14.
5. B.T. Poh and NG, C.C., *Eur. Polym. J.*, **34**, (1998), 975.
6. R.H. Hess, H.H. Hoekje, J.R. Creasey, F. Strain, (to PPG industries Inc. ), U.S. Pat. 3,768,537 (30-101973).
7. P.E. Cassidy, B.J. Yager, *J. Macromol. Sci. - Revs. Polym. Technol.*, **1**, (1971), 1.

8. F. Thurn and S. Wolff, *Kautsch. Gummi Kunstst.*, **28**, (1975), 733.
9. S. Wolff, *Kautsch. Gummi Kunstst.*, **34**, (1981), 280.
10. S. Wolff, *Rubber Chem. Technol.*, **55**, (1982), 967.
11. S. Wolff, *Kautsch. Gummi Kunstst.*, **36**, (1983), 969.
12. S. Wolff, E.-H. Tan and J.-B. Donnet, *Kautsch. Gummi Kunstst.*, **47**, (1994), 485.
13. S. Wolff and M.J. Wang, *Kautsch. Gummi Kunstst.*, **47**, (1994), 17.
14. S. Wolff, *Rubber Chemistry Technology*, **69**, (1996), 325.
15. H.D. Luginsland, *Kautsch. Gummi Kunstst.*, **53**, (2000), 10.
16. J.W. Pohl, Rubber division, American Chemical Society, Cleveland, Ohio, USA, October 21-24, 1997.
17. J.L. Leblanc, A. Mongruel, *Progress in Rubber and Plastics Technol.*, **17**, (2001), 162.
18. R. Rauline, (to the Compagnie Generale des Etablissements Michelin - Michelin & Cie), EP 0 501227A1 (February 12, 1992).
19. J.W. Brinke ten, P.J. van Swaaij, L.A.E.M. Reuvekamp, J.W.M. Noordermeer, *Kautsch. Gummi Kunstst.*, **55**, (2002), 244.
20. C.M. Blow, *Polymer*, **14**, (1973), 309.
21. E. Sheng, Sutherland, I., Bradley, R.H., Freakley, P.K., *Eur. Polym. J.*, **32**, (1996), 35.
22. A. Hunsche, U. Görl, H.G. Koban, Th. Lehmann, *Kautsch. Gummi Kunstst.*, **51**, (1998), 525.
23. H.D. Luginsland, 11<sup>th</sup> international SRC meeting, Púchov, May 25-26, 1999.
24. H.D. Luginsland, A. Hasse, Rubber Division, American Chemical Society, Dallas, Texas, USA, April 4-6, 2000.



---

## Chapter 4

### *Effect of zinc oxide on the reaction of TESPT silane coupling agent with silica and rubber<sup>#</sup>*

---

The addition of a coupling agent to silica-rubber compounds enhances filler-matrix compatibility. The coupling agent under study, TESPT, can also act as a sulphur donor, which leads to premature scorch in the mixer. The effect of the presence of zinc oxide in the internal mixer at higher dump temperatures was demonstrated by dynamic mechanical testing. A lower tendency to scorch was seen when zinc oxide was omitted during the internal mixing stage and added only later together with the curing additives on a two-roll mill. Zinc oxide primarily interferes with the reaction between the coupling agent and the silica surface, as shown by the reaction rate constants obtained with rheological experiments. Further confirmation was obtained by HPLC experiments: the reaction rate constants of TESPT with silica for the samples with zinc oxide present, were lower at higher temperatures in comparison with samples without zinc oxide. XPS data confirmed that zinc oxide can indeed react with the silica surface. When zinc oxide is included in the internal mixer stage, shorter scorch times are obtained for curing when compared to compounds where no zinc oxide is included during mixing and only added later on. These shorter scorch times are the result of filler flocculation of the silica during the curing stage.

#### 4.1 Introduction

The silica-rubber compatibility can be improved by the addition of a coupling agent. Under certain mixing conditions the filler surface may be only partly covered by the coupling agent, which may have an adverse effect on the properties in the final product. Some coupling agents may act as sulphur donor in addition. The dump temperature employed during mixing and the length of time the compound is exposed to that temperature govern the reaction mechanisms of the coupling agent and determine whether the agent leads to the formation of a silica-rubber bond or acts as a sulphur donor. A temperature of at least 130°C is necessary to ensure that the reaction between the coupling agent and the silica proceeds, whereas the coupling agent starts to react with the rubber or to donate sulphur, resulting in scorch, at temperatures above 160°C.<sup>1,2</sup>

During mixing of e.g. a tyre tread compound, many additional ingredients are present which may influence the reaction between coupling agent and silica: Table 3.1 (Chapter 3).

---

<sup>#</sup> The work described in this chapter has been submitted for publication in Rubber Chem. Technol.

Silica contains different types of silanol groups, isolated, vicinal and geminal, which can react with these other ingredients. In particular, the silanol groups on the surface of silica are of acidic nature<sup>3</sup> and can therefore react with an alkali, such as zinc oxide. In 1959, Laning et al. already stated that zinc oxide can react with the silanol groups on the silica surface.<sup>4</sup> This implicitly reduces their availability for reaction with the coupling agent. Thurn and Wolff mentioned in 1975 that zinc oxide might have an effect on the reaction of the coupling agent with silica. They found that the presence of zinc oxide in a SBR compound filled with silica showed a rapid decrease in the compound viscosity as reflected in the mixing torque.<sup>5</sup> They interpreted the effect of zinc oxide as a catalyst for the coupling reaction.

New insights have been gained in the mean time on the reaction mechanism of the coupling agent bis-(triethoxysilylpropyl)tetrasulphide (TESPT) with silica.<sup>1,2,6-8</sup> The objective of the present chapter is to show the effects of zinc oxide on the reaction mechanism of TESPT with the silica surface and on the sulphur donating reaction of the TESPT to the rubber compound, in order to settle the apparent contradiction between the two mechanisms postulated before.<sup>4,5</sup>

## 4.2 Experimental

*Compound recipe.* — The compounds were mixed, cured and characterised according to the experimental paragraph of Chapter 3.

*Method of analysing the coupling reaction kinetics with a RPA 2000.* — A compound was mixed **without TESPT and zinc oxide** according to the procedure in Table 3.2 (Chapter 3) using only the first mixing step; the second mixing step was omitted. Subsequently, in all cases TESPT and in half the cases also zinc oxide were added on the two-roll mill at a low temperature:  $\leq 50^{\circ}\text{C}$ . Buttons were punched out of the rubber compound, suitable for RPA 2000 measurement. The buttons were placed in a Heraeus oven set at various temperatures, ranging from  $100^{\circ}\text{C}$  to  $140^{\circ}\text{C}$ . Every 2 minutes a sample was taken out of the oven and cooled in liquid nitrogen, to stop the coupling reaction. The  $G'$  at 0.56% strain was measured with the aid of the RPA 2000 at  $100^{\circ}\text{C}$  and 0.5 Hz, as a measure of the coupling reaction.

*Method of analysing the coupling reaction kinetics with a HPLC.* — In a 5 ml high pressure vessel, 0.2 g silica was added to 1.9 ml of n-decane. 0.1 ml of a solution of TESPT (2 g in 10 ml n-decane) was added to the mixture. The reaction vessel was sealed and brought into an oil bath at elevated temperatures. During the reaction the mixture was stirred with a magnetic stirrer. At fixed time intervals the vessel was taken out of the oil bath and cooled in ice. The reaction vessel was then opened and 2 ml of diethyleneglycolmonobutylether was added, after which the vessel was closed again and stirred vigorously for 5 minutes. The diethyleneglycolmonobutylether was added to remove all the physically bound TESPT from the silica surface. The suspension was then filtered over a  $0.45\ \mu\text{m}$  Spartan filter. From this solution 100  $\mu\text{l}$  was added to 5 ml of acetonitrile. The amount of non-reacted TESPT was measured using High Performance Liquid Chromatography (HPLC). The HPLC conditions are given in Table 4.1.

**Table 4.1** HPLC Parameters to determine the TESPT concentration.

Column	Nucleosil 100-5 C18 HD (reverse phase)
Mobile phase	97 Acetonitrile : 3 water (vol%)
Flow rate	1 ml/min.
Temperature	23°C
Detector	UV
Wavelength	254 nm
Injected volume	50 $\mu$ l

*XPS measurements.* — Small cleaned glass cover plates were placed in a 5 ml high pressure reaction vessel with 1.9 ml of n-decane. 0.1 ml of a solution of TESPT (2 g in 10 ml n-decane) or zinc oxide (0.014 g) or a combination of both was added to the mixture. The reaction vessel was sealed and was brought into an oil bath at 140°C. During the reaction the mixture was stirred with a magnetic stirrer. After 1 hour the sample was cooled in ice. The reaction vessel was then opened and 2 ml of diethyleneglycolmonobutylether was added, after which the vessel was closed again and stirred vigorously for 5 minutes. After this step the glass plate was washed with acetone and n-decane to remove the non-reacted components from the glass surface.

Next, the samples were moved into the XPS analysis chamber and normal spectra were obtained. The spectrometer used was a PHI Quantum 2000 scanning X-ray microprobe. The X-rays were produced by the Al anode with a power of 124.6 W. Survey scans of the entire energy spectrum were recorded.

*Contact angle measurements.* — All samples were characterised by static water contact angle measurements using the sessile drop method. The measurements were performed with a Contact Angle Measuring System G10/G40. The samples were measured by placing a water droplet (1-3  $\mu$ l) onto the sample with an electronically regulated syringe. For each sample, contact angles were determined at five different spots using fresh water for each new droplet.

### 4.3 Results

During mixing the batch temperature increases, causing the coupling reaction, and possibly also the silane-rubber reaction due to sulphur donation, to proceed at different rates. In our earlier work it was shown, that the dump temperature after mixing is the main parameter influencing the degree of reaction.<sup>1,2</sup> Dump temperature was varied by adjusting the mixer's rotor speed and fill factor, while keeping the other mixing conditions and the mixing time constant. We investigated the effect of the presence or absence of zinc oxide in the recipe during the first two mixing steps in the internal mixer, by measuring the dynamic mechanical properties of the uncured compounds, directly after step 2. As zinc oxide is an indispensable ingredient for sulphur vulcanisation, zinc oxide was included on the two-roll mill together with the other curatives, when not already added in the internal mixer. Mechanical properties were measured after subsequent curing. The reaction of TESPT with

the silica surface was also analysed with HPLC and XPS and compared with the dynamic mechanical results on the still uncured compounds.

### 4.3.1 Properties of uncured and cured compounds as a result of addition or absence of zinc oxide during mixing in the internal mixer, obtained at different dump temperatures

Compounds were mixed according to the procedure described in the experimental paragraph. After the second mixing step the  $G'$  at low strain (0.56%) and at high strain (100%) were measured with the RPA 2000. The results of those measurements are given in Figures 4.1 A and B.

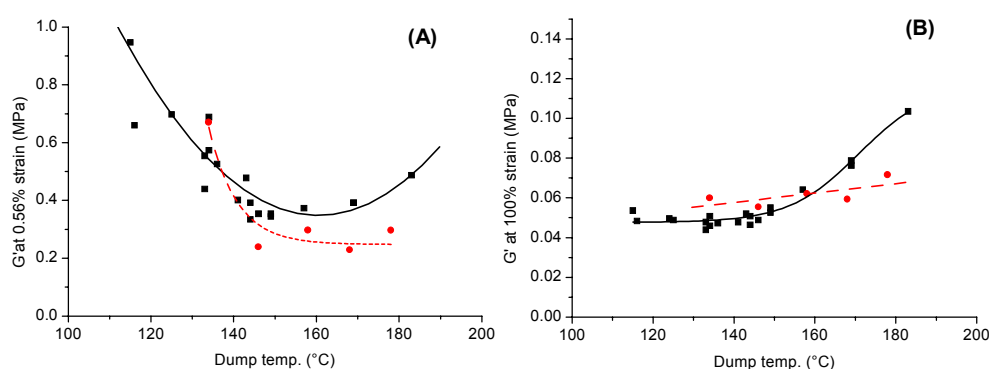


**Figure 4.1**  $G'$  at 0.56% strain (A) and 100% strain (B) as a function of the dump temperature; ■, with ZnO; ●, without ZnO, present in the internal mixer.

In Figure 4.1 A, the  $G'$  at low strain – a measure for the coupling reaction<sup>1,2</sup> – for a compound without zinc oxide decreases in the same manner as in the presence of zinc oxide. Above 140°C dump temperature the  $G'$  is lowest for the compound without zinc oxide. At dump temperature of 150°C and higher,  $G'$  at 100% strain – measure for the silane-rubber reaction – is increasing for a compound with zinc oxide. When no zinc oxide is present during mixing, the increase in the  $G'$  is less, indicating a lower reactivity of the silane towards the rubber.

The effect of zinc oxide on the coupling reaction is even more conspicuous when the elastic modulus is considered, after curing. When dump temperatures above 130°C are employed during mixing, the elastic modulus of vulcanised samples decreases as a function of dump temperature: Figure 4.2. When no zinc oxide is present during mixing – and only added later with the curatives on the mill – much lower elastic modulus values are obtained at comparable dump temperatures. On basis of our earlier work<sup>1,2</sup>, the lower elastic modulus is a sign of better hydrophobation of the silica by the coupling agent, leading to less filler-filler interaction and therefore a lower reinforcing power.

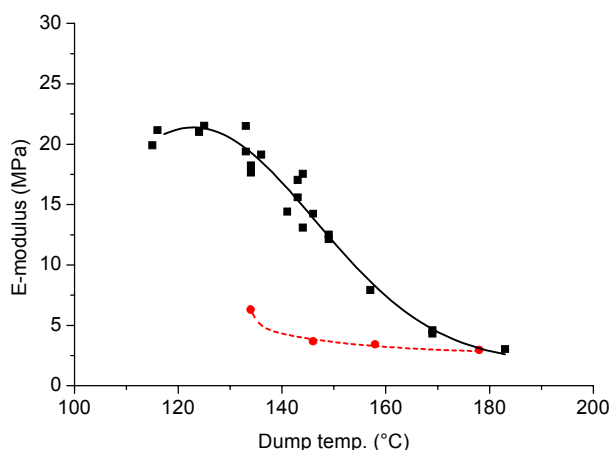


**Figure 4.2** Elastic modulus as a function of the dump temperature; symbols as in Fig. 4.1.

The other tensile properties of the vulcanised samples are listed in Table 4.2. There is no significant difference in properties between the compounds with and without zinc oxide being added during the first mixing steps in the internal mixer, except for the 300% modulus. With zinc oxide present in the mixer, the 300% modulus after curing remains practically constant up to a dump temperature of 150°C and then increases. The 300% modulus for the compound without zinc oxide added in the mixer is also increasing, but at a slower pace. The results of the dynamic measurements of uncured compounds at low and high strain amplitudes (Figures 4.1 A and B) show a striking resemblance to modulus measurements of vulcanised compounds at low vs. high strain amplitudes (Table 4.2), as exemplified earlier.<sup>1,2</sup>

**Table 4.2** Mechanical properties of the compounds with ZnO added in the mixer vs. on the two-roll mill, at different dump temperatures.

Dump Temp., (°C)	Addition of ZnO	E-modulus, (MPa)	100% modulus, (MPa)	300% modulus, (MPa)	Stress at break, (MPa)	Strain at break, (%)
134	In mixer	19.19	1.99	8.87	14.74	440.03
145	In mixer	14.43	1.83	8.73	15.30	452.41
157	In mixer	7.94	1.66	9.17	15.60	438.50
169	In mixer	4.47	1.80	11.56	16.10	376.42
183	In mixer	3.04	1.89	14.31	15.19	311.21
134	On two-roll mill	6.30	1.47	8.45	16.26	476.13
146	On two-roll mill	3.67	1.50	10.10	14.92	390.84
158	On two-roll mill	3.40	1.51	9.68	15.40	409.82
168	On two-roll mill	2.94	1.53	11.41	13.86	341.02
178	On two-roll mill	2.95	1.59	10.68	13.22	344.89

During the recording of the curing properties of the compound, prior to vulcanisation of the samples, the scorch time turned out to be another intriguing parameter. The scorch time ( $t_{02}$ ) of the rubber compound during vulcanisation, measured with the RPA 2000 at 160°C, is commonly defined as the onset of vulcanisation.<sup>9</sup> Figure 4.3 shows the scorch time as a function of the dump temperature for a compound where zinc oxide is present in the mixer and for a compound where zinc oxide is omitted and added later on the two-roll mill. When zinc oxide is present during mixing, an increase in scorch times at dump temperatures > 160°C is observed. Whereas compounds where zinc oxide is added on the two-roll mill result in a much earlier increase in scorch time at temperatures of 140°C already. The presence of zinc oxide in the internal mixer together with silica apparently has a strong effect on the curing behaviour of those silica filled compounds later on.

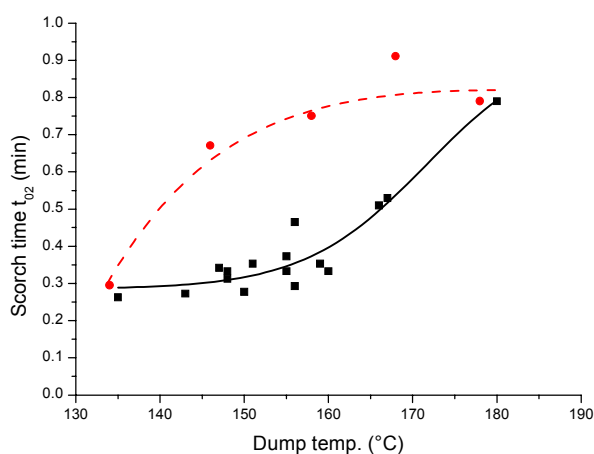


**Figure 4.3** Scorch time as a function of the dump temperature; symbols as in Fig. 4.1.

#### 4.3.2 Kinetic study of the reaction of TESPT with the silica surface as influenced by ZnO using rheological measurements

To further elucidate the effect of zinc oxide on the reaction mechanism of TESPT with silica, the kinetic rate constant of the coupling reaction in the rubber compound was measured by RPA 2000, as described in the experimental paragraph. The  $G'$  at 0.56% strain, measured after the various time/temperature combinations in the Heraeus oven, was plotted against reaction time (min.). Figure 4.4 A is an example of such a measurement for a compound at 130°C.

A reaction conversion can be calculated by using the following equation<sup>10</sup>:

$$x = \frac{G'(t) - G'(0)}{G'(\infty) - G'(0)} \quad (4.1)$$

Where  $G'(t)$  is the storage modulus after heating time  $t$  and  $G'(0)$  the storage modulus at time 0 min.  $G'(\infty)$  is the storage modulus at heating time 60 min, because at this time the  $G'$

has become constant. The reaction between TESPT and silica turns out to follow first order kinetics.<sup>11</sup> Therefore, the following equation can be used to calculate the reaction rate constant for the coupling reaction:

$$\ln(1-x) = -k^1 \cdot t \quad (4.2)$$

where  $k^1$  is the reaction rate constant ( $\text{min}^{-1}$ ). By plotting  $-\ln(1-x)$  versus time a straight line should appear, Figure 4.4 B. The slope of this line corresponds to  $k^1$ .

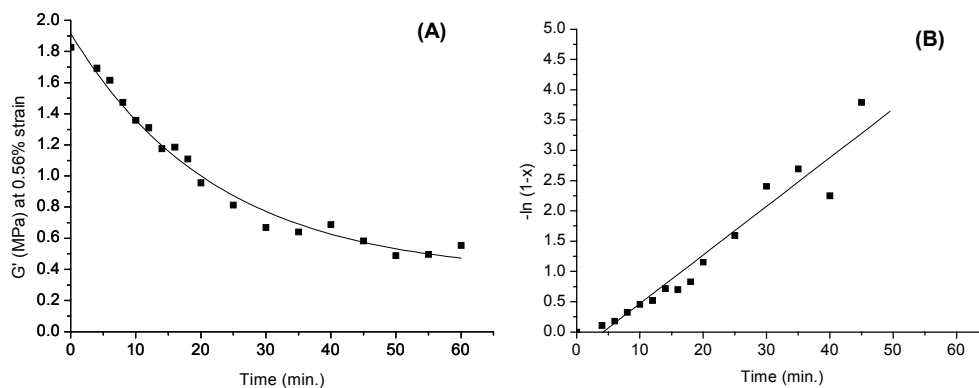


**Figure 4.4** Decrease of  $G'$  at 0.56% strain as a function of the reaction time at 130°C (A); logarithmic display of the reaction conversion as a function of the reaction time (B).

The results for the compounds, with and without zinc oxide added later on the mill, are represented in Table 4.3. From these results it can be seen, that the reaction rate constant for the compounds without zinc oxide, increases with temperature. When zinc oxide is included with the TESPT in the recipe on the two-roll mill, the reaction rate constant is lower at 140°C: 0.07 vs. 0.09 ( $\text{min}^{-1}$ ). This is an indication that zinc oxide is blocking the reactive silanol groups on the silica surface.

**Table 4.3** Kinetic rate constants at different temperatures measured with RPA 2000.

Kinetic rate constant, ( $\text{min}^{-1}$ )					
Temperature, (°C)	100	110	120	130	140
With ZnO	-	-	0.05	0.05	0.07
Without ZnO	-	-	0.04	0.05	0.09

It is very difficult to measure at and below temperatures of 120°C, because the reaction is then too slow to see a significant difference in  $G'$ . Temperatures above 120°C are needed to see a difference between the reaction rate constants, when looking at the compounds with and without zinc oxide.

### 4.3.3 Kinetic study of the reaction of TESPT with the silica surface as influenced by ZnO using HPLC measurements

To make sure that the decrease in  $G'$  at 0.56% strain, as seen in the previous paragraph, is not caused by a better dispersion of the silica, model studies were performed. These model studies in liquid suspension were done according to the work of Hunsche et al.<sup>11</sup>, except that in the present case also the effect of zinc oxide was studied. The extent of the reaction between TESPT and silica was determined by measuring the amount of unreacted TESPT by HPLC. For the calculations the summed peak areas of the different sulphur ranks were taken, Figure 4.5. The results are given in Table 4.4 for the kinetic rate constants of TESPT with and without zinc oxide present in the reaction mixture. The samples without zinc oxide show a clear increase in reaction rate constant with temperature, whereas the samples with zinc oxide present show a more or less constant reaction rate constant over the temperature range employed. The kinetic rate values are similar to the values obtained in the experiment described in the previous paragraph. In both cases the presence of zinc oxide is slowing down the reaction rate of TESPT with silica.

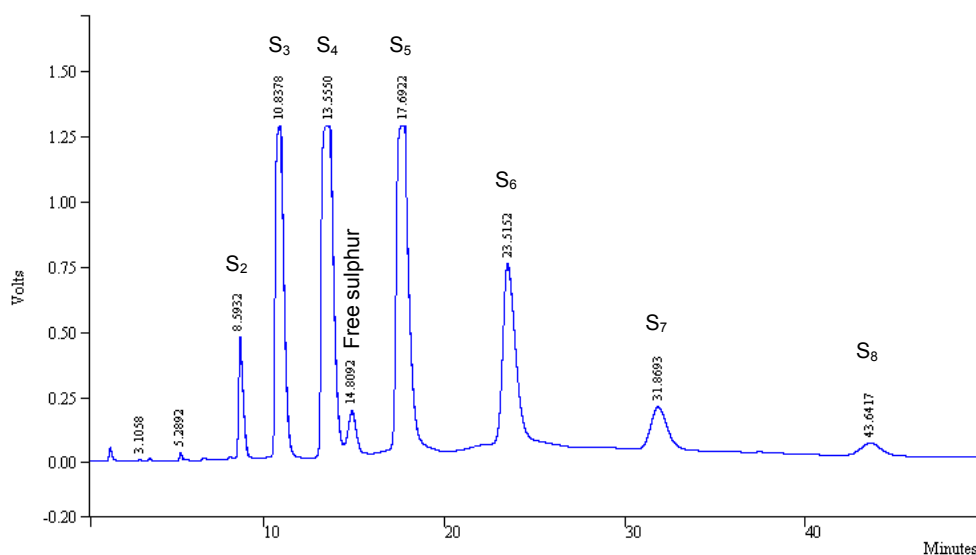


**Figure 4.5** HPLC chromatogram of TESPT, the different sulphur ranks and the free sulphur peak are indicated in the figure.

**Table 4.4** Influence of ZnO and stearic acid (in absence of ZnO) on the kinetic rate constants at different temperatures measured with HPLC.

Kinetic rate constant, ( $\text{min}^{-1}$ )					
Temperature, ( $^{\circ}\text{C}$ )	100	110	120	130	140
With ZnO	0.05	0.05	0.06	0.06	0.06
Without ZnO	0.04	0.05	0.04	0.06	0.09
With Stearic acid	0.03	0.04	0.04	0.06	0.08
Without Stearic acid	0.04	0.05	0.04	0.06	0.09

In the same way as with zinc oxide, HPLC measurements were also performed with stearic acid (SA) being omitted, on top of the absence of zinc oxide. The results from these experiments are also given in Table 4.4. They show, that there is no difference in the kinetic rate constants of TESPT with silica in presence or absence of stearic acid.

#### 4.3.4 XPS measurements on glass surface coated with TESPT and zinc oxide

From the results in the paragraphs above clear evidence is obtained, that zinc oxide reacts with the silica surface and therefore interferes with the reaction between TESPT and the silica surface. In order to confirm this in even more detail, glass samples (which also contain silanol groups) were coated with TESPT and/or zinc oxide as described in the experimental paragraph, and studied with XPS, a powerful tool for analysing surfaces. Figure 4.6 shows the XPS spectrum of a pure, non-coated glass sample. All spectra were corrected via the C1s peak. The different peaks are indicated in the figure. Around 1050 eV there are peaks from Zn. These are from the impurities, which are contained in the glass sample. At a binding energy of approximately 540 eV is the oxygen peak, at 100 and 170 eV are the peaks of Si. The spectrum of a glass sample, treated for 1 hour at 140°C with ZnO, is different as shown in Figure 4.7. The Zn peaks at 1050 eV are now much larger. The oxygen peak is also larger because there is zinc oxide present on the surface. The fact that Si peaks are still visible indicates, that this method is indeed sensing at the interface between the glass and zinc oxide. When the glass is only coated with TESPT, the Zn peaks are at the same level again as for the pure glass sample, Figure 4.8. The Si and O peaks are increased because of the Si and O atoms contained in TESPT. Figure 4.9 is a spectrum of a glass sample coated with both zinc oxide and TESPT. In comparison with the glass sample which has been coated with TESPT only (Figure 4.8), there is a difference in the amount of zinc. In the latter case there is more zinc oxide present on the glass surface and there is also a slight decrease in the amount of Si atoms. The decrease in Si atoms is caused by their reaction with zinc oxide.

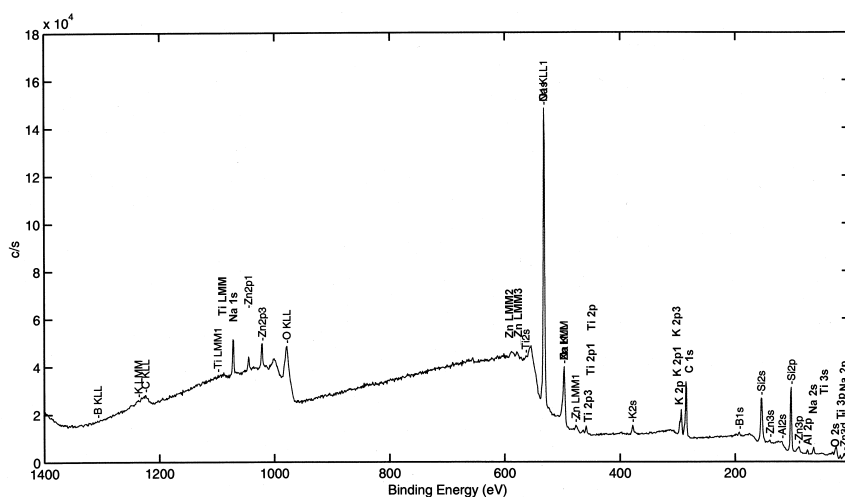


Figure 4.6 XPS measurement of untreated glass sample.

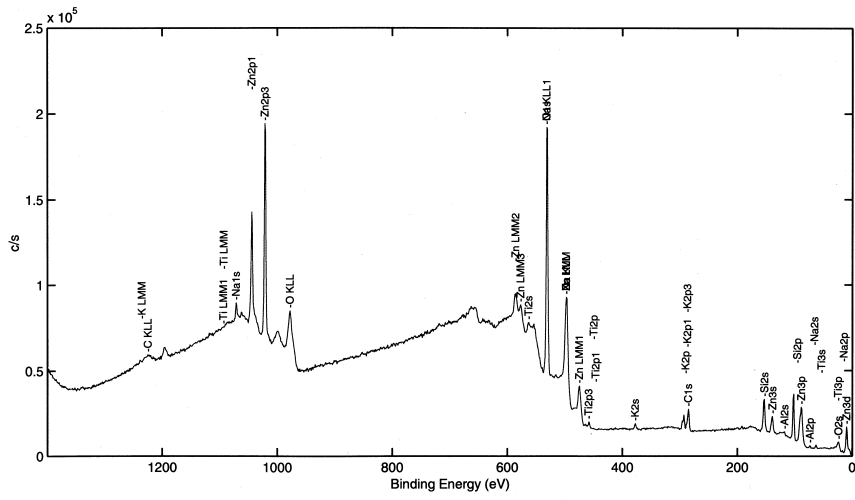


Figure 4.7 XPS measurement of glass sample coated with ZnO.

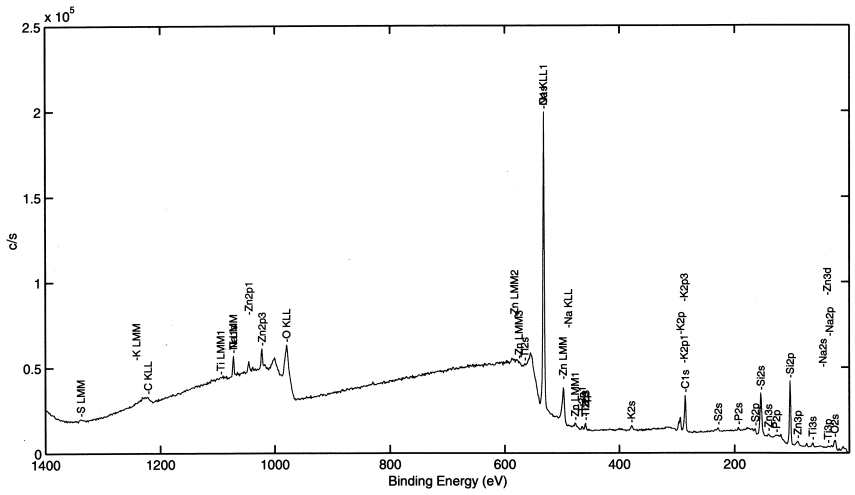


Figure 4.8 XPS measurement of glass sample coated with TESPT.

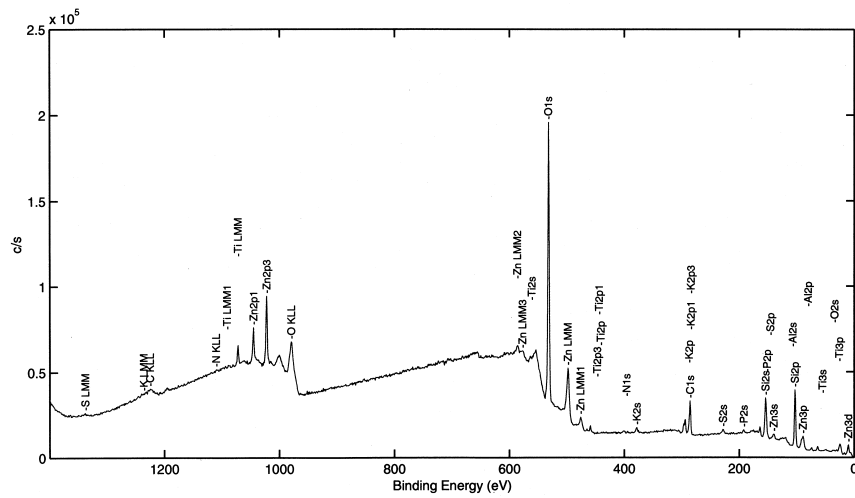


Figure 4.9 XPS measurement of glass sample coated with TESPT and ZnO.

### 4.3.5 Contact angle measurements

Contact angle measurements were performed to study the effect of the coupling agent and zinc oxide on the polarity of the silica surface. During this experiment glass was used to imitate the silica surface. In Figure 4.10 the contact angle is plotted for different kind of coatings on the glass surface.

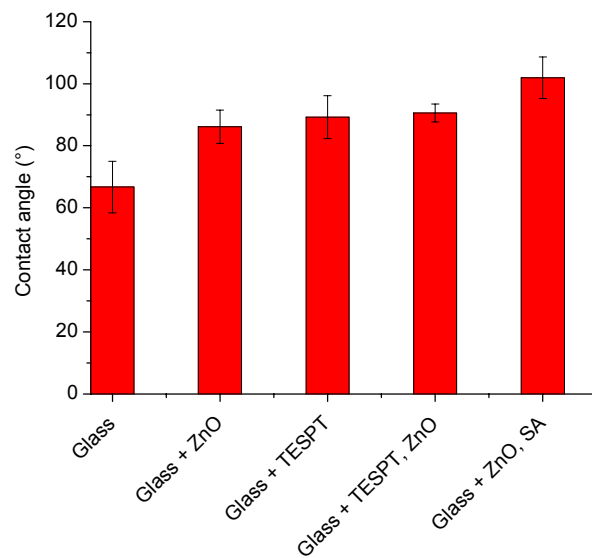


Figure 4.10 Contact angle for different types of coating on a glass surface.

A higher contact angle value means a higher hydrophobicity, whereas a lower value for the contact angle represents a more hydrophilic surface. First the surface of pure glass was measured, resulting in a contact value of approximately  $67^\circ$ . In all other cases, where a coating on the glass surface was applied, a higher value for the contact angle was obtained. When the glass surface is coated with zinc oxide, a more hydrophobic surface is obtained with the contact angle value being  $86^\circ$ . The coating with TESPT on the glass surface results in a slightly higher but comparable contact angle value. The combination of TESPT and zinc oxide as a coating layer on the glass surface also results in a comparable contact angle value. This is not surprising, because it is a combination of the values of pure TESPT and pure zinc oxide coating. When the glass surface is coated with zinc oxide and stearic acid, a significantly higher value for the contact angle is obtained. This might in turn be due to a complex which can be formed between the zinc oxide and the stearic acid; in this way the non-polar tail of the stearic acid will make the silica surface even more hydrophobic.

#### 4.4 Discussion

The results provide clear evidence that zinc oxide, present in the compound reacts with the silica surface in competition with TESPT. This effect is clearly visible in Figure 4.1 A. The fact that the  $G'$  at low strain above  $140^\circ\text{C}$  dump temperature is lower for the compound without zinc oxide added in the internal mixer, is an indication of better hydrophobation of the silica by the coupling reaction. At 100% strain (Figure 4.1 B), the increase in  $G'$  above  $150^\circ\text{C}$  dump temperature with zinc oxide present, was already explained by sulphur donation of TESPT to the rubber matrix or by the scorch reaction, resulting from coupling of the silica particle to the rubber matrix via the TESPT coupling agent.<sup>1,2</sup> For the compound where no zinc oxide is present the curve only shows a slight increase above  $150^\circ\text{C}$  dump temperature: Figure 4.1 B. Zinc oxide apparently acts as activator to enhance the reaction of the coupling agent with the rubber matrix, resulting in premature scorch. As a matter of fact, this agrees with the fact that TESPT after its development was first promoted as an accelerator.<sup>12</sup> As with the effects observed in the case of the storage modulus  $G'$  at low strain (Figure 4.1 A), the decrease in the elastic modulus (Figure 4.2) is also due to the coupling reaction between the silica and the coupling agent.

More evidence for the influence of zinc oxide on the coupling reaction was obtained from the kinetic experiments. The reaction between silica and zinc oxide became evident from the fact that the reaction rate constant for TESPT with silica was lower in the presence of zinc oxide in the compound. Similar results were obtained via HPLC measurements. This was also confirmed by the XPS data showing that, when zinc oxide and TESPT were applied at the same time to the glass surface, less Si atoms from TESPT were seen than on a glass surface only treated with TESPT. A possible acid-alkali reaction of zinc oxide with the silica surface via the silanol groups, the same groups where TESPT reacts with, is shown in Figure 4.11, similar to the reaction of water or alcohols with zinc oxide.<sup>13</sup>

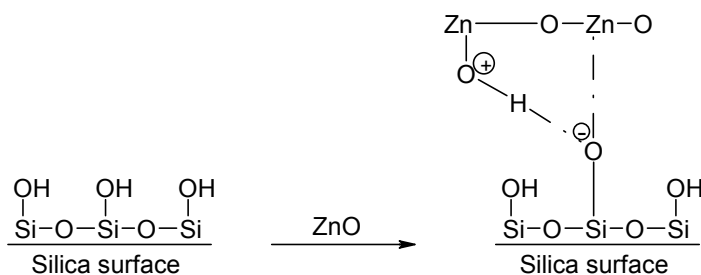


**Figure 4.11** Possible reaction of silica and zinc oxide.

From the contact angle experiments it is very clear that besides TESPT also zinc oxide converts the silica surface into a more hydrophobic surface. Especially when the zinc oxide is present in combination with stearic acid. In the silica containing tyre tread recipes zinc oxide and stearic acid are present during mixing of the silica and rubber. TESPT will compete with zinc oxide and stearic acid for the silanol groups on silica surface. As a conclusion, the interpretation by Thurn and Wolff<sup>5</sup> of the rapid decrease in compound viscosity, as reflected in mixing torque, as a catalytic effect of zinc oxide on the coupling reaction, must be questioned. All components make the surface more hydrophobic as can be seen from the contact angle measurements.

In order to properly understand the phenomenon of short scorch times for compounds with zinc oxide present in the internal mixer (Figure 4.3), it is important to note that for silica reinforced compounds the rheogram often shows two distinct regions, separated by a shoulder, sometimes even a plateau: Figure 4.12. It can easily be seen that this first increase, or the development of a shoulder or plateau in a rheogram results in short scorch times. This first increase in rheometer torque, can in principle be explained by: two different curing processes separated in time; or by filler flocculation.<sup>7</sup> Experiments with a “coupling agent” without a sulphur rank still showed a double increase in torque in the rheogram.<sup>7</sup> Therefore it is most common these days to interpret this first increase to be the result of filler flocculation, rather than two separate curing reactions. From literature it is known that even when a filler is well dispersed in a rubber, the filler tends to flocculate during post-mixing stages such as storage and vulcanisation. In this way the filler junction network will increase. This effect has been shown in the past by several authors for carbon black.<sup>14-16</sup>

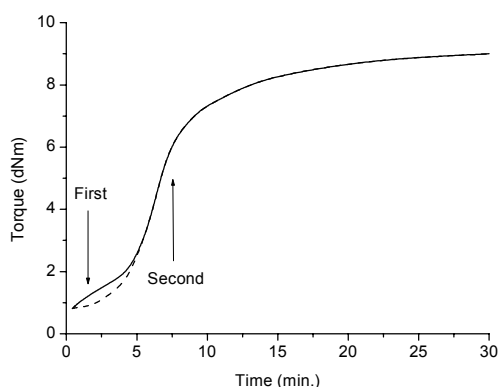


**Figure 4.12** Typical rheogram of a compound with short (—) and long (---) scorch time.

For filled rubbers, the surface energy between filler and polymer is always different. In the case of silica, being a hydrophilic filler, the difference in surface energy between silica and polymer is even more pronounced than for carbon black and polymer. On top of that, silica will tend to flocculate via hydrogen bonding, resulting in even stronger filler networks when compared to carbon black filler networks.<sup>16-18</sup> Surface treatment with coupling agents will lower the surface energy of silica.

The difference in surface energy between filler and polymer being the driving force, the flocculation process will also be influenced by the speed of diffusion of the filler aggregates. The main factor here is temperature, which will increase the diffusion rate.

The amount of surface treatment of the silica by the coupling agent therefore is the prime factor in lowering the difference in surface energy and decreasing the diffusion rate in filler flocculation.<sup>17</sup> At dump temperatures lower than 130°C, insufficient reaction between the coupling agent and silica is achieved, irrespective of presence or absence of zinc oxide in the internal mixer: the short scorch times are indicative of filler flocculation. In absence of zinc oxide and above 140°C sufficient coupling reaction takes place to suppress flocculation, as seen by the increased scorch time. In presence of zinc oxide in the internal mixer, apparently the proper reaction of the coupling is hampered. Dump temperatures of 160°C are necessary until the flocculation tendency will decrease to lead to long scorch times. From earlier work it is also known that at higher dump temperatures sulphur is donated towards the polymer or that the silica particle is coupled to the polymer.<sup>1</sup> This will result in a higher compound viscosity and consequently decrease the diffusion rate of the silica. The increase in scorch time in Figure 4.3 for the compound where zinc oxide is present in the mixer, therefore is most likely the result of donation of sulphur from the silane coupling agent to the polymer or coupling of the silica to the polymer. This raises the viscosity of the compound and consequently also suppresses flocculation.

An explanation for the trend of both lines in Figure 4.3 is now as follows. During mixing, zinc oxide reacts with the silica surface first and blocks in this way silanol groups on the silica, otherwise available for reaction with the silane coupling agent. When zinc oxide is omitted in the internal mixer and added later on the two-roll mill no reaction with the silica surface will take place. An optimal hydrophobation of the silica surface has already taken place in the internal mixer by the silane coupling agent. Therefore no filler flocculation will occur and as a result high scorch times are obtained.

The overall results presented in this paper strongly support the competing mechanism between zinc oxide and coupling agent for the silanol groups on the silica surface. It has become clear, that the reaction of the coupling agent with the silica is severely hampered by the presence of zinc oxide in the internal mixer. No signs have been found for a catalytic action of the zinc oxide on the coupling reaction, which contrary to earlier believes<sup>5</sup> would suggest, that it is better to leave out zinc oxide from the compound during mixing and add it at a later stage only, together with the curatives.

## 4.5 Conclusions

The dump temperature after mixing is a parameter of paramount importance in mixing silica and rubber in the presence of TESPT as a coupling agent. It turns out that the presence or absence of zinc oxide in the internal mixer is also an important additional factor. Presence of zinc oxide in the mixer provokes premature scorch of the compound, due to its

catalytic effect on the reaction between coupling agent and rubber. When mixing a compound without zinc oxide in the first mixing step, the scorch effect is largely reduced: it is possible to mix till higher dump temperatures without pre-scorch problems. A lower elastic modulus of the finally cured compound will be achieved when zinc oxide is omitted during the first step and added later on, together with the curatives, on the two-roll mill. An overall better hydrophobation of the silica surface is then obtained. This better hydrophobation is due to the fact that the coupling agent TESPT does not have to compete with zinc oxide over the silanol groups on the silica surface. Higher dump temperatures and/or absence of zinc oxide in the internal mixer result in longer scorch times due to a lower tendency of the silica filler to flocculate.

#### **4.6 References**

1. L.A.E.M. Reuvekamp, J.W. ten Brinke, P.J. van Swaaij, J.W.M. Noordermeer, *Kautsch. Gummi Kunstst.*, **55**, (2002), 41.
2. L.A.E.M. Reuvekamp, J.W. ten Brinke, P.J. van Swaaij, J.W.M. Noordermeer, *Rubber Chem. Technol.*, **75**, (2002), 187.
3. M.P. Wagner, *Rubber Chem. Technol.*, **49**, (1976), 703.
4. S.H. Laning, M.P. Wagner, J.W. Sellers, *J. Appl. Polymer Sci.*, **2**, (1959), 225.
5. F. Thurn and S. Wolff, *Kautsch. Gummi Kunstst.*, **28**, (1975), 733.
6. H.D. Luginsland, *Kautsch. Gummi Kunstst.*, **53**, (2000), 10.
7. J.W. Brinke ten, P.J. van Swaaij, L.A.E.M. Reuvekamp, J.W.M. Noordermeer, *Kautsch. Gummi Kunstst.*, **55**, (2002), 244.
8. J.W. Brinke ten, P.J. van Swaaij, L.A.E.M. Reuvekamp, J.W.M. Noordermeer, *Rubber Chem. Technol.* (in print).
9. W. Hofmann, *Rubber Technology Handbook*, Hanser Publishers, Munich (1996).
10. DIN 53 529 "Vulkametrie", Teil 2, (March 1983).
11. A. Hunsche, U. Görl, A. Muller, M. Knaack, Th. Gobel, *Kautsch. Gummi Kunstst.*, **50**, (1997), 881.
12. S. Wolff, *Kautsch. Gummi Kunstst.*, **30**, (1977), 516.
13. P.J. Nieuwenhuizen, Reedijk, J., Duin van, M., McGill, W.J., *Rubber Chem. Technol.*, **70**, (1997), 368.
14. G.G.A. Böhm, Nguyen, M.N., Cole, W.M., *Int. Rubber Conf.*, Kobe, Japan, Oct. 23-27, 1995.
15. G.G.A. Böhm, Nguyen, M.N., *J. Appl. Polymer Sci.*, **55**, (1995), 1041.
16. M.J. Wang, *Rubber Chem. Technol.*, **71**, (1998), 520.
17. C.-C. Lin, Hergenrother, W.L., Alexanian, E., Böhm, G.G.A, Rubber division, American Chemical Society, Cleveland, Ohio, USA, October 16-19, 2001.
18. T. Wang, Wang, M.-J., Shell, J., Tokita, N., *Kautsch. Gummi Kunstst.*, **53**, (2000), 497.



---

## Chapter 5

### *Influence of functional groups of TESPT coupling agent on dynamic and mechanical properties of tyre tread compounds*

---

Coupling agents with only one functional group i.e. only ethoxy groups or only sulphur group, resp. a coupling agent with only one ethoxy group on each side of the molecule, were synthesised. These coupling agents were used to study the effect of the different functional groups of TESPT on the vulcanised mechanical properties. In a tyre tread compound the usual coupling agent, e.g. TESPT was replaced by one of the synthesised coupling agents.

The experiments described in this chapter prove, that a proper balance in functionalities is required for a coupling agent to enhance the properties of silica-reinforced tyre tread compounds. TESPT proves to best comply with this balance, because it allows for the primary and secondary coupling reaction towards the silica via its tri-ethoxysilyl groups, resp. for a sulphur donation and a coupling reaction towards the rubber polymer via its sulphur moiety. Alternative coupling agents, allowing for only one of these functionalities lead to an inferior balance of properties. TESH with only a tri-ethoxysilyl group and no sulphur, does hydrophobise the silica and provides for a good dispersion like TESPT. However, the vulcanised properties are seriously poorer than those obtained with TESPT. On the other side TMeSPT, with only an active sulphur group, fails in its ability to properly disperse the silica and shows premature scorch effects at high mixer dump temperatures, like seen for TESPT. Again, the vulcanised properties are inferior to those obtained for TESPT. Adding two coupling agents, TESD and TMeSPT, with the functionalities independently divided over both, does result in a silica dispersion grossly comparable with the one obtained with TESPT. Also signs of scorch are seen at high mixer dump temperatures, like with TESPT. But still, the properties of vulcanised compounds are still grossly inferior to those obtained with TESPT.

A coupling agent with only one reactive ethoxy group attached to the silicium atom vs. three for TESPT, performs surprisingly well. This coupling agent can only perform the primary reaction with the silica, which leads to a very quick equilibrium during mixing and consequently low mixer torques. It comes closest to TESPT in vulcanised compound properties, particularly the  $\tan \delta$ , representative for tyre rolling resistance. Only the tensile strength is lower than the one achieved with TESPT.

Based on all the results a model is proposed, whereby TESPT releases sulphur to the compound in the vicinity of the silica particle during mixing or early stages of vulcanisation, thereby causing an crosslinked shell, trapping the silica particle in the rubber matrix. Later on, during vulcanisation, TESPT provides for chemical bridge formation between the silica particles and the rubber polymer.

## 5.1 Introduction

Bifunctional organosilanes, particularly bis-(triethoxysilylpropyl)tetrasulphide (TESPT), are very efficient silica-rubber coupling agents, as they can link non-interacting phases.<sup>1,2</sup> Especially in tyre tread compounds the combination of precipitated silica and sulphur functional organosilanes is used to reduce the rolling resistance and enhance wet traction.

The coupling by TESPT can be divided into two separate reactions. First, the ethoxy groups react with the silanol groups on the silica surface during mixing. Second, the tetrasulphide group reacts with the polymer under curing conditions and rubber to filler bonds are formed.<sup>2-4</sup> The reaction of the ethoxy groups of TESPT can in turn be divided into two steps. Reaction of the first ethoxy group of the coupling agent with silanol group on the silica surface: Primary reaction. Second, the remaining ethoxy groups of adjacent TESPT molecules already bound to the silica surface react with each other: Secondary reaction.<sup>5</sup>

The reactivity of the tetrasulphide group has been studied extensively by Görl et al.<sup>6,7</sup> The link of the TESPT polysulphide group was assumed to be brought about by the intermediate addition of accelerators. This reaction would subsequently lead to a covalent bond between rubber and filler, as mentioned before.

All reactions are depending on the temperature history during mixing. The primary reaction of the coupling agent during mixing takes place at a relatively slow rate at the moderate temperatures of for example 120°C, commonly employed as dump temperatures after mixing. Higher batch temperatures have to be used to achieve shorter reaction times. At such elevated temperatures, above 150°C, the reaction between the coupling agent and the rubber may occur, resulting in the problem of scorch.<sup>8-10</sup>

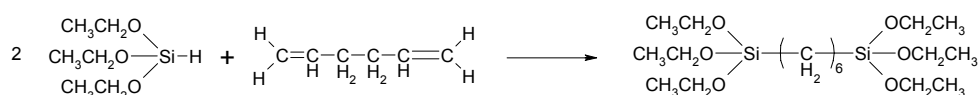
The present chapter describes investigations, carried out to study the effect of the different functional groups of TESPT on the various reactions mentioned before. For that purpose, coupling agents were synthesised with different functional groups. All compounds were mixed at different rotor speeds to achieve different dump temperatures. From literature it is known that TESPT can donate sulphur to the compound at high dump temperatures leading to scorch.<sup>9,11</sup> Therefore, a coupling agent without sulphur was synthesised to investigate if at high dump temperatures the scorch is indeed caused by the sulphur moiety in TESPT. Another coupling agent, without ethoxy groups but with a sulphur moiety, was synthesised to investigate if a silica particle will really be bound to the rubber during the vulcanisation procedure. The latter coupling agent can only donate sulphur to the rubber and is not able to couple the silica to the rubber. Further, as mentioned before, the coupling reaction of the ethoxy groups of TESPT can be divided in two reactions: primary and secondary. A coupling agent with only one ethoxy group on each side of the molecule was synthesised, which consequently cannot involve in the secondary reaction.<sup>12</sup> This allows us to investigate if the secondary reaction has an influence on the processing and material properties of a tyre tread compound.

## 5.2 Experimental

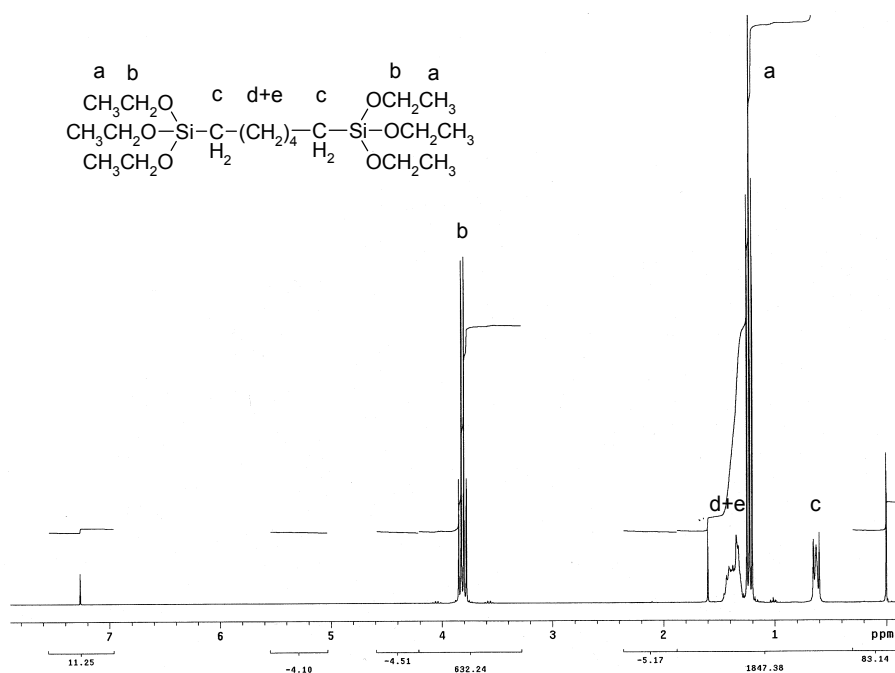
### 5.2.1 Synthesis and characterisation

#### 1,6-bis-(triethoxysilyl)hexane (TESH)

1,6-bis-(triethoxysilyl)hexane was synthesised through hydrosilation of 1,5-hexadiene, Scheme 5.1. A mixture of triethoxysilane, 1,5-hexadiene and a platinum-cyclovinylmethylsiloxane catalyst was stirred in toluene under a dry nitrogen flow for 48 hours. Vacuum distillation resulted in an 85% yield of colourless product with a boiling temperature of 150°C/0.07 mbar. The index of refraction of the product at 25°C was 1.4181. The product's structure was determined with the aid of <sup>1</sup>H-NMR, Figure 5.1. Peak assignments are listed in Table 5.1.



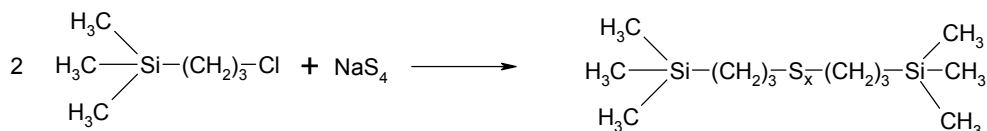
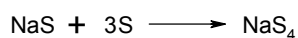
**Scheme 5.1** Formation of 1,6-bis-(triethoxysilyl)hexane.



**Figure 5.1** <sup>1</sup>H-NMR spectrum of 1,6-bis-(triethoxysilyl)hexane.

**Table 5.1** Chemical shifts  $\delta$  of protons of 1,6-bis-(triethoxysilyl)hexane.

Peak	Chemical shift, (ppm)	Type	Description
a	1.22	Triplet	CH <sub>3</sub>
b	3.82	Quartet	CH <sub>2</sub> , alkoxy side
c	0.62	Triplet	CH <sub>2</sub> , siloxane side
d	1.38	Quintet	CH <sub>2</sub> , siloxane side
e	1.44	Quintet	CH <sub>2</sub>

**Bis-(trimethylsilylpropyl)tetrasulphide (TMeSPT)****Scheme 5.2** Formation of bis-(trimethylsilylpropyl)tetrasulphide.

Bis-(trimethylsilylpropyl)tetrasulphide was synthesised in absolute ethanol under a nitrogen atmosphere by refluxing 3-chloropropyl trimethylsilane and sodiumsulphide, Scheme 5.2. After 13 hours of refluxing a yellow suspension was obtained. This suspension was filtered, after which ethanol was removed from the filtrate with the rotational evaporator, leading to a dark red suspension. The red suspension was diluted with diethylether. The ether layer was extracted 3 times with 10 ml of water to remove the sodiumsulphide salt. After this extraction the layer of ether was coloured yellow and the water was coloured red. The ether was dried with MgSO<sub>4</sub>, filtered followed by ether removal in the rotational evaporator which gave a yield of 82% of a gold/yellow clear liquid. The index of refraction of the product at 25°C was 1.5239. The product's structure was determined with the aid of <sup>1</sup>H-NMR, Figure 5.2. Peak assignments are listed in Table 5.2. The average sulphur rank was 3.89 as determined by elemental analysis, given in Table 5.3.

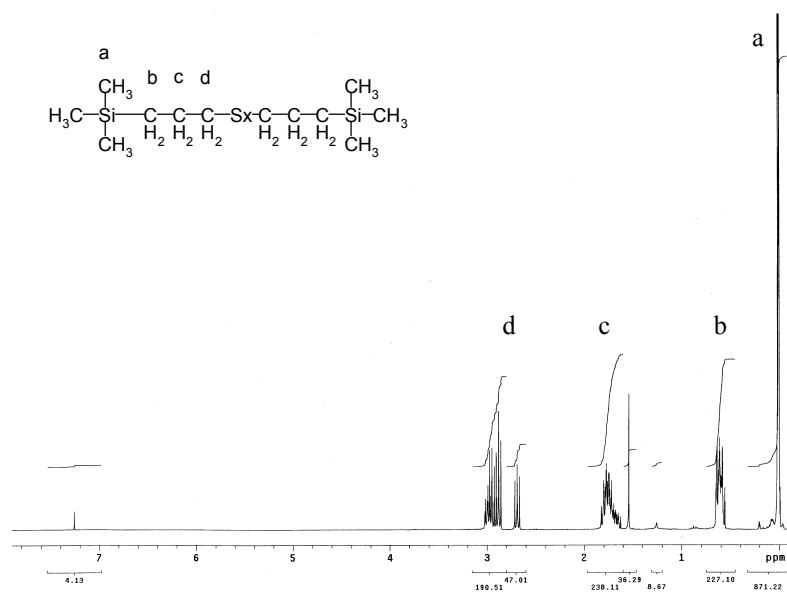


**Figure 5.2**  $^1\text{H}$ -NMR spectrum of bis-(trimethylsilylpropyl)tetrasulphide.

**Table 5.2** Chemical shifts  $\delta$  of protons of bis-(trimethylsilylpropyl)tetrasulphide.

Peak	Chemical shift, (ppm)	Type	Description
A	0.12	Singlet	$\text{CH}_3$
B	0.62	Triplet	$\text{CH}_2$ , siloxane side
C	1.78	Quintet	$\text{CH}_2$
D	2.98	Triplet	$\text{CH}_2$ , sulphur side

**Table 5.3** Elemental analysis of bis-(trimethylsilylpropyl)tetrasulphide.

Element	Mass %	Mass % theoretical
C	$40.41 \pm 0.11$	40.4
H	$8.45 \pm 0.14$	8.4
S	$35.46 \pm 0.11$	35.5

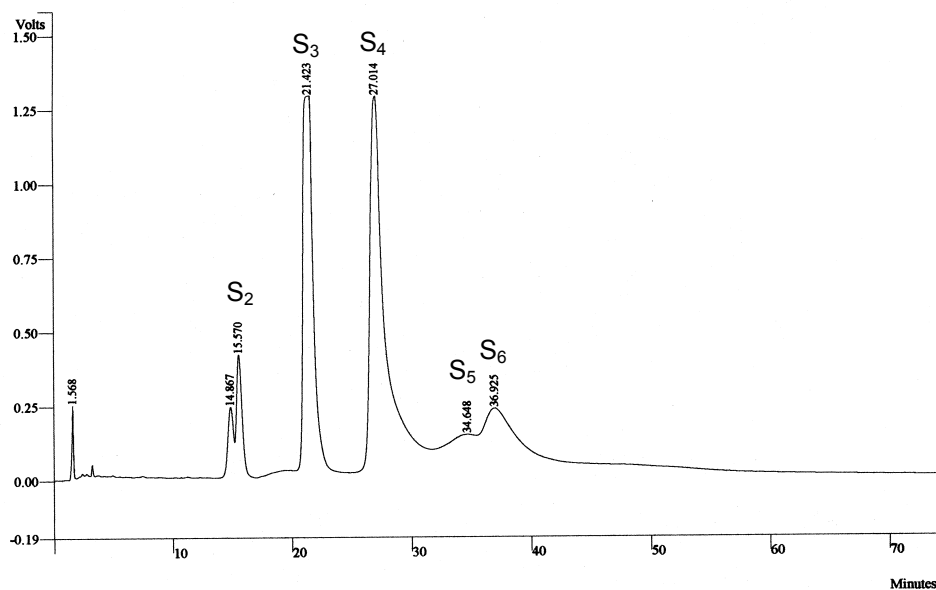


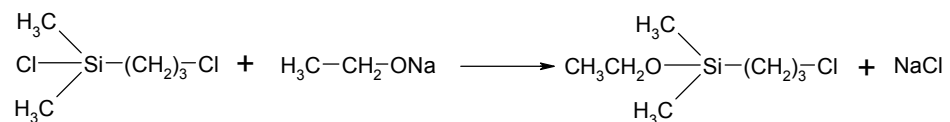
**Figure 5.3** HPLC chromatogram of bis-(trimethylsilylpropyl)tetrasulphide.

In Figure 5.2 several signals are visible at a chemical shift of 3 ppm. These signals are from the CH<sub>2</sub>-group next to a sulphur atom. The different signals indicate that the amount of sulphur atoms next to the CH<sub>2</sub>-group is different. Figure 5.3 shows the sulphur rank distribution of bis-(trimethylsilylpropyl)tetrasulphide as determined with HPLC according to the conditions in Table 4.1.<sup>10</sup> The different sulphur ranks are indicated in the figure. There is still free sulphur present in the mixture, but this peak is hidden under the tetrasulphide peak; therefore this peak has a slight tail.

### Bis-(dimethylethoxysilylpropyl)tetrasulphide (DMESPT)

Bis-(dimethylethoxysilylpropyl)tetrasulphide was synthesised by a two step synthesis. During the first step 3-chloropropyl dimethylethoxysilane was synthesised.

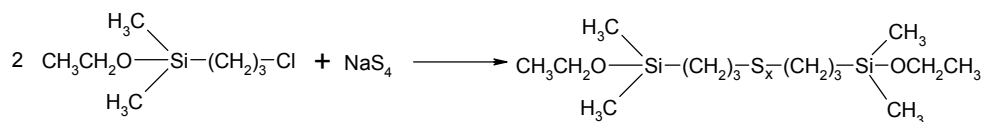
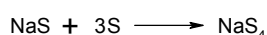
#### *3-chloropropyl dimethylethoxysilane*



**Scheme 5.3** Formation of 3-chloropropyl dimethylethoxysilane.

For the synthesis of 3-chloropropyl dimethylethoxysilane, a mixture of 3-chloropropyl dimethylchlorosilane and sodium ethanoate in 50 ml of ethanol was stirred under a dry nitrogen flow for 15 hours, Scheme 5.3. After the reaction the mixture was filtrated and the ethanol was removed with the aid of a rotational evaporator. The raw product, which had a yield of 86%, was purified via fractional vacuum distillation with a 20 cm vingreux column and a perkinson triangle. The distillation resulted in 72% of colourless product with a boiling temperature of 56-57°C/0.13 mbar. The product's structure was determined with the aid of <sup>1</sup>H-NMR (300 MHz, CDCl<sub>3</sub>) δ 3.65 (q, 2H), 3.5 (t, 2H), 1.80 (m, 2H), 1.18 (t, 3H), 0.68 (m, 2H), 0.10 (s, 6H).

***Bis-(dimethylethoxysilylpropyl)tetrasulphide***



**Scheme 5.4** Formation of bis-(dimethylethoxysilylpropyl)tetrasulphide.

Bis-(dimethylethoxysilylpropyl)tetrasulphide was synthesised in absolute ethanol in a nitrogen atmosphere by refluxing 3-chloropropyl dimethylethoxysilane and sodiumsulphide, Scheme 5.4. After 13 hours of refluxing a yellow suspension was obtained. This suspension was filtrated and ethanol was removed from the filtrate with the rotational evaporator which lead to a dark red suspension. The red suspension was diluted with diethylether. The ether layer was extracted 3 times with 10 ml of water to remove the sodiumsulphide salt. After this extraction the layer of ether was coloured yellow and the water was coloured red. The ether was dried with MgSO<sub>4</sub>, filtrated followed by ether removal in the rotational evaporator, which gave a yield of 88% of a gold/yellow clear liquid. The index of refraction of the product at 25°C was 1.5119. The product's structure was determined with the aid of <sup>1</sup>H-NMR, Figure 5.4. Peak assignments are listed in Table 5.4. The average sulphur rank was 3.89 as determined by elemental analysis, given in Table 5.5.

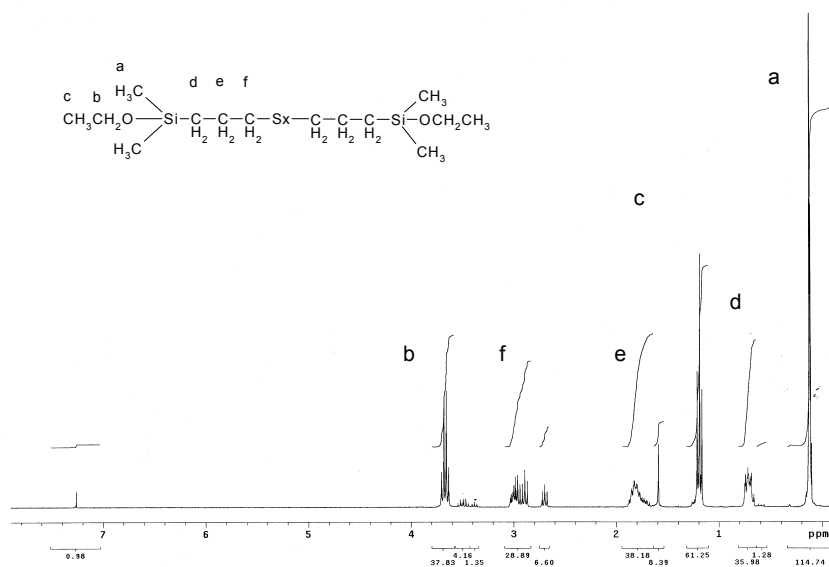


**Figure 5.4**  $^1\text{H-NMR}$  spectrum of bis-(dimethylethoxysilylpropyl)tetrasulphide.

**Table 5.4** Chemical shifts  $\delta$  of protons of bis-(dimethylethoxysilylpropyl)tetrasulphide.

Peak	Chemical shift, (ppm)	Type	Description
a	0.12	Singlet	$\text{CH}_3$
b	3.71	Quartet	$\text{CH}_2$ , alkoxy side
c	1.22	Triplet	$\text{CH}_3$
d	0.72	Triplet	$\text{CH}_2$ , siloxane side
e	1.82	Quintet	$\text{CH}_2$
f	3.00	Triplet	$\text{CH}_2$ , sulphur side

**Table 5.5** Elemental analysis of bis-(dimethylethoxysilylpropyl)tetrasulphide.

Element	Mass %	Mass % theoretical
C	$40.47 \pm 0.11$	40.5
H	$8.17 \pm 0.14$	8.2
S	$30.08 \pm 0.11$	30.0

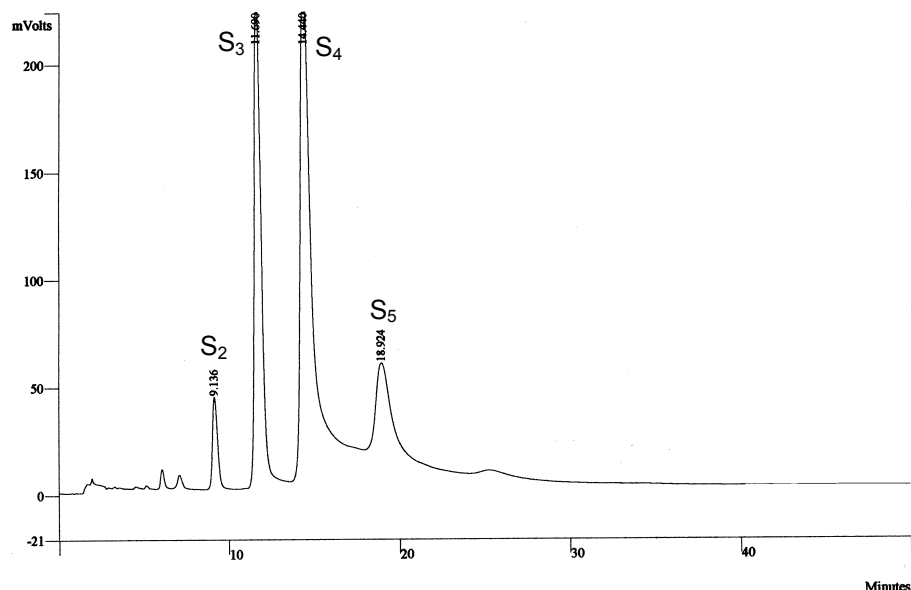


**Figure 5.5** HPLC chromatogram of bis-(dimethylethoxysilylpropyl)tetrasulphide.

In Figure 5.4 several signals are visible at a chemical shift of 3 ppm, these signals are from the CH<sub>2</sub>-group next to a sulphur atom. The different signals indicate that the amount of sulphur atoms next to the CH<sub>2</sub>-group is different. Figure 5.5 shows the sulphur rank distribution of bis-(dimethylethoxysilylpropyl)tetrasulphide as determined with HPLC according to the conditions in Table 4.1.<sup>10</sup> The different sulphur ranks are indicated in the figure. There is still free sulphur present in the mixture, but this peak is hidden under the tetrasulphide peak, therefore the peak has a slight tail.

## 5.2.2 Compound recipes

The experiments were based on a reference tyre tread composition which is shown in Table 5.6 and represent a “green tyre” recipe in accordance with the Michelin patent.<sup>13</sup> As the molar masses of the various coupling agents described in this chapter differ from that of TESPT, the quantities of the other coupling agents were adjusted to represent equimolar quantities. In the case of compounds containing both bis-(triethoxysilyl)decane (TESD) and TMeSPT, the TESD was adjusted to an equimolar quantity on basis of the ethoxy groups present in TESPT; the TMeSPT was adjusted to an equimolar quantity on basis of the sulphur moiety present in TESPT.

With TESPT as reference, TMeSPT shares the sulphur moiety with TESPT, but cannot couple to the silica; TESH can couple to the silica, but misses the sulphur group; TESD can couple to silica, and the sulphur moiety has been replaced by four methylene groups. DMESPT can couple to silica and the rubber but cannot undergo the secondary reaction. The compounds were mixed and characterised according to the experimental conditions described in Chapter 3.

**Table 5.6** Tyre tread recipe (phr) with the various coupling agents investigated.

Component	Type of coupling agent				
	TESH	TMeSPT	TESD + TMeSPT	DMESPT	TESPT
S-SBR (Buna <sup>®</sup> VSL 5025-1 HM) <sup>a</sup>	75	75	75	75	75
BR (Kosyn <sup>®</sup> KBR 01)	25	25	25	25	25
Silica (Zeosil <sup>®</sup> 1165 MP)	80	80	80	80	80
<b>Coupling agent</b>	<b>5.4</b>	<b>4.7</b>	<b>6.1 + 4.7</b>	<b>5.4</b>	<b>7</b>
Aromatic oil (Enerflex <sup>®</sup> 75)	32.5	32.5	32.5	32.5	32.5
ZnO	2.5	2.5	2.5	2.5	2.5
Stearic acid	2.5	2.5	2.5	2.5	2.5
Sulphur	1.4	1.4	1.4	1.4	1.4
CBS (Santocure <sup>®</sup> -GRS-2MM)	1.7	1.7	1.7	1.7	1.7
DPG (Perkacit <sup>®</sup> -PDR)	2	2	2	2	2
<b>Total</b>	<b>228.0</b>	<b>227.3</b>	<b>233.4</b>	<b>228.0</b>	<b>229.6</b>

<sup>a</sup> vinyl content is 50%, styrene content is 25% and the oil content is 37.5 phr.

## 5.3 Results

### 5.3.1 Effect of bis-(triethoxysilyl)hexane on material properties

In order to investigate the scorch effect of TESPT as described in Chapter 3, in greater detail, this coupling agent was replaced by 1,6-bis-(triethoxysilyl)hexane (TESH), unable to react with the rubber due to the absence of a sulphur moiety. TESH was mixed in the Brabender plasticorder at different rotor speeds to achieve different dump temperatures. The mixing curves are given in Figure 5.6. The TESPT containing compound is also given in this figure as a reference. All the mixing curves for TESH containing compounds are lower in end torque than for TESPT, indicating a lower compound viscosity at the end of the mixing cycle. This is a first indication of a good hydrophobation of the silica particles and therefore a proper dispersion of the silica filler in the rubber matrix.<sup>14</sup>

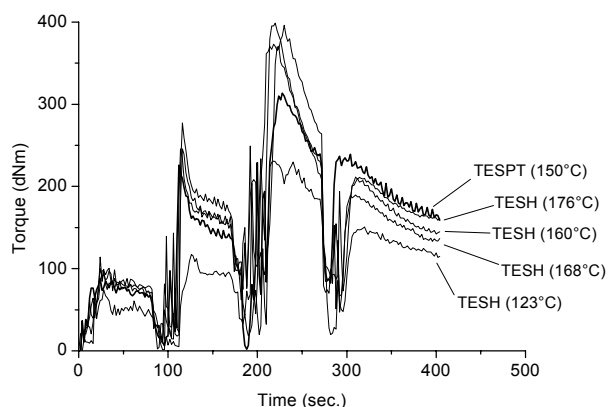


**Figure 5.6** Mixing curves of TESH– resp. TESPT– containing compounds with various dump temperatures indicated.

The effect of the good hydrophobation using TESH is also visible in the Payne effect. Figure 5.7 A shows the  $G'$  at 0.56% strain for different dump temperatures. The TESPT containing compounds are plotted in this figure as reference.<sup>10</sup> It can be seen, that the  $G'$  at 0.56% strain is decreasing with increasing dump temperatures for both coupling agents to more or less the same level at high dump temperatures. TESH is improving the dispersion of the silica filler particles with increasing dump temperature to a similar level as TESPT does.

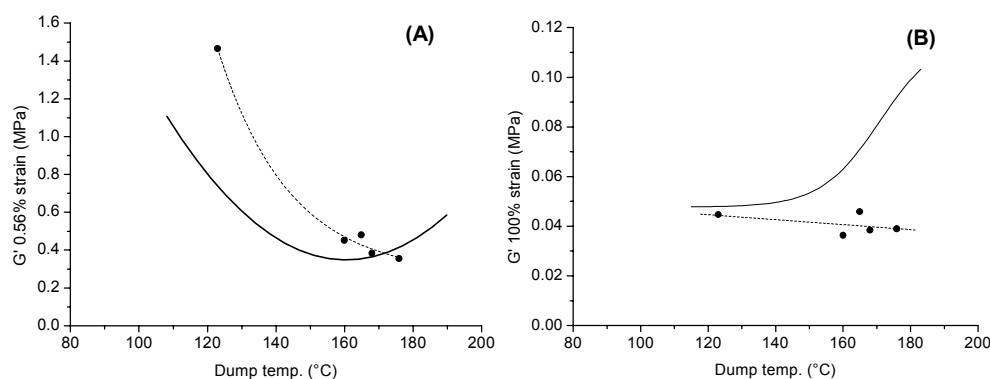


**Figure 5.7** Influence of dump temperature on the storage modulus at 0.56% strain (A) and 100% strain (B); (—), TESPT; (●), TESH.

On the high strain side, 100% strain, the filler-filler interactions are broken and network-effects prevail: Figure 5.7 B. The TESPT-containing compound shows a strong increase in  $G'$  at dump temperatures above 150°C. This effect is commonly interpreted as premature scorch of the compound due to: either donation of some sort of reactive, radical form of sulphur to the compound<sup>15</sup>; or the coupling reaction of the sulphur moiety of the TESPT, already coupled to the silica, to the rubber molecules. Both lead to some sort of crosslinking and increase in  $G'$  as result. It is clear that the sulphur group in TESPT is the reactive species towards the rubber matrix, because the  $G'$  at 100% strain for TESH remains more or less constant at a low level.

The tensile properties of TESH, in comparison with TESPT containing compounds after vulcanisation are plotted in graphs 5.8 A to D. Figure 5.8 A shows the elastic modulus of a TESH containing compound. The trend of the TESH containing compound is opposite to TESPT, the elastic modulus is increasing with increasing dump temperature for TESH, while it decreases for TESPT. The effect of the sulphur moiety in TESPT vs. TESH, is also very clear in the graph of the 300% modulus vs. dump temperature: Figure 5.8 B. In this figure the 300% modulus of the TESPT containing compound, after vulcanisation, increases at dump temperatures above 150°C, whereas the 300% modulus for TESH remains at a low level. This trend is similar to the  $G'$  at 100% strain: Figure 5.7 B. In Figure 5.8 C the tensile strength of vulcanised compounds is plotted against dump temperature. The main difference between the two coupling agents is, that for TESPT higher values of tensile strength are obtained when compared to TESH. Correspondingly, the elongation at break is higher for the TESH containing compounds as compared to the TESPT containing compounds: Figure 5.8 D.

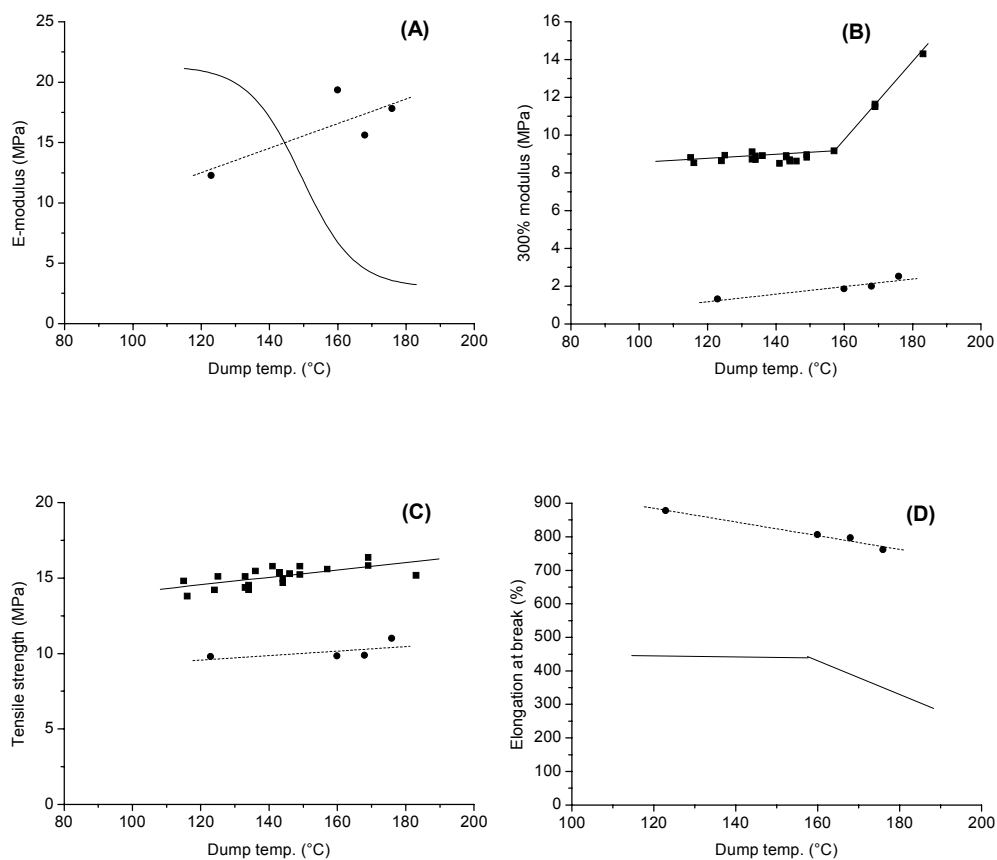


**Figure 5.8** Tensile properties as a function of dump temperature; (A) Elastic modulus, (B) 300% modulus, (C) Tensile strength, (D) Elongation at break; (—), TESPT, (●), TESH.

### 5.3.2 Effect of bis-(trimethylsilylpropyl)tetrasulphide on material properties

Bis-(trimethylsilylpropyl)tetrasulphide (TMeSPT) was mixed into the tyre tread compound to study the effect of the sulphur group of TESPT on the rubber matrix. TMeSPT cannot react with the silica surface, but contains a sulphur moiety to react with the rubber polymer matrix. Figure 5.9 A shows the  $G'$  at 0.56% strain for various dump temperatures, as a measure of filler-filler interaction. This shows, that the TMeSPT cannot react with the silica surface: the values of  $G'$  at the various dump temperatures are all much higher than those obtained for TESPT as coupling agent. Mixing of TMeSPT in the tyre tread compound appears equal to mixing silica without a coupling agent: Figure 3.1.<sup>10</sup> The silica filler particles are poorly dispersed in the rubber matrix and contribute to a high Payne effect.

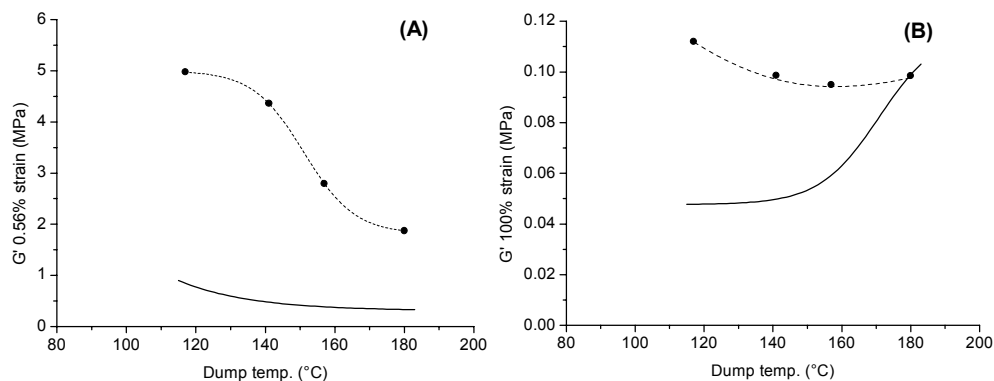


**Figure 5.9** Influence of dump temperature on the storage modulus at 0.56% strain (A) and 100% strain (B); (—), TESPT; (●), TMeSPT.

In  $G'$  at 100% strain the effect of the sulphur group of the coupling agent is visible for TESPT as an increase above 150°C dump temperature, see before: Figure 5.9 B. For TMeSPT this effect is not clear, it shows a small increase at best. The strong filler-filler network in presence of TMeSPT apparently prevails over the potential sulphur donation or scorch effect of TMeSPT.

Another method of measuring the reactivity of the sulphur group in TMeSPT is by a temperature sweep in the RPA 2000, as shown in Figure 5.10. The increase in  $G'$  starts for TMeSPT, like for TESPT, at the same temperature: approximately 160°C. In the case of TMeSPT the  $G'$  lies at an overall higher level, caused by the poor dispersion of the silica, as mentioned before.

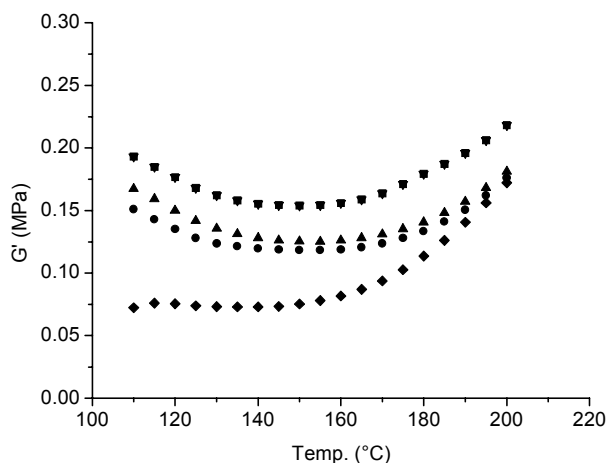


**Figure 5.10** Temperature sweep measurements for TMeSPT containing compounds with various dump temperatures; (■), 117°C; (▼), 141°C; (●), 157°C; (▲), 181°C and for TESPT (◆) with a dump temperature of 150°C.

The tensile properties of TMeSPT containing compounds, in comparison with TESPT, after vulcanisation are plotted in graphs 5.11 A to D. Figure 5.11 A shows the

elastic modulus of the TMeSPT containing compounds and is similar to TESPT. At dump temperatures above 160°C a somewhat higher value for the elastic modulus is obtained for TMeSPT. In Figure 5.11 B the 300% modulus is plotted against dump temperature. The values for TMeSPT are in general lower than for TESPT. At high dump temperature there is only a slight increase in the 300% modulus, in comparison with TESPT. The tensile strength is again lower for TMeSPT containing compounds than for TESPT, for the whole dump temperature range. The elongation at break is decreasing at higher dump temperatures for TMeSPT as well as for TESPT: Figure 5.11 D. The elongation at break is overall higher for TMeSPT than for TESPT.

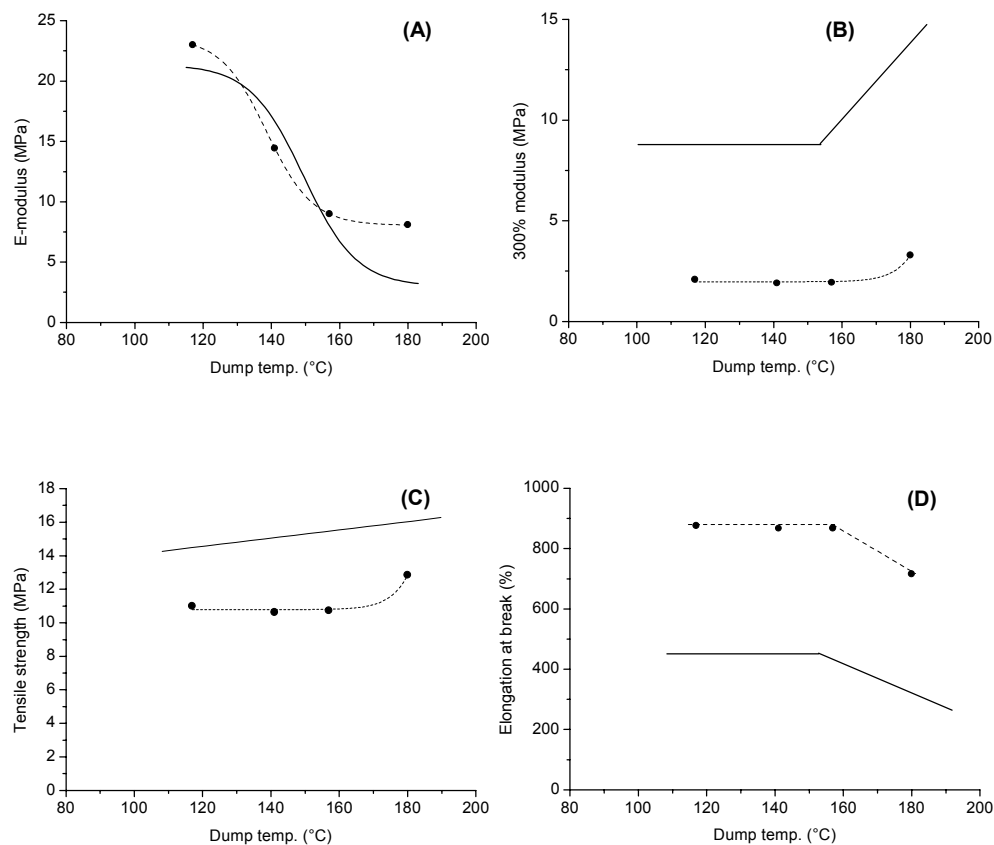


**Figure 5.11** Tensile properties as a function of dump temperature; (A) Elastic modulus, (B) 300% modulus, (C) Tensile strength, (D) Elongation at break; (—), TESPT; (●), TMeSPT.

**Table 5.7** Effect of dump temperature on  $\tan \delta$ .

Dump temp. (°C)	Tan $\delta$
117	0.198
141	0.213
157	0.183
181	0.154

The  $\tan \delta$  of TMeSPT containing compounds are listed in Table 5.7. With increasing dump temperature  $\tan \delta$  decreases. The value at 181°C is comparable with that for a TESPT containing compound: Figure 3.9. The values at the other dump temperatures are much higher when compared to TESPT.

### 5.3.3 Effect of a combination of bis-(trimethylsilylpropyl)tetrasulphide and bis-(triethoxysilyl)decane on material properties

Another way to mimic the reactions of TESPT with the silica surface on the one hand and the rubber polymer on the other hand, is to use two separate coupling agents, each capable of performing only one of the two functions. A possible way to do this is by using TMeSPT, as coupling agent to couple to the rubber polymer, and TESD to hydrophobise the silica surface as described in 5.3.1. For the present experiment bis-(triethoxysilyl)decane (TESD) was used, because from literature it was known that this coupling agent gives better results regarding the hydrophobation of the silica surface than TESH.<sup>14</sup> In this way the silica will be very well dispersed, although still no true coupling between the silica and the rubber can take place, because the two functionalities of TESPT are now divided over two “coupling agents”. An equal molar amount of TESD with regard to the amount of ethoxy groups was added to the compound. The same was done for TMeSPT for the amount of sulphur present in the coupling agent.

Due to the presence of TESD, low values for  $G'$  at 0.56% strain were obtained, indicating a good dispersion of the silica: Figure 5.12 A. Because of the good dispersion of the silica filler, the effect of sulphur donation by the other coupling agent TMeSPT is now slightly visible in the  $G'$  at 100% strain: Figure 5.12 B. The  $G'$  at 100% strain increases somewhat at dump temperatures above 150°C, similar to the TESPT data. A problem in this context is, that the hydrophobation by TESD is so good and the resulting viscosities of the compounds so low, that it is virtually impossible to reach dump temperatures well above 160°C. Therefore, the effect of scorch is not very well visible. TMeSPT cannot react with the silica and consequently, the increase in the  $G'$  at 100% strain must be the result of sulphur donation or coupling to the rubber matrix.

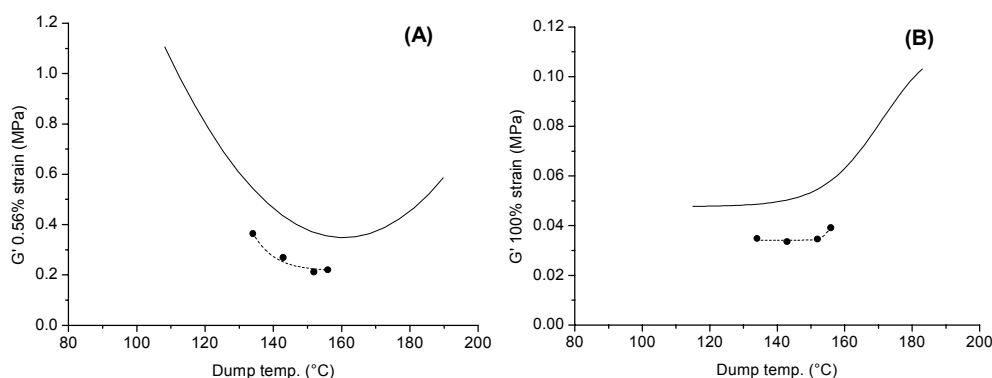


**Figure 5.12** Influence of dump temperature on the storage modulus at 0.56% strain (A) and 100% strain (B); (—), TESPT; (●), TESD + TMeSPT containing compounds.

Another indication that sulphur donation and coupling to the rubber matrix is taking place is observed in the Mooney viscosity of the compounds. The Mooney viscosity increases at high dump temperature, as a result of some crosslinks formed in the rubber matrix, Figure 5.13. A similar trend was observed for TESPT: at high dump temperatures a high Mooney viscosity was obtained, caused by the crosslinks created in the compound by sulphur donation.

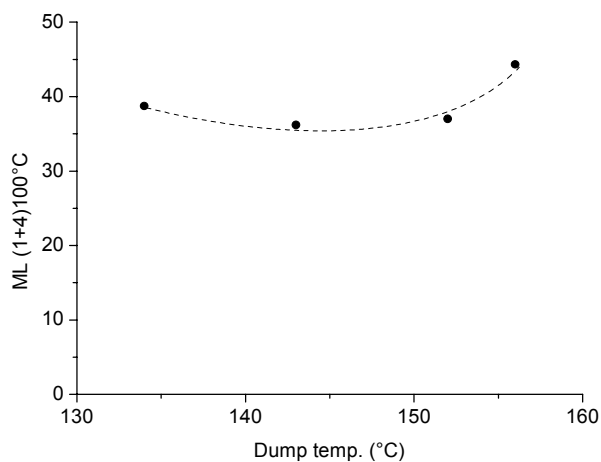


**Figure 5.13** Mooney viscosity as a function of the dump temperature; (●), TESD + TMeSPT containing compounds.

The tensile properties of a TESD + TMeSPT containing compound, in comparison with TESPT, after vulcanisation are plotted in graphs 5.14 A to D. Figure 5.14 A shows that the elastic modulus is lower for the TESD + TMeSPT containing compound, compared to TESPT. Figure 5.14 B shows the 300% modulus versus dump temperature. The values for TESD + TMeSPT are in general far lower than the values for TESPT. The 300% modulus is slightly increasing with increasing dump temperature. The tensile strength for TESD + TMeSPT shows the same trend as TESPT: Figure 5.14 C, but at a lower level: it increases with dump temperature. Figure 5.14 D shows the elongation at break as a function of the dump temperature: the elongation at break of TESD + TMeSPT containing compounds is higher than for TESPT. The elongation at break decreases with dump temperature.

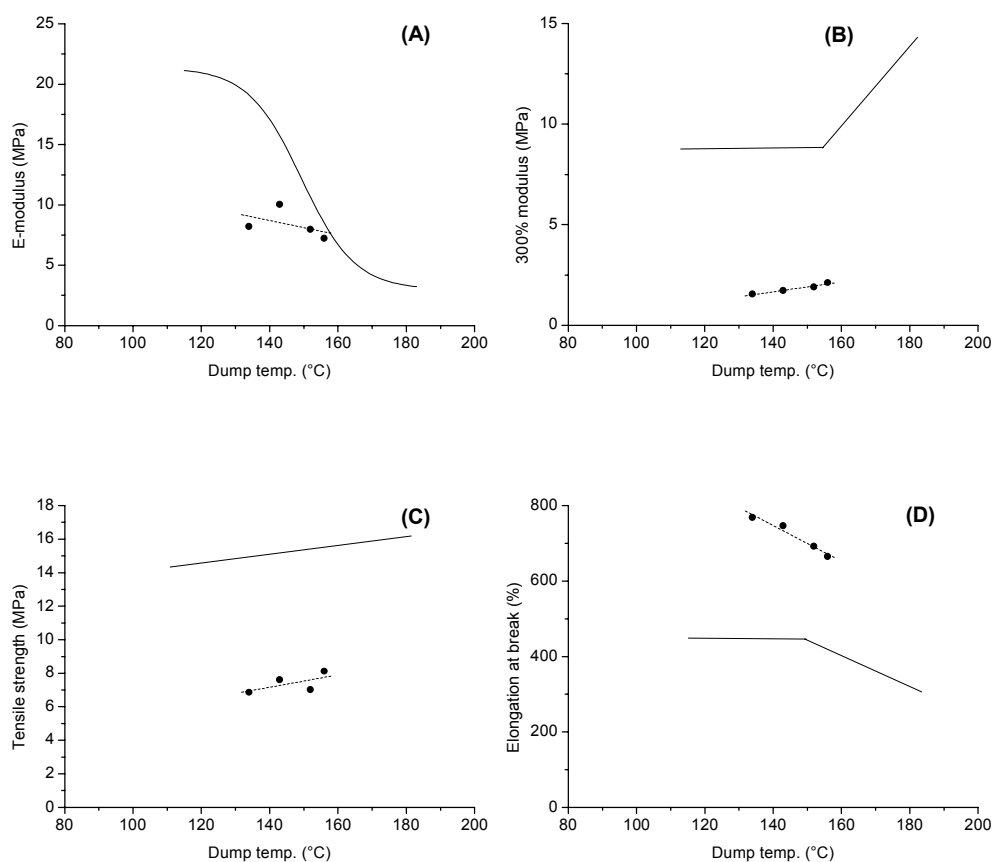


**Figure 5.14** Tensile properties as a function of dump temperature; (A) Elastic modulus, (B) 300% modulus, (C) Tensile strength, (D) Elongation at break; (—), TESPT; (●), TESD + TMeSPT.

**Table 5.8** Effect of dump temperature on  $\tan \delta$ .

Dump temp. (°C)	Tan $\delta$
134	0.174
143	0.186
152	0.183
156	0.211

The  $\tan \delta$  values of TESD + TMeSPT containing compounds are listed in Table 5.8. With increasing dump temperature  $\tan \delta$  increases. The values of  $\tan \delta$  are higher in comparison with TESPT: Figure 3.9.

### 5.3.4 Effect of bis-(dimethylethoxysilylpropyl)tetrasulphide on material properties

The tread compound with bis-(dimethylethoxysilylpropyl)tetrasulphide (DMESPT) as coupling agent was mixed at different rotor speeds to achieve different dump temperatures. Figure 5.15 shows the mixing curves for DMESPT containing compounds with dump temperature as parameter and for TESPT at 150°C dump temperature as a reference. This figure shows that DMESPT also brings about lower mixing torques than TESPT, like TESH did.

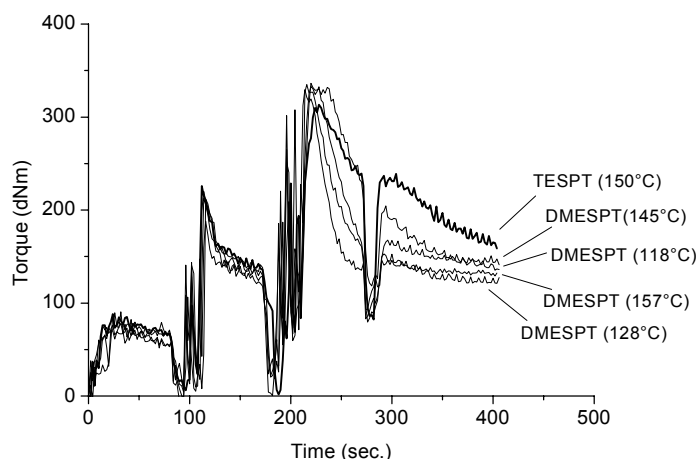


**Figure 5.15** Mixing curves of DMESPT– resp. TESPT– containing compounds with various dump temperatures indicated.

After adding the second batch of silica and silane at 170 seconds (Table 3.2) the decrease in torque for DMESPT containing compounds is more pronounced in comparison to TESPT. After 300 seconds of mixing, the torque curve becomes flat for DMESPT containing compounds; an indication that the primary reaction is finished. Implicitly, this indicates that the more gradual decrease in mixer torque seen with TESPT is due to the secondary reaction, known to be much slower and needing high temperatures.<sup>5</sup> By the Payne effect measured with a strain sweep, it turns out that for DMESPT (dump temp. of 157°C)  $G'$  at 0.56% strain after the first mixing step is already lower than for TESPT after the second mixing step: appr. 0.30 MPa for DMESPT versus appr. 0.35 MPa for TESPT.

Figure 5.16 A shows  $G'$  at 0.56% strain after the second mixing step of 5 minutes.  $G'$  at 0.56% strain is lower for DMESPT than for TESPT and any of the other systems investigated. In line with the foregoing, the lowest  $G'$  is interpreted as the result of the best dispersion of the silica filler particles in the rubber compound.

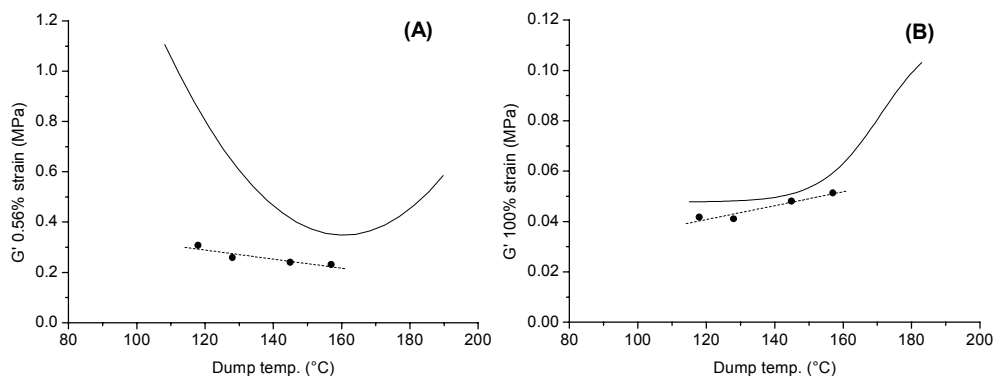


**Figure 5.16** Influence of dump temperature on the storage modulus at 0.56% strain (A) and 100% strain (B); (—), TESPT; (●), DMESPT.

For  $G'$  at 100% strain similar trends are visible between the DMESPT and TESPT, Figure 5.16 B. In the case of DMESPT containing compounds it is difficult to achieve a high dump temperature, because of the fast decrease of the mixing torque and consequent low energy dissipation in the compounds, like seen before in paragraph 5.3.3. This lower mixing torque consequently restricts the experiments to relatively low dump temperatures.

As an alternative method to sense the scorch sensitivity of the sulphur moiety in DMESPT, temperature sweeps were performed on the compounds in the RPA 2000: Figure 5.17. The lines for the temperature sweep for DMESPT and TESPT containing compounds show the same trend. In all cases the increase in  $G'$  starts at 160°C. This might have been expected, as the result of the same sulphur rank for both coupling agents: 3.89 for DMESPT and 3.83 for TESPT.

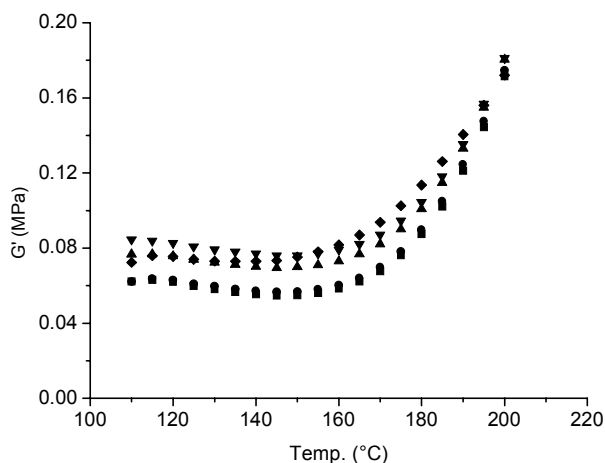


**Figure 5.17** Temperature sweep measurements for DMESPT containing compounds with various dump temperatures; (■), 118°C; (●), 128°C; (▲), 145°C; (▼), 157°C and for TESPT (◆) with a dump temperature of 150°C.

After the second mixing step, the curing additives were added on the two roll mill. The curing rheometer curves of the DMESPT and TESPT containing compounds for different dump temperatures are depicted in Figure 5.18. For DMESPT similar results are observed when compared to TESPT, higher dump temperature leads to a lower rheometer torque. At the beginning of the rheometer curve a small increase in torque is visible which is decreasing with increasing dump temperature. This effect is caused by filler flocculation, as already explained in Chapter 4. The rheometer curve for the DMESPT containing compound with a dump temperature of 157°C nearly coincides with the curve for TESPT. The only difference is that DMESPT containing compound cures slightly faster than for TESPT.

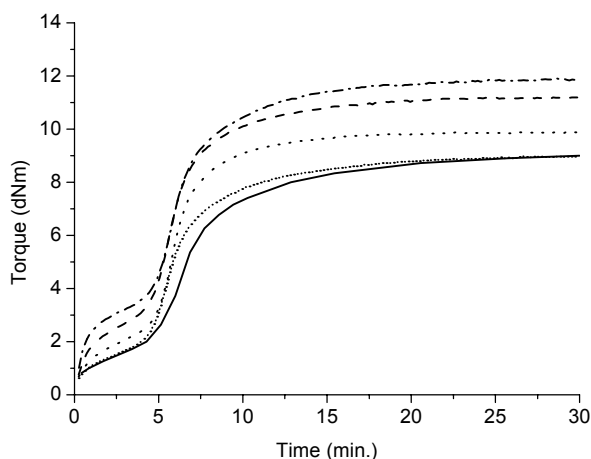


**Figure 5.18** Rheometer curves for DMESPT containing compounds with various dump temperatures; (.....), 118°C; (---), 128°C; (---), 145°C; (.....), 157°C and for TESPT (—) with a dump temperature of 150°C.

The tensile properties for this coupling agent are shown in the Figures 5.19 A to D. In Figure 5.19 A the elastic modulus is plotted against dump temperature for TESPT and DMESPT containing compounds. At lower dump temperatures a lower elastic modulus is achieved for DMESPT. The 300% modulus is similar for both compounds, Figure 5.19 B. The 300% modulus behaves in a similar manner as  $G'$  at 100% strain, Figure 5.16 B. The tensile strength is lower for DMESPT than for TESPT, Figure 5.19 C. Figure 5.19 D shows the elongation at break as a function of the dump temperature: the elongation at break of DMESPT containing compounds being a bit lower at higher dump temperatures than for TESPT.

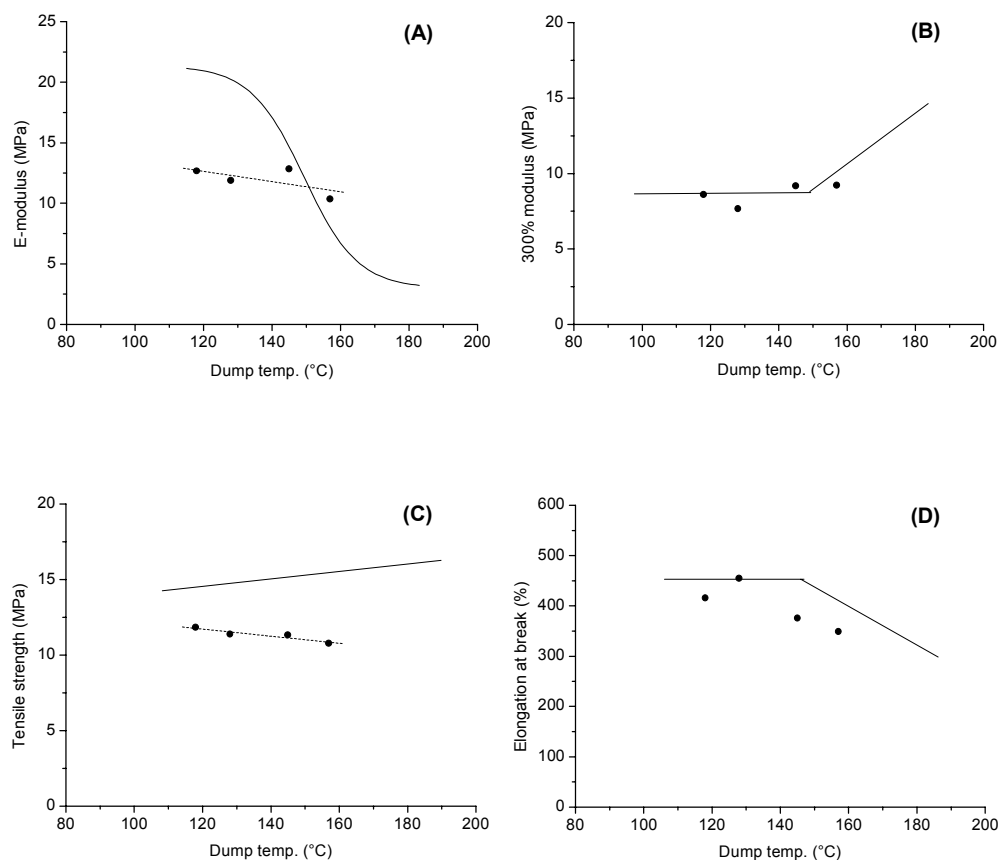


**Figure 5.19** Tensile properties as a function of dump temperature; (A) Elastic modulus, (B) 300% modulus, (C) Tensile strength, (D) Elongation at break ; (—), TESPT; (●), DMESPT.

**Table 5.9** Effect of dump temperature on  $\tan \delta$ .

Dump temp. (°C)	Tan $\delta$
118	0.179
128	0.174
145	0.173
157	0.171

The  $\tan \delta$  of the DMESPT containing compounds at different dump temperatures are listed in Table 5.9. With increasing dump temperatures a slight decrease in  $\tan \delta$  is observed. This decrease is so small, because already at low dump temperatures an excellent silica dispersion was achieved. The values of the  $\tan \delta$  of DMESPT containing compounds are comparable with the values of TESPT containing compounds: Figure 3.9.

## 5.4 Discussion

All the effects of the different functional groups, i.e. ethoxy- and sulphur-groups, on the dynamic and mechanical properties of the tyre tread compound are summarised in Table 5.10. The different reactions that are possible are indicated in the table.

When no coupling agent is applied, then the primary and secondary reaction as well as the reaction of the sulphur group are not possible. This leads to high values for  $G'$  at 0.56% strain and 100% strain as compared to a TESPT containing compound. The mechanical properties are all very poor: high values for the elastic modulus and the elongation at break, and low values for the 300% modulus and tensile strength.

In the case of TESH, the primary and secondary reaction potentially take place, however a reaction of a sulphur group is not possible. No full coupling of silica to rubber can happen. A similar silica dispersion is reached as for TESPT, as shown by the  $G'$  at 0.56% strain. There are no signs of premature scorch during mixing due to the absence of the sulphur group. The 300% modulus and tensile strength are lower, and the elastic modulus and the elongation at break higher than for TESPT: poor mechanical properties. The lower values of the 300% modulus and the tensile strength for TESH containing compounds are apparently due to the absence of coupling between the silica particle and the rubber matrix; a similar combination of effects was obtained when no coupling agent was applied at all.<sup>10</sup>

For the compound containing TMeSPT the opposite situation exists: neither the primary reaction nor the secondary reaction can take place, but a reaction of the sulphur moiety with the rubber polymer can potentially happen. Consequently, also no full coupling of the silica to the rubber is possible. As it turns out, this leads to high values for  $G'$  at 0.56% and 100% strain, compared to the values for a TESPT containing compound; primarily because of poor dispersion of the silica. At high mixer dump temperatures scorch problems occur, like for TESPT. The 300% modulus and tensile strength turn out low: generally poor mechanical properties. The fact that the 300% modulus is lower for the TMeSPT containing compound is due to no coupling between the silica and the rubber polymer during vulcanisation. The sulphur donating effect of the TMeSPT is visible in the fact, that at high dump temperature a slight increase in the 300% modulus occurs.

For the compound containing TESD and TMeSPT, the primary and secondary reaction potentially take place and also the reaction of the sulphur moiety with the rubber polymer is possible. Still no full coupling of the silica to the rubber is within reach. An improved silica dispersion is obtained, comparable to TESPT, as shown by the  $G'$  at 0.56% strain. The  $G'$  at 100% strain is higher than for TESPT and increases at dump temperatures above 160°C, indicating scorch. The elastic modulus, 300% modulus and the tensile strength are lower, and the elongation at break is higher than for TESPT: again poor properties due to the absence of full coupling.

In the case of DMESPT, the primary reaction potentially takes place, but the secondary reaction is not possible. A reaction of the sulphur moiety with the rubber polymer can also take place and full coupling of the silica to the rubber is possible. Surprisingly, a better dispersion of the silica is even reached than with TESPT, as shown by the lower  $G'$  at 0.56% strain. The tensile strength of the DMESPT containing compound is lower when compared to TESPT, but all other mechanical properties are similar to TESPT. DMESPT and TESPT only differ in the amount of ethoxy groups present in the molecules. The presence of only one ethoxy group on each side of the coupling agent prevents the occurrence of the secondary reaction. The lower tensile strength must be the result of the lower amount of ethoxy groups. The results with DMESPT are considered as very promising

in the sense, that this coupling agent allows for a large reduction needed to obtain a good dispersion. The latter is one of the major disadvantages of the silica technology. It is worth to try to overcome the lower tensile strength by slight adjustments of the compound recipe.

**Table 5.10** Effect of possible reactions of the various coupling agents on the dynamic and mechanical properties of the tyre tread compound; (+), possible; (-), not possible; (↓), lower than for TESPT; (↑), higher than for TESPT; (=), equal to TESPT.

	No coupling agent	TESH	TMeSPT	TESD+TMeSPT	DMESPT	TESPT
Primary reaction	-	+	-	+	+	+
Secondary reaction	-	+	-	+	-	+
Sulphur donation	-	-	+	+	+	+
Silica rubber coupling	-	-	-	-	+	+
G' (0.56%)	↑	=	↑	↓	↓	ref
G' (100%)	↑	↓	↑	↓	=	ref
E-mod.	↑	↑	=	↓	=	ref
300% mod.	↓	↓	↓	↓	=	ref
Tensile strength	↓	↓	↓	↓	↓	ref
Elongation at break	↑	↑	↑	↑	=	ref
Tan δ	↑	↑ <sup>1</sup>	↑	↑	=	ref

<sup>1</sup> Data obtained from literature<sup>14</sup>

In Chapter 3 it was explained, when applying TESPT as coupling agent, that a high  $M_{300}/M_{100}$  and lower  $\tan \delta$  are both indicative of a low rolling resistance, Figure 3.9. A conclusion from this figure would be, to mix till dump temperatures above 150°C to obtain low  $\tan \delta$  and high  $M_{300}/M_{100}$  values. However, at these temperatures processing problems arise due to scorch of the compound in the mixer. The question may be addressed at this point, whether the sulphur donation by the coupling agent, causing the scorch problems in the mixer, is a prerequisite for obtaining low  $\tan \delta$ ? Or that there is a way around this problem? The experiments with TMeSPT and the combination TESD + TMeSPT – in both cases full coupling between the silica and rubber via the coupling agent is not possible – show, that at elevated dump temperatures the  $M_{300}$  increases, when sulphur is present in the coupling agent. Consequently,  $M_{300}/M_{100}$  increases and  $\tan \delta$  decreases at the same time. This can be taken as an indication, that at high dump temperatures, i.e. above 150°C, the coupling agent TESPT donates sulphur to the rubber matrix and that this sulphur causes a surplus in the neighbourhood of the silica particle. This creates extra crosslinks in the rubber matrix around the silica particle. In this way the silica filler particle is trapped within the rubber matrix. During vulcanisation at a later stage, the silica particle is then coupled via the coupling agent to the rubber. The end result is a very tightly crosslinked interfacial shell around the silica particle, next to the silica-rubber coupling via the coupling agent. A schematic depiction of this model is given in Figure 5.20. Earlier work has shown<sup>14</sup>, that reducing the amount of sulphur in the coupling agent TESPT from 4 to 2 increases the scorch safety during mixing, but at the same time increases  $\tan \delta$ . It was shown, that the increased  $\tan \delta$  could be corrected for by adjusting the sulphur level in the curing package later on. This is consistent with the model drafted here above.

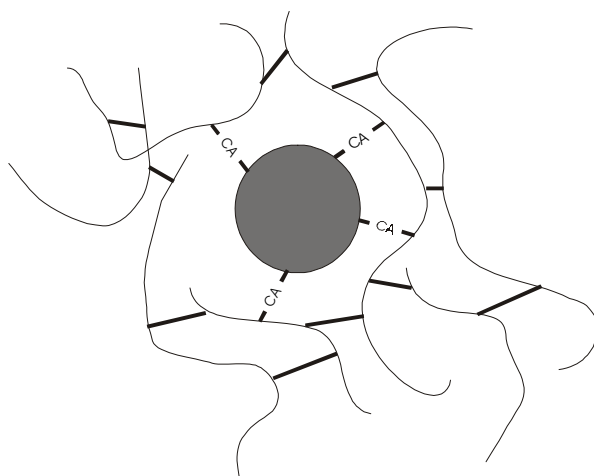


**Figure 5.20** Schematic representation of crosslink configuration around a silica particle; (—) sulphur crosslink, (—CA—) silica-coupling agent-rubber bond.

## 5.5 Conclusions

The experiments described in this chapter have shown, that a proper balance in functionalities is required for a coupling agent to enhance the properties of silica-reinforced tyre tread compounds. TESPT proved to best comply with this balance, because it allows for the primary and secondary coupling reaction towards the silica via its tri-ethoxysilyl groups, resp. for a sulphur donation and a coupling reaction towards the rubber polymer via its sulphur moiety.

Alternative coupling agents, allowing for only one of these functionalities lead to an inferior balance of properties. TESH with only a tri-ethoxysilyl group and no sulphur, does hydrophobize the silica and provides for a good dispersion like TESPT. However, the vulcanised properties are seriously poorer than those obtained with TESPT. On the other side TMeSPT with only an active sulphur group, fails in its ability to properly disperse the silica, shows premature scorch effects at high mixer dump temperatures like seen for TESPT. Again, the vulcanised properties are inferior to those obtained for TESPT.

Adding two coupling agents, TESD and TMeSPT, with the functionalities independently divided over both, does result in a silica dispersion grossly comparable with the one obtained with TESPT. Also signs of scorch are seen at high mixer dump temperatures, like with TESPT. But still, the properties of vulcanised compounds are still grossly inferior to those obtained with TESPT.

A coupling agent with only one reactive ethoxy group attached to the silicium atom vs. three for TESPT performs surprisingly well compared to TESPT. This coupling agent can only perform the primary reaction with the silica, which leads to a very quick equilibrium during mixing and consequently low mixer torques. It comes closest to TESPT in vulcanised compound properties, particularly the low  $\tan \delta$ , representative for low tyre rolling resistance.

Only the tensile strength is lower than the one achieved with TESPT. It is anticipated that the latter can be overcome by slight adjustments of the compound recipe.

Based on all the results a model is proposed, whereby TESPT releases sulphur to the compound in the vicinity of the silica particle during mixing or early stages of vulcanisation, thereby causing a crosslinked shell, trapping the silica particle in the rubber matrix. Later on, during vulcanisation, TESPT provides for chemical bridge formation between the silica particles and the rubber polymer.

## 5.6 References

1. H.D. Luginsland, *Kautsch. Gummi Kunstst.*, **53**, (2000), 10.
2. S. Wolff, *Tire Sci. Technol.*, **15**, (1987), 276.
3. A. Hunsche, U. Görl, A. Müller, M. Knaack, Th. Gobel, *Kautsch. Gummi Kunstst.*, **50**, (1997), 881.
4. S. Wolff, *Kautsch. Gummi Kunstst.*, **34**, (1981), 280.
5. A. Hunsche, U. Görl, H.G. Koban, Th. Lehmann, *Kautsch. Gummi Kunstst.*, **51**, (1998), 525.
6. U. Görl, A. Parkhouse, *Kautsch. Gummi Kunstst.*, **52**, (1999), 493.
7. U. Görl, J. Munzenberg, H.D. Luginsland, A. Müller, *Kautsch. Gummi Kunstst.*, **52**, (1999), 588.
8. J.W. Pohl, 152<sup>nd</sup> Technical Meeting and Rubber Expo '97, American Chemical Society, Rubber division, Cleveland, Ohio, USA, October 21-24, 1997.
9. L.A.E.M. Reuvekamp, J.W. ten Brinke, P.J. van Swaaij, J.W.M. Noordermeer, *Kautsch. Gummi Kunstst.*, **55**, (2002), 41.
10. Chapter 3 of this thesis.
11. L.A.E.M. Reuvekamp, J.W. ten Brinke, P.J. van Swaaij, J.W.M. Noordermeer, *Rubber Chem. Technol.*, **75**, (2002), 187.
12. T.F.E. Materne, Kayser, (to Goodyear Tire & Rubber), Eur. Pat 1 061 097 A1 (20-12-2000).
13. R. Rauline, (to the Compagnie Generale des Etablissements Michelin - Michelin & Cie), Eur. Pat. 0 501 227 A1 (12-02-1992).
14. J.W. ten Brinke, P.J. van Swaaij, L.A.E.M. Reuvekamp, J.W.M. Noordermeer, *Kautsch. Gummi Kunstst.*, **55**, (2002), 244.
15. S.C. Debnath, J.W.M. Noordermeer, *Rubber Chem. Technol.*, (in print).



---

## Chapter 6

### *A study of the influence of the reactivity of the TESPT-sulphur group by model vulcanisation*

---

The coupling agent, TESPT can react with rubber under high temperature even in absence of crosslinking agents. This can cause pre-crosslinking during mixing, which leads to a rise in compound viscosity and therefore makes the processing of the compound more difficult. This undesirable phenomenon should be avoided. In order to avoid this effect, it is necessary to study the reaction and elucidate which mechanism is taking place. The present study focused on the study of the reaction, which takes place between the coupling agent and the polymer. This was done by using Model Compound Vulcanisation, in order to analyse the products with standard analytical techniques.

The model 3-methyl-1-pentene (representative of the vinyl structure of butadiene rubber) is more reactive than trans-3-hexene (representative of the trans structure of butadiene rubber) and trans-3-hexene in turn is more reactive than 2,3-dimethyl-2-butene. Reactions with sulphur or TESPT lead to the same reaction products, indicating that TESPT is donating sulphur rather than coupling itself to the model compounds. During those reactions zinc oxide has no influence on the reaction conversion rate.

Experiments with only TESPT and a model showed, that TESPT is first incorporating free elemental sulphur during the first 5 minutes of reaction before donating it in an activated form to the model compound mixture. The disulphide variant of TESPT does not react with the model olefin.

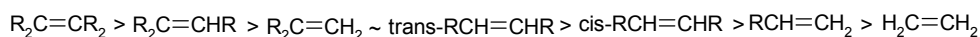
#### 6.1 Introduction

In the previous chapters studies were performed with a S-SBR/BR blend, where it was observed that TESPT silane coupling agent on the one hand couples the silica to the rubber matrix, and on the other hand donates sulphur to the rubber polymer at temperatures of 160°C and higher.<sup>1, 2</sup> The latter causes pre-crosslinking during mixing, which leads to a rise in compound viscosity and therefore makes the processing of the compound difficult. In order to investigate whether this effect can be avoided, it was decided to study the reaction between TESPT and rubber in detail and to elucidate its mechanism. Emphasis will be laid on the configuration of the polymer, that is most reactive to the coupling or sulphur donation reaction.

Little is known about the mechanism of the reaction between bis-(triethoxysilylpropyl)tetrasulphide (TESPT) silane coupling agent and the rubber matrix. Görl studied the reaction of the polysulphidic silane moiety with the rubber matrix.<sup>3</sup> His conclusions were that TESPT can react with the rubber matrix during processing in three

different ways. First, a disproportionation of the long chain polysulphide and subsequent bonding to the polymer, starting at temperatures over 150°C, as was found by others as well.<sup>4-6</sup> Second, accelerators such as CBS are able to react with the long chain polysulphide of TESPT and form in this way a silane/polymer bond, without the need for extra sulphur. Third, when elemental sulphur is present in the rubber compound, TESPT and the accelerator will compete for it. TESPT will incorporate part of the sulphur into its own sulphur chain, which results in longer polysulphidic units. This has been observed by others too.<sup>7-9</sup> The latter effect influences the TESPT/accelerator reaction, whereby the rubber-filler bonds formed are assumed to quantitatively and qualitatively be of a different nature than those formed without sulphur. All three reactions can take place during vulcanisation and lead to rubber/filler bonds. The relative contribution that each of these reactions plays is not known.

In the rubbers S-SBR or BR used for our investigations, different configurations of the butadiene part occur in the polymer chain. In the case of BR, three configurations are possible: cis, trans and vinyl. From literature it is known, that the stability of alkenes depends on their structure.<sup>10</sup> If TESPT is to react with the butadiene part of the BR and S-SBR, assuming that the styrene groups are non-reactive, it can therefore react with different kinetic rate constants with the different butadiene configurations. The stability of alkenes can be depicted in the following way, starting with the most stable alkene and ending with the less stable, the latter being the most reactive structure:



where R is alkyl. An increase of the number of alkyl substituents results in more stable alkenes, which is due to the inductive effect of alkyl groups. The difference in stability between the trans- and cis-configuration is mainly due to steric hindrance of the alkyl substituents.

Structural analysis of rubber vulcanisates is experimentally very difficult. The variety of crosslinked structures, the low concentrations as well as the insolubility of the elastomer network contribute to the problems encountered, when applying various chemical methods of analysis. As an alternative approach, it is therefore common to perform studies using low molecular weight model systems.<sup>10, 11</sup> Model Compound Vulcanisation (MCV) is defined as the vulcanisation of a low molecular weight model as a substitute for the reactive unit of a rubber.<sup>12</sup> The models used during model compound vulcanisation should be as much as possible representative for the reactive unit of the polymer. This means, that the chemical behaviour during vulcanisation should be similar to the behaviour of the reactive unit of the polymer. Despite the advantage MCV's are having, the main disadvantage is that those models have a high concentration of end groups. These end groups, in most cases methyl groups, have a reactivity different from the methylene and methyne groups, which form the majority of reactive groups in a real polymer.

Most MCV studies have dealt with sulphur vulcanisation and have employed models for rubbers that contain unsaturations. It is essential in sulphur MCV to have at least one allylic hydrogen atom, since crosslink formation commonly involves the substitution of a hydrogen for a sulphur link at this allylic position.<sup>12</sup>

Vulcanisation of unsaturated low molecular weight models has been studied by Versloot et al.<sup>10</sup> by treatment of these olefins with a mixture of zinc oxide, sulphur and tetramethylthiuramdisulphide (TMTD) at 140°C. They found that isomerisation of the double bond can take place during the reaction. The position of the double bond is determined by

the crosslink formation mechanism and by isomerisation, which takes place at higher temperatures.

The butadiene moiety in the S-SBR polymer, used in the previous chapters, consists for 50% of the vinyl-configuration. The BR used in the experiments consists for more than 96% of the cis-configuration. In literature several low molecular weight models are described, as a substitute for the different configurations of BR. 3-methyl-1-pentene is a good substitute for the vinyl-configuration. Finding a suitable substitute for the cis-configuration is much more complicated. Cyclohexene and 1,5-cyclooctadiene are sometimes used in literature as model compounds. However, due to the cyclic structure and the ring strain in the molecules, crosslinking occurs in a different manner than in BR.<sup>13</sup> Skinner studied conventional sulphur vulcanisation of cis-3-hexene. He showed that with this type of model a whole variety of products is formed, which makes the analysis of the reaction products very complicated. This is not favourable for a model compound vulcanisation study. The present study will therefore focus primarily on the vinyl-configuration, being the most reactive species anyway. The reactivity of the cis-configuration can then be estimated on basis of the stability/reactivity scheme above.

The models used for this study are: 2,3-dimethyl-2-butene (tetramethyl ethylene, TME), 3-methyl-1-pentene and trans-3-hexene. Characterisation of the reaction products of the models with elemental sulphur is necessary before the reaction mechanism of TESPT with the model can be elucidated. The model 3-methyl-1-pentene is used for the reaction with TESPT, because this model represents the most common vinyl-configuration, present in the S-SBR polymer used in the previous chapters.

## 6.2 Experimental

*Materials.* — The materials, which were used during the experiments, are listed in Table 6.1. The compositions of the samples are listed in Table 6.2. The alkene-model compounds used during the experiment as described in Table 6.2 are TME, 3-methyl-1-pentene or trans-3-hexene, respectively. The compositions of the reaction mixtures are divided into 3 parts: experiments with model compound and sulphur only; experiments with model compound, sulphur and zinc oxide; experiments with only the model compound and TESPT present.

**Table 6.1** Materials.

Material	Source
2,3-dimethyl-2-butene (TME)	Merck
3-methyl-1-pentene	Merck
trans-3-hexene	Merck
Sulphur	Merck
TESPT A1289	OSi Crompton Corporation
Zinc oxide	Merck

**Table 6.2** Composition of the reaction mixtures.

Sulphur		Sulphur and Zinc oxide		TESPT	
Material	Amount (g)	Material	Amount (g)	Material	Amount (g)
Model compound	0.5000	Model compound	0.5000	Model compound	0.5000
Sulphur	0.0070	Sulphur	0.0070	TESPT	0.0350
		Zinc oxide	0.0125		

*Model vulcanisation.*— The mixture was weighed into a glass ampoule. Before closing the ampoule by melting the glass neck, a flow of nitrogen was passed through the ampoule to remove oxygen. The closed ampoule was then placed in a thermostatic oil bath during a fixed time. During the reaction, the mixture was constantly stirred with a magnetic stirrer inside the ampoule. The ampoule was also covered with aluminium foil to avoid an UV influence. After a definite time the reaction was arrested by removing the ampoule from the oil bath and by immersion in an ice bath.

*Analysing the reaction product.*— After opening the ampoule, the reaction product was filtered over a 0.45 µm porous filter. Next, 50 µl of the filtered sample was diluted in 2.5 ml of acetonitrile and filtered again. Of this sample 50 µl was then injected onto the HPLC-column for analysis according to the conditions described in Table 6.3. After obtaining the chromatogram, the area of the elemental sulphur or TESPT peak was determined. Reaction conversions were calculated by dividing the amount of sulphur consumed during 1 hour of reaction, by the starting concentration and expressed in percents.

Whenever useful, <sup>1</sup>H-NMR spectroscopy (Bruker 300 MHz) was used to characterise the structure of the reaction products obtained. The solvent used for these experiments was CDCl<sub>3</sub>.

**Table 6.3** HPLC conditions.

Column	Nucleosil 100-5 C18 HD (reverse phase)
Length of column	250 mm
Intern diameter of column	4.6 mm
Mobile phase	97 Acetonitrile : 3 Water (vol%)
Flow rate	1 ml/min
Temperature	23°C
Detector	UV
Wavelength	254 nm
Injected volume	50 µl

### 6.3 Results

In the paragraphs 6.3.1-6.3.3, the results obtained with three different alkene models, 2,3-dimethyl-2-butene (TME), 3-methyl-1-pentene (3-m-1-p) and trans-3-hexene (t-3-h) are described. The reactions were done according to the experimental paragraph in the presence of elemental sulphur. TME was used to compare the results with literature.<sup>8, 11</sup> 3-Methyl-1-pentene was used as a substitute for the vinyl-configuration in BR, whereas trans-3-hexene was used as a substitute for the trans-configuration in BR. The experiments were performed at different temperatures and times to study the kinetics of the reaction between sulphur and the alkene model. The reaction products were analysed with HPLC and <sup>1</sup>H-NMR. In particular the characterisation of the reaction products, obtained after the reaction between elemental sulphur and 3-m-1-p, is important. These results are necessary to later be able to elucidate the reaction mechanism of TESPT with 3-m-1-p, see paragraph 6.3.5. Also the effect of ZnO on the reaction rate constant was studied. In paragraph 6.3.4 the results of the reaction of elemental sulphur with the three models are compared with each other.

In paragraph 6.3.5, TESPT was reacted with 3-m-1-p to test if the reaction proceeds in a similar way to the reaction with elemental sulphur. After the reaction, the products obtained were analysed with the aid of HPLC. Finally, in paragraph 6.3.6 the results of the reaction of 3-m-1-p with TESPT resp. elemental sulphur are compared.

#### 6.3.1 Reaction of 2,3-dimethyl-2-butene (TME) with elemental sulphur, with and without ZnO present

TME was reacted during one hour in the presence of sulphur at three different temperatures: 140, 150 and 160°C, which represent the vulcanisation temperatures commonly applied for rubber compounds. Figure 6.1 A shows the sulphur concentration in the reaction mixture after 1 hour of reaction as a function of the reaction temperature, as analysed with HPLC.

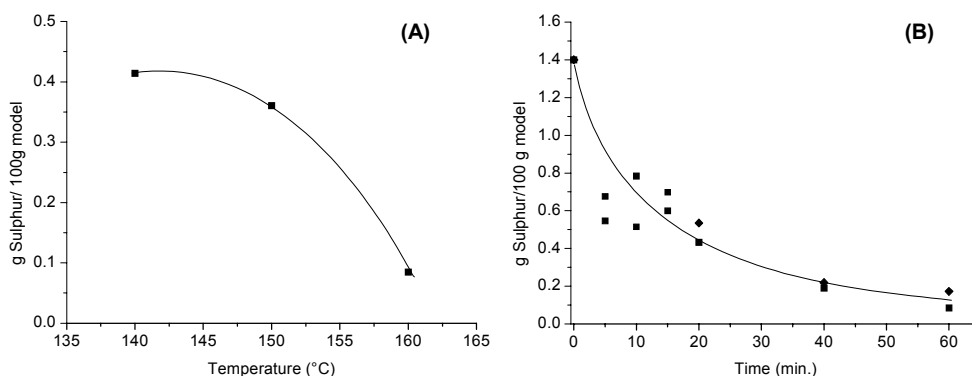


**Figure 6.1** (A), Sulphur concentration after 1 hour at different temperatures of reaction; (B), sulphur concentration after reaction at 160°C as a function of the reaction time; (■), without ZnO; (◆), with ZnO.

From Figure 6.1 A it can be seen that after 1 hour of reaction between sulphur and TME, the remaining sulphur decreases with increasing temperature. The reaction goes much faster at a temperature of 160°C, as more sulphur is consumed during this reaction. The effect of reaction time is given in Figure 6.2 B. From this figure it is evident, that the sulphur concentration is decreasing exponentially in time. At 5, 10 and 15 minutes the reactions were done twice to check the repeatability of the system.

The fact that the reaction at 160°C proceeds much faster when compared with the other two temperatures, is also clear from the reaction conversion: Table 6.4. The values for the reaction conversion are calculated with the amount of sulphur that remained after 60 minutes of reaction. Almost all the starting material has been converted into product at 160°C.

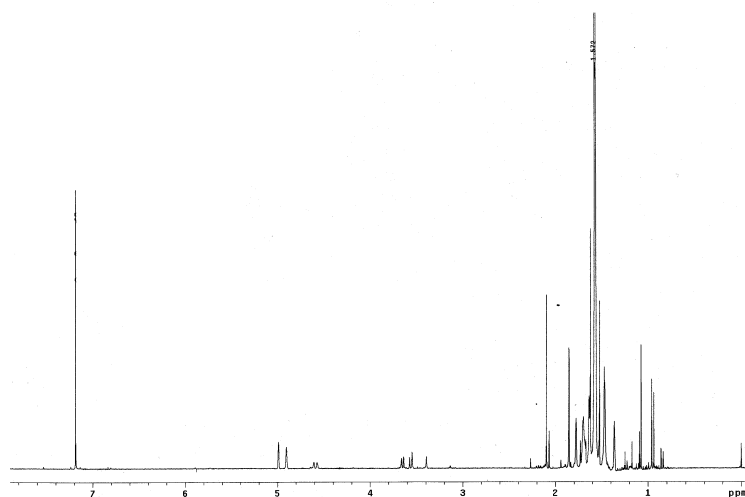
**Table 6.4** Reaction conversion of TME and sulphur

Temperature (°C)	Conversion (%)
140	70.43
150	72.24
160	93.95

At a reaction temperature of 160°C the experiment was repeated in the presence of ZnO and elemental sulphur. When ZnO was present during the reaction, the decrease in sulphur amount was the same: Figure 6.1 B. ZnO is therefore not activating this reaction.

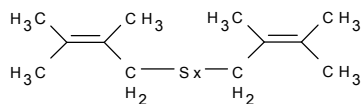
Assuming first order reaction conditions, plotting the logarithm of instantaneous sulphur concentration divided by the starting concentration against time, should give a straight line. The slope represents the kinetic rate constant. In this way a value of  $0.041 \text{ min}^{-1}$  is obtained as the kinetic rate constant for the reaction of TME with sulphur at 160°C.

Figure 6.2 shows the  $^1\text{H-NMR}$  spectrum of the reaction product mixture of TME with sulphur at 160°C. This spectrum shows, besides the signals for the starting material of TME, also some signals from methylene groups next to a sulphur bond, at 3.4-3.6 ppm chemical shift.

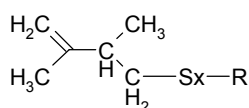


**Figure 6.2**  $^1\text{H-NMR}$  spectrum of the reaction product of TME and sulphur after 1 hour at 160°C.

Versloot et al. have demonstrated, that two molecules of TME react with sulphur to create a structure as depicted in Scheme 6.1.<sup>10</sup> The formation of this product is mainly without isomerisation, but some isomerisation may occur. If isomerisation takes place, a product as depicted in Scheme 6.2 can be obtained, where R represents another TME molecule with or without isomerisation.



**Scheme 6.1** Structure of reaction product of TME and sulphur.



**Scheme 6.2** Product structure when isomerisation takes place.  
R represents another TME molecule with or without isomerisation.

A theoretical calculation of the chemical shift for the methylene groups in Scheme 6.1 (next to the sulphur bridge) gives a value of around 3.39 ppm. The signals of those groups at 3.4-3.6 ppm correspond well with the theoretical shift. Different sulphur chain lengths between the methylene groups cause the fact that more signals are present around 3.5 ppm. Figure 6.1 also shows a signal at 5 ppm, which was not present in the pure starting product, meaning that this is also due to a reaction product. This signal comes most likely from methylene groups next to a double bond of an isomerised product, Scheme 6.2. The theoretically calculated shift is at around 4.78-4.81 ppm, while in Figure 6.1 the signal is at 4.9-5 ppm.

### 6.3.2 Reaction of 3-methyl-1-pentene (3-m-1-p) with elemental sulphur, with and without ZnO present

3-methyl-1-pentene was used as a model for the vinyl-configuration in BR. The same reaction conditions were applied as for TME. The decrease in sulphur concentration with time at 160°C as measured with HPLC is shown in Figure 6.3. Again, the reactions at 5, 10 and 15 minutes were performed twice to study the repeatability of the procedure. From this graph it can be concluded that the major part of the reaction takes place during the first 5 minutes already; much faster than for TME.

In presence of ZnO, again no major difference is obtained in the reactivity. The reaction also mainly takes place during the first 5 minutes.

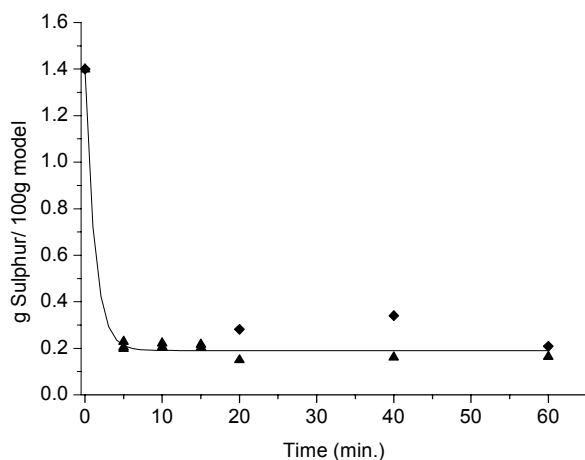


**Figure 6.3** Sulphur concentration as a function of reaction time for 3-m-1-p at 160°C; (▲), without ZnO; (◆), with ZnO.

Again, there is an exponential decay of the sulphur concentration. Whether this decay is really exponential is difficult to establish, because the reaction takes place very fast. Therefore, the kinetic rate constant cannot be calculated, but must be much larger than for the reaction with TME. An estimation of this kinetic rate constant can be done by taking only the conversion values at 0 and 5 minutes of reaction time. The rate constant then obtained is approximately  $0.39 \text{ min}^{-1}$  and indeed much larger than for TME.

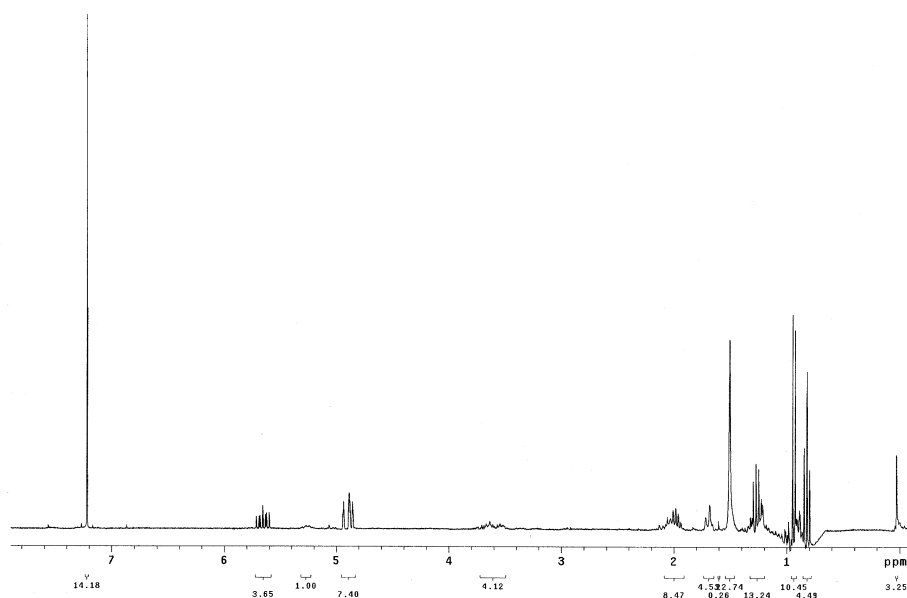
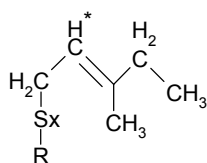


**Figure 6.4**  $^1\text{H}$ -NMR spectrum of the reaction product of 3-m-1-p and sulphur after 1 hour at 160°C.

The  $^1\text{H-NMR}$  spectrum obtained after 1 hour of reaction is different from the pure starting product: Figure 6.4. Similar to the results obtained with TME, there are signals of reaction products in the NMR spectrum. The signals appearing at 3.6 ppm are indicative of a methylene-group next to a sulphur. Based on experience gained with TME, similar products can be derived from this spectrum. The product, which is mainly formed during the reaction is (3-m-1-p)-S<sub>x</sub>-(3-m-1-p).

According to Versloot et al., also during the reaction with a vinyl-group and sulphur isomerisation is taking place.<sup>10</sup> Products as shown in Scheme 6.3 are the result. In the  $^1\text{H-NMR}$  there are some small signals at 5.35 ppm. The theoretical shift of the proton of the methyne group (\*; in Scheme 6.3) has a theoretical chemical shift of around 5.46 ppm. It is therefore most likely, that the signal obtained in the  $^1\text{H-NMR}$  is due to the isomerisation product of 3-m-1-p.



**Scheme 6.3** Product structure when isomerisation takes place.

R represents another molecule with or without isomerisation.

In the case of 3-m-1-p it is also interesting to look at the reaction products with the aid of HPLC, because this helps later with the interpretation of the chromatogram obtained after the reaction between TESPT and 3-m-1-p: paragraph 6.3.5. If the chromatograms of the samples reacted at 5 and 60 minutes are compared, Figures 6.5 and 6.6, it is seen that at 5 minutes the free sulphur peak (around 14.8 minutes) is more or less the same as after 60 minutes of reaction. This confirms, that the reaction of the free sulphur with the model olefin is already completed after 5 minutes. On the other hand, the peaks at around 8.3 and 6.6 minutes are increasing during the time interval. More peaks are appearing, indicating that more reaction products are formed. The peaks at 8.3 and 6.6 minutes increase fastest. Because these two products are present in a large quantity in the reaction mixture, it is reasonable to assume that those two peaks are responsible for the signals at 3.5 ppm in the  $^1\text{H-NMR}$  spectrum. As mentioned before with TME, more signals at around 3.5 ppm are caused by the fact that various sulphur chain lengths are present between the methylene groups.

Since the polarity of a compound in a common HPLC set-up determines the retention time in the chromatographic column, compounds with similar polarity have comparable retention times. The column used in the present experiment is a reverse phase column; therefore, the retention time of the products is now due to the non-polar part of the molecule, i.e. the sulphur chain. Separation now takes place on the sulphur chain length in the molecules. When comparing with the chromatogram of TESPT (Figure 4.5, Chapter 4) the peaks can be identified indirectly. For instance, all disulphidic molecules will appear at similar retention times. The disulphidic molecule of TESPT has a retention time of 8.4 minutes, which is similar to the peak at 8.3 minutes of the present reaction product. Therefore, it may be concluded that the peak at 8.3 minutes represents the combination of 2 molecules of 3-m-1-p, connected via a disulphide bridge. The peak at around 6.6 minutes in

the chromatogram corresponds to a more polar compound, than the one at 8.6 minutes. Since the peak at 6.6 minutes corresponds to a reaction product as well, the most likely is that this peak belongs to a monosulphidic link between two molecules of 3-m-1-p.

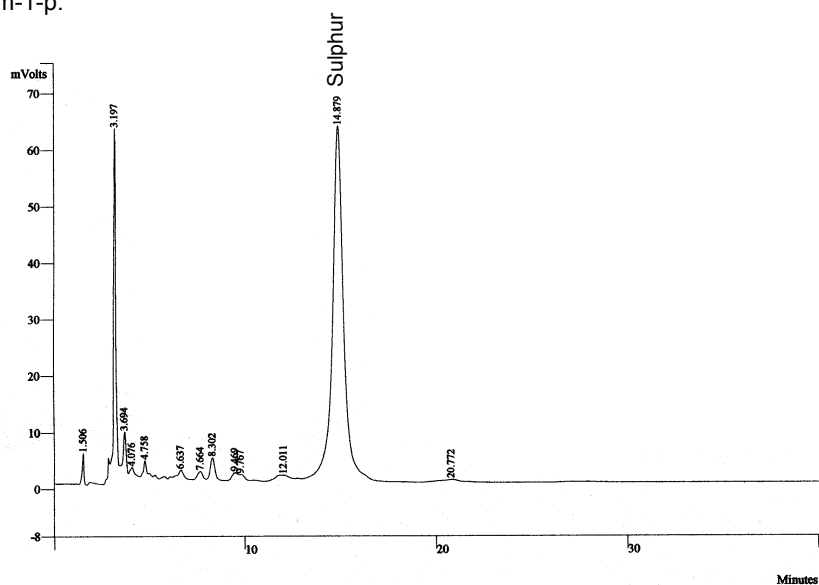


**Figure 6.5** HPLC chromatogram of the reaction product between 3-m-1-p and sulphur after 5 minutes of reaction at 160°C.

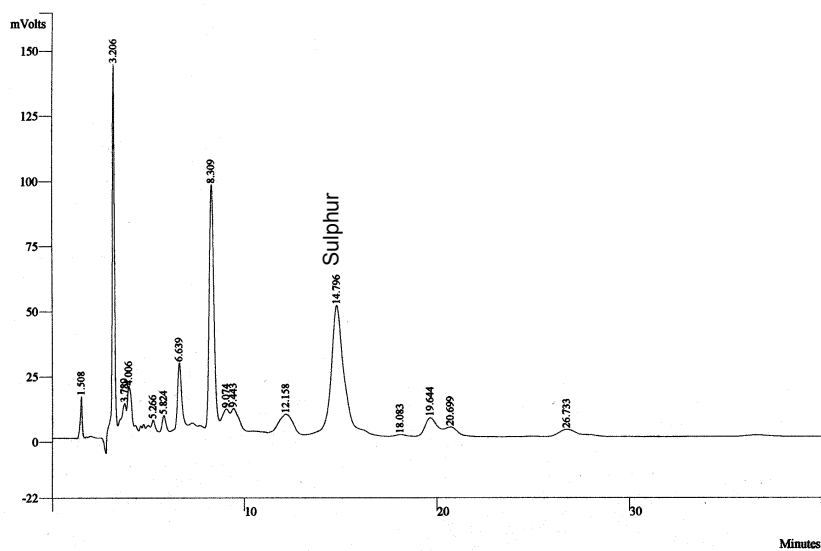


**Figure 6.6** HPLC chromatogram of the reaction product between 3-m-1-p and sulphur after 60 minutes of reaction at 160°C.

It was also tried to verify the product structures with GC-MS analysis, but due to the instability of the sulphur bond at high temperatures, this technique was not suitable. A milder technique is LC-MS. With this technique the products are separated with the aid of HPLC and determined with mass spectrometry. This technique did not clarify the structures of the reaction products either. Collecting the separate products from the HPLC-column, removing the mobile phase and determination of the structure with  $^1\text{H-NMR}$  also did not clarify the structures. It might be a subject of further research to try to further elucidate the structures of the reaction products.

Although no direct identification of the reaction products was possible, still an indirect identification was possible as shown before. The identification of the reaction products was necessary for the identification of the reaction products between TESPT and 3-m-1-p. Reaction products formed by sulphur donation of TESPT can then easily be found by comparison with the chromatograms obtained in the present paragraph.

### 6.3.3 Reaction of trans-3-hexene (t-3-h) with elemental sulphur

Trans-3-hexene was used as a substitute for the trans-configuration in BR. The same reaction conditions were applied as for TME and 3-methyl-1-pentene. The decrease in sulphur concentration with time at  $160^\circ\text{C}$  as measured with HPLC is shown in Figure 6.7. Again, the reactions at 5, 10 and 15 minutes were performed twice to study the repeatability of the procedure. From the figure it can be concluded that the sulphur concentration is decreasing again in a more or less exponential manner.

Because the experiment with ZnO did not show any significant difference in reactivity of sulphur towards a TME and 3-m-1-p, experiments with ZnO and t-3-h were not performed.

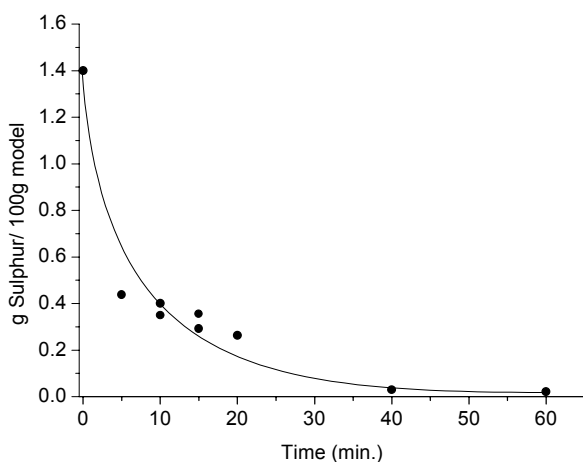


**Figure 6.7** Sulphur concentration as a function of reaction time at  $160^\circ\text{C}$  for trans-3-hexene.

A value of  $0.067 \text{ min}^{-1}$  was obtained for the kinetic rate constant for the reaction of trans-3-hexene with sulphur at  $160^\circ\text{C}$ .

### 6.3.4 Comparison of the three models with elemental sulphur

Versloot et al. have already shown, that the most reactive of the three models tested towards elemental sulphur is 3-methyl-1-pentene.<sup>10</sup> The less reactive model is TME, as explained in the introduction to this chapter. Figure 6.8 shows a comparison of the sulphur concentration as a function of the reaction time for the three models at 160°C. These results are in agreement with Versloot et al.<sup>10</sup> It can be clearly seen from this figure, that the amount of sulphur remaining after the reaction, is highest in the case of TME and smallest in the case of 3-methyl-1-pentene, while the trans-3-hexene is in between, at least up to about 20 minutes. For longer reaction times, 3-methyl-1-pentene leads to a higher amount of sulphur than TME and trans-3-hexene, maybe due to some reversion. Reversion is commonly associated with shortening of the sulphur chain length, which in the present experiment leads to sulphur being released from the reaction products and being added to the amount of free sulphur in the mixture.

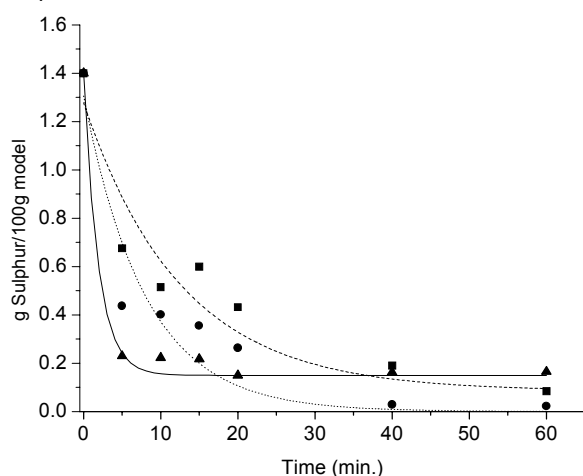


**Figure 6.8** Sulphur concentration at different times of reaction with the three models: (■), TME; (●), t-3-h; (▲), 3-m-1-p.

Since the BR in the S-SBR/BR blends used in our experiments consists mainly of cis-polybutadiene (with some vinyl and trans content) the reactivity of the cis-configuration towards sulphur is also of interest. The reactivity of the three models is following the order described in literature and therefore, the reactivity of the cis-configuration can be predicted. In view of the stability of the cis-configuration, it should end up between the lines of trans-3-hexene and 3-methyl-1-pentene, because the cis-configuration is a bit more reactive than the trans-configuration, as mentioned in the introduction to this chapter.

The possible reactions of elementary sulphur with the three model compounds having been studied, we can now proceed to investigate the possible reactions between TESPT and 3-m-1-p as the model compound. In the previous chapters S-SBR was used as the main polymer, which consists for 50% of vinyl-configuration. Therefore it is interesting to study the reaction of TESPT with the vinyl-configuration. The model 3-m-1-p was chosen because it represents the vinyl-configuration and it reacts very fast with TESPT, as it did with elemental sulphur as well. This results in more reaction products, which makes analysis easier.

### 6.3.5 Reaction of 3-methyl-1-pentene with TESPT

For reasons explained before, for the reaction with TESPT we restricted ourselves to the model compound 3-methyl-1-pentene. 3-m-1-p was reacted with TESPT at 160°C for different time intervals. The results were evaluated with HPLC by summing all the peaks of the various sulphur chains of TESPT, i.e. area of S<sub>2</sub>, + area of S<sub>3</sub> etc. as explained in Chapter 4. The summed TESPT peak areas were calculated back to the corresponding weight of TESPT per 100 gram of model compound. Free sulphur was not included in the calculation. The results obtained from this experiment are shown in Figure 6.9.

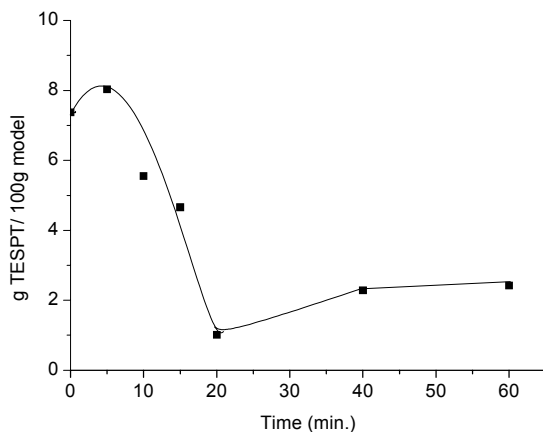


**Figure 6.9** Sulphur amount of TESPT as a function of time after reaction at 160°C.

Free sulphur is incorporated in the sulphur chain of the TESPT during the first 5 minutes of reaction. This sulphur originates from the free elemental sulphur present in the TESPT as an impurity. From 5 to approximately 20 minutes of reaction, TESPT is donating sulphur to the model compound. After 20 minutes of reaction, again sulphur is accepted by TESPT. This time the sulphur is coming from the reaction products of TESPT and free sulphur with the model compound. The reaction products with long sulphur chains are donating sulphur, which in turn is accepted by the TESPT.

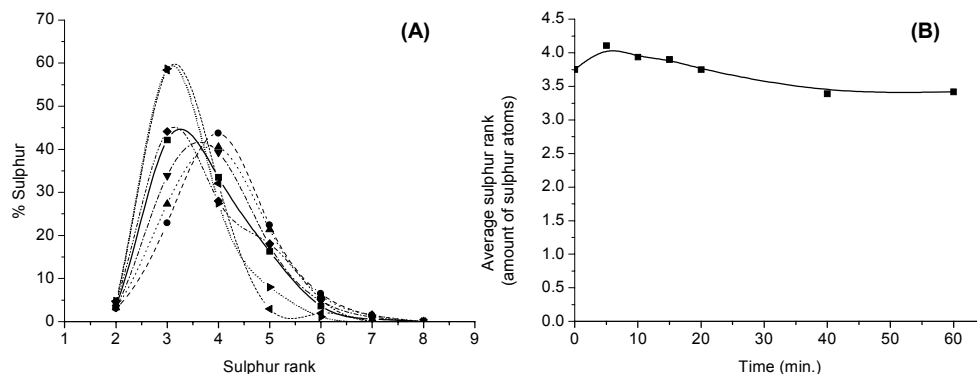


**Figure 6.10 (A)** Percentage of sulphur rank (2-8) of TESPT at different reaction times at 160°C; (■), 0 min; (●), 5 min; (▲), 10 min; (▼), 15 min; (◆), 20 min; (◄), 40 min; (►), 60 min; **(B)** Average sulphur rank as a function of the reaction time.

Due to the fact, that TESPT represents a mixture of sulphur ranks, ranging from 2 to 8, a rearrangement of the sulphur average is expected. Figure 6.10 A shows the relative amount of the different sulphur ranks present in the mixture as a function of the amount of sulphur atoms. It is plotted for different reaction times. The disulphide rank is very stable, because the amount remains more or less constant with increasing reaction time. On the other hand, the higher sulphide ranks are changing, especially the trisulphide varies significantly. At 40 and 60 minutes reaction time almost no sulphur rank higher than 5 is present anymore in the mixture. This influences the average sulphur rank as depicted in Figure 6.10 B. Again, the sulphur incorporating effect of TESPT is visible during the first 5 minutes, because the average sulphur rank is increasing. From 5 to 20 minutes, the average sulphur rank is decreasing due to the loss of sulphur towards the reaction products. After 20 minutes the sulphur average is levelling off. The reason why the sulphur rank average is affected by the reaction with the model compound can be explained by Figure 6.10 A. As mentioned before, the higher sulphur ranks are reacting faster as can again be seen from the figure. By the time the higher sulphur ranks are no longer contributing to the sulphur average, then the average will decrease. At 40 and 60 minutes of reaction time, trisulphide ranks are reformed, which makes the average sulphur rank go down.

The effect of renewed incorporation of sulphur in the TESPT after 20 minutes of reaction is also clearly visible when observing the HPLC peak area of one of the reaction products. Figure 6.11 shows the peak area of a reaction product with a high sulphur rank as a function of the reaction time at 160°C. The HPLC measurements show a long retention time (21.9 min) for this product. The actual structure of the product could not be clarified with analytical techniques such as  $^1\text{H-NMR}$  or LC-MS, as mentioned before. From the measurements with TESPT itself it is already known, that higher sulphur ranks elute at longer retention times. Therefore, because of the long retention time, this product does represent a species with a high sulphur rank.

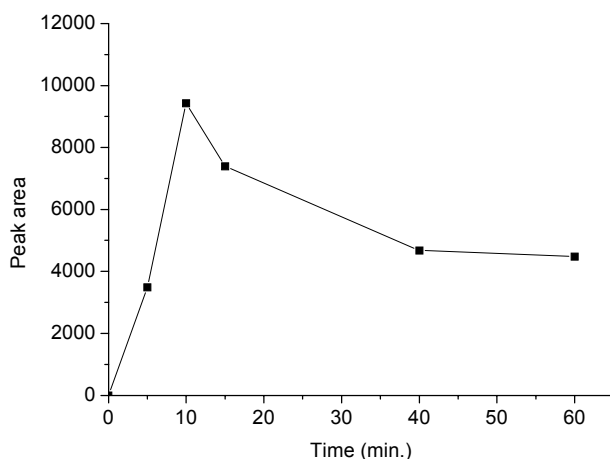


**Figure 6.11** Amount of reaction product with high sulphur rank as a function of time after reaction at 160°C.

From Figure 6.11 it is evident that the peak, corresponds to a reaction product, because during the first 10 minutes it is produced, i.e. increasing peak area. After 10 minutes, the amount of the product is then decreasing, indicating that sulphur is released for incorporation in TESPT: compare with Figure 6.9, wherein the amount of TESPT is

increasing again after 20 minutes. The fact, that the amount of TESPT is decreasing up to 20 minutes and the reaction product is formed only up to 10 minutes, can be explained as follows. During the sulphur donation of TESPT to the model compound, a variety of products is formed, as will be shown later in this paragraph. The products consist of different sulphur ranks. They are formed with different rates. This means, that one product may be donating sulphur back to the TESPT, whereas another product is still accepting sulphur. Overall, at long reaction times, the reaction products with longer sulphur chains are donating more sulphur back than incorporating sulphur, resulting in an increase of the amount of TESPT.

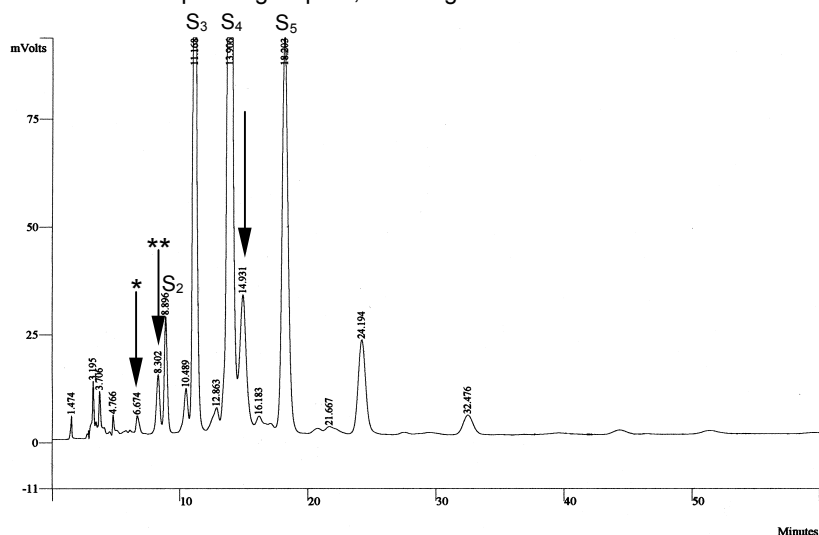


**Figure 6.12** HPLC chromatogram of the reaction mixture of 3-methyl-1-pentene and TESPT after 5 minutes of reaction at 160°C; the remaining TESPT peaks are indicated with S<sub>2</sub>, S<sub>3</sub>, etc.

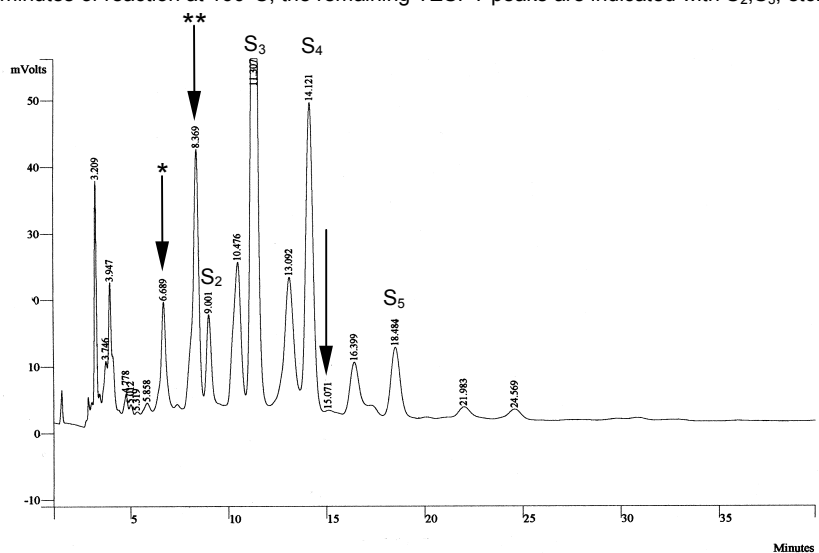


**Figure 6.13** HPLC chromatogram of the reaction mixture of 3-methyl-1-pentene and TESPT after 60 minutes of reaction at 160°C; the remaining TESPT peaks are indicated with S<sub>2</sub>, S<sub>3</sub>, etc.

Figures 6.12 and 6.13 show the HPLC chromatograms of the reaction mixture after 5 minutes of reaction, and after 60 minutes, respectively. In Figure 6.13 the peaks of TESPT are marked with the sulphur rank  $S_2$ ,  $S_3$ , etc. The peaks of TESPT are much smaller than in the chromatogram after 5 minutes of reaction: Figure 6.12. The free sulphur peak is marked with an arrow in both graphs, at a retention time of approximately 15 minutes. This peak is constantly decreasing in size during reaction. After 60 minutes of reaction almost all sulphur is gone.

Before every peak of TESPT a reaction product is appearing in the chromatogram. Since the retention times of the reaction products are similar to the retention times of the different sulphur ranks of TESPT, components with identical retention times have the same polarity. Therefore, the peaks of the reaction products are having the same sulphur rank as the peak of TESPT with an equal retention time.<sup>8</sup> The reaction products obtained are similar to the reaction products obtained after the reaction between elemental sulphur and 3-m-1-p. The structure of the reaction product is: (3-m-1-p)- $S_x$ -(3-m-1-p) where  $x$  is the amount of sulphur atoms.

At the start of the chromatogram several peaks are appearing. Especially in Figure 6.13 the peaks are clearly present. Identification of those peaks with LC-MS or collecting the fractions and analysing with  $^1\text{H-NMR}$  did not succeed to reveal the structure. To detect, if one of the peaks corresponds to the thiol-version of TESPT, triethoxysilylpropylthiol was analysed separately on the HPLC-column. In the chromatograms, no peak of the thiol-compound was detected. Also no TESPT attached to 3-m-1-p: (TESPT)-(3-m-1-p), could be detected. This was expected to be found, because this compound establishes the bond between a silica particle and the polymer. It is very likely however, that, based on the polarity of the (TESPT)-(3-m-1-p) product, the peak elutes at equal retention time as the peaks of TESPT and (3-m-1-p)- $S_x$ -(3-m-1-p). The resolution in the chromatograms is insufficient to detect the particular peak of (TESPT)-(3-m-1-p).

### 6.3.6 Comparison of the reactions of 3-methyl-1-pentene with elemental sulphur and with TESPT

If the HPLC chromatograms of the reaction products of 3-methyl-1-pentene and sulphur and 3-m-1-p with TESPT are compared, it becomes evident that some peaks are appearing at the same retention time. These peaks are most probably coming from the same type of products. As mentioned in the previous paragraph, two peaks are appearing very strongly in the chromatogram of 3-methyl-1-pentene and TESPT; marked in the Figures 6.12 and 6.13 (\* at 6.6 min. and \*\* at 8.3 min.). It was interesting to analyse these two peaks in more detail. Figure 6.14 A and B show the increase in amount of the two reaction products in time, measured with HPLC. Figure 6.14 A corresponds to the sulphur case, whereas in Figure 6.14 B TESPT was used.

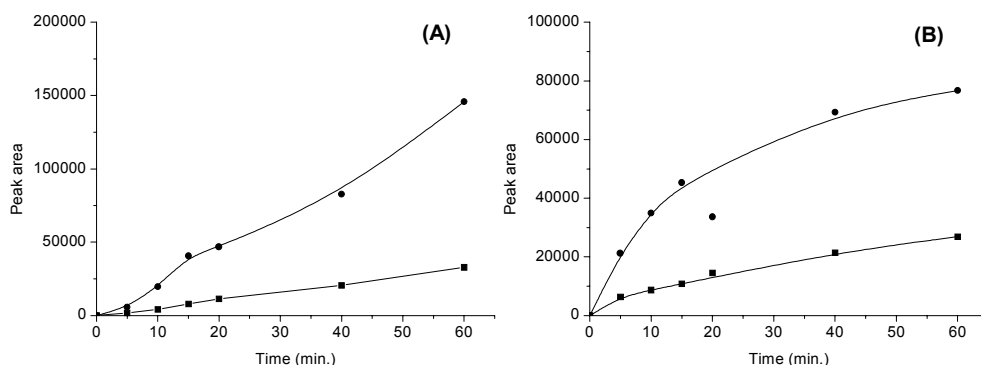


**Figure 6.14** Amount of reaction products as a function of reaction time for (A), 3-methyl-1-pentene with sulphur; (B), 3-methyl-1-pentene with TESPT; retention time of the reaction products: (■), 6.6 min; (●), 8.3 min.

In both cases the reaction product with a retention time of approximately 8.3 minutes increases faster than the product that has a retention time of 6.6 minutes. Because the product peak at 8.3 minutes in the chromatogram is of considerable size, it should also prevail in a  $^1\text{H-NMR}$  spectrum. In the  $^1\text{H-NMR}$  spectrum of the reaction mixture of elemental sulphur with 3-m-1-p, Figure 6.4, signals are appearing indicating a disulphidic product, as mentioned before.

The reaction product, which gives a signal at 6.6 minutes in the chromatogram, is even more difficult to identify. Based on the retention time this peak corresponds to a smaller sulphur bridge in the product. This can then only be a monosulphidic product.

The monosulphidic product is formed in a slightly faster way for the reaction with TESPT than with sulphur. The disulphidic reaction product is formed even significantly faster when TESPT is present during the model compound vulcanisation with 3-m-1-p. The sulphur that is released from the TESPT is apparently more reactive than the elemental sulphur itself. This can be explained by the fact that elemental sulphur is ring-shaped. At elevated temperatures the ring must open before the sulphur can react with the alkene model and create a crosslink.<sup>8</sup>

## 6.4 Discussion

Where model vulcanisation is often invoked as a technique to elucidate chemical mechanisms in real rubber vulcanisates, the present chapter shows, that even then it is a difficult task to reach clear conclusions. The main reason is, that with the sulphur chemistry involved a great many reaction products are formed. To separate all those products and subsequently analyse their chemical structure, without changing the sulphur rank during these procedures, is virtually impossible. With the currently available analytical techniques we are facing the limits of what is possible. This limits the foundation of conclusions and makes them a bit speculative.

From the results shown it is clear, that the reaction rate of elemental sulphur with alkene model compounds differs greatly. 3-methyl-1-pentene reacts faster with elemental sulphur than trans-3-hexene, which in turn reacts faster than TME. After the reaction of 3-

methyl-1-pentene with elemental sulphur, several reaction products were obtained. The reaction products contained different sulphur ranks, as observed with  $^1\text{H-NMR}$  and HPLC. The reaction between elemental sulphur and 3-m-1-p is explained first before discussing in more detail the reaction between TESPT and 3-m-1-p.

Elemental sulphur is a ring-shaped  $\text{S}_8$ -compound, having a melting point of approximately  $116^\circ\text{C}$ . Above this temperature some more energy is still needed to open the ring for the formation of the sulphur radicals, which ultimately become involved in the vulcanisation reaction. Some investigators have stated that the mechanism of vulcanisation indeed involves free sulphur radicals<sup>14-16</sup>; others have postulated mechanisms involving ionic species.<sup>17</sup> In the present system where only 3-m-1-p is present next to sulphur, there is no other ingredient, which can initiate the formation of sulphur radicals.<sup>8</sup> A mechanism can therefore be postulated involving free radicals as shown in Scheme 6.4. This mechanism is in accordance with the radical mechanism proposed by Coran.<sup>18</sup>

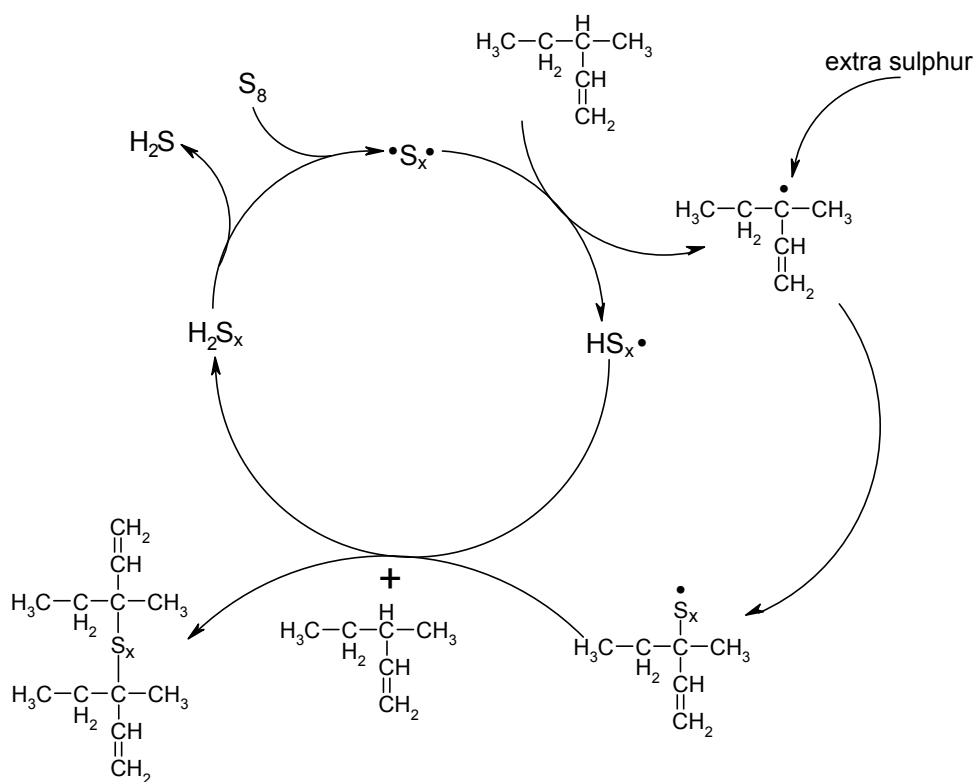
From the experiments with TESPT and 3-m-1-p it has become clear, that TESPT first incorporates sulphur and subsequently donates it to the model compound, as was observed by Debnath et al.<sup>8</sup> A mechanism is postulated in Scheme 6.5. TESPT first accepts sulphur and increases the concentration of the higher sulphides as shown in Figures 6.9 and 6.10. Subsequently, the higher sulphides being in dynamic equilibrium with lower sulphides, donate sulphur back to the reaction mixture as active sulphur moieties. That the sulphur is more active is seen in Figure 6.14. The reaction products formed with the sulphur from TESPT are generated in a faster way than with elemental sulphur. The active sulphur involves itself in the vulcanisation reaction without the help of accelerators, according to the same mechanism as described in Scheme 6.4. Crosslinked products with different sulphur length are obtained. The TESPT can also dissociate, as described in Scheme 6.5, and couple directly to the alkene model. At elevated temperatures longer sulphur chains between the TESPT and the alkene model, will also donate active sulphur that subsequently participates in the vulcanisation reaction: Scheme 6.4. TESPT will react "in rubber" with the vinyl-configuration of BR, because this reaction will have the fastest kinetic rate constant as shown in paragraph 6.3.2. A side product that should be formed is triethoxysilylpropylthiol.

Yet an alternative route for the vulcanisation reaction with TESPT is depicted in Scheme 6.6. The crosslinking reaction is not initiated by active sulphur, but by the dissociated TESPT. The side product that is formed according to this reaction scheme is again triethoxysilylpropylthiol. The rest of the reaction is similar to Scheme 6.5.

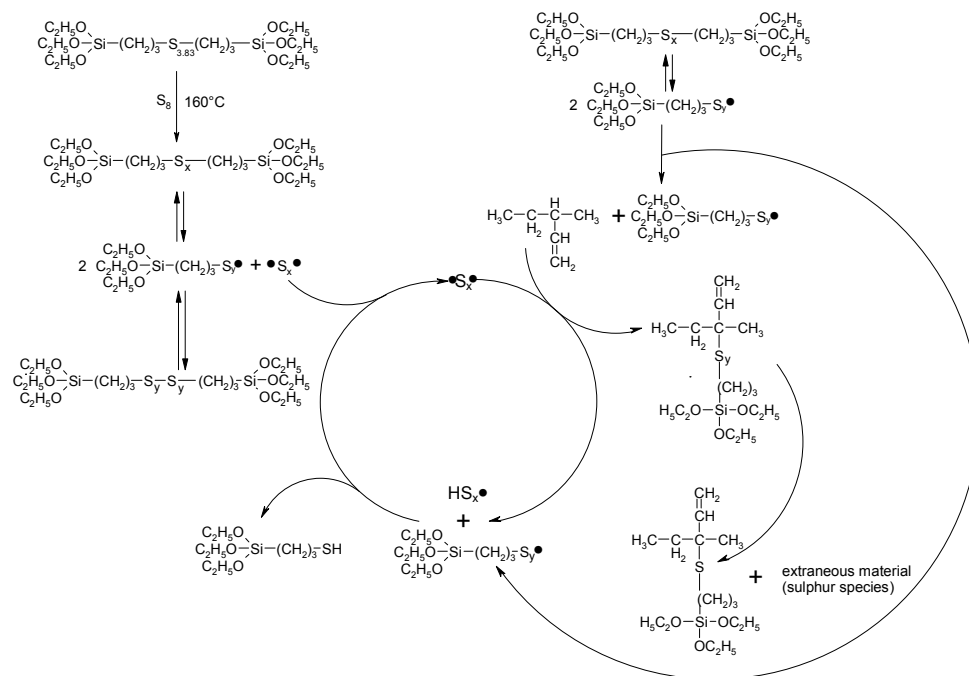
Both reaction schemes, Scheme 6.4 and 6.5, have triethoxysilylpropylthiol as a side product. However, this product was never found in the reaction mixture. An explanation for this seemingly contradictory fact could be, that the triethoxysilylpropylthiol reacts immediately itself with the model compounds: Scheme 6.7. Thurn and Wolff showed in 1975 already, that the triethoxysilylpropylthiol is an extremely reactive coupling agent in silica filled rubbers.<sup>19</sup> They showed that the use of triethoxysilylpropylthiol resulted in very short scorch times, indicating that the product is extremely reactive towards the polymer. A possible reaction mechanism of the triethoxysilylpropylthiol with a polymer was postulated by Gorski et al.<sup>20</sup> They showed that the addition reaction of thiols to the double bond takes place regioselectively at the vinyl and the cis-double bonds at very high speed.

The (TESPT)-(3-m-1-p) product was not found in the reaction mixture due to the low resolution in the chromatograms, as mentioned before. Another possible explanation can be that the TESPT first has to react with the silica before it can react with the polymer. The TESPT coupled to the silica particle reacts in a similar manner as the reaction depicted in Scheme 6.5. After incorporating sulphur and donating it back to the polymer,

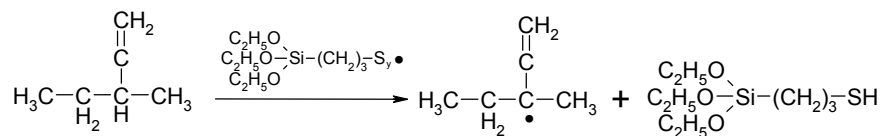
recombination of the remaining parts of the coupling agent is less favourable. The part of TESPT coupled to the silica containing a radical, is diffusion limited due to the large silica particle attached. Instead of reacting with another part of TESPT attached to another silica particle or at a distant place on the same silica particle, it is more favourable to react with the polymer chain. In the present study, silica was omitted. There are no diffusion limitations and therefore the remaining parts of the coupling agent will recombine to another coupling agent molecule with a lower sulphur rank. Experiments with silica, pre-treated with TESPT, and model compound were performed to study this effect. The result was a coagulated system which was impossible to analyse.



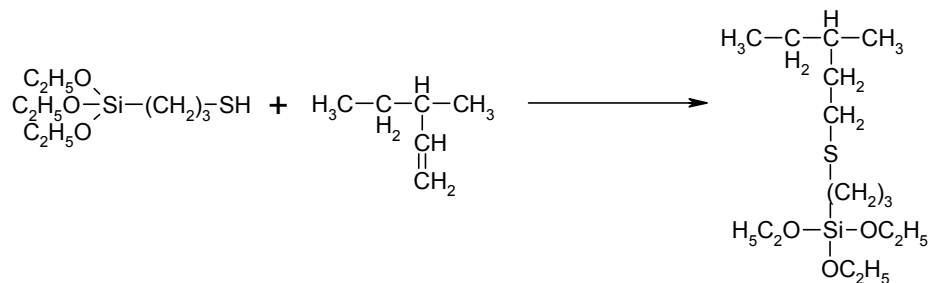
**Scheme 6.4** Postulated reaction of elemental sulphur with 3-m-1-p.



**Scheme 6.5** Postulated reaction of TESPT with 3-m-1-p.



**Scheme 6.6** Postulated initiation reaction of TESPT with 3-m-1-p under formation of triethoxysilylpropylthiol.



**Scheme 6.7** Addition reaction of triethoxysilylpropylthiol with 3-m-1-p.

## 6.5 Conclusions

The products of the reaction between the model olefins and sulphur mainly consist of two molecules of the model coupled by a mono- or disulphide bridge. Also some isomerisation of the model compound takes place during the reaction. The rate constant of the coupling reaction is higher for the 3-methyl-1-pentene (3-m-1-p) than for the trans-3-hexene (t-3-h). The trans-3-hexene in turn is faster than the 2,3-dimethyl-2-butene (TME). The presence of zinc oxide during those reactions does not influence the reaction rate constants.

Reaction of TESPT and 3-m-1-p model compound leads to similar types of reaction products as with elemental sulphur and 3-m-1-p, indicating that TESPT is primarily a sulphur-donor. During the first 5 minutes of reaction TESPT incorporates sulphur. After 5 minutes it starts to donate activated sulphur to the model compound. At long reaction times, TESPT is again incorporating sulphur but this time from the reaction products, when the sulphur bridges are shortening due to reversion reactions.

The main products that are formed when TESPT is used in combination with model olefin compounds are model-S-model and model-S<sub>2</sub>-model. No evidence is found that TESPT itself is bound to the model compound. From all the sulphide ranks available in TESPT, the disulphide rank is the most stable rank and not involved in any of the reactions above.

## 6.6 References

1. Chapter 3 of this thesis.
2. Chapter 5 of this thesis.
3. U. Görl, J. Munzenberg, H.D. Luginsland, A. Muller, *Kautsch. Gummi Kunstst.*, **52**, (1999), 588.
4. L.A.E.M. Reuvekamp, J.W. ten Brinke, P.J. van Swaaij, J.W.M. Noordermeer, *Kautsch. Gummi Kunstst.*, **55**, (2002), 41.
5. L.A.E.M. Reuvekamp, J.W. ten Brinke, P.J. van Swaaij, J.W.M. Noordermeer, *Rubber Chem. Technol.*, **75**, (2002), 187.
6. H.D. Luginsland, presented at a meeting of ACS, Rubber Division, Chicago, Illinois, April 13-16, 1999.
7. H.D. Luginsland, *Kautsch. Gummi Kunstst.*, **53**, (2000), 10.
8. S.C. Debnath, J.W.M. Noordermeer, presented at a meeting of ACS, Rubber Division, Savannah, Georgia, April 29 - May 1, 2002.
9. J.W. ten Brinke, P.J. van Swaaij, L.A.E.M. Reuvekamp, J.W.M. Noordermeer, *Kautsch. Gummi Kunstst.*, **55**, (2002), 244.
10. P. Versloot, J.G. Haasnoot, P.J. Nieuwenhuizen, J. Reedijk, *Rubber Chem. Technol.*, **70**, (1997), 106.
11. P. Versloot, J.G. Haasnoot, J. Reedijk, M. van Duin, E.F.J. Duynstee, J. Put, *Rubber Chem. Technol.*, **65**, (1991), 343.
12. P.J. Nieuwenhuizen, J. Reedijk, M. van Duin, W.J. McGill, *Rubber Chem. Technol.*, **70**, (1997), 368.
13. P.J. Nieuwenhuizen, J.G. Haasnoot, J. Reedijk, *Kautsch. Gummi Kunstst.*, **53**, (2000), 144.

14. E.H. Framer, F.W. Shipley, J. Polym. Sci., **1**, (1946), 293.
15. E.H. Framer, J. Chem. Soc., (1947), 1519.
16. E.H. Framer, J. Soc. Chem. Ind., **66**, (1947), 86.
17. L. Bateman, C.G. Moore, M. Porter, J. Chem. Soc., (1958), 2866.
18. A.Y. Coran, "Science and Technology of Rubber", Academic Press, New York, 1978.
19. F. Thurn and S. Wolff, Kautsch. Gummi Kunstst., **28**, (1975), 733.
20. U. Gorski, E. Klemm, Die Angewandte Makomolekulare Chemie, **254**, (1996), 11.

---

## **Chapter 7**

### ***Distribution of silica filler particles in relation to material properties***

---

The effect of dump temperatures on macro- as well as microdispersion of silica have been studied. It has been found that the dump temperatures do not influence macrodispersion of a highly dispersible silica. On the contrary, the microdispersion as observed with AFM measurements does depend on the dump temperature. With higher dump temperatures a better microdispersion is obtained, as characterised by an increased amount of primary particles.

The macro- as well as microdispersion are influenced by different silica samples with various structures (DBP-values). It has been found that low structured (conventional) silicas show a poor macrodispersion as compared to medium structured/semi dispersible and highly structured/highly dispersible silicas. No improvements were observed on macrodispersion by addition of TESPT to the recipe. Microdispersion measurements revealed an increased level of primary silica particles for higher structured silicas, where the highly dispersible silicas are primarily dispersed to the microdispersion level, with only 15-20% remaining in the macrodispersion regime.

The dynamic and mechanical properties of a tyre tread compound turn out to primarily depend on the level of microdispersion. The filler-filler interactions responsible for poor dynamic mechanical properties, are mainly due to aggregates with a diameter of approximately 600 nm and larger. Also the tensile strength of the compounds is primarily influenced by the microdispersion, where lower tensile strength values are obtained, when aggregates with a diameter larger than 600 nm are present.

In addition to microdispersion measurements, AFM is also in a position to visualise pre-vulcanisation effects in the compounds: elliptical structures appear in the AFM phase image.

The overall conclusion is, that to obtain a tyre tread compound with a low rolling resistance, a highly dispersible/highly structured silica is preferred. This highly dispersible silica should mainly be dispersed to the microdispersion level, to result in primary particles and a low level of aggregates with a size between 100 and 200 nm.

#### **7.1 Introduction**

Amorphous precipitated silica has emerged as a major contributor to the reduction of tyre tread rolling resistance.<sup>1</sup> In contrast to carbon black, the surface properties of

precipitated silica cause a number of difficulties in the use of this material as reinforcing agent, particularly in hydrocarbon elastomers. The surface of hydrated, precipitated silica is highly polar and hydrophilic as a result of its polysiloxane structure and the presence of numerous silanol groups. Due to this hydrophilic surface, mixing with a hydrophobic elastomer is difficult. To achieve good dispersion of the silica filler in the elastomeric matrix use of so-called coupling agents are necessary.<sup>2-6</sup>

One of the most widely used coupling agents to improve the dispersion of the silica filler is bis-(triethoxysilylpropyl)tetrasulphide (TESPT).<sup>7-9</sup> The role of this coupling agent is to shield the silica surface and make it more hydrophobic and, second, to couple the silica particle to the rubber.<sup>10-12</sup> The first reaction is of interest in the dispersion of silica. If the reaction of the coupling agent is improved, then the silica will disperse to a better level, i.e. more primary particles.

Different types of silica are available and all have different physical properties, which may influence the dispersion of the silica. Silicas can be classified as conventional, semi dispersible or highly dispersible silicas, depending on the amount of silica dispersed to a level smaller than approximately 1  $\mu\text{m}$ . There is always a bimodal distribution with a main peak at approximately 10  $\mu\text{m}$ : Figure 7.1. This peak is attributed to the initial structure with large agglomerates of silica. Particles with a size larger than 5  $\mu\text{m}$  are commonly designated as part of the "macrodispersion", and the particles with a diameter smaller than 1  $\mu\text{m}$  belong to the "microdispersion".

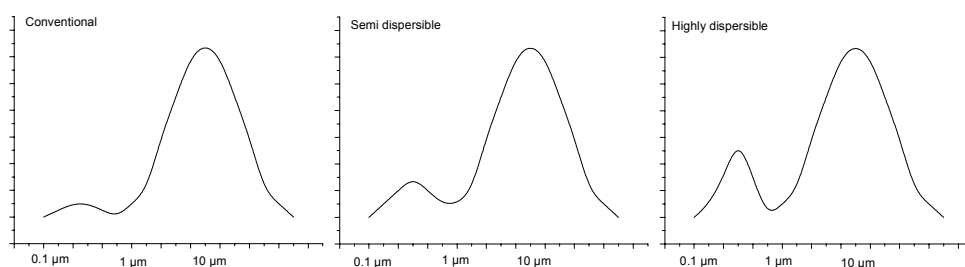


**Figure 7.1** Particle size distribution for different classes of silica.

A classical method to determine the structure of fillers is the DBP value. This method was developed for the characterisation of carbon black and describes the void volume in the filler structure available for dibutyl phthalate (DBP) penetration. A high DBP value corresponds to a high structure of the filler. A silica with a DBP value lower than 180 is commonly designated as conventional (C); with a DBP value between 180 and 200 is designated as semi dispersible (SD) and with a DBP value higher than 200 as highly dispersible (HD).<sup>13</sup>

Especially for tyre applications, highly dispersible silica (HDS) has become of great importance.<sup>14-16</sup> Highly dispersible silica can disperse more easily to the level of primary particles. The extent of dispersion then has a major influence on dynamic mechanical properties.

In order to optimise the morphology-property relationships in polymeric systems, knowledge of microscopic morphology and physical properties are essential.<sup>17,18</sup> In the past, optical and electron microscopy have been the primary methods for determining the dispersion of various fillers in rubber. Scanning Tunneling Microscopy (STM), which can be used to study the surfaces of conducting materials, has been used successfully to image the surface structure of carbon black.<sup>19-24</sup>

The Atomic Force Microscope (AFM) is another version of the scanning tunnelling microscope. Both systems were developed by Binnig and co-workers and have the potential for atomic resolution.<sup>25,26</sup> The AFM has rapidly developed into a powerful tool, which can image surface topology of both insulating and conductive samples. Since its invention in 1986, the AFM has been applied extensively in polymer science and technology. The operation is based on detecting the cantilever deflection, which is caused by small forces acting between a sharp tip on the cantilever and the sample surface. Recently it has been demonstrated, that AFM can also be applied for determining the dispersion of fillers in rubbers.<sup>21, 22</sup>

In the previous chapters only one type of highly dispersible silica was used. The aim of this chapter is to quantify the effects of silica dispersibility, using representative silica samples of all three classes. The first part of the present chapter focuses on the effect of the dump temperature on the macro- and micro-dispersion of a highly dispersible silica. In the second part of this chapter several silicas are tested from the different classes; conventional, semi and highly dispersible. The experiment is performed in the absence and presence of TESPT coupling agent. Macrodispersion and microdispersion measurements are performed on the compound recipes containing the different classes of silica. The macrodispersion is obtained with optical light microscopy and the microdispersion is obtained with the aid of AFM. Dynamic and mechanical properties of the different compounds are measured and related to the macro- and micro-dispersion.

## 7.2 Experimental

*Compound recipe.* — The different types of silica, that were used, are listed in Table 7.1. The silicas are ordered by increasing DBP value. Also their BET-specific surface area is mentioned as an indication of primary particle size. The last column in Table 7.1 is a classification of the different types of silica; (C), conventional; (SD), semi dispersible; (HD), highly dispersible, according to the classification proposed by Blume.<sup>13</sup> All experiments were performed using a tyre tread composition as shown in Table 7.2, representing a silica filled recipe corresponding to the fuel-saving green-tyre technology.<sup>27</sup> The compounds were mixed, cured and characterised according to the procedures described in the experimental paragraph of Chapter 3.

**Table 7.1** Types of silica

Silica	Source	BET (m <sup>2</sup> /g)	DBP (g/100g)	Class
Grace® PQks408 gr	Akzo	190	151	C
Ultrasil® VN3	Degussa	175	176	C
Hisil® dxr 115 gr	PPG	168	192	SD
Zeopol® 8745 gr	Huber	175	200	HD
Zeosil® 1165 MP	Rhodia Silices	160	202	HD
Ultrasil® 7005p	Degussa	185	217	HD

**Table 7.2** Tyre tread recipe (phr) with the various silicas investigated.

Component	Recipe					
	I	II	III	IV	V	VI
S-SBR (Buna <sup>®</sup> VSL 5025-1 HM) <sup>a</sup>	75	75	75	75	75	75
BR (Kosyn <sup>®</sup> KBR 01)	25	25	25	25	25	25
Grace <sup>®</sup> PQks408 gr	<b>80</b>	-	-	-	-	-
Ultrasil <sup>®</sup> VN3	-	<b>80</b>	-	-	-	-
Hisil <sup>®</sup> dxr 115 gr	-	-	<b>80</b>	-	-	-
Zeopol <sup>®</sup> 8745 gr	-	-	-	<b>80</b>	-	-
Zeosil <sup>®</sup> 1165 MP	-	-	-	-	<b>80</b>	-
Ultrasil <sup>®</sup> 7005p	-	-	-	-	-	<b>80</b>
Coupling agent	7	7	7	7	7	7
Aromatic oil (Enerflex <sup>®</sup> 75)	32.5	32.5	32.5	32.5	32.5	32.5
ZnO	2.5	2.5	2.5	2.5	2.5	2.5
Stearic acid	2.5	2.5	2.5	2.5	2.5	2.5
Sulphur	1.4	1.4	1.4	1.4	1.4	1.4
CBS (Santocure <sup>®</sup> -GRS-2MM)	1.7	1.7	1.7	1.7	1.7	1.7
DPG (Perkacit <sup>®</sup> -PDR)	2	2	2	2	2	2
Total	229.6	229.6	229.6	229.6	229.6	229.6

<sup>a</sup> vinyl content is 50%, styrene content is 25% and the oil content is 37.5 phr.

*Macrodispersion measurements.* — Vulcanised samples were cut with a razor blade and measured on ten different spots. Macrodispersion measurements were performed with two types of optical light microscopes. A Dispergrader Optigrade 100 reflective optical light microscope was used to examine the effect of dump temperature on the morphology of a tyre tread compound. A Leica Quantimet 500 IW optical microscope was used to examine the effect of different types of silica on the morphology of a tyre tread compound. For both microscopes the magnification was 100 times. Particle sizes of 5  $\mu\text{m}$  and larger can be detected with this method.

*Microdispersion measurements.* — Atomic Force Microscopy experiments were conducted using a NanoScope III multimode scanning force microscope (Digital Instruments (DI), Santa Barbara, CA, USA) in Tapping Mode with phase imaging. Standard Si Nanosensor probes were used to conduct the measurements. Unvulcanised samples for the AFM observation were prepared by microtoming the surface of the samples with a rotary Leica microtome at  $-130^{\circ}\text{C}$ , with a diamond knife. Particle sizes of 1  $\mu\text{m}$  and smaller can be detected with this method.

*Particle size distribution calculation.* — The particle size distributions were calculated with a Leica Quantimet 500 IW software system. First, the area of the silica particles are counted in the microscopic image. Second, for the calculation of the diameter of the silica particles, perfectly round particles were assumed. Particles with a similar diameter were counted and the relative amount of particles, with a particular diameter were plotted in a histogram. The white area percentage was calculated by dividing the total area of all the particles visible in the microscopic image, by the total area of the image and then multiplying by a factor of 100.

### 7.3 Results and discussion

The first experiment that was carried out was to study the effect of the dump temperature on the macro- and micro-dispersion. In paragraph 7.3.1 the compounds were mixed at different rotor speeds and fill factors to achieve different dump temperatures. In paragraph 7.3.2 and 7.3.3, all the compounds with the different types of silica and in presence of TESPT silane coupling agent were mixed up to a dump temperature of 150°C.

#### 7.3.1 Effect of dump temperature on the macro- and microdispersion of silica

The typical tyre tread compound recipe V in Table 7.2 was mixed up to different dump temperatures with TESPT as the silane coupling agent, according to the procedure outlined in Chapter 3. After curing, the compounds were prepared for dispersion measurements according to the experimental paragraph.

##### *Macrodispersion*

A first indication whether the dispersion of the silica filler is improved with increasing dump temperature, is the white area percentage: Figure 7.2. From this figure it can be concluded that an increase in dump temperature does not have a huge influence on the macro dispersion. The white area percentage remains more or less constant up to dump temperature of 165°C. At a dump temperature of 180°C a higher white area percentage is observed, which indicates a worse dispersion of the silica filler in the rubber compound. This is unexpected because in Chapter 3 it was observed, that higher dump temperatures led to better dispersion of silica filler.

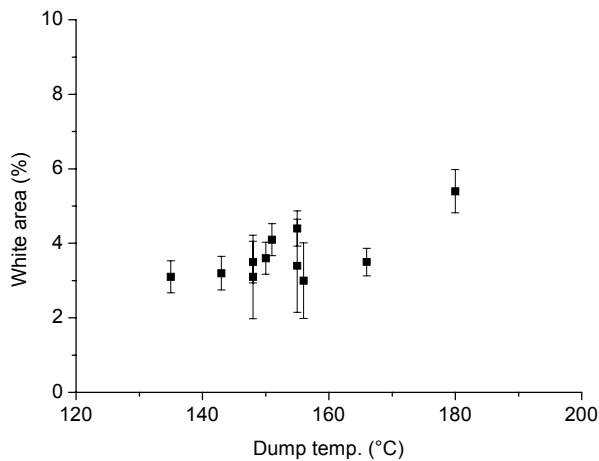


**Figure 7.2** White area percentage as a function of dump temperature.

A closer look at the particle size diameter, shows that a large amount of the particles has a diameter of approximately 10  $\mu\text{m}$ : Figure 7.3. Second, the dump temperature has no influence on the silica particle size distribution. For all dump temperatures, ranging from 135°C to 180°C, the distribution is similar with a peak at 10  $\mu\text{m}$ .

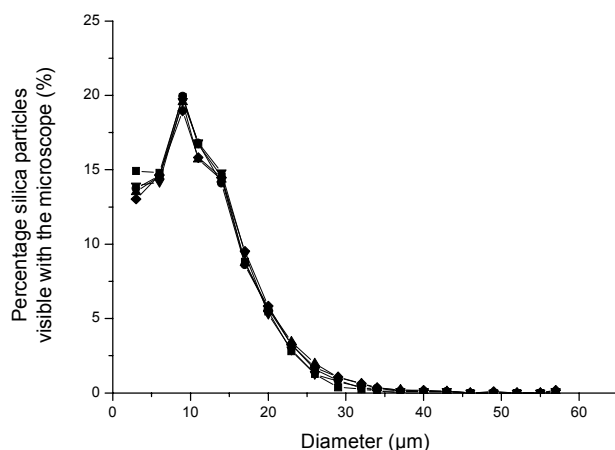


**Figure 7.3** Percentage silica particles visible with the microscope vs. the silica particle size for different dump temperatures; ■, 135°C, ●, 151°C, ▲, 155°C, ▼, 166°C, ◆, 180°C.

If the silica is perfectly dispersed, 20% v/v should be silica according to the compound recipe, Table 7.2. This means that at any given section of the sample, 20% of the area should consist of silica. As observed in Figure 7.2 only 3 to 4% of the microscopic image contains silica; corresponding with 15 to 20% of the total silica amount. This means that the 80 to 85% of the silica is dispersed to a level, which is not detectable with optical light microscopy; smaller than 5  $\mu\text{m}$ . This dispersion level is commonly called the microdispersion level.

The silica in recipe V used for the experiment above, is a highly dispersible silica<sup>28</sup>: Table 7.1. Because of this fact, the silica may be dispersed to the primary particle size of approximately 30 nm. This size is far too small to detect with visible light and therefore other techniques are necessary to study the dispersion. One technique, which was already successfully applied at an earlier occasion on silica filled rubbers, is Atomic Force Microscopy (AFM).<sup>22</sup>

### Microdispersion

Figure 7.4 shows the microdispersion of highly dispersible silica in the rubber matrix, recipe V. The difference between the two figures is the dump temperature: the compound in Figure 7.4 A was mixed up to a dump temperature of 135°C, whereas the compound in Figure 7.4 B was mixed up to a dump temperature of approximately 180°C. In both figures, the silica particles are visible as white spots. Filler particles are readily distinguished, having a bright contrast in the dark rubber matrix. The bright contrast can be associated with a higher stiffness of the filler particles as compared to the rubber matrix. At first sight it seems, that in Figure 7.4 A not many silica particles are present, but also the darker spots contain silica, covered with a thin layer of polymer. Figure 7.4 B shows more

silica particles, which are mainly primary particles. The particles seem to end up in channel-like-structures, which are interconnected. The width of the channel-like-structures is wider in Figure 7.4 B. The channel-like-structures will be discussed in more detail in Chapter 8. Also light elliptical structures are appearing in this AFM image; marked with an arrow in the image. These structures are caused by the pre-vulcanisation of the compound in the mixer, due to the high mixing temperature, Chapter 3. Because of the crosslinks in these parts of the polymer, it is stiffer and appears as a white structure. These structures are also visible when fully vulcanised samples are submitted to AFM measurements.<sup>22</sup> The polymer domains between the channel-like-structures are larger in Figure 7.4 B than in Figure 7.4 A.

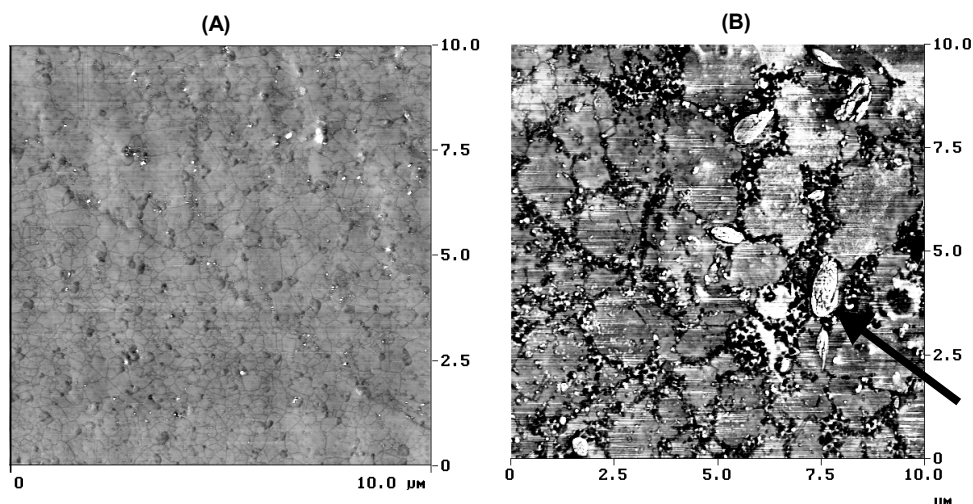


**Figure 7.4** AFM phase images of recipe V filled with highly dispersible silica mixed up to different dump temperatures: (A), 135°C; (B), 180°C.

The microdispersion of the silica particles is better in the compound with a dump temperature of 180°C than for the compound with a dump temperature of 135°C. A quantitative picture of the silica size distribution is given in Figure 7.5. The amount of silica with a particular diameter is plotted versus the corresponding diameter of the particle. The inserts in Figure 7.5 are enlargements, emphasising the higher particle diameter fraction. At 180°C dump temperature more primary particles are obtained, as was seen in the AFM image. The fact that the compound at 180°C results in more primary particles, i.e. better dispersion, corresponds with the low  $G'$  values at 0.56% strain for this compound as shown in Chapter 3.

For both dump temperatures the macrodispersion does not differ significantly, as already seen in Figure 7.3. The AFM measurement shows a difference in dispersion of the silica on microdispersion level. At first sight it looked in Figure 7.4 B that more silica was present. However, this effect can be explained by the fact that for the compound with the lower dump temperature, i.e. 135°C, more aggregates and agglomerates are still present in the compound. Furthermore, during the AFM measurements only areas on the surface are measured where no large aggregates or agglomerates are present. Otherwise the image would be partly filled with one aggregate or agglomerate of silica. This is a somewhat subjective aspect of all sorts of microscopy on such a small scale.

The compound, which reached a dump temperature of 180°C, shows relatively more primary particles in comparison with the one which reached 135°C. Therefore, less aggregates are present in the compound again in agreement with the  $G'$  values obtained at low strain.

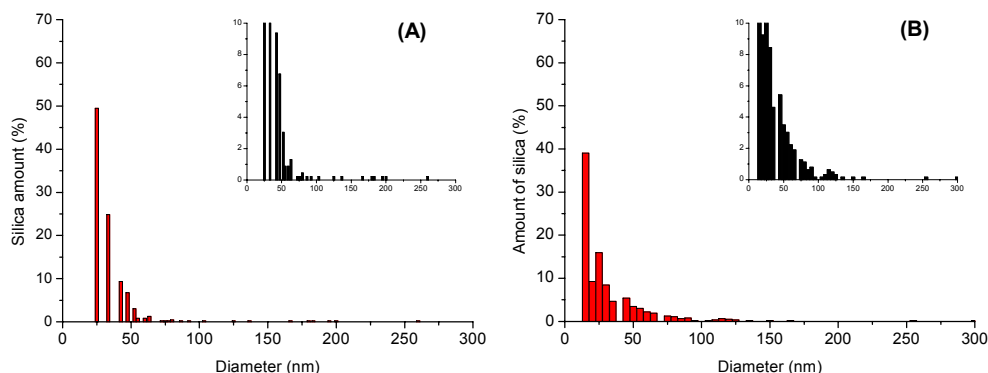


**Figure 7.5** Silica size distribution (microdispersion) for recipe V and mixed at different dump temperatures; (A), 135°C; (B), 180°C.

The combined results of macro- and microdispersion indicate the following picture. What is observed in the macrodispersion measurement is just a left over of very hard, sintered silica agglomerates, which will not disperse at any rate, representing at best 15-20% of the silica added. These hard agglomerates are an impurity rather than that they play an important role in reinforcing the rubber. The 80-85% dispersed to the micro level is the real reinforcing part, whose dispersion can be linked to the earlier observations of the  $G'$  values at low strain, as measures for dispersion as well as filler-filler interactions.

### 7.3.2 Dispersion of different types of silica in absence of TESPT coupling agent

Novel precipitated silicas are normally prepared with a BET specific surface ranging from about 140 to 200  $m^2/g$ . They exhibit an outstanding capacity for deagglomeration and dispersion<sup>14, 28, 29</sup>. The dispersion coefficient of silica also largely depends on the DBP value. A higher DBP value also results in better dispersion of the silica.<sup>13</sup>

Several types of silicas are available but show different material end properties. The silicas used during the experiments were listed in Table 7.1 and are classified in three different categories: conventional, semi dispersible, highly dispersible. The following paragraphs shows the effect of the macro- and microdispersion of silica on the dynamic and mechanical properties of a tyre tread compound in the absence or presence of TESPT silane coupling agent: Recipe I to VI: Table 7.2.

### Macrodispersion

The macrodispersion was measured for compounds with the different types of silica mentioned in Table 7.1, prepared in absence of TESPT coupling agent, with a Leica system according to the procedure described in the experimental paragraph. Table 7.3 shows the white area percentage of silica in the rubber compound. From this table it is evident that two types of silica differ from the others; compound recipes I and II. These compounds contain conventional silicas and correspond to the fact, that there is a relatively high amount of agglomerates still present in the compound. All other recipes (III to VI) result in equal macrodispersion. Recipe V stands out slightly better, because the white area percentage is lowest.

The distribution of the silica particle sizes is depicted in Figure 7.6. The figures are truncated at the left side at 5  $\mu\text{m}$ , being the smallest particle size visible in the microscope. Particles with a diameter of approximately 5  $\mu\text{m}$  are in all cases present in the highest amount. Recipe I and II show the lowest amount for a particle diameter of 5  $\mu\text{m}$ . There are relatively more larger particles present, as was already shown in Table 7.3. Recipe VI results in the highest amount of particles with a diameter of 5  $\mu\text{m}$  and the distribution is very narrow. Recipe V shows the lowest amount of white area, but the distribution is broader than for recipe VI. The silica in recipe V does not show any particles with a diameter larger than 50  $\mu\text{m}$ .

**Table 7.3** White area percentage of different types of silica.

Recipe	White area (%)
I	11.9
II	11.4
III	4.8
IV	4.9
V	3.1
VI	4.5

Based on the observations in the former paragraph, it has to be noted though, that we only see the left-over of the silica in the macrodispersion. Obviously, the industrial definition of high dispersion is based on macrodispersion measurements. Of real importance is the microdispersion which will be discussed next.

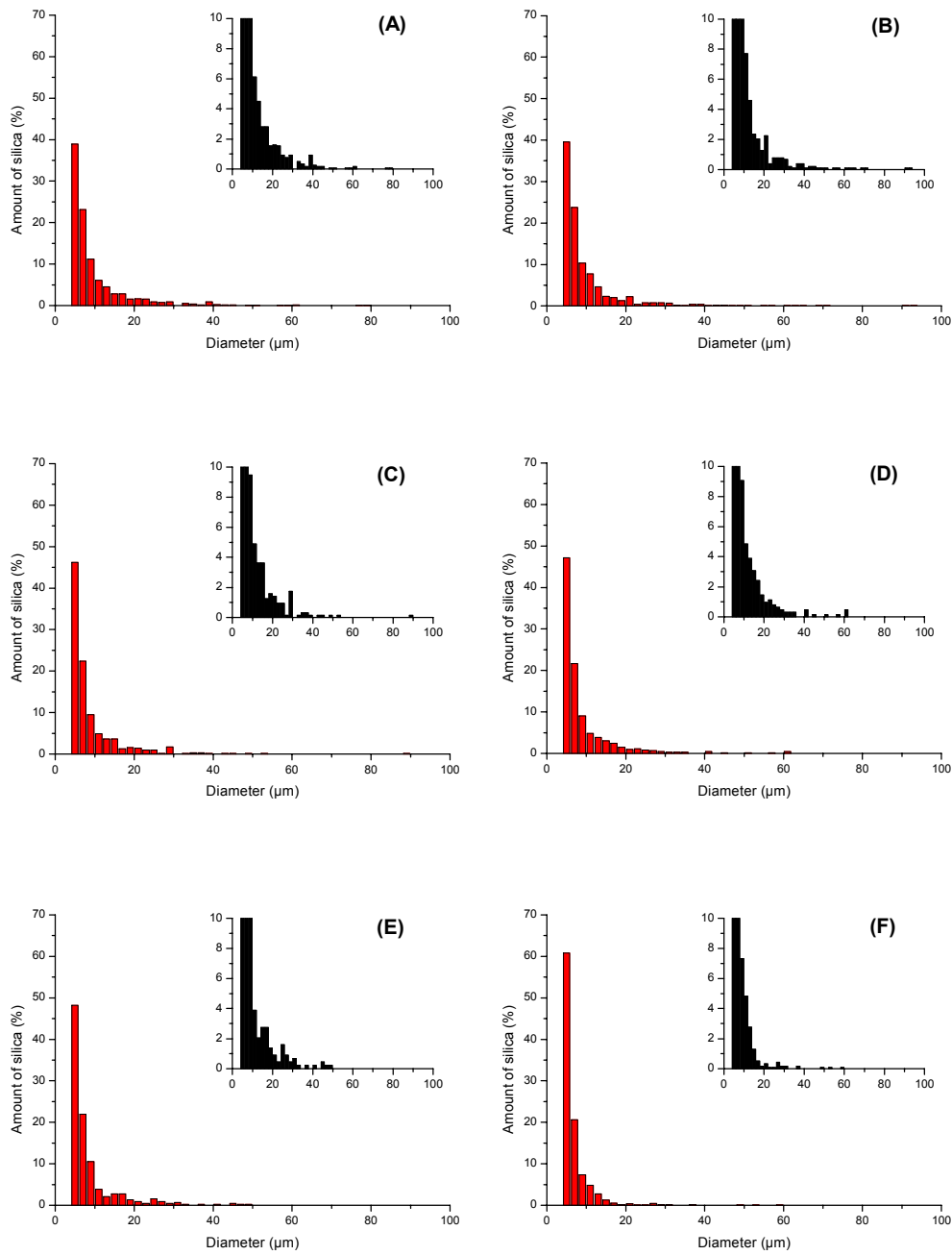


**Figure 7.6** Silica size distribution (macrodispersion) for different recipes in absence of TESPT; (A), I; (B), II; (C), III; (D), IV; (E), V; (F), VI.

### *Microdispersion*

The differences in microdispersion are much more conspicuous between the different types of silica than the macrodispersion. Figure 7.7 shows the AFM images of the compounds filled with the different types of silica. The left image is always the height image whereas the right image is the phase image. The height image shows the 3-D topography of the investigated surface. Different grey colours correspond to different heights from black for the lowest to white for the highest. A first impression when observing the images is, that the silica in recipe I is mainly dispersed to the primary particle size. Only a few aggregates are present in the compound. On the other hand, recipe I showed a large white area in the macrodispersion meaning that the overall dispersion is not good. In the case of recipe II, Figure 7.7 B and recipe III, Figure 7.7 C also a good microdispersion is obtained. Recipe I and recipe II show a similar behaviour: both have a relatively good microdispersion, but the macrodispersion resulted in the largest amount of white area. Recipe III on the other hand, resulted in a good microdispersion and also a good macrodispersion. Figure 7.7 F represents recipe VI. Large aggregates are visible with a diameter up to 500 nm, the rest of this silica in recipe VI is dispersed to single primary particles. The structure of the aggregates is very grainy. Also in recipe IV relatively large aggregates are present, Figure 7.7 D. Recipe V also shows several aggregates, but the main part of the silica is still dispersed to the primary particle size.

The quantification of the distribution of the silica particle sizes is represented in Figure 7.8. When observing the amount of silica with a certain diameter in percentages, two types of silica attract particular attention. Recipes I and II show the lowest amount of silica, which is dispersed to the primary particle diameter of approximately 20-30 nm. Recipe III possesses the narrowest silica size distribution, in the image there are no particles with a size larger than 200 nm. Almost all of the silica in recipe VI is dispersed to primary particles, but there are still a few large aggregates present in the compound. Recipe IV shows also a very narrow silica size distribution. Again the main part of the silica has a diameter smaller than 100 nm although some percentages of the silica have a size up to 400 nm. In the case of recipe V, the silica is partly very well dispersed to the level of primary particles. A large percentage of the silica is dispersed up to a level with a diameter below the 100 nm. The difference with the other silicas is, that there are also very large aggregates present. Diameters of large aggregates of approximately 700 nm are obtained, which was not the case for the other types of silica.

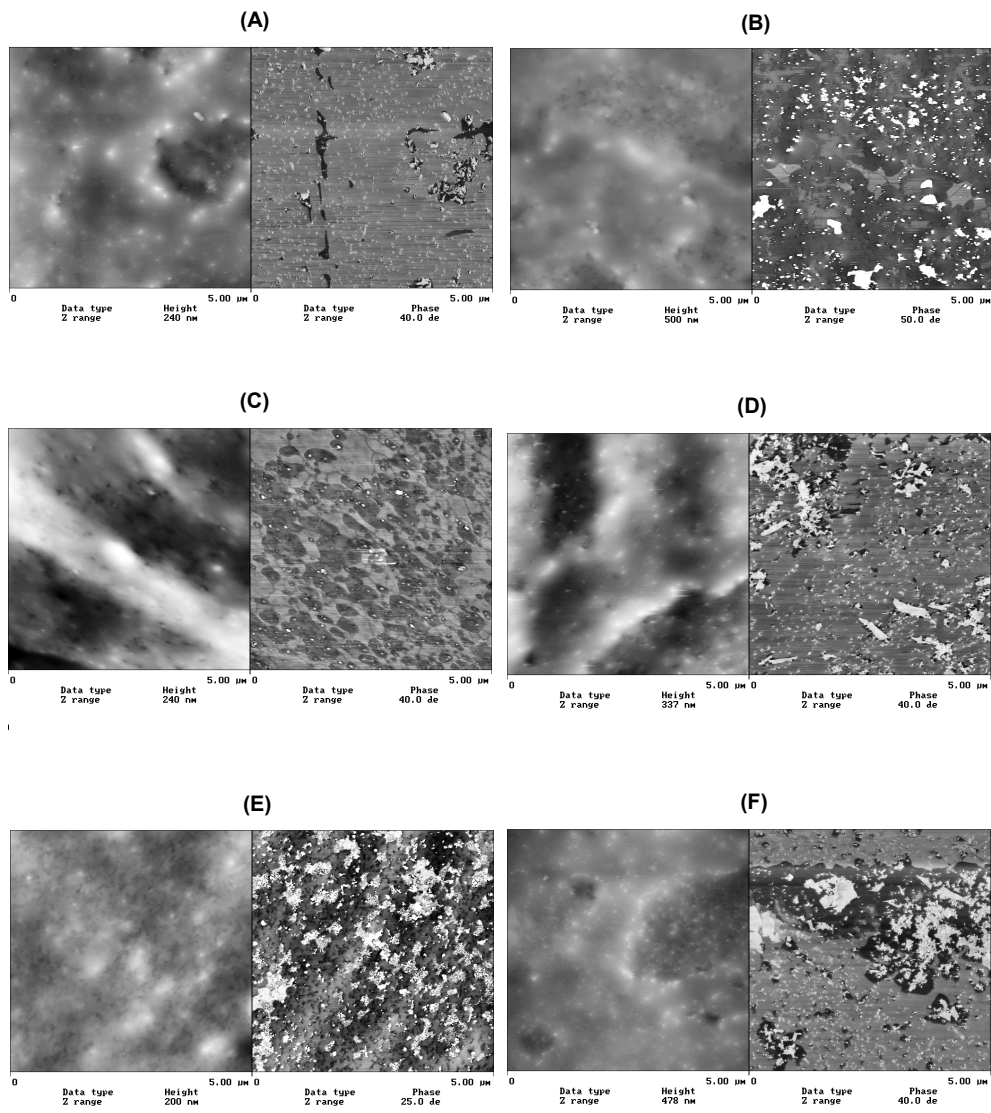


**Figure 7.7** AFM images of the silica distribution (microdispersion) for different recipes in absence of TESPT; (A), I; (B), II; (C), III; (D), IV; (E), V; (F), VI.

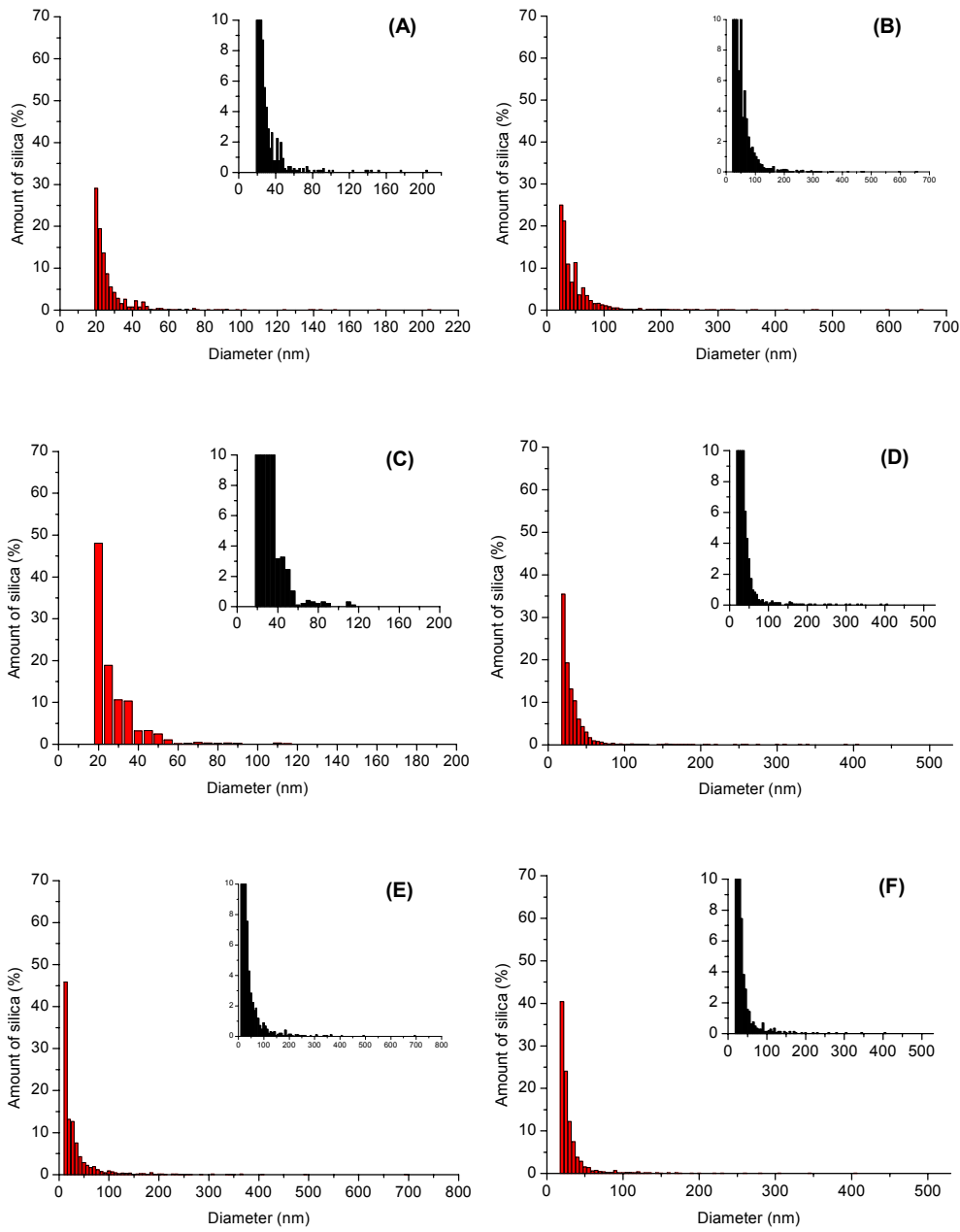


**Figure 7.8** Silica size distribution (microdispersion) for different recipes in absence of TESPT; (A), I; (B), II; (C), III; (D), IV; (E), V; (F), IV.

## Dynamic mechanical properties

After the second mixing step dynamic mechanical measurements were performed on the compounds to study the dispersion of the silica filler in the compound. Figure 7.9 shows the effect on the storage modulus ( $G'$ ) after the second mixing step. The highest  $G'$  at 0.56% strain is obtained for recipes II and V. There is a high amount of filler-filler interactions, which contribute to  $G'$ . The lowest  $G'$  at 0.56% strain is observed for recipe IV.

When comparing the results of the dynamic mechanical measurement with the macrodispersion, no correlation is found. Recipe I showed the highest amount of white area percentage but shows a lower  $G'$  than recipe V, which had the lowest amount of white area percentage.

A better correlation can be obtained between the microdispersion and the  $G'$  at low strain: recipes II and V are the only compounds that contain silica aggregates with a size larger than 600 nm. Apparently these aggregates contribute most prominently to the filler-filler interactions. The lowest value for  $G'$  is for recipe IV. In this case the silica size distribution is narrow as mentioned before. There are no aggregates > 600 nm remaining in this compound, resulting in low filler-filler interactions. Recipe III still shows a high value for the  $G'$  at low strain although the microdispersion was the narrowest. A closer look at the AFM images shows that not many silica particles are present in the image, Figure 7.7 C. Due to the relatively large aggregates present in recipe VI, also a larger value for  $G'$  at low strain is obtained. Recipe I has a narrow silica size distribution but the compound shows also a very poor macrodispersion. This confirms, that macrodispersion apparently has a negligible influence on the  $G'$  values.

The tensile properties of the different compounds are highly comparable, Figure 7.10. There is practically no correlation between the microdispersion of the silica and the mechanical properties. Only the recipes II and V show a somewhat lower tensile strength, caused by the aggregates with a size larger than 600 nm. For all the other compounds the tensile properties are more or less the same.

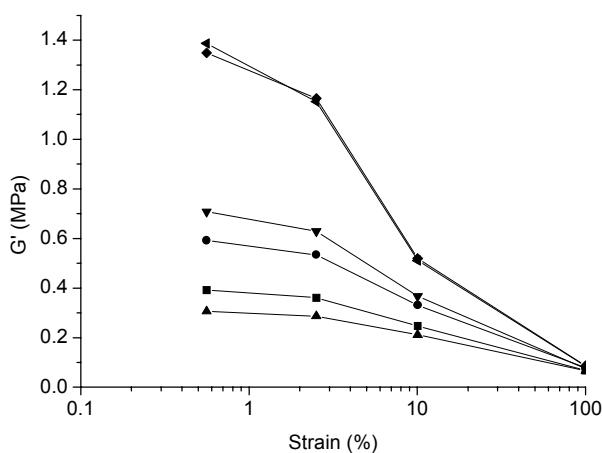


**Figure 7.9** Storage modulus as a function of the deformation; (■), I; (◄), II; (▼), III; (▲), IV; (◆), V; (●), VI.

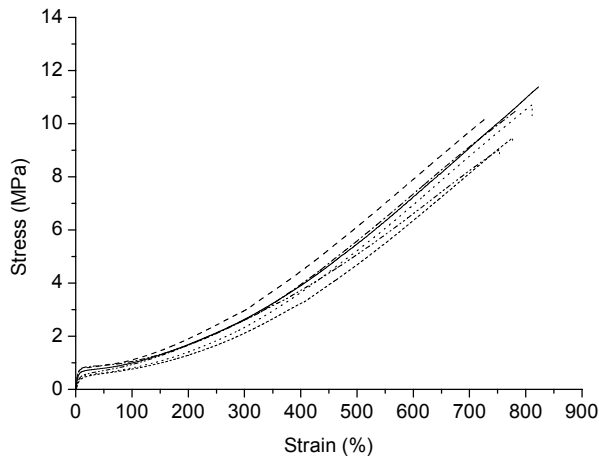


**Figure 7.10** Stress strain curves; (—), I; (---), II; (-.-), III; (-.-.-), IV; (.....), V; (-.-.-), VI.

**Table 7.4** Effect of macro- and microdispersion on dynamic and mechanical properties in absence of TESPT; (-), poor; (+), good; (X) not present; (O), present.

Recipe	Macrodispersion	Large aggregates > 600 nm	G' (0.56%) (MPa)	Tensile strength (MPa)
I	-	X	0.3921	11.4
II	-	O	1.3867	8.9
III	+	X	0.7077	10.5
IV	+	X	0.3060	10.2
V	+	O	1.3484	9.4
VI	+	X	0.5929	10.3

Table 7.4 shows a summary of the results of the present paragraph. A low DBP value (conventional silica) only has a negative influence on the macrodispersion. High DBP values (semi or highly dispersible silica) result in a good macrodispersion. In absence of TESPT, no significant differences are obtained in microdispersion between the different classes of silica.

### 7.3.3 Dispersion of different types of silica in presence of TESPT

If the silica filler is included in the presence of TESPT as coupling agent, significantly better dispersions in the rubber matrix are obtained. First indications for this better dispersion are obtained from the macrodispersion.

*Macrodispersion*

Table 7.5 shows the white area percentage for the different types of silica in the presence of TESPT in the rubber compound. The highest white area percentage is found for recipe I and II, although there is a decrease in white area, apparently due to the presence of the coupling agent. The white area percentage for recipe V is higher compared to the same recipe in the absence of coupling agent, Table 7.5 resp. Table 7.3. The lowest white area percentage is now observed for recipe IV.

The distributions are depicted in Figure 7.11. Recipe VI shows the narrowest silica size distribution, with the highest amount of silica having a diameter of approximately 5  $\mu\text{m}$ . Recipes I and II contain agglomerates that are larger than 60  $\mu\text{m}$ . This is also the case for recipe IV but in this case the overall distribution is narrower: there are less particles in the 20 and 40  $\mu\text{m}$  interval. Recipe III results in more or less the same distribution of silica size as compared with recipe IV, but in the case of recipe III there are more particles present in the compound which have a size larger than 20  $\mu\text{m}$ . Recipe V shows a similar silica size distribution as recipe IV. Further, the distribution in silica sizes is more or less the same as compared to the compounds without coupling agent.

The addition of TESPT leads to lower amounts of white area percentages, compare Table 7.3 with Table 7.5. The largest decrease in white area due to the presence of TESPT is obtained for recipes I and II. The distribution of the silica in recipes I to VI is less affected by the presence of TESPT: Figure 7.6 versus Figure 7.11.

**Table 7.5** White area percentage of different types of silica coated with TESPT.

Recipe	White area (%)
I	6.9
II	7.5
III	3.1
IV	2.8
V	3.9
VI	4.0

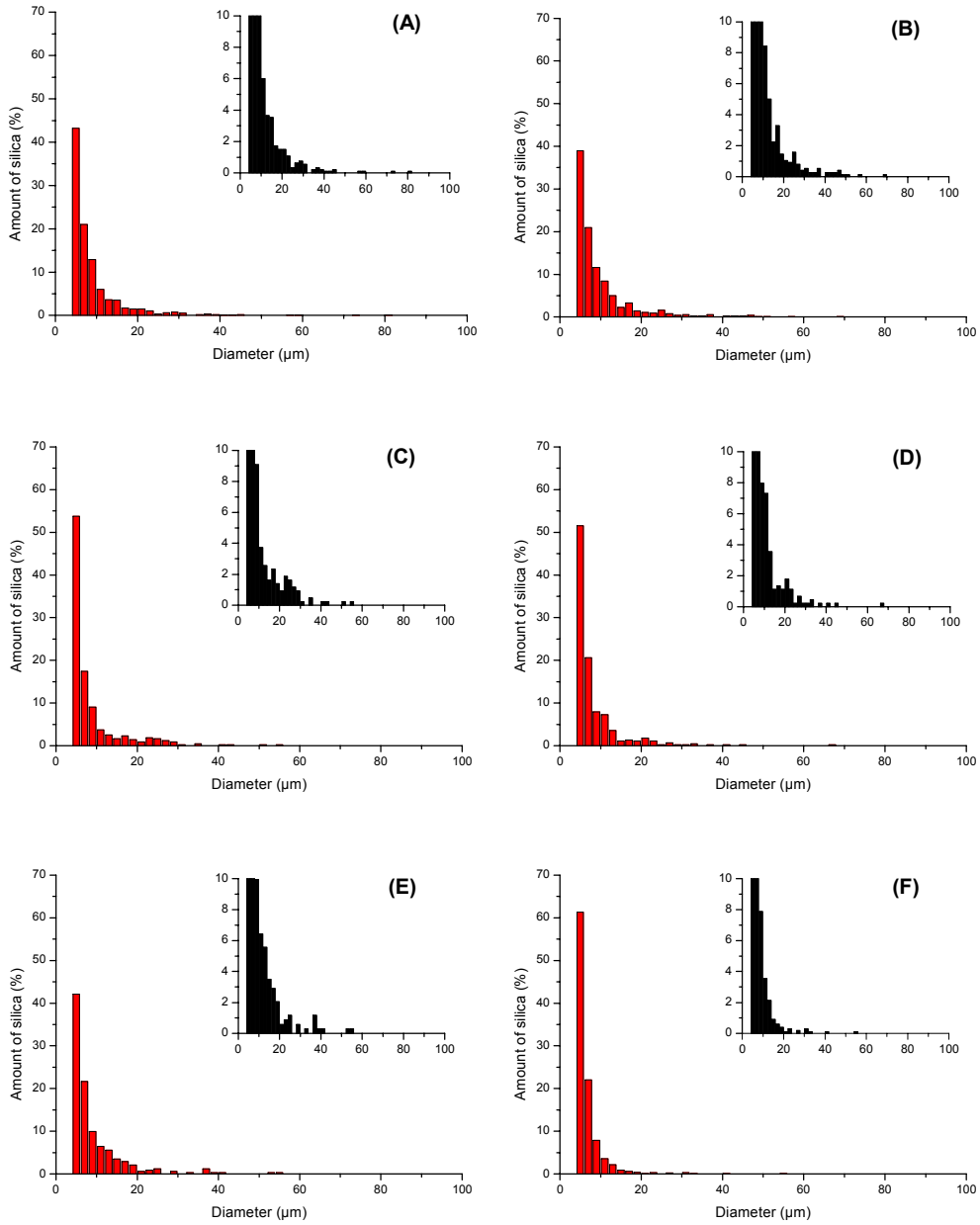


**Figure 7.11** Silica size distribution (macrodispersion) for different recipes in presence of TESPT; (A) I; (B), II; (C), III; (D), IV; (E), V; (F), VI.

### *Microdispersion*

The AFM images of the compounds with different types of silica prepared in the presence of TESPT silane coupling agent, are depicted in Figure 7.12. The compound recipes I and III were difficult to measure but show almost no aggregates: Figure 7.12 A and 7.12 C. This is also reflected in silica size distribution: Figure 7.13 A and 7.13 C. Almost all silica particles have a diameter below 100 nm. The other samples are easier to interpret. Recipe VI shows the best dispersion, almost only primary particles can be observed: Figure 7.12 F. This is also visible from the silica size distribution plot: Figure 7.13 F. The main part of the particles has a diameter below 100 nm. The large white area's on the surface are not silica but are thin sections of the compound that remained on the surface after microtoming. The silica in recipes IV and V is also well dispersed to a level of primary particles but still possess several aggregates in the compound, which clearly show up in the AFM phase images: Figure 7.12 D and 7.12 E. Both types of silica have a narrow silica size distribution, but also show a small amount of aggregates between 100 and 200 nm: Figure 7.13 D and 7.13 E. The silica in recipe II is also well dispersed, but there is a higher amount of aggregates present in the compound. This is also clear in the silica size distribution graph: Figure 7.13 B. Although a large part of the silica is dispersed to the primary particle level, still a high percentage consists of aggregates with a size between 200 and 700 nm.

Overall, the effect of the TESPT coupling agent is clearly visible on the silica microdispersion as obtained with the AFM in comparison with the data shown in paragraph 7.3.2. Due to the presence of TESPT less aggregates and more primary particles are present in the compound.

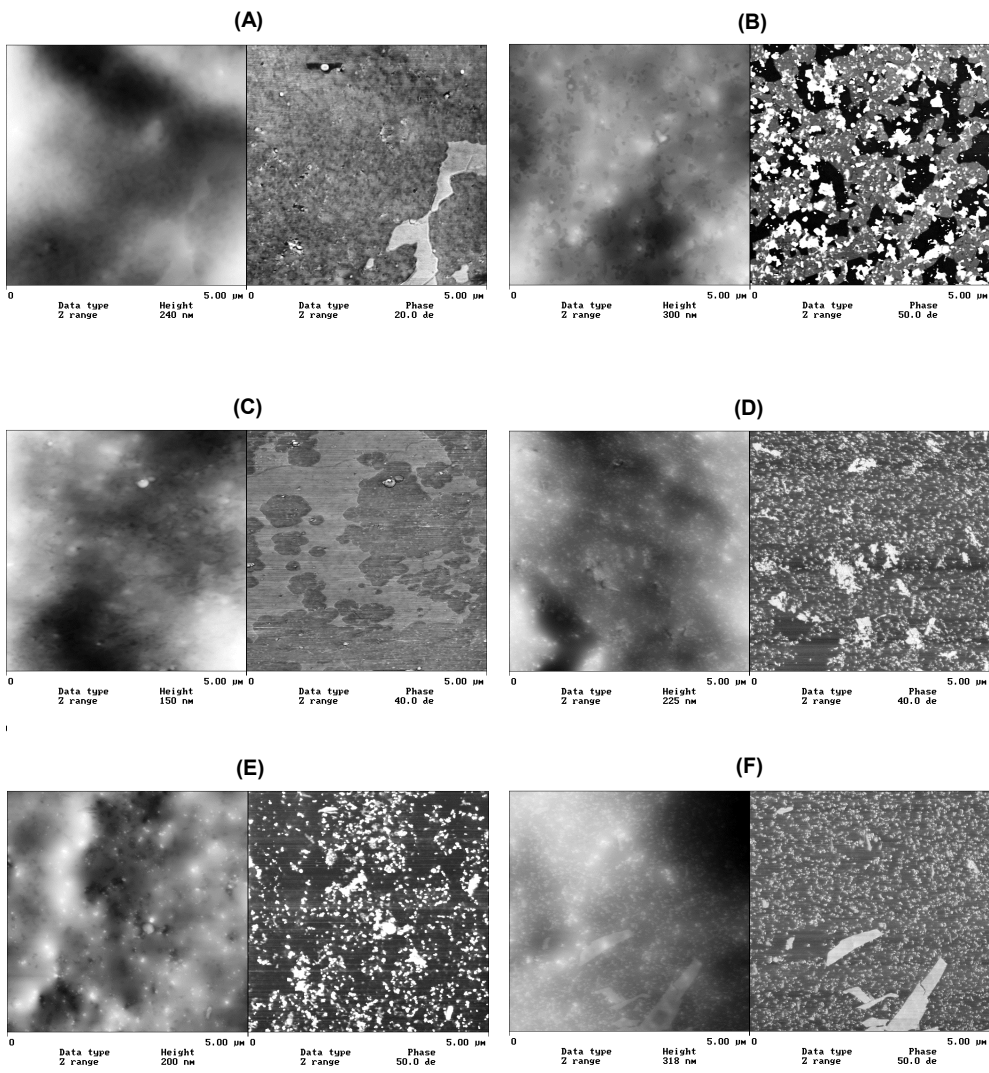


**Figure 7.12** AFM images of the silica distribution (microdispersion) for different recipes in the presence of TESPT; (A), I; (B), II; (C), III; (D), IV; (E), V; (F), VI.

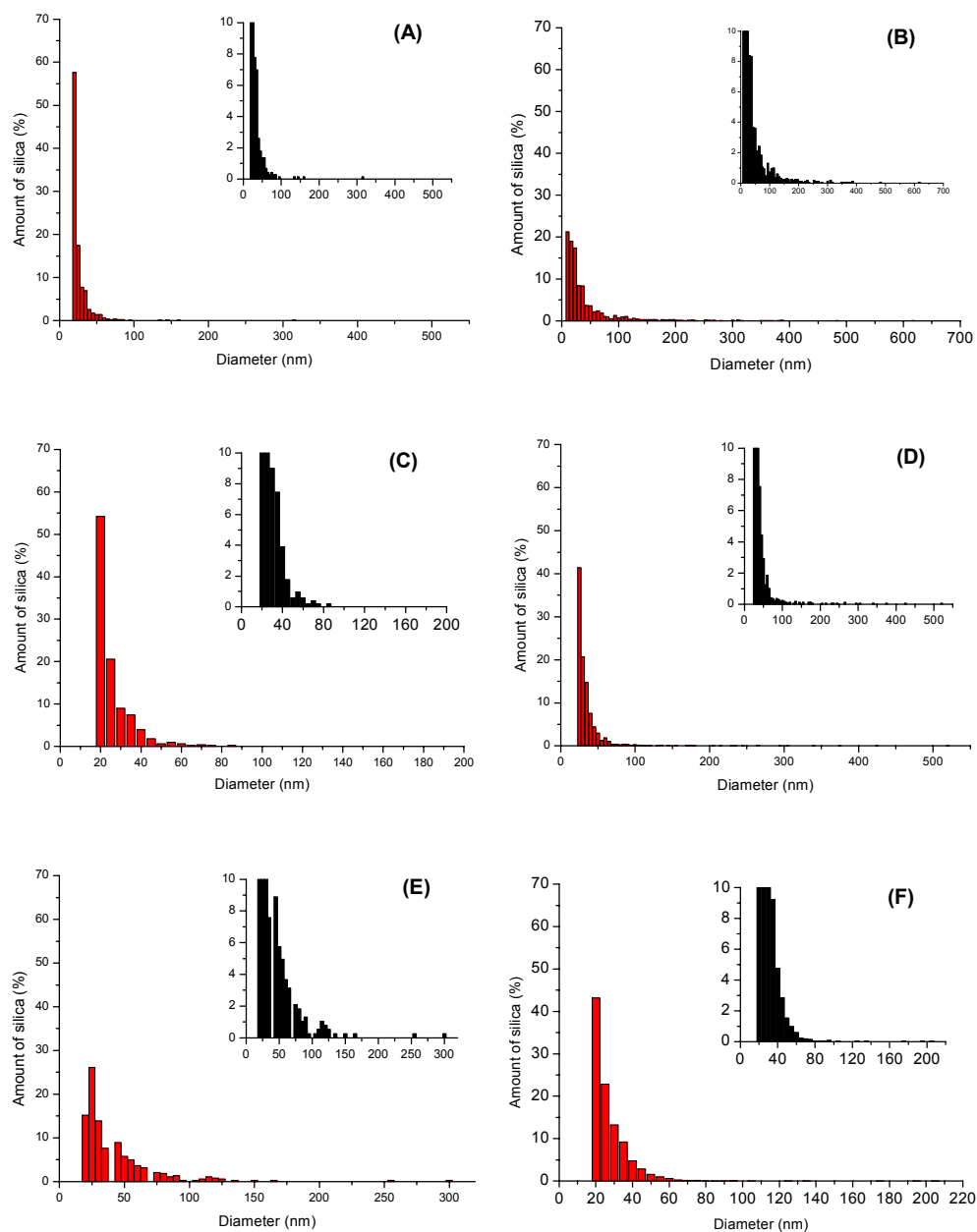


**Figure 7.13** Silica size distribution (microdispersion) for different recipes in presence of TESPT; (A), I; (B), II; (C), III; (D), IV; (E), V; (F), VI.

Dynamic mechanical properties

The dynamic measurements again show a good correlation with the microdispersion, Figure 7.14. As seen before, the silica in recipe II resulted in a relatively high amount of aggregates: large aggregates with a size of > 600 nm were still present. As seen before, those aggregates most prominently result in a large filler-filler network and consequently a high  $G'$  value at low strain. For the silicas in the other recipes the  $G'$  at low strain are now all more or less comparable. Also the silica size microdistributions for those types of silica are more or less the same.

The effect of the coupling agent on the different types of silica is more outspoken in the tensile properties: Figure 7.15. Recipe IV shows a steeper increase in the stress-strain curve as compared to the other recipes. The most inferior properties are obtained with recipe II, which again contains large aggregates with a size larger than 600 nm. The other types of silica are all comparable in the tensile properties. Recipe I also results in relatively good tensile properties, although the macrodispersion was poor. On the other hand the microdispersion was very good. The results of this paragraph again show the primary role of microdispersion in determining the mechanical properties of silica-reinforced rubber compounds.

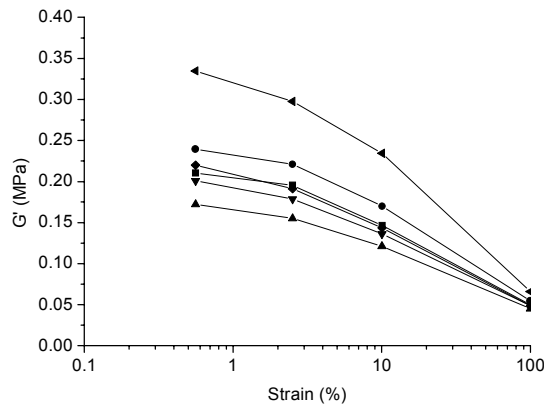


Figure 7.14 Storage modulus as a function of the deformation in the presence of TESPT; (■), I; (◄), II; (▼), III; (▲), IV; (◆), V; (●), VI.

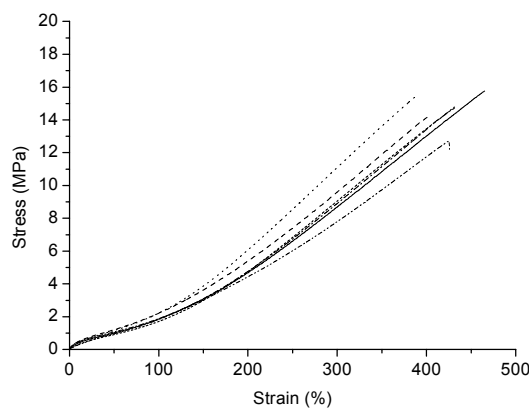


Figure 7.15 Stress-strain curve; (—), I; (-·-·-), II; (- - -), III; (- · - · -), IV; (·····), V; (- - -), VI.

**Table 7.6** Effect of macro- and microdispersion on dynamic and mechanical properties in presence of TESPT; (-), poor; (+), good; (X) not present; (O), present.

Recipe	Macrodispersion	Large aggregates > 600 nm	G' (0.56%) (MPa)	Tensile strength (MPa)
I	-	X	0.2104	15.8
II	-	O	0.3347	12.2
III	+	X	0.2008	14.8
IV	+	X	0.1721	15.6
V	+	X	0.2200	14.7
VI	+	X	0.2391	14.1

Table 7.6 shows a summary of the results of the present paragraph. A low DBP value (conventional silica) again, has only an influence on the macrodispersion. High DBP values (semi or highly dispersible silica) result in a good macrodispersion. In presence of TESPT, significant differences are obtained in microdispersion between the different classes of silica. Silica with a DBP value of approximately 200, recipes IV and V, show aggregates with a size between 100 and 200 nm. If the DBP value is higher, recipe VI, the compound contains only primary particles.

### 7.3.4 Comparison of the compounds with and without TESPT coupling agent with respect to morphology and implications for tyre application

In the former paragraphs it was demonstrated, that there is a clear trend between the microdispersion of the different silica filled compounds and their dynamic mechanical properties of those compounds. A better dispersion, i.e. less aggregates, leads to a lower Payne effect. The macrodispersion showed no correlation with this Payne effect, therefore it is taken as proof that the filler-filler interaction is only caused by large aggregates with a minimum size of approximately 600 nm till a maximum of 1  $\mu\text{m}$ . In the presence of a coupling agent, the G' at low strain decreases very clearly. This decrease in the G' at low strain is another proof of less filler-filler interactions. The coupling agent causes the silica surface to behave more hydrophobic and this leads to the better dispersion of the silica in the rubber matrix.

In case of the mechanical properties the primary factor is the microdispersion. The presence of large aggregates with a diameter of approximately 600 nm and larger decreases the tensile strength significantly. The macrodispersion has little or no influence on the mechanical properties.

From the experiments it can be observed that silicas with a high DBP value, i.e. more structured silica, disperse to more primary particles. This was best observed in the absence and in the presence of TESPT as coupling agent. The conventional silicas, low DBP value, have the highest amount of white area for the macrodispersion, a high percentage of silica is not dispersed to the level of primary particles. The difference between the semi dispersible and the highly dispersible silica is less outspoken, comparable DBP

values. The silica used in recipe VI has the highest amount of primary particles, especially in the presence of TESPT. The type of silica used in this recipe has the highest DBP value.

The results show that for all classes of silica the main part is dispersed to the microdispersion level. The difference between the classes of silica is the amount that is dispersed to the microdispersion level. A schematic depiction is given in Figure 7.17. The first peak in all three pictures is related to the microdispersion level and the second peak is related to the macrodispersion level. The difference is, that with increasing DBP value, more silica is dispersed towards the microdispersion level. The pictures are the opposite to what was supposed by Blume, and explained in the introduction of the present chapter.<sup>13</sup>

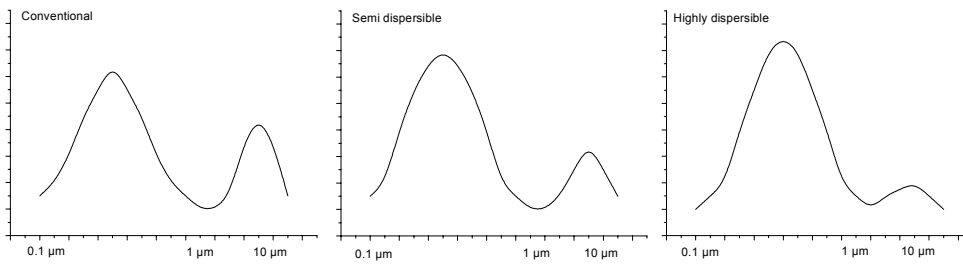


**Figure 7.17** Schematic representation of the amount of silica, that is dispersed to the micro- and macrodispersion level for three different types of silica.

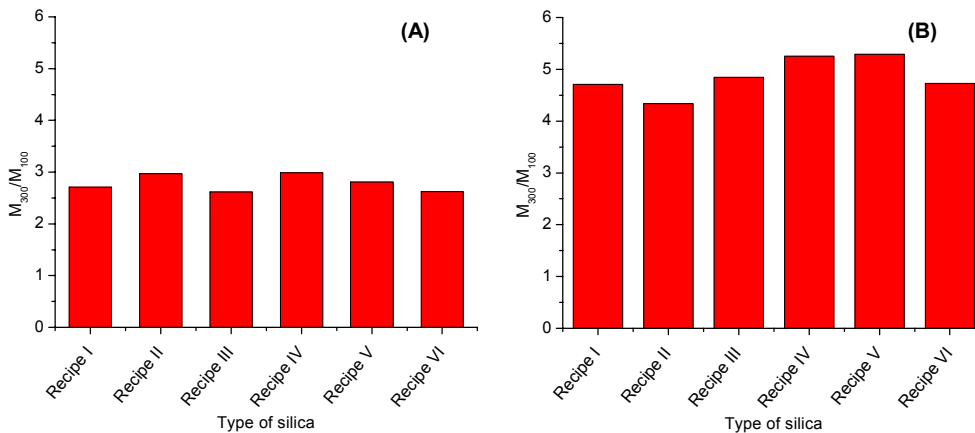


**Figure 7.18**  $M_{300}/M_{100}$  for different recipes with and without TESPT coupling agent; (A), without TESPT; (B), with TESPT.

In case of a tyre tread application, the rolling resistance is an important parameter, see Chapter 2. An alternative measure for  $\tan \delta$ , the rolling resistance, is the  $M_{300}/M_{100}$ .<sup>5</sup> A high value for the  $M_{300}/M_{100}$  indicates a low rolling resistance. The  $M_{300}/M_{100}$  is not influenced by the macrodispersion of the silica in the polymer, see Figures 7.18 A and B. Recipe I and II showed the highest amount of white area in the macrodispersion in the absence and presence of TESPT. The  $M_{300}/M_{100}$  for these two recipes is not significantly different from that of the other recipes. The only difference between recipes I and II and the other four recipes can be found in the microdispersion. Amongst the compounds treated with TESPT,

two recipes stand out. Recipes IV and V result in the highest  $M_{300}/M_{100}$  and consequently the lowest rolling resistance. Recipe IV and V are the only compounds, which contain aggregates in the range of 100 to 200 nm in the presence of TESPT. When the silica is dispersed to the microdispersion level, it is important that not only primary particles are obtained but also a few aggregates. The silica in recipe VI is mainly dispersed to the primary particle level but still does not result in the highest  $M_{300}/M_{100}$ . The aggregates with a size in the range of 100 to 200 nm apparently play an important role. An explanation can be as follows.

Primary silica particles can only be attached to the polymer via the coupling agent. This results in an increase of the  $M_{300}/M_{100}$ , compare Figure 7.18 A and B for recipe VI. If aggregates, i.e. in the range of 100 to 200 nm, are present in the compound then small pores, i.e. nano-pores, are present in the silica.<sup>30</sup> For those types of silica, coupling takes place via the coupling agent to the polymer and physical interaction takes place in the nano-pores between the silica and the polymer.

There is one restriction to this explanation. The polymer should be linear to be able to penetrate into such a nano-pore. To obtain good mixing of silica with polymers, the polymer should be forced into the nano-pores, which is easier for a linear polymer. The restricted geometry of the nano-pore competes with the connectivity among the polymer segments. The connectivity is expressed through the spectral dimension  $D_s$  of the fractal polymer object. A polymer that is linear has a  $D_s$  equal to 1 and a polymer that is highly branched has a  $D_s$  equal to 4/3. Whenever the connectivity of branched polymers is larger than a threshold value  $D_s^*$  the fractals do not interpenetrate as do linear polymers.<sup>31</sup>

The polymer that is used during the experiments is a blend of solution-styrene-butadiene-rubber (S-SBR) and butadiene rubber (BR). The S-SBR is a linear polymer and can therefore penetrate into the nano-pores in the aggregates. If this penetration is taking place, then, besides the chemical attachment of the silica particle to the rubber matrix, also strong physical interaction takes place, also called polymer-filler interlocking. More interaction between the filler and the polymer results in a steeper increase in the stress-strain curve. This will consequently lead to a higher  $M_{300}/M_{100}$  and therefore a lower rolling resistance.

## 7.4 Conclusions

The dump temperature reached during mixing has no significant influence on the macrodispersion of a highly dispersible silica. On the other hand, the microdispersion as observed with AFM measurements does depend on the dump temperature. With higher dump temperatures a better microdispersion is obtained, as characterised by an increased amount of primary particles.

When comparing different silica samples with various structure (DBP values) large differences are seen in the macro- and microdispersion. Low structured (conventional) silicas show a poor macrodispersion in comparison with medium structured/semi dispersible and highly structured/highly dispersible silicas. This poor macrodispersion is not improved by the admixture of TESPT to the recipe. Microdispersion measurements revealed an increased level of primary silica particles for higher structured silicas, where the highly dispersible silicas are primarily dispersed to the microdispersion level, with only 15-20% remaining in the macrodispersion regime.

The dynamic and mechanical properties of a tyre tread compound turn out to primarily depend on the level of microdispersion. The filler-filler interactions responsible for poor dynamic mechanical properties, are mainly due to aggregates with a diameter of approximately 600 nm and larger. Also the tensile strength of the compounds is primarily influenced by the microdispersion, where lower tensile strength values are obtained, when aggregates with a diameter larger than 600 nm are present.

In addition to microdispersion measurements, AFM is also useful to visualise pre-vulcanisation effects in the compounds: elliptical structures appears in the AFM phase image.

The overall conclusion is, that to obtain a tyre tread compound with a low rolling resistance, a highly dispersible/high structured silica is preferred. This highly dispersible silica should mainly be dispersed to the microdispersion level, to result in primary particles and a low level of aggregates with a size between 100 and 200 nm.

## **7.5 References**

1. M.P. Wagner, *Rubber Chem. Technol.*, **49**, (1976), 703.
2. S. Wolff, *Kautsch. Gummi Kunstst.*, **34**, (1981), 280.
3. S. Wolff, *Rubber Chem. Technol.*, **55**, (1982), 967.
4. S. Wolff, *Tire Sci. Technol.*, **15**, (1987), 276.
5. Chapter 3 of this thesis.
6. Chapter 5 of this thesis.
7. B.T. Poh, C.C. NG, *Eur. Polym. J.*, **34**, (1998), 975.
8. R.H. Hess, H.H. Hoekje, J.R. Creasey, F. Strain, (to PPG industries Inc.), U.S. Pat. 3,768,537 (30-10-1973).
9. P.E. Cassidy, B.J. Yager, *J. Macromol. Sci. - Revs. Polym. Technol.*, **1**, (1971), 1.
10. R.W. Cruse, M.H. Hofstetter, L.M. Panzer, R.J. Pickwell, *Rubber & Plastics News*, (1997), 14.
11. A. Hunsche, U. Görl, A. Muller, M. Knaack, Th. Gobel, *Kautsch. Gummi Kunstst.*, **50**, (1997), 881.
12. A. Hunsche, U. Görl, H.G. Koban, Th. Lehmann, presented at a meeting of ACS, Rubber Division, Louisville, Kentucky, October 8-11, 1996.
13. A. Blume, *Kautsch. Gummi Kunstst.*, **53**, (2000), 338.
14. Y. Chevallier, M. Rabeyrin, (to Rhone-Poulenc Chimie), U.S. Pat. 5,403,570 (4-4-1995).
15. P. Cochet, L. Barriquand, Y. Bomal, S. Touzet, presented at a meeting of ACS, Rubber Division, Cleveland, Ohio, October 17-20, 1995.
16. W.H. Dokter, I.I.M. Tijnburg, (to AkzoNobel), WO 01/07364 A1 (1-2-2001).
17. S. Maas, W. Gronski, *Rubber Chem. Technol.*, **68**, (1995), 652.
18. I.H. Jeon, H. Kim, S.G. Kim, presented at a meeting of ACS, Rubber Division, Cleveland, Ohio, October 16-19, 2001.
19. R.J. Seward, *Rubber Chem. Technol.*, **43**, (1970), 1.
20. J. Kruse, *Rubber Chem. Technol.*, **46**, (1973), 653.
21. W.M. Hess, C.R. Herd, P.C. Vegvari, *Rubber Chem. Technol.*, **66**, (1993), 329.
22. D. Trifonova-van Haeringen, H. Schönherr, G.J. Vancso, L. van der Does, J.W.M. Noordermeer, P.J.P. Janssen, *Rubber Chem. Technol.*, **72**, (1999), 862.

23. W. Niedermeier, J. Stierstorfer, S. Kreitmeier, O. Metz, D. Göritz, *Rubber Chem. Technol.*, **67**, (1994), 148.
24. Y. LI, M.J. Wang, T. Zhang, F. Zhang, X. Fu, *Rubber Chem. Technol.*, **67**, (1994), 693.
25. G. Binnig, H. Rehrh, C. Gerber, E. Weibel, *Phys. Rev. Lett.*, **49**, (1982), 57.
26. G. Binnig, C.F. Quate, C. Gerber, *Phys. Rev. Lett.*, **56**, (1986), 930.
27. R. Rauline, (to Compagnie Generale des Etablissements Michelin - Michelin & Cie), *Eur. Pat.* 0 501 227 A1 (02-09-1992).
28. Y. Chevallier, M. Rabeyrin, (to Rhone-Poulenc Chimie), U.S. 5,587,416 (20-8-1996).
29. Y. Chevallier, J.-C. Morawski, (to Rhone Poulenc Chimie), *Eur. Pat.* 0157703 (31-5-1989).
30. Z. Pu, J.E. Mark, G. Beaucage, *Rubber Chem. Technol.*, **72**, (1999), 138.
31. G. Heinrich, paper no. 2 presented at a meeting of Deutsche Kautschuk Gesellschaft, Fortbildungsseminar "Soft Matter Nano-Structuring and Reinforcement", Hannover, Germany, May 22, 2001.

---

## Chapter 8

### *Effect of polymer structure on the morphology of rubber compounds as measured with AFM*

---

In the previous chapter interconnected channel-like-structures were observed in the AFM phase images of the S-SBR/BR blends. Several interpretations are given in literature for the grainy structure or soft interstices that are present in AFM phase images or TEM micrographs of rubber polymers. The present study proves that the soft interstices seen in AFM phase images are not the actual crosslinking system as was mentioned in literature. Preparation of the sample at room temperature or cooling with liquid nitrogen, before measuring with AFM, resulted in the same observations. Both sample preparation procedures resulted in soft interstices in the AFM phase images of oil extended S-SBR. Therefore, the soft interstices are also not caused by microcracks introduced by cooling of the sample.

There is a correlation observed between the presence of soft interstices in AFM phase images and the polymer structure. Linear polymers, such as S-SBR or EPDM with a narrow molecular weight distribution, showed soft interstices, whereas branched polymers did not show any in the AFM phase image. The soft interstices are interpreted as a manifestation of mastication on a nano-scale. The consequence of such soft interstices or grains is, that fillers as well as vulcanisation ingredients tend to preferentially be included in these softer phases, thereby rendering the resulting compounds intrinsically inhomogeneous.

#### 8.1 Introduction

In the previous chapter interconnected channel-like-structures were observed in the AFM phase images, when determining the microdispersion of silica in S-SBR/BR blends. Those structures were visible as dark regions in the AFM phase image: Figure 7.4 A and B. The darker contrast in the AFM phase images can be associated with a low stiffness of the pertinent material.

The phenomenon of softer segments in a rubber matrix has more often been described in literature and was sometimes designated as grainy structures. Several explanations were given for the nature of the grainy structures. Shiibashi and Tinker observed the grainy structures in TEM micrographs of swollen vulcanisates and swollen vulcanised blends of natural rubber.<sup>1,2</sup> Shiibashi found that the grain size was decreasing with increasing network density and felt that he saw the actual crosslink network. Similar grainy structures were observed by measurements of EPDM rubber with AFM.<sup>3</sup> The grain boundaries seen for EPDM would then correspond to different viscoelastic properties

between the grains and the boundaries. Engelbert van Bevervoorde-Meilof et al. found no correlation between the network chain density and the grain size, as quoted by Shiibashi.<sup>3</sup>

Kilian suggested that the grainy structure is a visualisation of an aggregate structure of liquids.<sup>4</sup> AFM images of glassy layers of polymethyl methacrylate revealed similar heterogeneous structures. They reflect the many equivalent microstructures a liquid is constantly running through. The microstructures or aggregates are considered as dynamic subsystems (reversible aggregation) with a broad and asymmetric size distribution. Rubbers have much lower glass transition temperatures than glasses, but at the high frequencies of the AFM tapping mode experiments, quasi-stationary structures of the rubber surface should become visible. According to Kilian it might be expected that chemical crosslinks are formed preferentially in the boundaries between the grains and might therefore be heterogeneously distributed.

Another somewhat speculative explanation is given by Engelbert van Bevervoorde-Meilof et al. They suggest, that the grains reflect striae created during the mixing of the compounds.<sup>3</sup> The boundaries constitute masticated sheared rubber, surrounding globules of non-masticated material. While all shearing and mixing thus is concentrated in the boundaries, also the vulcanisation ingredients tend to concentrate in the boundaries. Their further transport into the grains is controlled by diffusion. This means, that the crosslinking preferentially takes place in the boundaries. Another explanation they gave was, that the striae are merely showing a viscoelastic behaviour different from the matrix, because the material in the striae is masticated and the matrix not.

From the foregoing it is clear that different explanations are postulated to explain the soft-segments or grainy structures visible in AFM phase images or TEM micrographs of rubber compounds. The present chapter is meant to shed further light on what is causing the formation of the soft segments or grainy structure in the rubber compounds.

## 8.2 Experimental

*Materials.* — The experiments described in paragraph 8.3.1 were performed using a tyre tread composition as shown in Table 8.1. The compounds were mixed, according to the procedure described in Chapter 3.

For the experiments where different types of polymer were investigated, paragraph 8.3.2, the polymers are listed in Table 8.2. The pure polymers were mixed for 6.45 minutes in a 390 ml Brabender Plasticorder. The starting temperature was 50°C and the cooling water was kept at a constant temperature of 50°C. After this mixing step the compounds were sheeted out on a Schwabenthan 100 ml two-roll mill.

**Table 8.1** Tyre tread recipe (phr).

Component	
S-SBR (Buna <sup>®</sup> VSL 5025-1 HM) <sup>a</sup>	75
BR (Kosyn <sup>®</sup> KBR 01)	25
Silica (Zeosil <sup>®</sup> 1165 MP)	80
Coupling agent (TESPT)	7
Aromatic oil (Enerflex <sup>®</sup> 75)	32.5
ZnO	2.5
Stearic acid	2.5
Total	224.5

<sup>a</sup> vinyl content is 50%, styrene content is 25% and the oil content is 37.5 phr.

**Table 8.2** Type of polymers.

Polymer type	Source	Mooney viscosity values (MU)
S-SBR (Buna <sup>®</sup> VSL 5025-1 HM) <sup>a</sup>	Bayer AG	68.4
S-SBR (Buna <sup>®</sup> VSL 2525-0 M)	Bayer AG	52.0
BR (Kosyn <sup>®</sup> KBR 01)	Korea Kumho Petrochemical Co. Ltd.	44.4
NR (SIR 20)		93.7
E-SBR (Krylene <sup>®</sup> 1500)	Bayer AG	49.8
EPDM (Keltan <sup>®</sup> 4802) <sup>b</sup>	DSM Elastomers	110.8; 74.5 <sup>d</sup>
EPDM (Keltan <sup>®</sup> 812) <sup>c</sup>	DSM Elastomers	116.7; 78.1 <sup>d</sup>

<sup>a</sup> oil content is 37.5 phr.

<sup>b</sup> narrow molecular weight distribution.<sup>5</sup>

<sup>c</sup> broad molecular weight distribution.<sup>5</sup>

<sup>d</sup> measurement performed at 125°C.

**Characterisation.** — The Mooney viscosity ML(1+4) at 100°C, Table 8.2, was measured with the aid of a Mooney viscometer 2000E from Alpha Technologies. The EPDM samples were also measured at 125°C, the common temperature for these types of polymers.

**Sample preparation.**— Unvulcanised samples for the AFM were prepared by microtoming the surface of the samples with a rotary Leica microtome at –130°C, with a diamond knife. For the samples cut at room temperature a scalpel was used.

**Atomic Force Microscopy measurements.**— The AFM experiments were done using a NanoScope III multimode scanning force microscope (Digital Instruments (DI), Santa Barbara, CA, USA) in tapping mode with phase imaging under ambient conditions. Standard Si Nanosensor probes were used to conduct the measurements.

**Tan  $\delta$  measurements.**— Frequency sweep measurements were performed with the RPA 2000 to measure the tan  $\delta$ . The measurement was performed at a temperature of 100°C and a strain of 14%. The frequency was varied from 0.05 to 200 rad/s.

### 8.3 Results and discussion

Paragraph 8.3.1 focuses on the effect of sample preparation and the influence of oil on the occurrence of soft segments in the AFM phase images. Also the assumption postulated by Shiibashi<sup>1</sup>, that the actual crosslinking network is visible, is discussed. Paragraph 8.3.2 focuses on the mechanism postulated by Engelbert van Bevervoorde-Meilof et al.<sup>3</sup>. For this part several types of polymers were investigated.

#### 8.3.1 Soft interstice boundaries: influence of oil content and sample preparation

Figure 8.1 A to C shows the AFM phase images of an unvulcanised S-SBR/BR blend filled with silica, Table 8.1. Soft interstices are present in the shape of interconnective channel-like structures, approximately 50 nm in width. At the junctions of the channels larger soft domains are present. In the images it can be seen that the soft interstice structures are randomly distributed throughout the rubber compound. Figure 8.1 C shows an image with an area of  $1 \mu\text{m}^2$ . The silica present in the compound is clearly visible as white particles. The main part of these silica particles tends to end up in the softer channels.

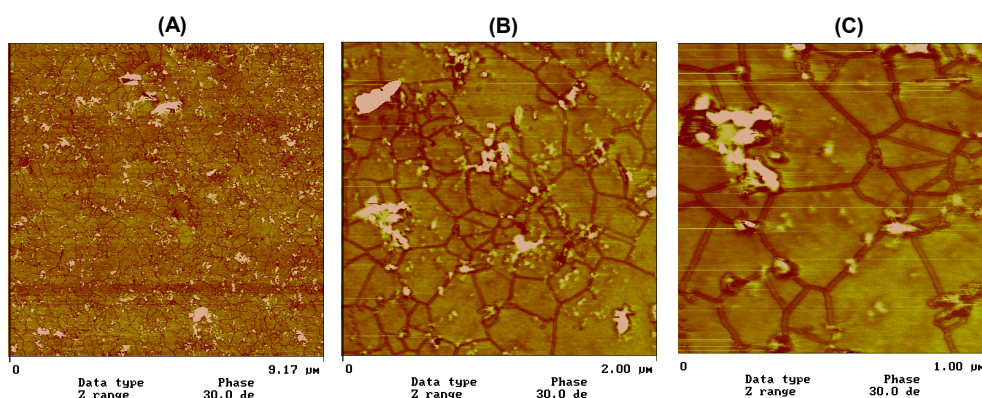


**Figure 8.1** AFM phase images of a S-SBR/BR blend filled with silica with different image sizes; (A),  $9 \times 9 \mu\text{m}$ ; (B),  $2 \times 2 \mu\text{m}$ ; (C),  $1 \times 1 \mu\text{m}$ .

It may be questioned if the soft interstices in the S-SBR/BR blends are not caused by low molecular weight material in the polymer such as oil. The S-SBR used in the compound is oil extended: Table 8.1. To investigate if the oil in the S-SBR is causing the soft interstices, non-oil extended S-SBR was measured with the AFM after mixing in the internal mixer. Several measurements were performed, but no image could be made of this type of polymer. The polymer was too sticky for the AFM measurements. Also, the sample was not stiff enough and started to vibrate with the frequency of the AFM-tip.

By measuring a typical tyre tread compound, Table 8.1, an indirect proof was obtained that the oil present in the compound did not cause the occurrence of soft interstices. The compound was measured several times on exactly the same position: Figure 8.2 A to C. Although there are no channel-like-structures visible, there is some oil

visible in the images as dark spots. The lighter points are the silica particles. Measuring on exactly the same position increases the oil spot in the image: Figure 8.10 B, second time measuring and C, third measurement. This effect can be explained by the fact that the AFM measurement is performed in tapping mode. The oil that is present in the compound is squeezed out of the polymer and ends up at the surface, where it is spread out by the AFM-tip.

The measurements with AFM on the sample surfaces where soft interstices were present, were performed several times on the same position. The AFM phase image did not change at all, every time the same image was obtained. This is an indirect indication, that the soft interstices are not caused by the oil in the compound.

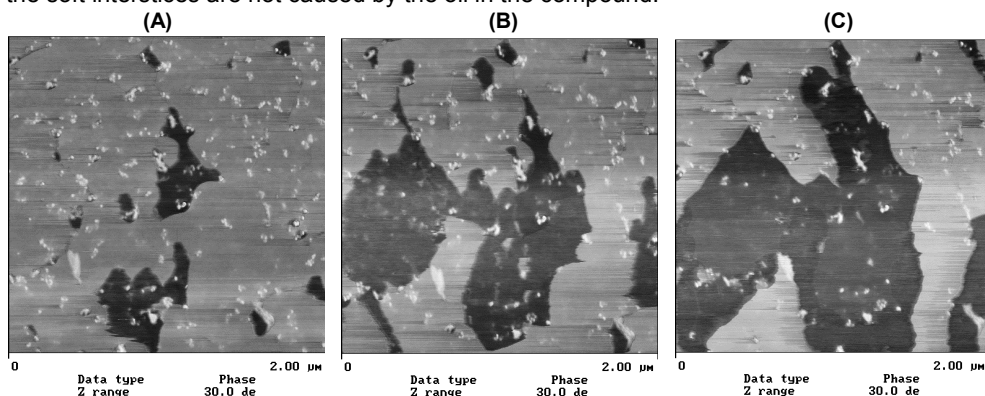


**Figure 8.2** AFM phase images of a S-SBR/BR blend filled with silica measured several times on exactly the same position; (A), first measurement; (B), second measurement; (C), third measurement.

Another possible experimental artefact leading to the occurrence of the soft interstices is the preparation of the AFM samples. Cooling of the sample in liquid nitrogen for microtoming, might result in microcracks throughout the sample, which could become visible as soft interstice structures in the AFM phase image. To check this, the sample preparation was performed at room temperature. Although the surface is rough after cutting with a scalpel, still images could be obtained: Figure 8.3. The soft interstices are again clearly visible in the AFM phase image. This indicates that the soft interstices are not created by the sample preparation.

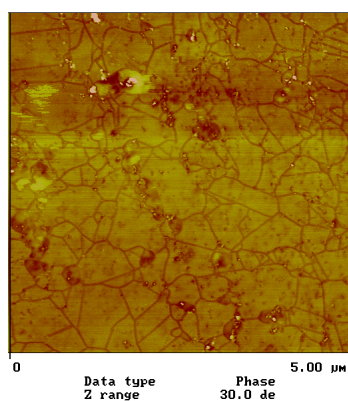


**Figure 8.3** AFM phase image of a S-SBR/BR blend filled with silica; sample preparation at room temperature.

In the introduction several explanations were postulated, what might cause the appearance of the soft interstices in a rubber blend. Shiibashi interpreted the soft interstices as the crosslinking network.<sup>1</sup> The compound recipe used for the AFM image in Figure 8.1, is described in Table 8.1 and does not contain a vulcanisation system. Although no vulcanisation system is present, still soft segments are visible in the AFM phase image; an indication that the crosslinking system cannot cause the appearance of this structure.

### 8.3.2 Soft interstice boundaries: effect of polymer branching on softening

Another explanation was given by Engelbert van Bevervoorde-Meilof et al.; they suggested that the soft segments or grainy structures are reflecting striae created during the mixing of the compounds.<sup>3</sup> The striae are representing the masticated polymer. This explanation seems to be very plausible. During mixing, the molecular weight of the polymer is lowered by breaking of polymer chains. The ease of molecular weight decrease is affected by the branching or linearity of the polymer chains.

It is well known, that  $\tan \delta$ , as measured in a dynamic mechanical test, can be used as an indicator of branching.<sup>6,7</sup> Branching greatly influences the viscosity of a compound, especially for EPDM. At low frequencies the  $\tan \delta$  is indicative for the linearity or branching of a polymer. A high value for  $\tan \delta$  represents a linear polymer whereas a low value represents a branched polymer. The  $\tan \delta$  values at high frequencies give an indication of the absolute molecular weight. High values for  $\tan \delta$  at high frequencies represent low molecular weights, whereas low values for  $\tan \delta$  represent high molecular weights.

All the polymers listed in Table 8.2 were subjected to a frequency sweep, whereby the  $\tan \delta$  was measured. Comparison between the polymers is only possible when polymers are having comparable Mooney viscosity values. Figure 8.4 shows the  $\tan \delta$  as a function of frequency for the two types of EPDM. The two types of EPDM are having similar Mooney viscosity values: Table 8.2. There are clear differences in the  $\tan \delta$  values at low frequency. The highest value for  $\tan \delta$  at low frequency is obtained for the EPDM with a narrow molecular weight distribution. The  $\tan \delta$  at low frequency obtained for the EPDM with the broad molecular weight distribution is the lowest. This indicates that the EPDM with the narrow molecular weight distribution is more linear than the EPDM with the broad molecular weight distribution.

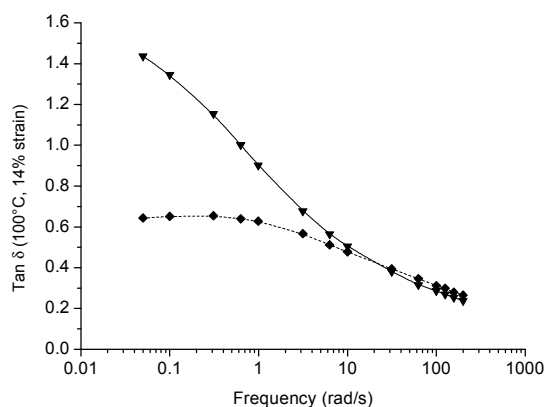


**Figure 8.4**  $\tan \delta$  vs. frequency for two types of polymers; (▼), EPDM with narrow MWD; (◆), EPDM with broad MWD.

The AFM phase image of the EPDM with the narrow molecular weight distribution is shown in Figure 8.5 A. This image shows a large amount of soft interstices. The interstices are not present in the polymer as channels, but more as grainy structures, as was mentioned before in literature for EPDM.<sup>3</sup> Still, the grainy structures are darker and therefore represent a softer part in the polymer. These soft interstices are interconnected.

In Figure 8.5 B the AFM phase image of EPDM with a broad molecular weight distribution is depicted. Dark and light regions are present in the polymer, but these are different in shape compared to the EPDM with the narrow molecular weight distribution. The difference in the phase image between the two types of EPDM is most probably due to surface roughness and not to the fact that soft interstices are present.

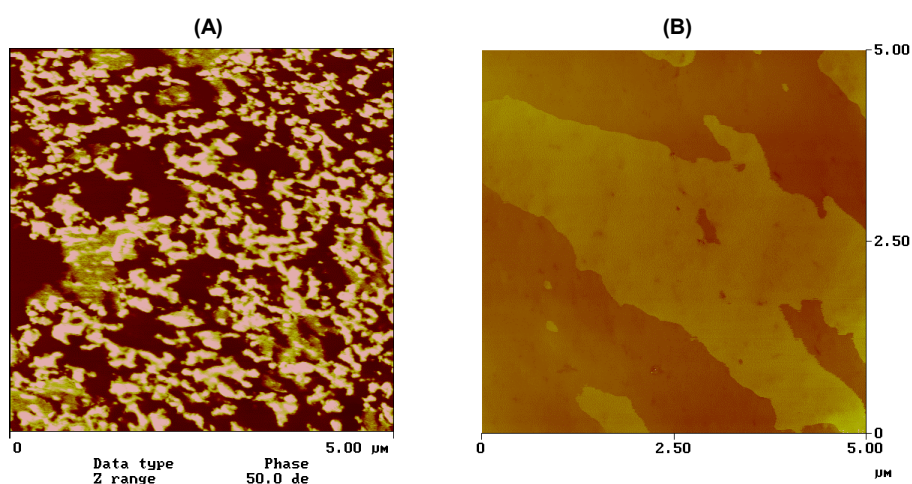


**Figure 8.5** AFM phase image of EPDM; (A), with narrow MWD; (B), with broad MWD.

The E-SBR and the S-SBR without oil also have similar Mooney viscosity values: Table 8.2. In Figure 8.6 the  $\tan \delta$  as a function of the frequency is plotted for the two polymers. The difference in the  $\tan \delta$  between the two polymers is less outspoken as was the case for the two types of EPDM. The value for  $\tan \delta$  at low frequency is higher for the S-SBR without oil than the value for the E-SBR. This is an indication that the S-SBR is more linear than the E-SBR, which corresponds with literature.<sup>8</sup>

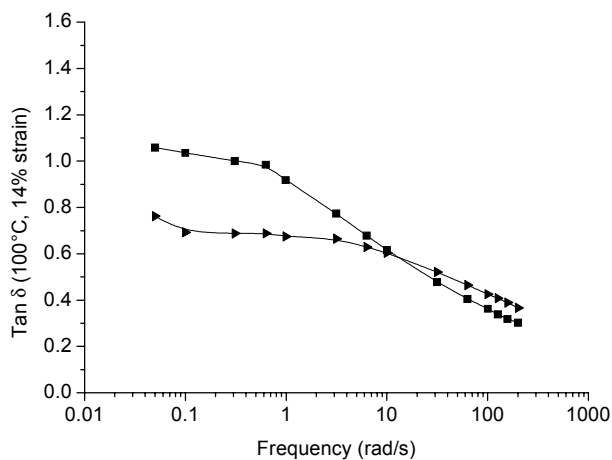


**Figure 8.6** Tan  $\delta$  vs. frequency for two types of polymers; (■), S-SBR without oil; (▴), E-SBR.

The AFM phase image of E-SBR is shown in Figure 8.7. The image shows no soft interstices or grainy structures. White structures are present on the polymer surface. These structures are most likely caused by the surfactants present in the E-SBR. As mentioned in paragraph 8.3.1, AFM measurements of S-SBR without oil were not possible.

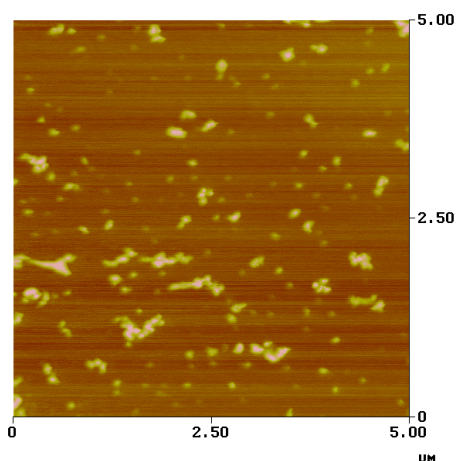


**Figure 8.7** AFM phase image of E-SBR.

All the other polymers listed in Table 8.2 have different Mooney viscosity values. Therefore, comparison of the different polymers is more speculative. The S-SBR normally used in the “green tyre” compound is oil extended. Frequency measurements were also performed on this type of pure S-SBR polymer. The results of the frequency measurements are depicted in Figure 8.8, E-SBR is plotted as a reference. The value of the tan  $\delta$  at low frequency for the oil extended S-SBR is lower than for the E-SBR. The Mooney value of the oil extended S-SBR is higher when compared to the Mooney viscosity value of E-SBR. Therefore, it is not possible to conclude if the oil extended S-SBR is more linear than for the E-SBR. An indirect conclusion can be made with the pure non-oil extended S-

SBR. This polymer was more linear than the E-SBR and therefore it is expected that the oil extended S-SBR is also more linear than the E-SBR.

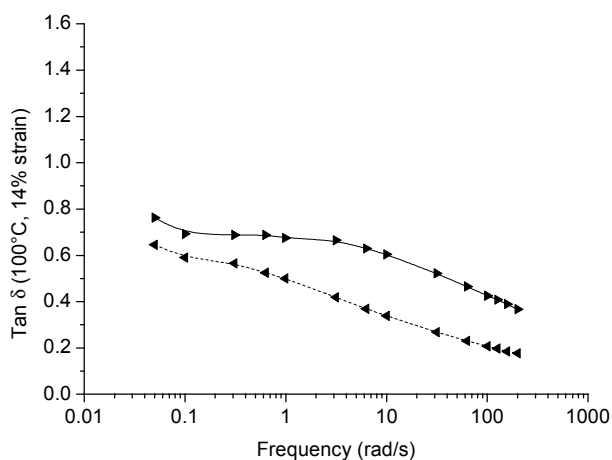


**Figure 8.8** Tan  $\delta$  vs. frequency for two types of polymers; ( $\blacktriangleleft$ ), S-SBR with oil; ( $\blacktriangleright$ ), E-SBR.

The AFM phase image of the oil extended S-SBR is depicted in Figure 8.9. In this phase image it is clearly seen that soft interstices are present again. The soft interstices are slightly smaller than in the standard S-SBR/BR compound filled with silica: Figure 8.1. The dark spot in the middle of the AFM phase image is oil that is present in the rubber and exuded to the sample surface.

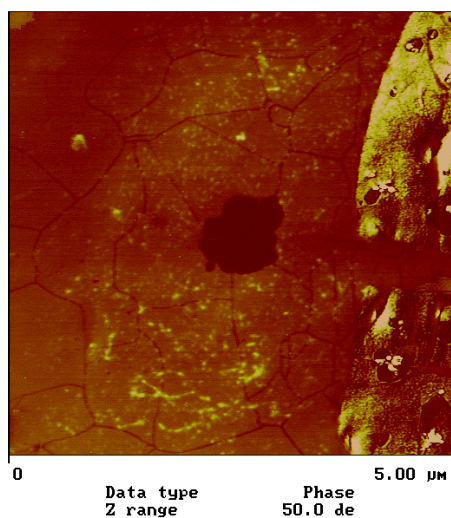


**Figure 8.9** AFM phase image of oil extended S-SBR.

NR and BR are both having different Mooney viscosity values and compositions and therefore, cannot be compared with any other polymer in Table 8.2 with respect to level of branching. According to literature, both polymers are branched.<sup>8</sup> The AFM phase image of NR is depicted in Figure 8.10 A. This figure shows a plain image. In this AFM phase image no soft interstices are present. The white structures on the surface of the sample are

most likely proteins or impurities present in the NR. The latter is due to the fact that it is a natural product. The AFM phase image of BR is shown in Figure 8.10 B. Similar to the NR, the BR phase image shows a plain picture. There are no indications of soft interstices or grainy structures.

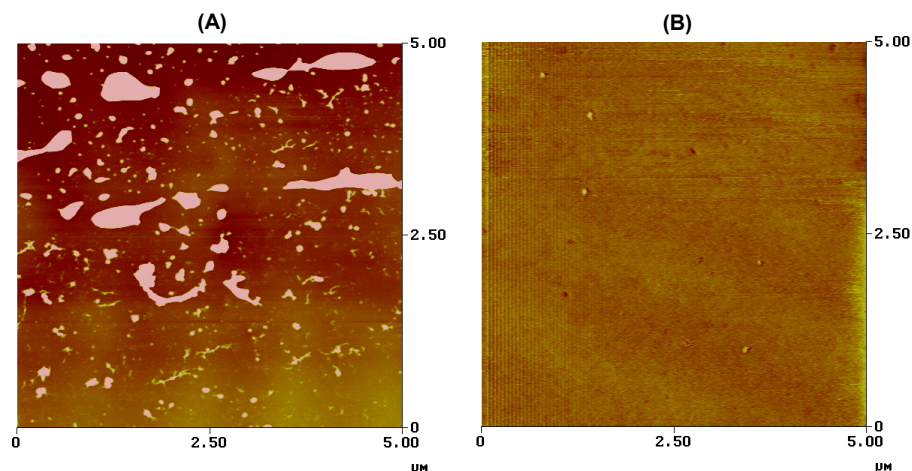


**Figure 8.10** AFM phase image of (A), NR; (B), BR.

In Table 8.3 the results of the present paragraph are summarised. Out of the six polymers, two polymers showed soft segments in the AFM phase images after mixing. The S-SBR resulted in channel-like-structures whereas the EPDM with the narrow molecular weight distribution resulted in grainy structures. All the other polymers did not show soft segments in the AFM phase images.

Although the different polymers were compared with each other on basis of their Mooney viscosity values, a comment has to be made about the  $\tan \delta$  experiment. The  $\tan \delta$  measurement was not optimised for each type of polymer. Improvements can be expected with this type of measurement by fine-tuning of the test method. Therefore all the results cannot completely be compared with each other.

**Table 8.3** Summary of the results; +, present; -, not present.

Polymer	Polymer structure	Presence of soft interstices or grainy structure
S-SBR	Linear	+
BR	Branched	-
NR	Branched	-
E-SBR	Branched	-
EPDM (narrow $M_w$ distribution)	Linear	+
EPDM (broad $M_w$ distribution)	Branched	-

The results summarised in Table 8.3 show that only two polymers exhibit soft interstices. The polymers showing these soft interstices are the two predominantly linear polymers. Apparently, the structure of the polymer has a major influence on the occurrence

of soft interstices in the polymer after mixing. In the AFM phase images it was observed that the amount of soft interstices was much larger for the EPDM with the narrow molecular weight distribution than for the S-SBR. EPDM with the narrow molecular weight distribution results in a higher  $\tan \delta$  at low frequency than the EPDM with a broad molecular weight distribution, an indication that the EPDM with the narrow molecular weight distribution is more linear. The S-SBR was compared with the E-SBR and also showed a higher  $\tan \delta$  at low frequency, indicating that S-SBR is more linear.

Overall, only the predominantly linear polymers were showing soft segments in an AFM phase image, after mixing in an internal mixer. According to one of the explanations postulated by Engelbert van Bevervoorde-Meilof et al., the polymers are masticated in the internal mixer.<sup>3</sup> During the mixing process, the molecular weight of the polymer decreases by breaking down the molecular chain due to the high shear forces. A linear polymer crumbles due to a low cohesive strength by lack of branching, and the fragments are then pasted together during the mixing process. This effect is related to the well-known Tokita regime 3 behaviour of rubbers on a mill.<sup>9</sup> In this way the soft interstices or grainy structures are appearing in the rubber compound and represent lower molecular weight material.

The consequence for the homogeneity of compounds are significant. If the soft interstices are indeed a manifestation of mastication of the polymers on a nano-scale, it is to be expected, that rigid fillers as well as the vulcanisation ingredients will preferentially be included in these softer interstices (as far as their dimensions do not surpass these of the thickness of the interstices). Such compounds are then intrinsically inhomogeneous with the consequence, that random filler distribution or even random crosslinking throughout the rubber is most likely not happening in the case of predominantly linear polymers, showing this Tokita regime 3 behaviour. Apparently the mechanical properties of the rubber compounds are not negatively influenced to a large extent, as long as these phenomena play a role on a nano-scale.

## **8.4 Conclusion**

Several interpretations are given in literature for the grainy structure or interstices that are visible in AFM phase images or TEM micrographs of various rubbers: e.g. S-SBR and EPDM. The present study proves that the interstices seen in AFM phase images is not the actual crosslinking system, as postulated by Shiibashi.<sup>1</sup> Preparation of the sample at room temperature or cooling with liquid nitrogen, before measuring with AFM, resulted in the same observations. Both sample preparation procedures resulted in soft interstices in the AFM phase images. Therefore, the soft interstices are also not caused by microcracks introduced by cooling of the sample.

There is a correlation observed between the presence of soft interstices in AFM phase images and the polymer structure. Linear polymers, such as S-SBR or EPDM with a narrow molecular weight distribution, showed soft interstices or a grainy structure, whereas branched polymers did not show these soft interstices in the AFM phase image. The cause of these soft interstices is related to a low cohesive strength of linear polymers due to lack of branching, leading to Tokita regime 3 behaviour. The interstices are a manifestation of mastication on a nano-scale.

The consequence of such soft interstices or grains is, that fillers as well as vulcanisation ingredients will tend to preferentially be included in these softer phases, thereby rendering the resulting compounds intrinsically inhomogeneous.

## 8.5 References

1. T. Shiibashi, *Int. Polym. Sci. Technol.*, **14**, (1987), T/33.
2. A.J. Tinker, *Blends of Natural Rubber*, Chapman & Hall, London (1998).
3. E.W. Engelbert van Bevervoorde-Meilof, D. van Haeringen-Trifonova, G.J. Vancso, L. v. d. Does, A. Bantjes, J.W.M. Noordermeer, *Kautsch. Gummi Kunstst.*, **53**, (2000), 426.
4. H.-G. Kilian, B. Zink, R. Metzler, *J. Chem. Phys.*, **107**, (1997), 8697.
5. Technical brochure of DSM products.
6. H.C. Booij, *Kautsch. Gummi Kunstst.*, **44**, (1991), 128.
7. K.P. Beardsly, C.C. Ho, *J. Elastomers Plastics*, **16**, (1984), 20.
8. W. Hofmann, *Rubber Technology Handbook*, Hanser Publishers, Munich, (1996).
9. N. Tokita, J.L. White, *J. Appl. Polym. Sci.*, **10**, (1966), 1011.

---

## Chapter 9

### *The effect of silica/coupling agent combinations versus carbon black on the dynamic and mechanical properties of an EPDM-based engine mount compound*

---

Addition of highly dispersible silica to EPDM in combination with TESPT coupling agent reinforces the rubber, while leaving the dynamic properties at a good level. The tear strength of reinforced EPDM is very poor in comparison with a NR reinforced compound. Adding less silane has a positive effect on the mechanical properties, but a negative effect on the dynamic properties. Addition of no silane causes a bad dispersion of the silica in the rubber matrix, resulting in poor dynamic properties.

Addition of highly dispersible silica to NR reinforces this rubber as well. In such reinforced NR the mechanical properties are better than for EPDM, while the dynamic properties are worse. Comparing silica to carbon black, silica shows stronger reinforcing capabilities and better dynamic properties. This is the case for NR compounds, as well as for EPDM compounds.

Blending some NR into EPDM has a reinforcing effect on the mechanical properties of the compounds. The tear strength is increased with a factor 3 when using a 90/10 EPDM/NR blend, vulcanised with a slow NR system, relative to the pure EPDM vulcanised with its own ultra-fast vulcanisation system.

The development of an engine mount compound based on silica reinforced EPDM is not possible with only EPDM as the polymer. The major problem of the EPDM based engine mount recipes is to obtain a high value for the tear strength. This can be solved to some extent by addition of some NR. The tear strength is improved significantly, without loss of the dynamic properties. The main polymer in that engine mount compound is still EPDM, therefore providing a good high temperature as well as improved ageing resistance.

#### 9.1 Introduction

In recent years, passenger cars have achieved higher performance: lower fuel consumption, improved safety and greater riding comfort. This riding comfort depends to a large extent on the engine mount and the tyre performance. The engine mount is the linkage between the engine and the bodywork of the automobile. It consists for a large part of rubber and is the key factor in isolating noise from the engine.<sup>1-3</sup>

In past years, engine mounts have always been produced from natural rubber (NR). NR has excellent dynamic properties: low  $\tan \delta$ , low dynamic stiffness over a high frequency range and low heat-build-up, compared to other rubbers. However, the service temperature of NR has its limitations. Temperatures above 100°C drastically change the properties. Because of the unsaturated backbone in NR, this type of rubber is very sensitive to oxidative degradation. This effect becomes more pronounced at higher temperatures.

Stronger engines (more heat production) and better aerodynamics of the car bodies (less air-cooling) have raised the temperature under the hood up to 120°C.<sup>4</sup> Another reason for increase in the temperature under the hood is a new set of European gas outlet regulations (Euro IV).<sup>5</sup> To comply with these new laws, drastic steps such as upstream movement of the catalytic converter from the engine compartment are necessary. This leads to a stepwise temperature increase of at least 10°C at the rear mount of the engine.<sup>6</sup> As a result, the car industry is developing better temperature resistant engine mounts as compared to NR. One possible solution is to produce engine mounts using Ethylene-Propylene-Diene-Rubber (EPDM). EPDM is much better resistant to high temperatures due to its saturated backbone.<sup>7, 8</sup>

In the past, several investigations were performed to develop an EPDM based engine mount reinforced with carbon black.<sup>9, 10</sup> The results of those experiments showed that EPDM filled with carbon black results in comparable dynamic properties, but in inferior mechanical properties, as compared to the existing NR-based engine mounts reinforced with carbon black.<sup>9</sup> A possible explanation is given by Klüppel et al.<sup>11</sup> They suggested that there is a high affinity between the  $\pi$ -electrons of carbon black and double bonds in polymers. In EPDM, double bonds are rare, causing a poor compatibility between EPDM and carbon black. A way to improve the mechanical properties of EPDM compounds is to add highly dispersible silica as active filler. Highly dispersible silica might be a suitable filler, because this filler has shown to provide excellent dynamic properties in tyres, which might also be applicable to the EPDM-case.<sup>12</sup>

The performance of an engine mount can be divided into 3 major functions.<sup>13</sup> The primary function of an engine mount is to support the weight of the engine. Secondly, it should dampen large motions near its resonance frequency, for which a large damping is required at that frequency. The last major function is to isolate the high frequency noise, generated by the engine, to the passenger compartment. This condition requires a proper elastic modulus.

To isolate the vibrations caused by the engine, low elastic stiffness and low damping are needed, as the forces transmitted to the structure are dependent on the stiffness and damping of the mount. A measure for the vibration amplitude that is passed on to the bodywork is the transmissibility. The transmissibility (T) is defined as the ratio of a displacement transmitted, relative to the excited displacement. A general expression for T is given by:

$$T^2 = \frac{1 + [\tan \delta(\omega)]^2}{[1 - (\omega / \omega_0)^2 G'(\omega_0) / G'(\omega)]^2 + [\tan \delta(\omega)]^2} \quad (9.1)$$

where  $\omega_0$  is the resonance frequency,  $G'(\omega_0)$  is the corresponding storage shear modulus at resonance frequency,  $\omega$  is the actual frequency of the vibrating system, and  $G'(\omega)$  and  $\tan \delta$  are the corresponding storage shear modulus and loss tangent. A graphical representation of the transmissibility is given in Figure 9.1.

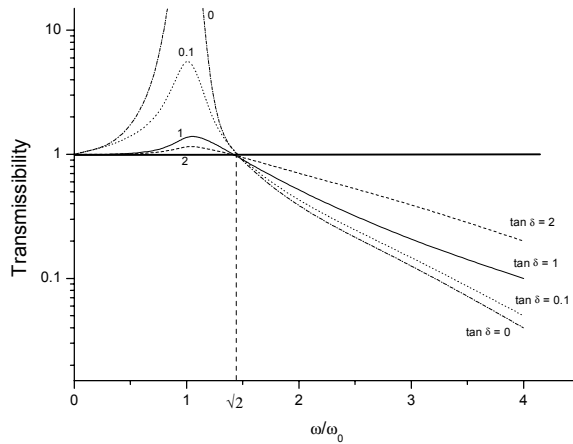


Figure 9.1 Transmissibility vs. frequency-ratio.

Vibration isolation corresponds to transmissibilities lower than 1. The isolation of input vibrations begins at a frequency of roughly  $\omega/\omega_0 = \sqrt{2}$ , above which the transmissibility is less than 1. As vibration isolation is primarily used to isolate noise at higher frequencies, it is the high frequency isolation which counts. Also note that isolation at high frequencies decreases as the damping in the system at resonance frequency increases. Unfortunately, the better the vibration isolation at higher frequencies, the higher the resonance at lower frequencies. This is an intrinsic aspect of noise isolation, which has to be overcome by mechanical means.<sup>6</sup>

Engine mounts should support the engine in the static state and dampen the large vibrations at low frequencies. At high frequencies, damping is not so much necessary, because the amplitudes are normally not so high as compared to low frequencies. For the high frequency range, noise isolation is the main function, meaning that any small deformations suffocate in the rubber part and do not reach the other side.

At high frequencies,  $\omega/\omega_0$  is large, and equation 9.1 simplifies to:

$$T = (\omega / \omega_0)^{-2} [G'(\omega) / G'(\omega_0)] [1 + (\tan \delta(\omega))^2]^{1/2} \quad (9.2)$$

for  $\omega/\omega_0 \gg 1$ . This shows that the transmissibility decreases by the second power of frequency for constant  $G'(\omega)$  and  $\tan \delta(\omega)$ . Engine mounts are therefore designed to have a resonance frequency considerably below the frequencies for which isolation is desired. According to equation 9.2, the ideal engine mount should have a constant or nearly constant shear modulus for many decades in frequency.

To isolate the engine vibrations in the high frequency range, mounts should be soft, having a low elastic stiffness. As mentioned before, an anti-vibration mounting is ideally required to give small transmissibility at all frequencies. This would provide a stable performance over a wide frequency range. Therefore, very high loss angle values at low frequencies combined with very low loss angles at high frequencies would be needed. Clearly, no single rubber matrix (natural or synthetic) is capable to behave in this way: moreover, a slow growth of stiffness ( $G'$  or  $E'$ ) with frequency is closely related to small values of  $\tan \delta$ .<sup>15</sup> To meet the requirement of isolating vibrations at high frequency, a low stiffness ratio is needed. The dynamic stiffness ratio is defined as:<sup>8, 16</sup>

$$\text{Stiffness ratio} = \frac{\text{dynamic stiffness at high frequency}}{\text{static stiffness at low frequency}} = \frac{K_d}{K_s} \quad (9.3)$$

where the stiffness in the high frequency range is depicted as  $K_{\text{dynamic}}$  or  $K_d$  and the stiffness in the low frequency range or at zero frequency as  $K_{\text{static}}$  or  $K_s$ . The stiffness,  $K$ , of an engine mount is composed of two components:<sup>6</sup>

$$K = G^* \cdot S \quad (9.4)$$

where  $K$  is the stiffness (dynamic or static),  $G^*$  is the complex shear modulus and  $S$  is a shape factor determined by the design of the mount. Substituting equation 9.4 for the dynamic and static stiffness in equation 9.3 removes the shape factor from the equation. Therefore, measuring the modulus at high and low frequency results in the stiffness ratio.

The present chapter describes the influence of silica in combination with a coupling agent versus carbon black, on the dynamic and mechanical properties of EPDM and NR engine mount compounds. The effects of the dump temperature on the dynamic and mechanical properties of silica filled EPDM and NR compounds are also discussed.

## 9.2 Experimental

**Materials.** — The compounds for the experiments contained: EPDM (Keltan<sup>®</sup> 7441 A, DSM Elastomers B.V.) with an ENB content of 7.8 wt% and extended with 75 phr of paraffinic oil, or NR (SIR 20); Silica (Zeosil<sup>®</sup> 1165 MP, Rhodia silices); Carbon black (N220, Cabot Corporation); Coupling agent (TESPT Silquest<sup>®</sup> A-1289, OSi Specialties group/Crompton Corporation); Aromatic oil (Enerflex<sup>®</sup> 75, BP Oil Europe); Zinc oxide (Merck); Stearic acid (Merck); Sulphur (J.A. Baker); Tetramethylthiuramdisulphide (TMTD) (Aldrich); Dipentamethylenethiuramtetrasulphide (DPTT; Perkacit<sup>®</sup> DPTT, Flexsys B.V.); N-cyclohexyl-2-benzthiazolesulphenamide (CBS; Santocure<sup>®</sup> CBS, Flexsys B.V.); MBT (Merck); diphenylguanidine (DPG; Perkacit<sup>®</sup> DPG, Flexsys B.V.).

**Compound recipes.**— The engine mount compound recipes are listed in Table 9.1. In recipe I to IV the amount of reinforcing filler and the amount of coupling agent TESPT is varied. The amounts of silica, carbon black and coupling agent are given in the paragraphs containing the results of the experiments: 9.3. Recipe V is a blend of EPDM and NR; the relative amounts of NR blended with EPDM are described in the respective paragraph 9.3.7.

**Table 9.1** Engine mount recipes (phr) for NR and EPDM with silica or carbon black.

Component	I	II	III	IV	V
EPDM	175	175	-	-	Var
NR	-	-	100	100	Var
Silica	var	-	var	-	50
Carbon black	-	var	-	var	-
Coupling agent	var	-	var	-	5
Aromatic oil	-	-	5	5	-
ZnO	5	5	3	3	5
Stearic acid	1	1	1	1	1

Two different curing systems were used, an EPDM and a NR curing system. Which system is used will be explained in the respective paragraph 9.3.

**Table 9.2** Curing systems (phr).

Chemical	NR-system	EPDM-system
Sulphur	0.3	1
TMTD	-	0.8
DPTT	-	0.8
MBT	-	1.5
CBS	3	-
DPG	1.5	1.5

*Mixing.* — The compounds were mixed in three steps. For most of the compounds, the first two mixing steps were effected in a Brabender Plasticorder Labstation 390 ml internal mixer. The carbon black containing compounds were mixed in a Farrel Bridge 1600 ml, internal mixer. The mixing procedure was kept the same for all mixes, as given in Table 9.3. The internal mixers were filled to an extent of 70%. The dump temperature was varied by varying the rotor speed. The starting temperature was 50°C and the cooling water was kept constant at a temperature of 50°C. After each mixing step, the compounds were sheeted out on a Schwabenthan 100 ml two-roll mill. In the case of carbon black filled compounds, a Schwabenthan 1000 ml two-roll mill was used to sheet out the compounds.

**Table 9.3** Mixing procedure.

Step 1:

Time, (min.sec.)	Action
0.00	Open ram; add rubbers
0.20	Close ram
1.20	Open ram; add silica, silane, oil, ZnO and stearic acid
2.20	Close ram
4.20	Open ram; sweep
4.30	Close ram
6.30	Dump

## Step 2:

Time, (min.sec.)	Action
0.00	Load compound
5.00	Dump

*Curing.*— The compounds' curing properties were determined using a RPA 2000 dynamic mechanical rheological tester from Alpha Technologies at a temperature of 170°C. To vulcanise, sheets were pressed in a Wickert laboratory press WLP 1600/5\*4/3 at 100 bar for a period corresponding to  $t_{90}$ , as determined with the RPA 2000. The cured specimens measured 90\*90\*2 mm (for the tensile tests) and 110\*110\*2 mm (for the trouser tear tests).

*Characterisation.*—The Mooney viscosity ML(1+4) at 100°C of the mixed compounds was measured using a Mooney viscometer 2000E from Alpha Technologies.

Dynamic measurements of the uncured compounds (strain sweeps) were performed with the aid of the RPA 2000 from Alpha Technologies at 100°C at a frequency of 0.5 Hz.

The stiffness ratio was measured as a function of frequency with the RPA 2000 at 60°C with 0.56% dynamic strain, after first curing the compounds in the RPA 2000 at 170°C for  $t_{90}$  and subsequently cooling to 60°C. The  $K_s$  was measured at a frequency of 0.01 Hz, whereas the  $K_d$  was measured at a frequency of 30 Hz.

The cured compounds' tensile properties were measured on a Zwick Z020 tensile tester according to ISO-37 and the tear strength, with a trouser shape, was measured according to ISO-34.

The hardness of the cured samples was determined according to DIN-53505.

### 9.3 Results

In the present study EPDM and NR are compared as polymers for an engine mount application. The polymers are reinforced with carbon black or with silica, to compare the effects of these filler systems on the dynamic and mechanical properties of such engine mounts. Carbon black has less reinforcing power than silica; therefore, for the experiments where carbon black and silica are compared, different levels of filler loading are used. The mixer dump temperature is used as the main parameter in the experiments where silica is used as the filler, in accordance with previous chapters in this thesis.

#### 9.3.1 Dynamic and mechanical properties of unfilled compounds

Unfilled (gum) compounds were prepared according to Table 9.1 recipes I and III, with silica, coupling agent and carbon black omitted. This experiment was performed to compare the effect of the polymer NR vs. EPDM on the dynamic and mechanical properties, and in particular on the stiffness ratio  $K_d/K_s$ . The material properties of recipes I and III, and vulcanised after addition of the respective curing systems given in Table 9.2, are listed in Table 9.4.

**Table 9.4** Material properties of unfilled NR and EPDM vulcanised compounds.

Property	NR	EPDM
Tan $\delta$ , (-)	0.07	0.02
$K_d/K_s$ , (-)	1.15	1.07
E-modulus, (MPa)	1.04	1.68
Tensile strength, (MPa)	9.29	1.1
Elongation at break, (%)	533	185
Hardness Shore A, (-)	34	34
Tear strength, (N/mm)	5	0.1

The dynamic properties such as  $\tan \delta$  and the stiffness ratio,  $K_d/K_s$ , are both lower for the EPDM compound as compared to the NR compound. These dynamic properties are surprisingly better for the EPDM gum compounds than for those made on basis of NR! However, the mechanical properties of the NR compound, are far better than for the EPDM compound: high tensile strength, elongation at break and tear strength. These higher mechanical properties are well known to result from the ability of NR to crystallise under strain, a property which virtually all synthetic rubbers are lacking.<sup>17</sup> Reinforcement with fillers is needed to upgrade the EPDM properties to acceptable levels, usually at the cost of the dynamic properties. At the same time, addition of a filler is necessary to obtain acceptable hardness values, approximately 50 – 60 Shore A commonly needed for passenger car engine mounts.<sup>15</sup>

### 9.3.2 Dynamic and mechanical properties of EPDM compounds filled with silica or carbon black

As mentioned in the introduction to this chapter, highly dispersible silica might also be a suitable filler for EPDM, because this filler has shown to provide excellent dynamic properties in tyres, which might also be applicable for the EPDM-case.<sup>12</sup>

Recipes I and II from Table 9.1 were used with variable amounts of silica and carbon black. The silica-coupling agent ratio was set at 10:1. The compounds were mixed according to the procedure described in the experimental paragraph and dumped at a temperature of approximately 150°C. Curing was done with the EPDM system: Table 9.2.

Figures 9.2 A to E represent the dynamic and mechanical properties of the EPDM compounds, reinforced with different amounts of silica or filled with different amounts of carbon black. As can be seen, the stiffness ratio ( $K_d/K_s$ ) increases with increasing amount of silica: Figure 9.2 A. However, the stiffness ratio values of the compounds filled with 50 phr silica are still very good: close to 1. The values for the stiffness ratio for the carbon black filled EPDM compound are even higher than for the silica filled EPDM compound. Also in EPDM rubber, the silica/silane combination shows its superior dynamic performance over carbon black. The point at 60 phr carbon black is comparable to the silica filled compound but probably an experimental outlier. The elastic modulus increases with increasing amount of filler: Figure 9.2 B, as normally observed. Silica and carbon black are resulting in similar elastic moduli. The tensile strength is more dependent on the type of active filler: Figure 9.2

C. A much higher tensile strength and elongation at break are obtained with silica when compared to the carbon black filled compound. The tear strength is also much improved when applying an active filler: Figure 9.2 E. The increase in tear strength is more pronounced when applying silica as filler, similar to the tensile strength. Remarkable is that the tear strength of an EPDM compound filled with carbon black remains more or less the same with increasing amount of carbon black. The fact that the values for the tear strength are varying a lot for the silica-filled compounds, for instance at 50 phr of silica, is due to the type of measurement: a representative tear strength value greatly depends on the way the crack is propagating through the sample, being rather erratic for the trouser tear test.

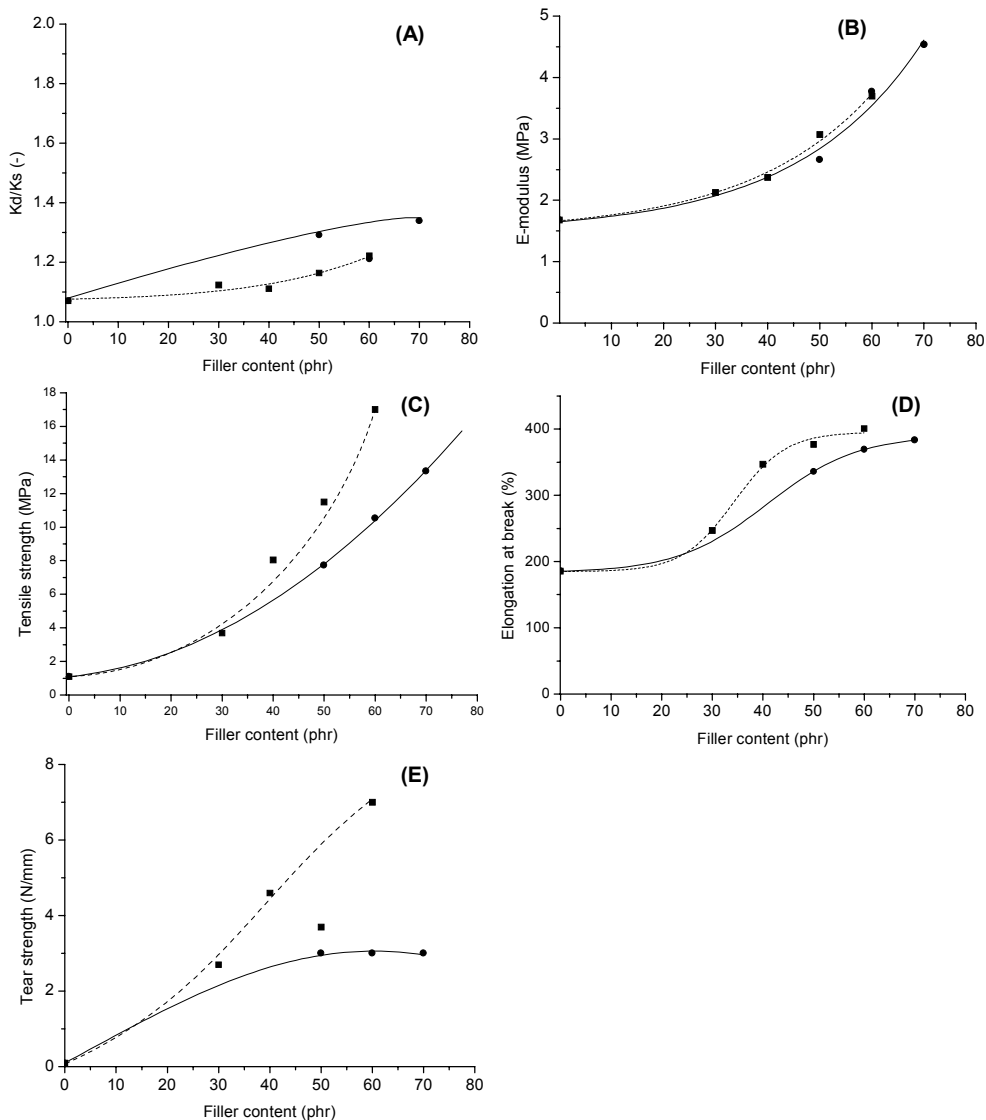


**Figure 9.2** Dynamic and mechanical properties as a function of the filler content; (■), EPDM with silica, (●), EPDM with carbon black; (A), Stiffness ratio; (B), Elastic modulus; (C), Tensile strength; (D), Elongation at break; (E), Tear strength.

### **9.3.3 Dynamic and mechanical properties of NR compounds filled with silica or carbon black**

Recipe III and IV were used with variable amounts of silica and carbon black. The silica-coupling agent ratio was again set at 10:1. The compounds were mixed according to the procedure described in the experimental paragraph and dumped at a temperature of approximately 150°C. The curing was done with the NR system: Table 9.2.

Figures 9.3 A to E represent the dynamic and mechanical properties of the NR compound, reinforced with different amounts of silica or filled with different amounts of carbon black, as indicated in the figure. According to Figure 9.3 A, an increase in the amount of carbon black and silica leads to a higher stiffness ratio. The increase in stiffness ratio is very pronounced, when carbon black is applied as filler in the NR compound. The stiffness ratio remains at a surprisingly low level for even up to 50 phr silica applied. The increase in elastic modulus is for both fillers more or less comparable: Figure 9.3 B. The tensile strength, Figure 9.3 C, is higher for compounds filled with silica and not influenced by the amount of silica within the loading range of 30-60 phr. On the other hand, it seems that the optimum loading with carbon black has been surpassed for this compound: its value decreases already at higher carbon black contents. The elongation at break decreases with increasing amount of filler: Figure 9.3 D. There is no significant difference in the elongation at break between the compounds filled with carbon black and silica. The tear strength increases with increasing amount of filler: Figure 9.3 E. For silica as well as for carbon black the tear strength values are more or less comparable.

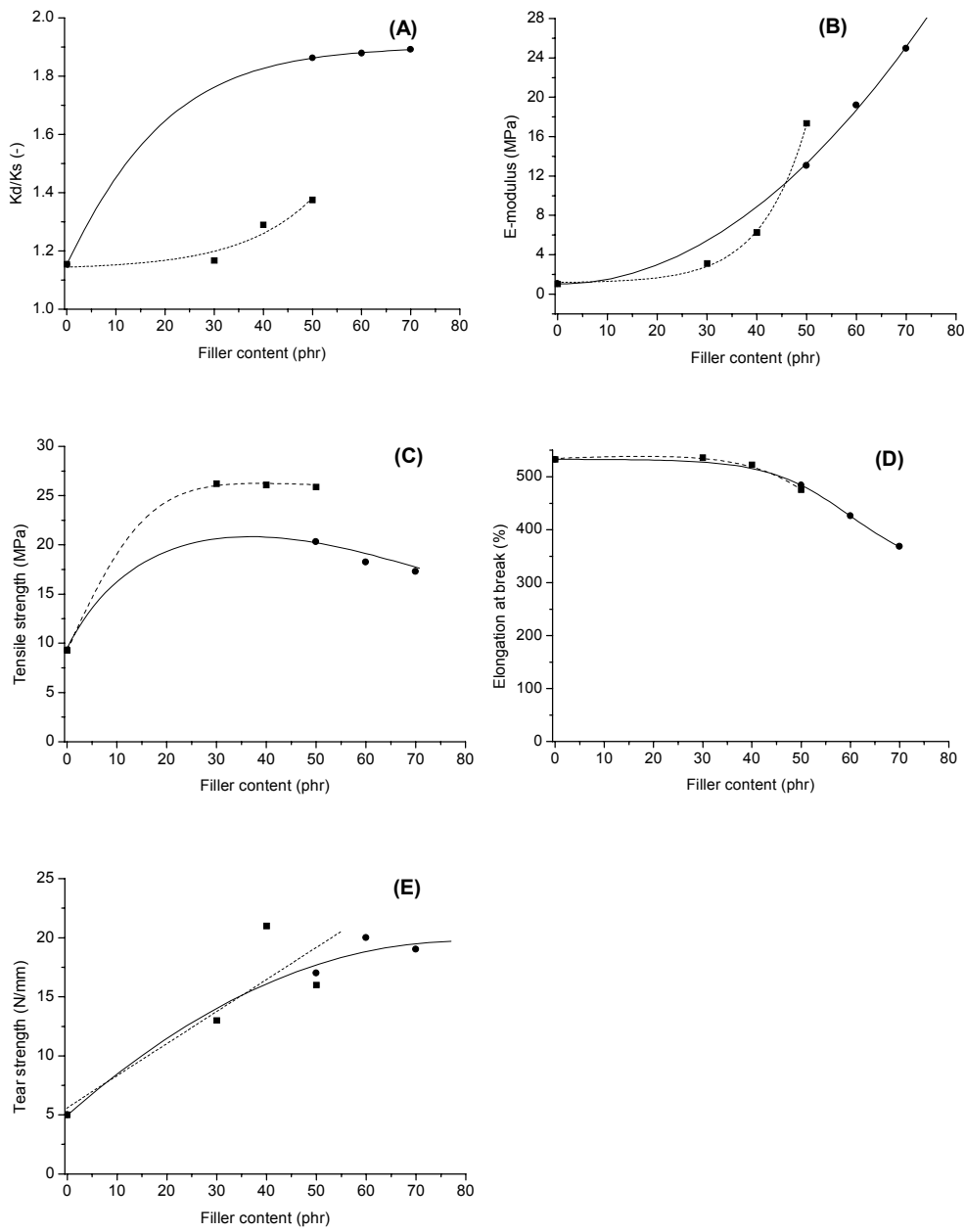


**Figure 9.3** Dynamic and mechanical properties as a function of the filler content; (■), NR with silica, (●), NR with carbon black; (A), Stiffness ratio; (B), Elastic modulus; (C), Tensile strength; (D), Elongation at break; (E), Tear strength.

### 9.3.4 Effect of mixer dump temperature on dynamic and mechanical properties of silica filled EPDM compounds

In Chapter 3 it was shown, that the dump temperature has a significant effect on the dynamic and mechanical properties of a tyre tread compound. The present paragraph shows the effect of dump temperature on the EPDM engine mount compound filled with silica. For this experiment recipe I was used with variable silica contents and a silica-coupling agent ratio of 10:1. All the compounds were cured with the EPDM curing system: Table 9.2. The effects of dump temperature on the dynamic and mechanical properties as influenced by the silica loading, are given in Figures 9.4 A to F.

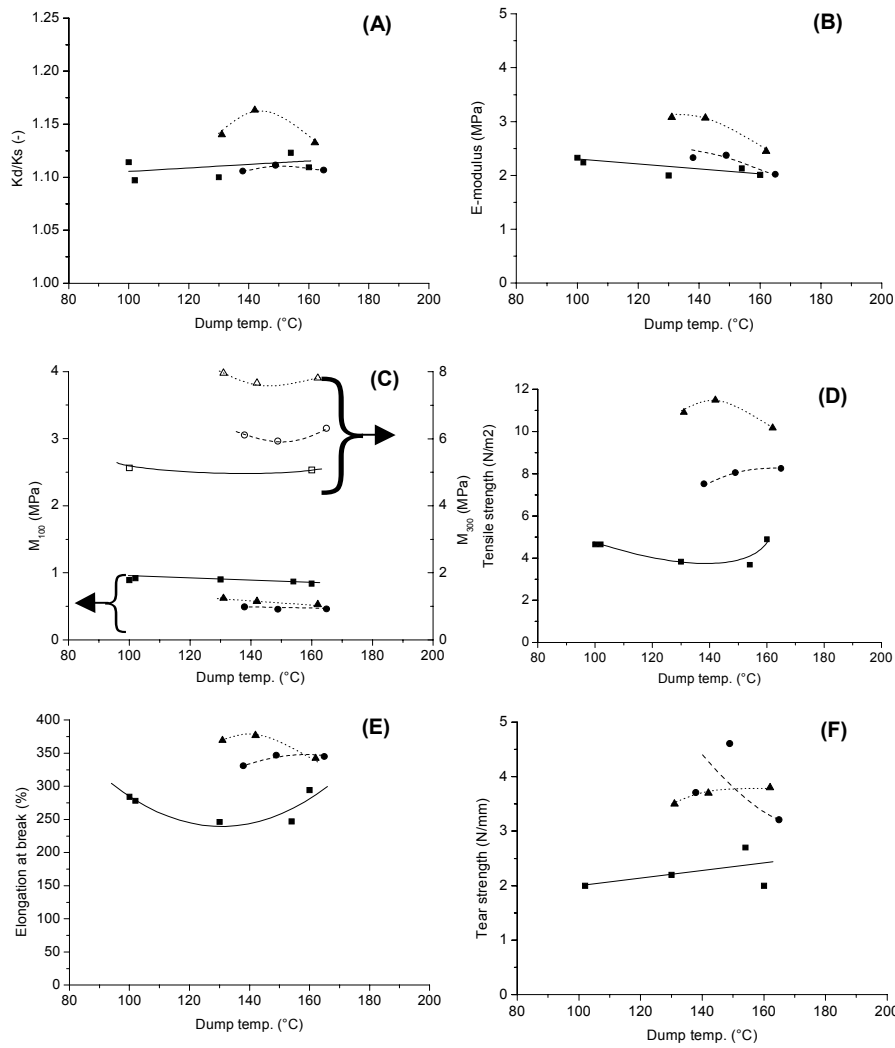


**Figure 9.4** Dynamic and mechanical properties of EPDM compounds with different amounts of silica as a function of the dump temperature; (■), 30 phr silica; (●), 40 phr silica; (▲), 50 phr silica; (A), Stiffness ratio; (B), Elastic modulus; (C), 100 and 300% Modulus; (D), Tensile strength; (E), Elongation at break; (F), Tear strength.

The dump temperature does not have a significant influence on the stiffness ratio: Figure 9.4 A. Higher amounts of silica lead to higher overall E-moduli: Figure 9.4 B, versus a value of 1.68 MPa for the unfilled compound, Table 9.3, as normally would be expected. In this graph there is again no significant effect of the dump temperature visible. At dump temperatures above 150°C, the E-modulus decreases slightly. This effect is most visible at the highest levels of silica. The 100% and 300% modulus are plotted in Figure 9.3 C. Some values for the compounds filled with 30 phr silica are not given for the 300% modulus. This is, because in those cases the sample was already broken before 300% strain was reached. In this graph no significant differences at the 100% modulus can be seen for the different compounds and dump temperatures. This is in accordance with what would be expected. Possible effects of scorching at very high temperatures can only be seen in the 300% modulus and not in the 100% modulus.<sup>18</sup> Figure 9.4 D shows the tensile strength. The reinforcing effect of the silica can again be seen by higher values at increased loadings. Upon adding more silica, the tensile strength increases from around 4 MPa (30 phr silica) till around 10 MPa (50 phr silica). From Table 9.3, it can be seen that adding no silica gives a tensile strength of 1.10 MPa. The dump temperature again does not show an influence on the tensile strength. Filling a compound with active filler leads to higher elongations at break: Figure 9.4 E. This is also in line with the unfilled compound, which has an elongation at break of only 186%: Table 9.3. In this graph again no significant effect of the dump temperature can be seen. The results of the tear strength experiments are shown in Figure 9.4 F. It can be seen, that the tear strength of the 30 phr compound is almost half the value of the 40 phr and 50 phr compound. However, when these results are compared with the values for conventional engine mount compounds based on NR, the difference is very outspoken. Normal NR-based engine mount compounds have tear strengths of 20 N/mm or more<sup>15</sup>, whereas these EPDM compounds have tear strengths of at most 5 N/mm; see also Figure 9.3 E. The unfilled EPDM compound has an even worse tear strength; actually this tear strength is below the limit of detection.

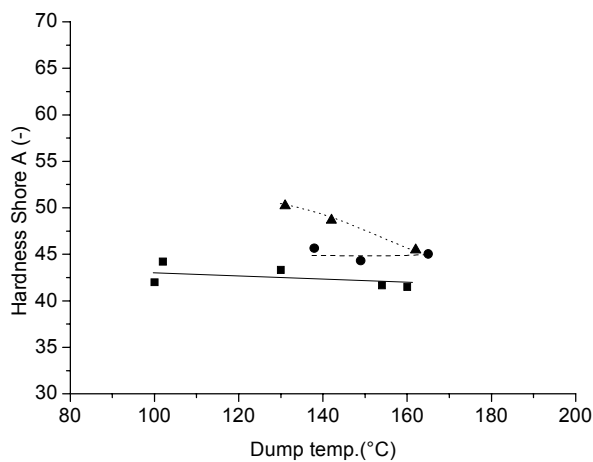


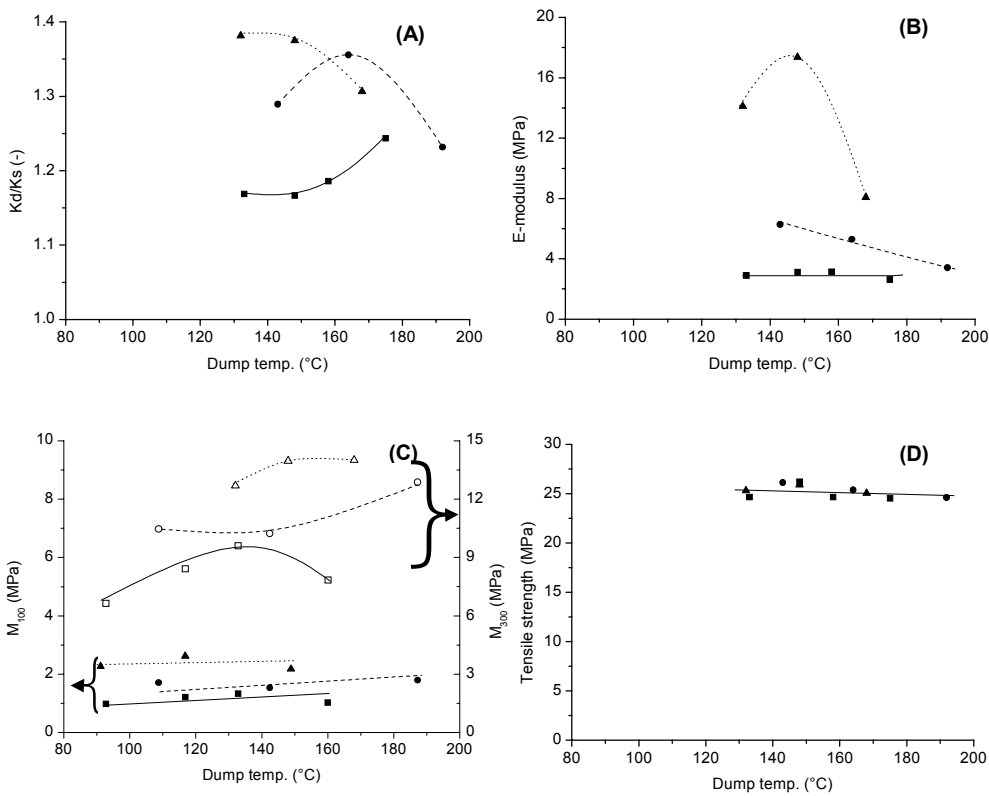
**Figure 9.5** Hardness of EPDM compounds filled with different amounts of silica and with different dump temperatures; (■), 30 phr silica; (●), 40 phr silica; (▲), 50 phr silica.

In Figure 9.5 it can be seen, that an increasing amount of silica leads to an increase in hardness. The value for the unfilled EPDM compound is in line with this

observation; the hardness for the unfilled compound was 34 Shore A, Table 9.3. In Figure 9.5, there is a significant influence of the dump temperature on the hardness. At higher dump temperatures lower hardness values are obtained, especially for the compounds filled with 50 phr of silica.

### 9.3.5 Effect of mixer dump temperature on dynamic and mechanical properties of silica filled NR compounds

The present paragraph shows the effect of dump temperature on the NR engine mount compound reinforced with silica. For this experiment recipe III was used with a silica-coupling agent ratio of 10:1. All the compounds were cured with the NR curing system: Table 9.2. The influences of the addition of silica and of the dump temperature on the dynamic and mechanical properties are given in Figure 9.6.



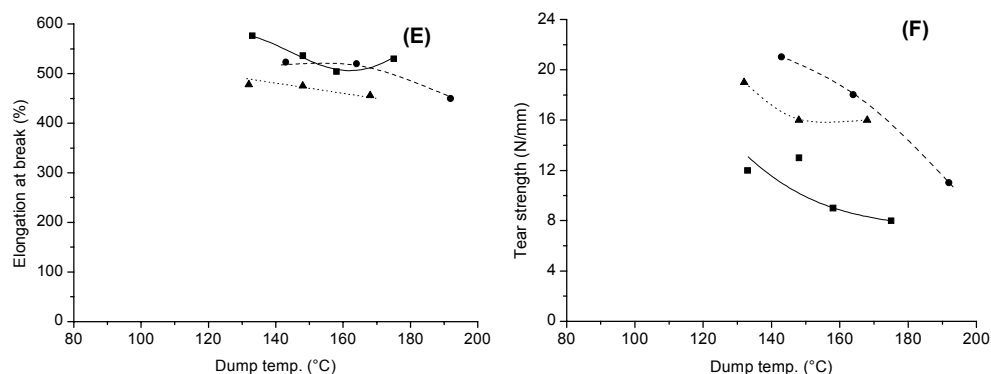


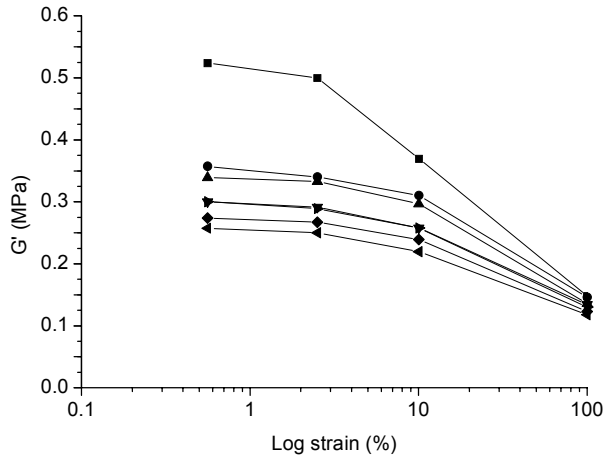
**Figure 9.6** Dynamic and mechanical properties of NR compounds with different amounts of silica as a function of the dump temperature; (■), 30 phr silica; (●), 40 phr silica; (▲), 50 phr silica; (A), Stiffness ratio; (B), Elastic modulus; (C), 100 and 300% Modulus; (D), Tensile strength; (E), Elongation at break; (F), Tear strength.

If the results of the stiffness ratio, Figure 9.6 A, are compared to the results of the compound without silica, Table 9.4, it can be seen that upon adding silica, the stiffness ratio increases. In this figure, the influence of dump temperature is not clearly visible. At higher levels of filling, 40 and 50 phr, the stiffness ratio decreases with increasing dump temperature. The elastic modulus is increasing with increasing amount of filler: Figure 9.6 B. Similar as to the stiffness ratio, with 40 and 50 phr of silica, the elastic modulus is decreasing. This is an indication of better dispersion of the silica filler in the rubber, similar to the observations in Chapter 3. The 100% modulus is more or less the same for all amounts of filler: Figure 9.6 C. The 300% modulus is increasing with increasing amount of filler: Figure 9.6 C. For both properties no significant influence of the dump temperature is observed. The tensile strength remains unaffected by the amount of filler: Figure 9.6 D. The tensile strength is also not influenced by the dump temperature. The elongation at break remains also more or less the same with increasing amount of filler: Figure 9.6 E. The dump temperature has only an influence on the compounds with 40 and 50 phr of silica; the elongation at break decreases with increasing dump temperature, similar to the observations with the tyre tread compound in Chapter 3. The tear strength increases with increasing amount of filler and is influenced by the dump temperature. The tear strength decreases with increasing dump temperature. The effect of the dump temperature on the dynamic and mechanical properties for the silica reinforced NR compounds is more pronounced than for the silica reinforced EPDM compounds, see paragraph 9.3.4.

### 9.3.6 Effect of coupling agent variation on dynamic and mechanical properties of silica filled EPDM compounds

In order to obtain a better insight into the influence of the amount of coupling agent in the silica filled EPDM compound, the effect of the silica/coupling agent ratio was studied. The compounds were prepared according to recipe I described in Table 9.1, with 50 phr of

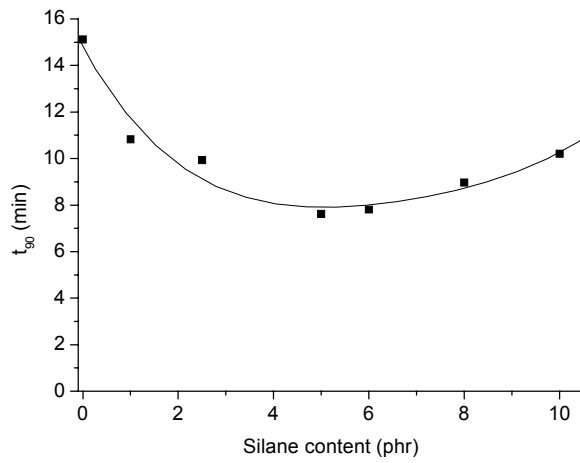
silica and a variable amount of coupling agent. The compounds were all mixed up to a dump temperature of approximately 150°C. The results for dynamic strain sweep measurements are shown below in Figure 9.7 in order to judge the level of filler-filler interaction in a similar manner as done with the green tyre recipes in Chapter 3.



**Figure 9.7** Payne effect shown for EPDM compounds filled with 50 phr silica, with different amounts of coupling agent added; (■), 0 phr; (●), 1 phr; (▲), 2.5 phr; (▼), 5 phr; (▷), 6 phr; (◆), 8 phr; (★), 10 phr.

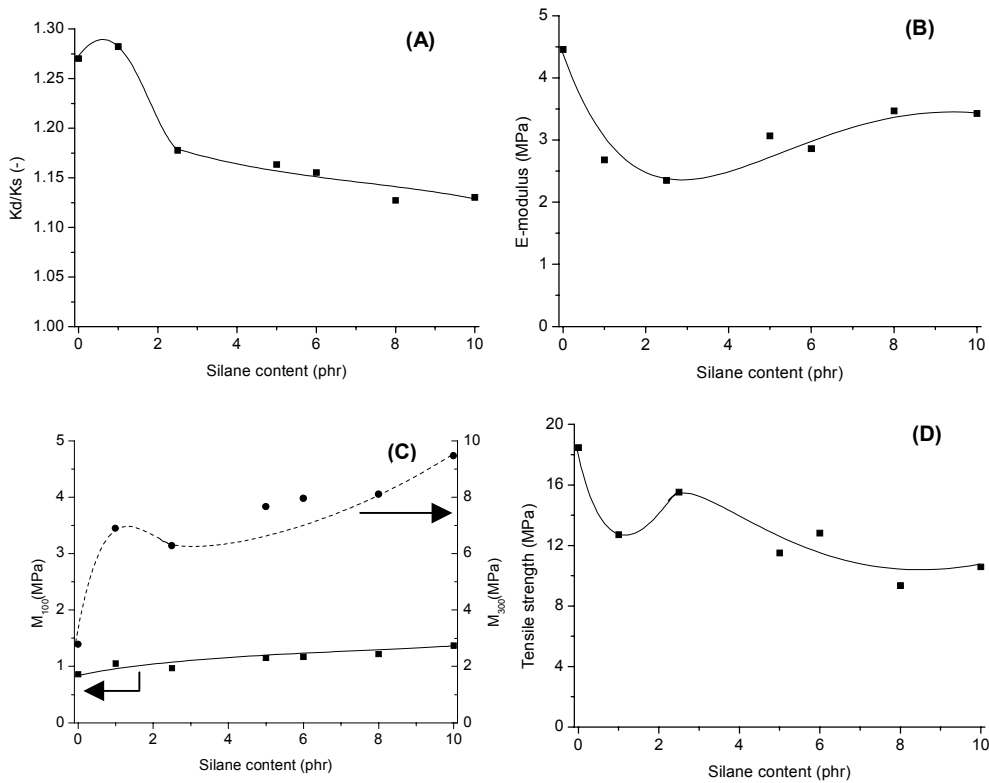
In this figure, two effects of the coupling agent/silica ratio are visible. The first effect is, that adding a coupling agent has a strong influence on the modulus at low strain. In a similar manner, as seen in Chapter 3, the silica particles are not well dispersed in the polymer in absence of silane coupling agent. When already a small amount of coupling agent is added, the surface of the silica is made more hydrophobic and the silica is better dispersed in the polymer. Upon gradual addition of more coupling agent, the effect of making the silica surface more hydrophobic is stronger. This effect reaches a maximum at about 5 phr coupling agent (1/10 of the amount of silica). Adding 6 phr coupling agent has the same effect as adding 5 phr. If the amount of coupling agent is still further increased, another effect of the coupling agent comes into play. As the coupling agent is a liquid, it also has a so-called 'plasticizer' effect. When a suitable liquid is added to a polymer, this liquid lowers the viscosity or the rigidity of the polymer or rubber compound in the present context.<sup>4</sup> This results in a decrease of the modulus at all strains.

When observing the  $t_{90}$  of the compounds with different amounts of coupling agents, the same optimal coupling agent/silica ratio is found, as seen in Figure 9.8. In this graph, two effects of the coupling agent/silica ratio are visible. From 0 phr to 5 phr of coupling agent, there is the effect that the vulcanisation is accelerated. This can be explained by the fact that after the coupling to the silica, the adverse effects of the acidic silica surface on sulphur vulcanisation are neutralised. The vulcanisation reaction preferably takes place in a basic environment, so covering the acidic groups on the silica surface has an accelerating effect.<sup>4</sup> When more than 6 phr coupling agent is added, it can be seen that the  $t_{90}$  increases again. This can be explained by the fact, that the coupling agent itself donates 'free' sulphur atoms to the compound.<sup>19</sup> This causes longer curing times, because more sulphur is donated to the system.



**Figure 9.8**  $t_{90}$  values for EPDM compounds filled with 50 phr silica and various silane coupling agent contents.

In order to find the optimal silica/coupling agent ratio for the dynamic and mechanical properties, the vulcanised compounds were further investigated. The results are given in Figures 9.9 A to F.



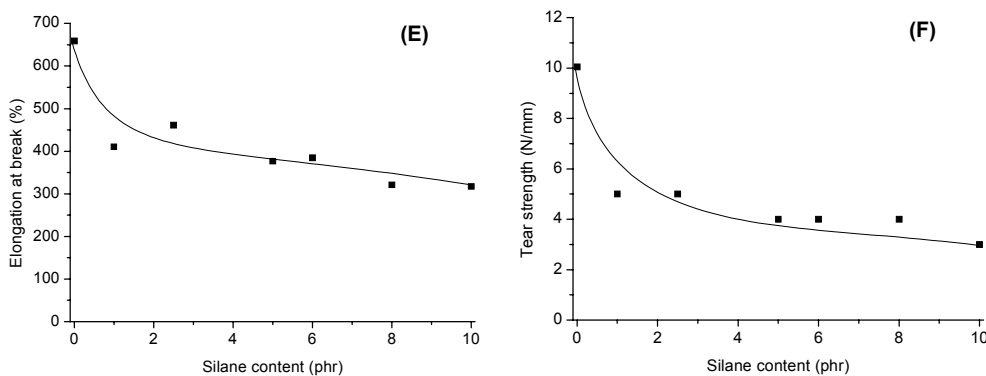


**Figure 9.9** Dynamic and mechanical properties of vulcanised EPDM compounds as a function of the amount of coupling agent added; (A), Stiffness ratio; (B), Elastic modulus; (C), 100 and 300% Modulus; (D), Tensile strength; (E), Elongation at break; (F), Tear strength.

The figure of the stiffness ratio shows a very clear effect of the addition of coupling agent: Figure 9.9 A. If no coupling agent is added, the compound has a rather high stiffness ratio. Upon adding an amount of 4 phr coupling agent, the stiffness ratio decreases to values of approximately 1,12-1,15. The E-moduli for all compounds in this series are very close to each other: Figure 9.9 B. The value for the compound without coupling agent is the highest: 4,5 MPa; the other compounds in this series have E-moduli in the range of about 2,5 to 3,5 MPa. In the plot for the 100% modulus and the 300% modulus versus the coupling agent content, the effect of adding a little amount of coupling agent can be seen very well. Upon adding a small quantity of coupling agent, the 300% modulus increases sharply. For the compound without coupling agent, the 300% modulus is around 3 MPa; upon addition of coupling agent, the value is increased to around 7 to 8 MPa. The results of the tensile strength are decreasing with increasing amount of coupling agent: Figure 9.9 D. In the present case there is no large difference between adding no coupling agent or only 1 phr. The elongation at break is decreasing with increasing amount of coupling agent: Figure 9.9 E. Without the addition of a coupling agent, the highest value for the elongation at break is obtained. The tear strength also decreases with increasing amount of coupling agent: Figure 9.9 F. The strongest decrease in the tear strength already happens between no addition of coupling agent and the addition of only 1 phr.

### 9.3.7 Dynamic and mechanical properties of blends of EPDM and NR compounds

In the previous paragraphs it was observed that the dynamic properties of EPDM compounds are better in comparison to NR compounds. NR compounds, on the contrary, resulted in better mechanical behaviour in comparison with the EPDM compounds. It is interesting to see, whether it is possible to combine the two characteristics in one

compound. A possibility is to blend the two compounds. For example, blending of EPDM and NR has been quoted to be successfully applied in tyre sidewall compounds.<sup>20</sup>

For this experiment recipe V was used, as listed in Table 9.2. The compounds were mixed according to Table 9.3 and dumped at a temperature of 150°C. Blending though, may cause problems when adding ingredients, like fillers or the vulcanisation system. Ingredients usually show a preference for one of the two phases. This may for instance result in the phenomenon, that all the silica will end up in the NR phase of the blend, leaving the EPDM phase almost without silica. This obviously represents a bad distribution of the filler in the compound. A way to overcome this problem is, to first add the complete filler and vulcanisation systems to both polymers separately, resulting in two masterbatches. From these masterbatches the suitable amounts are blended, resulting in the desired compounds with a good distribution of the ingredients. This way of blending two polymers with fillers is commonly known as Y-mixing. In the present experiments also Y-mixing was applied. Two masterbatches with filler and their own vulcanisation system were blended on the two-roll mill in the desired ratios.

Figure 9.10 A shows the stiffness ratio ( $K_d/K_s$ ) for the polymer blend as a function of the amount of NR blended with the EPDM. The stiffness ratio first increases with increasing amount of NR. A maximum in stiffness ratio occurs at 75% EPDM and 25% NR. The different vulcanisation systems show the same behaviour. Applying the Y-mixing procedure results in the best stiffness ratio; close to 1. Independent of the amount of NR, the Y-blends result in the lowest values of the stiffness ratio.

The elastic modulus increases with increasing NR content, Figure 9.10 B. The NR vulcanisation system causes somewhat lower elastic moduli, while with Y-mixing the elastic moduli are somewhat higher. For the tensile strength versus the NR content, a non-linear behaviour is observed. From 0 to 7.5% NR, there is a sharp increase in tensile strength. The maximum values come close to the tensile strength of a 100% NR compound. From 7.5% to 25% NR the tensile strength decreases, with the tensile strength for the 75/25 blend being equal to or even lower than for the 100% EPDM compound. The 50/50 blend is somewhat better, especially for the EPDM vulcanisation system. Finally, the values for the 100% NR are very good again. The NR vulcanisation system results in the best properties.

The elongation at break results in more or less the same trend as for the tensile strength, Figure 9.10 D. From the 100/0 EPDM compound to the 85/15 blend, the elongation at break increases. From that point onwards, the values are decreasing to the value for the 0/100 NR compound. The NR vulcanisation system again accounts for the best results. The Y-mixing procedure results in elongations at break comparable to those for the EPDM vulcanisation system.

Figure 9.10 E represents the tear strength values of the EPDM/NR blends. From this figure it can be observed, that there is a local maximum and a local minimum. The maximum in tear strength is reached at the 90/10 blend. From that point onwards, the tear strength decreases to low values at the 50/50 blend. The 100% NR value for the tear strength is the highest value in comparison to all blends and the 100% EPDM compound. The NR vulcanisation system results in the highest values for the tear strength, whereas the Y-mixing procedure and the EPDM vulcanisation system result in similar but lower values.

The shape of the different tear strength plots shows an interesting phenomenon. EPDM compounds show an increase in stress till a certain value is reached and, after the first cut, the EPDM tears on at more or less the same stress level: Figure 9.11. For a NR compound the tear strength plot results in a strong zigzag-pattern: Figure 9.12. The NR compound builds up a large stress without tearing, then suddenly the cut grows till a certain

point, after which a new large stress is built up and the whole process repeats itself. Apparently, for a compound to show a good tear strength, it is important that it shows this type of zigzag-pattern. Figure 9.13 represents a EPDM/NR (90/10) blend, in which it can be observed, that after the first cut in the sample this zigzag-pattern already appears to a significant extent. Only 10% NR is already causing this effect.

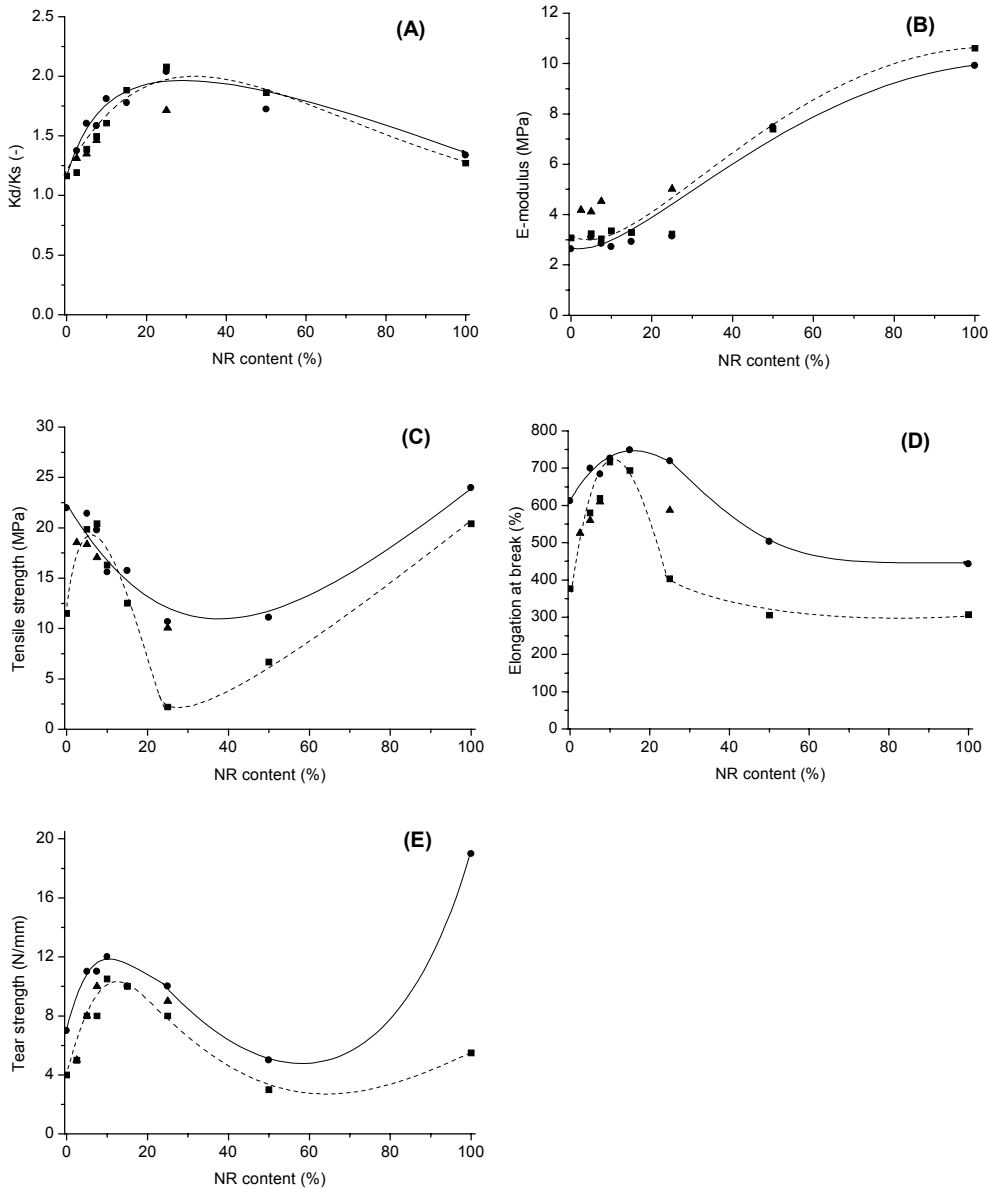


**Figure 9.10** Dynamic and mechanical properties as a function of the NR content; (A), Stiffness ratio; (B), Elastic modulus; (C), Tensile strength; (D), Elongation at break; (E), Tear strength; (■), EPDM curing system; (●), NR curing system; (▲), Y-mixing.

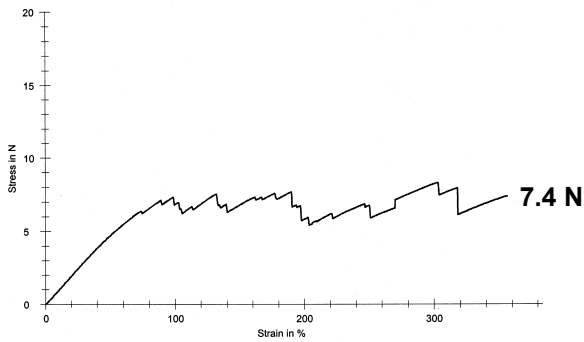


Figure 9.11 Tear strength measurement of EPDM filled with 50 phr silica.

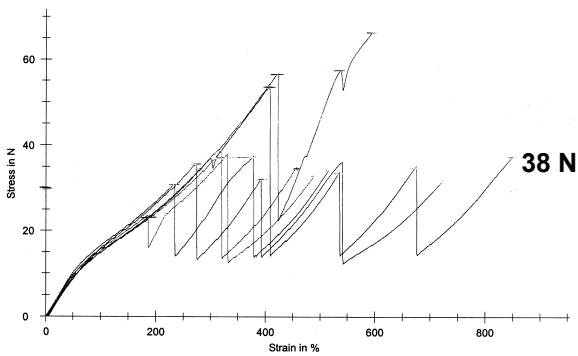


Figure 9.12 Tear strength measurement of NR filled with 50 phr silica.

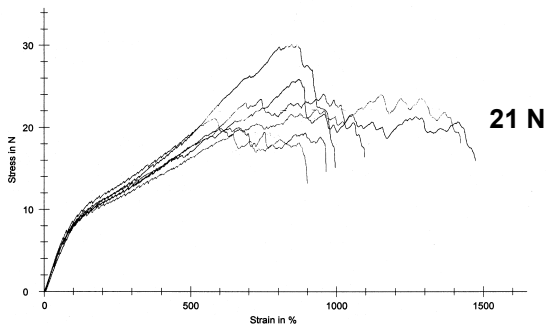


Figure 9.13 Tear strength measurement of EPDM/NR (95/5) filled with 50 phr silica.

## 9.4 Discussion

In order to meet the requirements for engine mounts as described in the introduction, a rubber compound should have a good level of dynamic and mechanical properties. Pure EPDM and NR compounds do not meet these conditions. Although good

values for the dynamic properties were obtained, especially in the case of EPDM, the mechanical properties were too poor.

The addition of fillers was investigated as a means to improve the mechanical properties. Two sorts of active fillers are normally used: carbon black and/or silica. When looking at silica filled EPDM, the mechanical and dynamic properties were better in comparison with carbon black filled EPDM. The use of silica resulted in lower dynamic stiffness ratios in comparison with carbon black and provided higher values for the tensile and tear strength. This can be explained by the fact, that silica particles can be attached to the polymer network via the silane coupling agent, as described in Chapter 2. Upon deformation, these silica particles move along with the network, instead of being loose filler, slipping in the rubber network. In the case of NR, similar results were obtained, lower dynamic stiffness ratios and higher mechanical properties at the same amounts of silica added, compared to carbon black. To obtain the same mechanical properties as for a carbon black filled compound, less filler is needed in NR when applying silica. In that case, relatively more polymer is present in the compound and that has a positive effect on the dynamic properties.

In the present work, no significant effects of the dump temperature could be seen in a NR or EPDM compound, contrary to the 'green tyre technology'.<sup>23</sup> This can be explained by the fact, that in the case of EPDM not many double bonds are present in its structure, like in SBR or BR and NR. The ENB content of the EPDM used in this work, is 7,8 wt% and is of the vinylidene-type. These double bonds are necessary to provide the allylic hydrogen atoms, which form the reactive site for the coupling reaction between the silica/silane and the polymer backbone. In NR, there are a lot of double bonds, so in this polymer there should be an effect of the dump temperature on the properties like in SBR/BR. However, just like for EPDM, this was not the case. Only small effects of the dump temperature on the dynamic and mechanical properties of the NR compound were visible, and only at filler loadings of 40 and 50 phr. An explanation could be the type of double bonds that are present in NR. In Chapter 6 it was observed that cis and trans-type double bonds are not so reactive towards TESPT coupling agent as vinyl-type double bonds. In SBR/BR, there are a lot of these vinyl-double bonds, while in NR there are only cis-double bonds present.<sup>19</sup>

Addition of TESPT as coupling agent is necessary to obtain good dynamic and mechanical properties. If 50 phr silica is added, then the addition of 1 phr of TESPT improves the properties already significantly. On the other hand, if more than 5 phr is added, no further improvement is obtained but rather a deterioration due to a plasticising effect. The optimum silica:coupling agent ratio is 10:1.

The results show, that silica filled EPDM compounds have better dynamic properties than NR, whereas silica filled NR compounds show better mechanical properties. The tear strength is a property for which NR outperforms EPDM greatly. The reason for this big difference is, that NR allows for strain crystallisation. When the polymer chains in NR are stretched, the glass transition temperature is shifted above room temperature.<sup>17</sup> This results in crystallisation of the polymer chains. These rigid polymer crystals provide for ad hoc reinforcement with the very high tear strength as a result. Unlike NR, EPDM does not show this behaviour.

According to the results obtained for EPDM filled with silica, there is a great opportunity to improve the mechanical properties. The addition of a few percentages of NR already gave a large positive effect on the mechanical properties. The tensile strength and the tear strength are raised to a higher level, without the complete loss of the good dynamic characteristics of the EPDM.

With respect to the vulcanisation system that was applied, a difference in properties was observed, dependent on the vulcanisation system. This can be explained by the type of crosslinks that are formed. Longer crosslinks, which are formed in slower vulcanisation systems, like the NR-system Table 9.2, can build up higher strengths. This can be seen in the tensile strength and the tear strength plot. Shorter crosslinks, which are formed with ultra accelerator vulcanisation systems, like the EPDM-system Table 9.2, give the compound better dynamic properties.

## 9.5 Conclusions

Addition of highly dispersible silica to EPDM in combination with TESPT coupling agent reinforces the rubber. The dynamic properties of the EPDM remain good with the addition of moderate quantities of silica. Addition of 50 phr silica provides for a good hardness value and E-modulus, as requested in the specifications for engine mounts. The tear strength of reinforced EPDM is very poor in comparison with a NR reinforced compound. The optimal silica:silane ratio is 10:1. Adding less silane has a positive effect on the mechanical properties, but a negative effect on the dynamic properties. Addition of no silane causes a bad dispersion of the silica in the rubber matrix, resulting in poor dynamic properties.

Addition of highly dispersible silica to NR reinforces this rubber as well. In such reinforced NR the mechanical properties are better than for EPDM, while the dynamic properties are worse. Comparing silica to carbon black, silica shows stronger reinforcing capabilities and better dynamic properties. This is the case for NR compounds, as well as for EPDM compounds.

Blending some NR into EPDM has a reinforcing effect on the mechanical properties of the compounds. The tear strength is increased with a factor 3 when using a 90/10 EPDM/NR blend, vulcanised with a slow NR system, relative to the pure EPDM vulcanised with its own ultra-fast vulcanisation system.

The development of an engine mount compound based on silica reinforced EPDM is not possible with only EPDM as the polymer. Replacing carbon black by silica in an EPDM compound greatly improves the mechanical properties of the compound without significant loss of the dynamic properties. The major problem with the EPDM based engine mount recipes is to obtain a high value for the tear strength. This can be solved to some extent by addition of a small quantity of NR. The tear strength is improved significantly, without loss of the dynamic properties. The main polymer in that engine mount compound is still EPDM, therefore a good high temperature resistance can be achieved.

## 9.6 References

1. H.C. Lord, U.S. Pat. 1,778,503 (14-10-1930).
2. K.A. Brown, N.J. Westwood, E.S. Taylor, (to Wright Aeronautical Corporation, Paterson), U.S. Pat. 2,175,825 (10-10-1939).
3. W. Hutter, A. Wöfl, *Kautsch. Gummi Kunstst.*, **51**, (1998), 506.
4. S. Slayer, *Jahrestagung Elastomerverarbeitung des VDI-K, Mannheim*, (1999).

5. Official Journal of the European Communities, (1999).
6. DSM, *Closing the gap between NR and EPDM*, 1999, internal publication at DSM.
7. O.M.J. Shinichiro, (to Exxon chemicals patents inc.), U.S. Pat. 5,904,220 (18-05-1999).
8. P.M. van de Ven, M.J.M. Theunisse, H. Shimada, International Rubber Conference, Kobe, Japan, October, 23-27, 1995.
9. J. Dato, W.F. Cousins, W. Von Hellens, D. Wall, presented at a meeting of ACS, Rubber Division, Anaheim, California, USA, May 6-9, 1997.
10. M. Hofmann, EPDM conference, Brussels, May 11, 2000.
11. M. Klüppel, R.H. Schuster, J. Schaper, Rubber Chem. Technol., **72**, (1999), 91.
12. Chapter 3 of this thesis.
13. A. Ueda, T. Ohyama, H. Watanabe, A. Yoshioka, presented at a meeting of ACS, Rubber Division, Cincinnati, Ohio, USA, October 18-21, 1988.
14. A.R. Payne, R.E. Whittaker, Rubber Chem. Technol., **44**, (1971), 440.
15. S. Caldari, M. Demaio, The engineering society for advancing mobility land sea air and space, SAE, Detroit, Michigan, USA, February 28- March 3, 1994.
16. R.P. Brown, Physical Testing of Rubbers, Applied Science Publishers, London, UK (1979).
17. W.R. Krigbaum, R.-J. Roe, J. Appl. Polym. Sci., **2**, (1964), 4391.
18. L.A.E.M. Reuvekamp, J.W. ten Brinke, P.J. van Swaaij, J.W.M. Noordermeer, Kautsch. Gummi Kunstst., **55**, (2002), 41.
19. Chapter 6 of this thesis.
20. F.G. Corvasce, (to Goodyear Tire & Rubber Company), Eur. Pat. 1 038 696 A1 (27-09-2000).



---

## Main symbols and abbreviations

---

$\delta$	chemical shift	[ppm]
$\phi$	volume fraction of the filler	[-]
$\gamma$	strain	[-]
$\gamma_0$	maximum strain	[-]
$\eta$	viscosity of filled compound	[Pa.s]
$\eta_0$	viscosity of unfilled compound	[Pa.s]
$\sigma$	stress	[MPa]
$\sigma_0$	maximum stress	[MPa]
$\nu$	number of moles of elastically effective network chains per unit volume	[m <sup>-3</sup> ]
$\omega$	angular frequency	[rad/s]

E-modulus	Young's modulus for small strains of the stress-strain curve	[MPa]
f	shape factor	[-]
G	modulus of filled compound	[MPa]
G'	storage modulus	[MPa]
G''	loss modulus	[MPa]
G <sub>0</sub>	modulus of unfilled compound	[MPa]
k	Boltzmann constant	[J/K]
k <sub>b</sub>	rate constant	[min <sup>-1</sup> ]
k <sub>m</sub>	rate constant	[min <sup>-1</sup> ]
k <sub>a</sub>	kinetic rate constant; primary reaction	[min <sup>-1</sup> ]
k <sub>b</sub>	kinetic rate constant; secondary reaction	[min <sup>-1</sup> ]
K <sub>d</sub>	dynamic stiffness	[N/m]
K <sub>s</sub>	static stiffness	[N/m]
M <sub>100</sub>	stress at 100% strain	[MPa]
M <sub>300</sub>	stress at 300% strain	[MPa]
N	number of surviving contacts	[-]
P	mixer torque	[Nm]
R <sub>b</sub>	rate of breakage	[min <sup>-1</sup> ]
R <sub>m</sub>	rate of reagglomeration	[min <sup>-1</sup> ]
S <sub>BET</sub>	specific surface area	[m <sup>2</sup> ]
T	transmissibility	[-]
T <sub>g</sub>	glass transition temperature	[K]
t <sub>02</sub>	scorch time	[min.]
t <sub>90</sub>	optimum vulcanisation time	[min.]

3-m-1-p	3-methyl-1-pentene
AFM	atomic force microscopy
BR	butadiene rubber
C	conventional silica

*Main symbols and abbreviations*

---

CBS	N-cyclohexyl-2-benzothiazolesulphenamide
CDCl <sub>3</sub>	deuterated chloroform
DMESPT	bis-(dimethylethoxysilylpropyl)tetrasulphide
DPG	diphenylguanidine
DPTT	dipentamethylenethiuramtetrasulphide
EPDM	ethylene-propylene-diene rubber
EtO	ethoxy
EtOH	ethanol
HD	highly dispersible silica
<sup>1</sup> H-NMR	proton nuclear magnetic resonance
HPLC	high performance liquid chromatography
MBT	mercaptobenzothiazole
MCV	model compound vulcanisation
NR	natural rubber
phr	parts per hundred rubber
ppm	parts per million
RPA 2000	rubber process analyser
S	sulphur
SD	semi dispersible silica
S-SBR	solution-styrene-butadiene-rubber
t-3-h	trans-3-hexene
TESH	bis-(triethoxysilyl)hexane
TESD	bis-(triethoxysilyl)decane
TESPT	bis-(triethoxysilylpropyl)tetrasulphide
TME	2,3-dimethyl-2-butene, tetramethylene
TMeSPT	bis-(trimethylsilylpropyl)tetrasulphide
TMTD	tetramethylthiuramdisulphide
XPS	X-ray Photoelectron Spectroscopy
ZnO	zinc oxide

---

## Summary

---

In recent years a steady growth has been seen in the use of silica as reinforcing filler in tyre tread compounds. Silica greatly reduces the rolling resistance of tyres, when compared with carbon black. However, the use of silica as a reinforcing filler is considered to be difficult. Since rubber and carbon black are both hydrophobic substances, problems seldomly arise when the two are mixed. However, when silica is mixed with the commonly non-polar olefinic hydrocarbon rubbers, there will be a greater tendency towards hydrogen-bond interactions between surface silanol groups in silica agglomerates, than to interactions between polar siloxane or silanol groups on the silica surface and the rubber polymers. So mixing silica with rubber involves major problems. For this reason, there is great interest in enhancing the compatibility of hydrocarbon rubbers and precipitated silica by modification of the surface of the silica. Bifunctional organosilanes are commonly used as coupling agents to chemically modify silica surfaces in order to promote interactions with hydrocarbon rubbers. The coupling agent most commonly used for these applications is bis-(triethoxysilylpropyl) tetrasulphide (TESPT). From a processing point of view, two chemical reactions have to take place via the coupling agent. First, a reaction to bind the organosilane to the silica surface and second, a reaction to couple the organosilane to the rubber polymer.

The objective of the research described in the present thesis was to gain understanding of the mechanism of the reactions described above, during mixing of silica and rubber in the presence of coupling agent. This is needed to optimise the reinforcing mechanism in silica filled rubbers. This can only be done when more insight is gained about the reaction mechanisms that are taking place between the coupling agent and the silica, respectively with the rubber matrix.

An introduction in topics relevant for the present thesis was presented in **Chapter 2**. Emphasis was laid on the effect of fillers on the dynamic mechanical properties of elastomers, in relation to their role in tyre performance. The processes of dispersion of fillers during mixing were also briefly reviewed. Special attention was given to the mixing of silica, regarding the reactions that are to take place in the presence of a silane coupling agent.

The influence of processing parameters on the dynamic and mechanical properties of silica reinforced tyre tread compounds was discussed in **Chapter 3**. The addition of TESPT as a coupling agent to silica-rubber compounds significantly enhanced the filler-matrix compatibility. This coupling agent may also act as sulphur donor and thereby get involved in premature curing reactions: scorch during mixing. The dump temperature, one of the main processing parameters employed during mixing, and the length of time that the compound is exposed to that temperature, governed the reaction mechanisms of the coupling agent and determined whether the agent lead to the formation of a bond to the silica or even acted as a curing agent. A temperature of at least 130°C was necessary to ensure, that the reaction between the coupling agent and the silica proceeded, whereas the coupling agent started to react with the rubber or to donate sulphur, resulting in scorch, at temperatures above 160°C. An increase in the 300% modulus and/or  $G'$  at 100% strain above 150°C dump temperature was an indication of this scorch caused by the sulphur donor capability of the coupling agent. It was observed that the coupling agent must be mixed with the silica for at least 10 minutes at 150°C to obtain a sufficient degree of coupling between the two.

The influence of other ingredients such as zinc oxide was investigated in **Chapter 4**. The effect of the presence of zinc oxide in the internal mixer at high dump temperatures was studied by dynamic mechanical testing. A lower tendency to scorch was seen when zinc oxide was omitted during the internal mixing stage and added only later, together with the curing additives on a two-roll mill. Zinc oxide primarily interfered with the reaction between the coupling agent and the silica surface, as shown by the reaction rate constants obtained with rheological experiments. Further confirmation was obtained by HPLC experiments: the reaction rate constants of TESPT with silica for the samples with zinc oxide present, were lower at higher temperatures in comparison with samples without zinc oxide. XPS data confirmed that zinc oxide can indeed react with the silica surface. Another interesting phenomenon observed was, that when zinc oxide is included in the internal mixer stage, shorter scorch times are obtained for curing when compared to compounds where no zinc oxide was included during mixing, and added later on. These shorter scorch times are the result of filler flocculation of the silica during the curing stage.

The experiments described in **Chapter 5** proved, that a proper balance in functionalities is required for a coupling agent to enhance the properties of silica-reinforced tyre tread compounds. TESPT proved to best comply with this balance, because it allows for the coupling reaction towards the silica via its triethoxysilyl groups, resp. for a sulphur donation and a coupling reaction towards the rubber polymer via its sulphur moiety. Alternative coupling agents, allowing for only one of these functionalities, led to an inferior balance of properties. Bis-(triethoxysilyl)hexane (TESH) with only a triethoxysilyl group and no sulphur, did hydrophobise the silica and provided for a good silica dispersion, like TESPT. However, the vulcanised properties were seriously poorer than those obtained with TESPT. On the other side bis-(trimethylsilylpropyl)tetrasulphide (TMeSPT), with only an active sulphur group, failed in its ability to properly disperse the silica and showed premature scorch effects at high mixer dump temperatures, like seen for TESPT. Again, the vulcanised properties were inferior to those obtained for TESPT. Adding two coupling agents, bis-(triethoxysilylpropyl)decane (TESD) and TMeSPT, with the functionalities independently divided over both, did result in a silica dispersion grossly comparable with the one obtained with TESPT. Also signs of scorch were seen at high mixer dump temperatures, like with TESPT. But still, the properties of vulcanised compounds were still grossly inferior to those obtained with TESPT.

A coupling agent with only one reactive ethoxy group attached to the silicium atom, vs. three for TESPT, performed surprisingly well. This coupling agent can only perform coupling with the silica via one Si-O-bridge, which leads to a very quick dispersion equilibrium during mixing and consequently low mixer torques. It came closest to TESPT in vulcanised compound properties, particularly for the  $\tan \delta$ , representative for tyre rolling resistance. Only the tensile strength was lower than the one achieved with TESPT.

Based on all the results, a model was proposed whereby TESPT releases sulphur to the compound in the vicinity of the silica particle during mixing or in the early stages of vulcanisation, thereby causing a crosslinked polymer shell, trapping the silica particle in the rubber matrix. Later on, during vulcanisation, TESPT provides for chemical bridge formation between the silica particles and the rubber polymer.

In Chapters 3 and 5 it was observed that TESPT reacts with rubber under high temperature conditions even in absence of crosslinking agents. This causes the pre-crosslinking or scorch during mixing, which leads to a rise in compound viscosity and therefore makes processing of the compound difficult. In order to look for a solution to this problem, it was necessary to study this reaction and elucidate its mechanism. **Chapter 6**

focused on the reactions, which take place between the coupling agent and the polymer. This was done by using Model Compound Vulcanisation, in order to be able to analyse the reaction products with standard analytical techniques. The model 3-methyl-1-pentene (representative of the vinyl structure of butadiene rubber) was more reactive than trans-3-hexene (representative of the trans structure of butadiene rubber), and trans-3-hexene was more reactive towards elemental sulphur than 2,3-dimethyl-2-butene. Reactions with sulphur or TESPT lead to the same reaction products, indicating that TESPT indeed donates sulphur. Experiments with only TESPT and a model showed, that TESPT first incorporates free elemental sulphur during the first 5 minutes of reaction and later donates it to the model compound.

The effect of dump temperature on the morphology of the silica-filled compound was studied in **Chapter 7**. The dump temperature obtained during mixing had no significant influence on the macrodispersion of a highly dispersible silica. On the other hand, the microdispersion as observed with AFM measurements, was influenced by the dump temperature. At high dump temperatures a better dispersion, i.e. more primary particles, was obtained. Also effects of pre-vulcanisation could be visualised by the AFM. Elliptical structures appeared in the AFM phase image.

The structure of the silica has a major effect on the macro- and microdispersion. Low structured silica (conventional silica) resulted in a poor macrodispersion. Microdispersion measurements showed that higher structured silica results in more primary particles. Highly dispersible, highest structured silicas are mainly dispersed to the microdispersion level, with only 15-20% of the silica remaining on the macrodispersion level. The filler-filler interactions were mainly caused by aggregates with a minimal diameter of 600 nm. The tensile strength of the compounds based on the various silicas was primarily influenced by the microdispersion. Lower tensile strengths were obtained when a significant amount of aggregates were present in the compound with a diameter greater than 600 nm.

To obtain a tyre tread compound with a low rolling resistance, a highly dispersible silica is needed. The highly dispersible silica should mainly be dispersed to the microdispersion level, where it should consist out of primary particles and a few aggregates with a size between 100 and 200 nm.

In the previous chapter interconnected, soft channel-like-structures were observed in the AFM phase images. Several interpretations are given in literature for grainy structure or soft interstices that are present in AFM phase images or TEM micrographs of various rubbers. In **Chapter 8** it was shown, that the soft interstices seen in AFM phase images containing the S-SBR/BR rubber blend used for the tyre tread compound, are not the actual crosslinking system. Preparation of the samples at room temperature or cooling with liquid nitrogen, before measuring with AFM, resulted in identical observations. Both sample preparation procedures resulted in soft interstices in the AFM phase image. The soft interstices are also not caused by microcracks introduced by cooling of the sample.

There was a correlation found between the presence of soft interstices in AFM phase images and the polymer structure. Linear polymers, such as S-SBR or EPDM with a narrow molecular weight distribution, show soft interstices, whereas branched polymers do not show these soft phases in the AFM phase image. The cause of these soft interstices is related to a low cohesive strength of linear polymers due to lack of branching, leading to Tokita regime 3 behaviour. The interstices are a manifestation of mastication on a nano-scale.

In **Chapter 9** the knowledge gained in the previous chapters was applied to a different dynamic application: an engine mount, commonly made out of Natural Rubber.

Adding highly dispersible silica to EPDM in combination with TESPT coupling agent reinforced the rubber. Also the dynamic properties of the EPDM were good. Addition of 50 phr silica provided a good hardness value and E-modulus, as requested in the specifications for engine mounts. However, the tear strength of the silica-reinforced EPDM was very poor in comparison with a NR carbon black reinforced compound. The optimal silica:silane ratio was 10:1. Adding less silane had a positive effect on the mechanical properties, but a negative effect on the dynamic properties. Addition of no silane caused a bad dispersion of the silica in the rubber matrix, resulting in poor dynamic properties.

Adding highly dispersible silica to NR, reinforced this rubber as well. In reinforced NR the mechanical properties were better than in EPDM, while the dynamic properties were worse. Comparing silica to carbon black, silica showed stronger reinforcing capabilities and better dynamic properties. This was the case for NR compounds, as well as for EPDM compounds.

Blending some NR into EPDM had a strong reinforcing effect on the mechanical properties of the compounds. The tear strength increased with a factor 3 when using a 90/10 EPDM/NR blend, vulcanised with a slow NR system, instead of the pure EPDM vulcanised with its own ultra-fast vulcanisation system.

The development of an engine mount compound based on silica-reinforced EPDM was not possible with EPDM as the only polymer. Replacing carbon black by silica in an EPDM compound greatly improved the mechanical properties of the compound without significant loss of dynamic properties. The major problem of the EPDM based engine mount was to obtain a sufficiently high value for the tear strength. This could be overcome by a small addition of NR. The tear strength was improved significantly, without significant loss of dynamic properties. The main polymer in the engine mount compound is still EPDM, therefore, a good high temperature resistance could in principle be achieved.

This thesis has been devoted to a great many different aspects of the technology of silica reinforcement of rubber, with emphasis on tyre applications. Although silica reinforcement of rubber is not entirely new, it has advanced significantly during recent years due to its introduction in low rolling resistant tyres. It is a technology with great potential, but more susceptible to processing problems than reinforcement with carbon black. Overall, mixing of silica in the presence of a coupling agent with rubber can be considered as "reactive" mixing, a new technology in the rubber field. It is a versatile technology, whereby many processing parameters play an important role. The research described in this thesis has contributed to an understanding of many of these mechanistic parameters, allowing for a better control of this technology.

---

## Samenvatting

---

In de afgelopen jaren is er duidelijke toename van het gebruik van silica als versterkende vulstof in bandenloopvlakmengels op te merken. In vergelijking met roet wordt de rolweerstand van banden sterk verminderd door het gebruik van silica als vulstof. Het gebruik van silica als een versterkende vulstof wordt echter als zeer lastig beschouwd. Rubber en roet zijn beide hydrofobe substanties waardoor zelden problemen zullen ontstaan tijdens het mengen. Wanneer echter silica wordt gemengd met de gebruikelijke apolaire rubbers zal er een grotere tendens zijn tot de vorming van waterstofbruginteracties in silica-agglomeraten dan interacties tussen de polaire siloxaan of silanol groepen aan het silica-oppervlak en het rubber. Hierdoor kunnen er grote problemen ontstaan tijdens het mengen van silica en rubber. Vanwege deze reden is er grote belangstelling om de compatibiliteit van rubbers en geprecipiteerde silica te vergroten middels modificatie van het silicaoppervlak. Over het algemeen worden bifunctionele organosilanen gebruikt als “coupling agents” om het silica-oppervlak chemisch te modificeren zodat interactie met het rubber wordt bevorderd. De meest gebruikte “coupling agent” voor dit soort toepassingen is bis-(triethoxysilylpropyl)tetrasulfide (TESPT). Vanuit een proces punt gezien moeten er twee chemische reacties plaatsvinden met behulp van de “coupling agent”. Eerst een reactie om de organosilaan aan het silica-oppervlak te binden en vervolgens een reactie om de organosilaan aan het rubber te binden.

Het doel van het onderzoek beschreven in dit proefschrift, was om een beter inzicht te verkrijgen in de reactiemechanismen die plaatsvinden tijdens het mengen van silica en rubber in de aanwezigheid van een “coupling agent” zoals in de voorgaande paragraaf beschreven staat. Deze kennis is noodzakelijk om het versterkingsmechanisme van silica in rubber te optimaliseren. Dit is alleen mogelijk als er meer inzicht is in de reactiemechanismen die plaatsvinden tussen de “coupling agent” en silica resp. rubber.

Een introductie in thema's die relevant zijn voor dit onderzoek is beschreven in **Hoofdstuk 2**. Nadruk is gelegd op het effect van vulmiddelen op de dynamisch mechanische eigenschappen van elastomeren, in relatie tot de rol in bandenprestatie. Het dispersieproces van vulmiddelen tijdens het mengen is ook kort behandeld. Speciale aandacht is gegeven aan het mengen van silica, betreffende de reacties die plaatsvinden in de aanwezigheid van een “coupling agent”.

De invloed van procesparameters op de dynamisch mechanische eigenschappen van silica versterkte bandenloopvlakmengsels staat beschreven in **Hoofdstuk 3**. Het toevoegen van TESPT als de “coupling agent” aan silica-rubbermengsels geeft een significante verbetering van de vulstof-rubbermatrix compatibiliteit. Deze “coupling agent” kan ook als een zwavel donor optreden en daarbij betrokken raken in een voortijdige vulcanisatie van het rubbermengsel. De dump temperatuur is een van de meest belangrijke procesparameters die tijdens het mengen wordt toegepast, tevens is ook de tijdsduur waarbij het mengsel aan een bepaalde temperatuur is blootgesteld van belang. Beide parameters beïnvloeden het reactiemechanisme van de “coupling agent” en bepalen of de “coupling agent” leidt tot een binding tussen silica en het rubber of resulteert in zwavel donatie. Een temperatuur van tenminste 130°C is nodig om de reactie tussen de “coupling agent” en silica plaats te laten vinden, terwijl de reactie tussen de “coupling agent” en het rubber of de zwavel donatie-reactie begint bij een temperatuur van 160°C. Een toename in de 300% modulus en/of de G' bij 100% rek bij dump temperaturen van hoger dan

150°C was een aanwijzing voor prevulcanisatie veroorzaakt door de zwaveldonatie mogelijkheid van de “coupling agent”. Het is waargenomen dat de “coupling agent” gemengd moet worden met silica gedurende tenminste 10 minuten bij een temperatuur van 150°C zodat een goede reactie kan plaatsvinden tussen de “coupling agent” en silica.

De invloed van andere ingrediënten, zoals bijvoorbeeld zinkoxide, is bestudeerd in **Hoofdstuk 4**. Het effect van de aanwezigheid van zinkoxide in de interne menger bij hogere dumptemperaturen is bestudeerd met behulp van dynamisch mechanische testen. Een lagere tendens tot prevulcanisatie is waargenomen wanneer zinkoxide niet aanwezig was tijdens de interne mengstap, maar werd toegevoegd tijdens de laatste mengstap op de wals samen met de vulcanisatieingrediënten. Zinkoxide interfereerde hoofdzakelijk in de reactie tussen de “coupling agent” en het silica-oppervlak, zoals aangetoond met de reactiesnelheidsconstanten verkregen via reologische experimenten. Verdere bevestiging werd verkregen door middel van HPLC-experimenten: de reactiesnelheidsconstanten van TESPT met silica monsters in de aanwezigheid van zinkoxide waren lager bij hogere temperaturen dan de monsters zonder zinkoxide. XPS-data bevestigde dat zinkoxide inderdaad kan reageren met het silica-oppervlak. Een ander interessant fenomeen dat is waargenomen, is dat de aanwezigheid van zinkoxide tijdens het mengen in de interne menger resulteert in kortere scorchtijden in vergelijking tot mengsels waarbij zinkoxide niet aanwezig is tijdens het mengen in de interne menger. Deze kortere scorchtijden zijn het resultaat van vulmiddel flocculatie van silica tijdens de vulcanisatie-stap .

De experimenten beschreven in **Hoofdstuk 5** bewijzen dat een juiste balans tussen de functionaliteiten van de “coupling agent” noodzakelijk is om de eigenschappen van silica versterkte bandenloopvlakmengsels te verbeteren. TESPT heeft bewezen hier het beste aan te voldoen, omdat het kan koppelen aan het silica-oppervlak via drie ethoxy-groepen resp. zwavel kan doneren en koppelen aan het rubber via zijn eigen zwavelhoeveelheid. Alternatieve “coupling agents” die maar een van deze functionaliteiten bezitten, resulteerden in een inferieure balans van eigenschappen. Bis-(triethoxysilyl)hexaan (TESH) heeft alleen maar ethoxy-groepen, hydrofobeerde het silica-oppervlak en zorgde voor een goede silicadispersie net zoals TESPT. De eigenschappen na vulcanisatie waren echter veel slechter dan wanneer TESPT wordt gebruikt. Bis-(trimethylsilylpropyl)tetrasulfide (TMeSPT), met alleen een actieve zwavelgroep, faalde in het goed dispergeren van silica en vertoonde voortijdige vulcanisatie bij hoge menger dumptemperaturen, zoals waargenomen met TESPT. Het toevoegen van twee “coupling agents”, bis-(triethoxysilylpropyl)decaan (TESD) en TMeSPT, waarbij de functies onafhankelijk zijn verdeeld over de twee “coupling agents” resulteerde in een silicadispersie die vergelijkbaar is met die van TESPT. Ook is er scorch waargenomen bij hoge menger dumptemperaturen, zoals bij TESPT. De eigenschappen van de ge vulcaniseerde mengsels waren nog steeds inferieur in vergelijking tot die van TESPT. Een “coupling agent” met maar een reactieve ethoxygroep aan het silicium atoom vs. drie voor TESPT werkte verbazingwekkend goed. Deze “coupling agent” kan alleen maar via een Si-O brug koppelen, dit resulteert in een snelle dispersie van silica tijdens het mengen en derhalve worden lage mengkoppels verkregen. De ge vulcaniseerde mengsel eigenschappen zijn vergelijkbaar met die van TESPT, in het bijzonder de tan  $\delta$ , hetgeen representatief is voor de rolweerstand. Alleen de treksterkte was lager dan voor TESPT bevattende mengsels.

Gebaseerd op alle resultaten is er een model voorgesteld waarbij TESPT zwavel doneert naar het mengsel in de nabijheid van een silicadeeltje tijdens het mengen of tijdens het begin stadium van het vulcaniseren. Hierdoor wordt een gecrosslinkte laag om het

silicadeeltje gevormd en wordt silica in de rubbermatrix gevangen. Tijdens de vulcanisatie stap zorgt de “coupling agent” voor de koppeling tussen het silicadeeltje en het rubber.

In hoofdstukken 3 en 5 was het waargenomen dat TESPT met het rubber reageert onder hoge temperatuur condities zelfs in de afwezigheid van vulcanisatiemiddelen. Dit veroorzaakt pre-vulcanisatie of scorch tijdens het mengen en leidt tot een stijging in de viscositeit van het mengsel waardoor de verwerkbaarheid van het mengsel moeilijker wordt. Om een oplossing voor dit probleem te vinden is het noodzakelijk om de reactie te bestuderen en het mechanisme op te helderen. **Hoofdstuk 6** behandelt de reacties die plaatsvinden tussen de “coupling agent” en het rubber. Deze studie is gedaan met behulp van modelvulcanisatie zodat analyse van de reactieproducten met standaard technieken mogelijk is. Het model 3-methyl-1-penteen (representatief voor de vinyl-configuratie van butadiëenrubber) was reactiever dan trans-3-hexeen (representatief voor de trans-configuratie in butadiëenrubber) en trans-3-hexeen was reactiever met zwavel dan 2,3-dimethyl-2-buteen. Reactie met TESPT leidde tot dezelfde reactieproducten; dit is een indicatie dat TESPT zwavel doneert. Experimenten met alleen TESPT en een model toonde aan dat TESPT vrij zwavel opneemt gedurende de eerste 5 minuten van de reactie alvorens het te doneren naar het model.

Het effect van de dump temperatuur op de morfologie van silica in gevulde mengsels is bestudeerd in **Hoofdstuk 7**. De dump temperatuur verkregen tijdens het mengen heeft geen significante invloed op de macrodispersie van hoog dispergeerbare silica. De microdispersie, gemeten met behulp van AFM metingen, wordt wel beïnvloed door de dump temperatuur. Bij hoge dump temperaturen wordt een betere dispersie verkregen; dit houdt in dat er meer primaire deeltjes aanwezig zijn. Ook zijn er effecten van pre-vulcanisatie zichtbaar met behulp van AFM. Elliptische structuren zijn zichtbaar in het AFM-plaatje.

De structuur van silica heeft een grote invloed op de macro- en de microdispersie. Laag gestructureerde silica (conventionele silica) resulteerde in een slechte macrodispersie. Microdispersiemetingen toonde aan dat hoog gestructureerde silica meer primaire deeltjes oplevert. Hoog dispergeerbare silica (hoogst gestructureerde silica) wordt voor het merendeel gedispergeerd tot het microdispersie niveau, slechts 15-20% van de silica blijft achter in het macrodispersie gebied. De vulmiddel-vulmiddel interacties worden meestal veroorzaakt door aggregaten met een diameter van minimaal 600 nm. De treksterkte van de mengsels gebaseerd op de verschillende silica's wordt hoofdzakelijk beïnvloed door de microdispersie. Lage treksterktes werden verkregen wanneer een significante hoeveelheid aggregaten aanwezig was in het mengsel met een diameter groter dan 600 nm.

Om een bandenloopvlakmengsel te verkrijgen met een lage rolweerstand is het belangrijk dat een hoog dispergeerbare silica wordt gebruikt. De hoog dispergeerbare silica moet voor het grootste deel tot op het microdispersie niveau worden gedispergeerd, waarbij het dan hoofdzakelijk bestaat uit primaire deeltjes en een paar aggregaten met een diameter tussen de 100 en 200 nm.

Voor de korrelige of zachte gebieden die aanwezig zijn in AFM- of TEM-plaatjes van verschillende rubbers worden in de literatuur verschillende verklaringen gegeven. In **Hoofdstuk 8** is aangetoond dat de zachte kanaalachtige structuren in een S-SBR/BR mengsel niet het eigenlijke vulcanisatienetwerk is. Behandeling van de monsters bij kamertemperatuur of koelen met vloeibare stikstof voordat gemeten werd met de AFM, resulteerde in identieke resultaten. Beide monsterbehandelingen resulteerden in zachte gebieden in het AFM-plaatje. De zachte gebieden worden ook niet veroorzaakt door microscheurtjes geïntroduceerd door het koelen.

Er is een samenhang gevonden tussen de aanwezigheid van zachte gebieden in het AFM-plaatje en de structuur van het polymeer. Lineaire polymeren zoals S-SBR of EPDM met een nauwe molgewichtverdeling vertoonden zachte gebieden, terwijl vertakte polymeren juist geen zachte gebieden vertoonden in het AFM-plaatje. De reden van het ontstaan van deze zachte gebieden is een lage cohesieve sterkte van lineaire polymeren door het ontbreken van vertakkingen. Dit leidt tot het Tokita 3 regime gedrag. De zachte gebieden zijn een manifestatie van masticatie op nanoschaal.

In **Hoofdstuk 9** is de kennis vergaard in de voorgaande hoofdstukken, toegepast op een andere dynamische applicatie: een motorophangblok, normaal gesproken gemaakt van natuurrubber. Het toevoegen van hoog dispergeerbare silica aan EPDM in combinatie met TESPT als de "coupling agent" versterkte het rubber. Ook waren de dynamische eigenschappen van EPDM goed. Een toevoeging van 50 phr silica leverde een goede waarde voor de hardheid en de E-modulus, zoals vereist voor een motorophangblok. De scheursterkte van silica versterkt EPDM was echter zeer slecht in vergelijking tot een NR mengsel versterkt met roet. De optimale silica:silaanverhouding was 10:1. Minder silaan toevoegen had een positief effect op de mechanische eigenschappen, maar had een negatief effect op de dynamische eigenschappen. Wanneer er geen silaan wordt toegevoegd, wordt een slechte dispersie van silica in de rubbermatrix verkregen, hetgeen resulteert in slechte dynamische eigenschappen.

Het toevoegen van hoog dispergeerbare silica heeft ook een versterkend effect op NR. In versterkt NR waren de mechanische eigenschappen beter dan in EPDM, terwijl de dynamische eigenschappen slechter waren. In vergelijking tot roet vertoonde silica een beter versterkend vermogen en betere dynamische eigenschappen. Dit was het geval voor NR mengsels als ook voor EPDM mengsels.

Het mengen van een kleine hoeveelheid NR in EPDM had een groot versterkend effect op de mechanische eigenschappen van de mengsels. De scheursterkte nam met een factor 3 toe wanneer een EPDM/NR mengsel werd gebruikt met een verhouding van 90/10 en ge vulcaniseerd met het NR systeem in vergelijking tot het pure EPDM met zijn eigen ultra-snelle vulcanisatiesysteem.

De ontwikkeling van een motorophangblok gebaseerd op EPDM versterkt met silica was niet mogelijk met alleen EPDM als polymeer. Vervanging van roet door silica in een EPDM mengsel verbetert de mechanische eigenschappen aanzienlijk, terwijl de dynamische eigenschappen niet verminderen. De scheursterkte verbeterde significant door toevoeging van een kleine hoeveelheid NR zonder dat een sterke afname van de dynamische eigenschappen optrad. EPDM blijft het voornaamste polymeer, daardoor is het nog steeds mogelijk om een goede temperatuursbestendigheid te verkrijgen.

In dit proefschrift komt een groot aantal aspecten aan de orde van de technologie van silicaversterking in rubber, met de nadruk op bandentoepassingen. Ook al is silicaversterking in rubber niet geheel nieuw, toch is het ver gevorderd in de loop der jaren dankzij de introductie van silica in lage rolweerstand banden. Het is een technologie met grote mogelijkheden, maar meer gevoelig voor procesproblemen dan versterking door middel van roet. Concluderend kan het mengen van silica in de aanwezigheid van een "coupling agent" en rubber worden beschouwd als "reactief mengen", een nieuwe technologie in de rubberwereld. Het is een veelzijdige technologie waarbij vele procesparameters een belangrijke rol spelen. Het onderzoek beschreven in dit proefschrift, heeft bijgedragen aan een beter begrip van veel van deze mechanistische parameters, zodat een betere beheersing van deze technologie mogelijk is.

---

## **Curriculum Vitae**

---

De auteur werd op 16 mei 1973 geboren te Heino. Na het behalen van zijn HAVO diploma in 1990 aan het Florens Radewijns college te Raalte, begon hij zijn studie aan het Hoger Laboratorium Onderwijs van de Rijkshogeschool IJsselland te Deventer in de richting van algemene analytische chemie. In 1994 rondde hij zijn afstudeeropdracht af bij Akzo Nobel te Deventer. In datzelfde jaar begon hij aan de studie Chemische Technologie aan de Universiteit Twente in Enschede. In 1998 sloot hij zijn studie af met een afstudeeropdracht binnen de vakgroep Rubbertechnologie, getiteld 'De invloed van versnellersystemen op de recycling van natuurrubber en EPDM'. Na het voltooien van deze studie begon hij in diezelfde groep als assistant in opleiding. Onder de supervisie van prof. dr. ir. J.W.M. Noordermeer heeft hij zijn promotieonderzoek uitgevoerd, waarvan de resultaten beschreven zijn in dit proefschrift.

